An Evaluation of Small Scale Shortwave Vegetation Index Imagery for Vegetation Mapping

by

Daniel Lloyd

A thesis submitted to the University of Bristol
in accordance with the requirements
for the degree of Doctor of Philosophy
in the Faculty of Science

Department of Geography,
University Road,
Bristol BS8 1SS.

Copy 6

July, 1988

Abstract

The spatial, radiometric, temporal and economic characteristics of small scale radiometric imagery produced by the United States National Oceanic and Atmospheric Administration Advanced Very High Resolution Radiometer (AVHRR) are described and compared with large scale multispectral radiometric imagery from other satellite-borne sensors. The physical and physiological bases of normalised difference vegetation index (NDVI) imagery, which may be derived from AVHRR data, and the purposes for which NDVI imagery has been used are reviewed with reference particularly to their phytophenological potential.

Two types of AVHRR NDVI imagery are analysed. Twelve full resolution AVHRR NDVI images for the Spring and Summer months of 1985 and 1986 are used to describe and classify the vegetation of northeastern and southern Spain and twenty-four monthly Global Vegetation Index images for the period January 1985 to December 1986 are used to describe and classify the vegetation of Africa. Phytophenological variables summarising in an accessible form the information relating to canopy photosynthetic activity contained in multidate NDVI imagery are derived from the basic data. The extent to which multidate AVHRR NDVI imagery may be used to map the vegetation of Spain and Africa is assessed using unsupervised and supervised classification techniques.

There are five conclusions. The first is that small scale shortwave vegetation index imagery is a unique source of synoptic information with immense potential. The second conclusion is that imagery of phytophenological variables, which describe spatial variations in the timing, intensity and duration of vegetation photosynthetic activity, is a useful, concise and appropriate form in which to compress the information contained in large volumes of multitemporal NDVI data. The third conclusion is that, for purposes of classifying multidate NDVI imagery, a supervised binary decision tree classification of phytophenological variables has distinct advantages over both cluster analysis and a minimum distance classifier. The fourth conclusion is that equal area radial projections are preferable to other map projections for purposes of displaying small scale radiometric imagery. The fifth conclusion is that Global Vegetation Index imagery would be improved if it were mapped to an equal area radial projection base map array and produced without drastic spatial subsampling.

Dedicated with love to my Mum and Dad

"Moon!" you cry suddenly, "Moon! Moon!"

The moon has stepped back like an artist gazing amazed at a work

That points at him amazed

(Ted Hughes)

Contents

Chapter Three. The Definition of Vegetation Cover Classes for use with Multidate AVHRR NDVI Imagery

Chapter Four. Vegetation Mapping Using Full Resolution AVHRR NDVI Imagery

List of Tables

List of Equations

List of Figures

Acknowledgements and Declaration

I should like to thank Eric Barrett for providing me with the opportunity to pursue a most interesting research project. He has, on occasions, helped, guided, provoked and cajoled in order to keep my investigations moving. However, his confidence in my ability to complete this research did not appear to falter and this, particularly, has been a continual source of encouragement to me. I should like to thank also the Natural Environment Research Council for financial assistance. In addition to a three-year maintenance grant (GT4/83/TLS/6), they provided satellite imagery of Spain and supported several field excursions to Spain. I also acknowledge the support provided by the Memorandum of Understanding between Bristol University Remote Sensing Unit and the National Oceanic and Atmospheric Administration in the United States which consisted of the supply of Global Vegetation Index imagery.

I have received help and encouragement from many people during the four-and-a-half years that I have been working on this thesis. I was introduced to digital image processing by George Kearn of the Royal Aircraft Establishment at Farnborough. More recently, the capable and friendly research group at Bristol have been a constant source of support. Giles D'Souza, in particular, has helped, encouraged and inspired me at every stage. Tim Richards, Andrew Harrison and Mike Beaumont have also made many helpful suggestions and comments. In addition, I am grateful to John Brush of Dundee University, who generously made his geodetic registration algorithm available to me, Rafael Ruiz-Fornells Gonzalez of the Spanish ministry of agriculture, who gave me a set of landuse maps of Spain, and Terry Hardaker of Oxford Cartographers, for his permission to use the illustration from the *Peters Equality Atlas of the World*. I should also like to thank my examiners, Dr. Edward Maltby (Exeter University) and Professor John Thornes, for their comments and criticisms of the original manuscript.

Throughout the period of this research I have been encouraged and supported by my friends and my family. In Bristol, Steve, Pips, Nick, Louise, Loz, Phil, Rache, Stuart, Ken, Pauline, Clare, Richard, Chris, Ben, Paul, Judy, Chris, Sue and Porters (all of them!) have helped keep work fun. In Spain, I received enthusiastic support for my field excursions from Dave, Julen, Txoli, Gerard, Rachel, Sarah, Antxon and Liz. They all helped to ensure that we were not tempted to stay too long at any of the more agreeable spots along the way.

Throughout my research I have enjoyed being a member of the Geography Department at Bristol. At this stage I should like to thank particularly the head of department, John Thornes, who allowed me to continue working in the department after my grant had finished, Tony Philpott, who helped me to produce the black-and-white photographs and figures, and Lilian Sherwood, who helped me to find maps, provided me with stationary, and soft-bound draft copies of the thesis. There is no typist to thank, although I am grateful to Ann French, Cathy Hole and Cyd Hammel of the University Computer Centre for their answers to my word-processing queries.

Finally, in accordance with the regulations, I declare that this thesis is my own work, except where acknowledgement is given in the text, and that it has not been submitted for a higher degree to this or any other university.

Daniel Lloyd.
July, 1988.

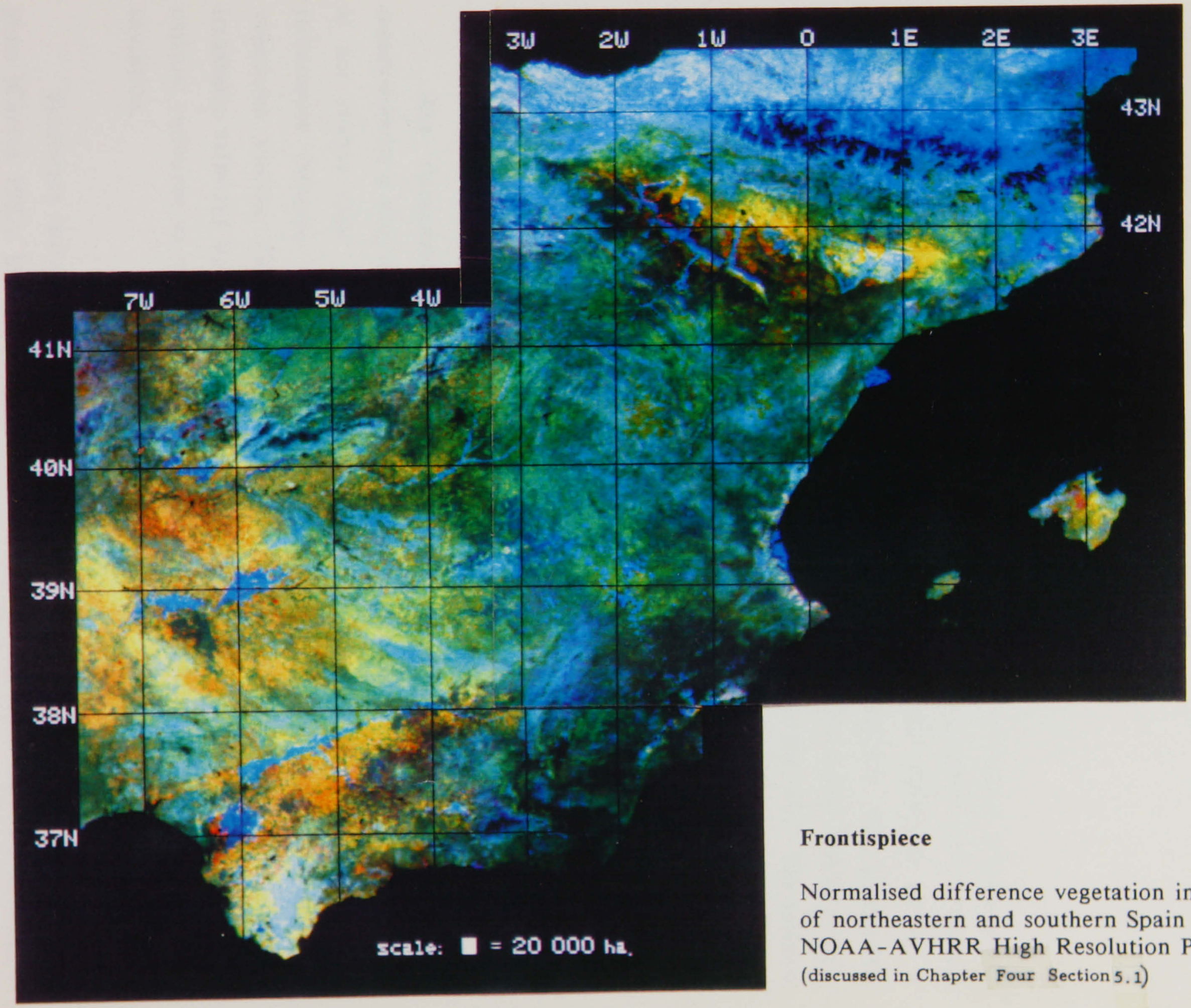

Frontispiece

Normalised difference vegetation index image of northeastern and southern Spain derived from NOAA-AVHRR High Resolution Picture Transmission.
(discussed in Chapter Four Section 5.1)

Chapter One

Introduction

1. Background

There are many approaches to the description and classification of vegetation. Vegetation maps may be based on vegetation floristics (Whittaker 1962[1],1973; Shimwell 1971), vegetation physiognomy (e.g. Fosberg 1967; Beard 1973; UNESCO 1973a), a combination of vegetation floristics and physiognomy (e.g. UNESCO 1983; Laubenfels 1975), vegetation phenology (Leith 1974a), landuse (e.g. Küchler 1969; MAPA 1988), climate (e.g. Walter 1985) or topography (e.g. Howard and Mitchell 1980). The relative merits of these different approaches depend ultimately upon how well they serve the needs of the study in hand (Küchler 1967; Whittaker 1973; Shimwell 1984). This thesis describes an evaluation of certain radiometric data derived from satellite-borne sensors for purposes of describing the vegetation cover of large areas and discusses the extent to which a phytophenological approach particularly can provide vegetation cover maps as a reference for the optimal assessment, planning, development and management of renewable resources.

The fundamental advantage of radiometric imagery over ground-based measurements is that the data are spatially comprehensive. Unfortunately their meaning is not always clear. Consequently, despite the availability of a wide variety of radiometric imagery (Colwell 1983), shortwave imagery particularly is used for vegetation studies. This is because the primary controls on the amount of solar irradiance reflected by a vegetation canopy are known and it is therefore possible to explain variations in vegetation shortwave response in terms of vegetation type and condition.

Shortwave radiometric imagery has been produced by airborne sensors for many years (Curran 1985). More recently, a wide variety of shortwave radiometric imagery from satellite-borne sensors has become generally available (tables 1, 2 and 3). The satellite imagery used most to study vegetation is produced by the Landsat and SPOT[2]

---

1 Reprinted Whittaker (1977)

2 Système Probatoire d'Observation de la Tierre

Table 1. Radiometric Characteristics and Imaging Frequency of Selected Satellite-Borne Electro-Optical Imaging Systems
(sources: Brimacombe 1981; USGS 1984; Kidwell 1986; NRSC 1987)

	Channel	Waveband (μm)	Bits Per Pixel	Repeat Period[a]
SPOT Panchromatic		0.51-0.73	6	26 days
SPOT Colour Mode	1	0.50-0.59	8	26 days
	2	0.61-0.68	8	26 days
	3	0.79-0.89	8	26 days
Landsat 4 Thematic Mapper	1	0.45-0.52	8	16 days
	2	0.52-0.60	8	16 days
	3	0.63-0.69	8	16 days
	4	0.76-0.90	8	16 days
	5	1.55-1.75	8	16 days
	6	10.4-12.5	8	16 days
	7	2.08-2.35	8	16 days
Landsat 4 Multispectral Scanner	1	0.50-0.60	6	16 days
	2	0.60-0.70	6	16 days
	3	0.70-0.80	6	16 days
	4	0.80-1.10	6	16 days
NOAA 9 AVHRR/2	1	0.58-0.68	10	12 hours
	2	0.72-1.06	10	12 hours
	3	3.55-3.93	10	12 hours
	4	10.3-11.3	10	12 hours
	5	11.5-12.50	10	12 hours
Meteosat 2	1	0.40-1.10	6	1 hour[b]
	2	5.70-7.10	8	30 minutes
	3	10.5-12.50	6	1 hour

a. SPOT, Landsat 4 and NOAA 9 are all polar-orbiting satellites. Their repeat period is defined as the time the satellite takes in order to return to approximately the same point on the Earth's surface. Meteosat is a geostationary satellite which hovers over the Gulf of Guinea at the intersection of the Equator and the Greenwich meridian and images the surface of the Earth visible from this position. The best Meteosat imagery is produced for the area bounded by 60 ° N, 60 ° S, 60 ° W and 60 ° E

b. Meteosat 2 channel 1 data is produced every thirty minutes during daylight hours at one of two spatial scales. Full resolution channel 1 imagery (2.5x2.5km) is produced when channel 3 imagery is not made and half spatial resolution channel 1 imagery (nominally 2.5x5.0km) is produced when channel 3 imagery is made. Usually Meteosat channel 3 data is produced every thirty minutes at night and every hour during the day (Eumetsat 1987)

imaging systems. However, although Landsat data were once relatively cheap due to subsidies from the Government of the United States (Baker 1987), often today it seems that there is no extra benefit obtained and considerable extra financial cost incurred from using Landsat or SPOT imagery instead of high resolution imagery from an airborne sensor (Watson 1981; Curran 1985). This is because the temporal characteristics

Table 2. Spatial Characteristics of Imagery from Selected Satellite-Borne Electro-Optical Imaging Systems
(sources: Brimacombe 1981; USGS 1984; Kidwell 1986; NRSC 1987)

	Pixel Size[a]	Pixels per 1.1km^2	Pixels Per 100km^2	Pixels To Cover Africa[b]
SPOT Panchromatic	10x10m	12 100	$1.0x10^8$	$9.2x10^{18}$
SPOT Colour Mode	20x20m	3025	$2.5x10^7$	$2.3x10^{18}$
Landsat 4 Thematic Mapper (channels 1, 2, 3, 4, 5 and 7)	30x30m	1344	$1.1x10^7$	$1.0x10^{18}$
Landsat 4 Multispectral Scanner (all channels)	80x80m[c]	265	$2.2x10^6$	$2.0x10^{17}$
Landsat 4 Thematic Mapper (channel 6)	120x120m	84	$6.9x10^5$	$6.4x10^{16}$
NOAA 9 AVHRR/2 HRPT[d] (all channels)	1.1x1.1km[e]	1	11 364	$1.0x10^{15}$
Meteosat 2 (channel 1)	2.5x2.5km	0.2	1600	$1.5x10^{14}$
Meteosat 2 (channels 2 and 3)	5x5km	0.05	400	$3.7x10^{13}$
NOAA 9 AVHRR GVI[f]	20x20km[g]	0.003	25	$2.3x10^{12}$

a. Area on the ground covered by the instantaneous field of view of the sensor at nadir (see also Chapter Two Section 3.6)
b. $30.3x10^6km^2$
c. For the purpose of the calculations in this table the area on the ground corresponding to one Landsat 4 Multispectral Scanner Pixel is taken as 80x57m (i.e. across-track pixel overlap is taken into account)
d. High Resolution Picture Transmission
e. For the purpose of the calculations in this table the area on the ground corresponding to one High Resolution Picture Transmission Pixel is taken as 0.8x1.1km (i.e. across-track pixel overlap is taken into account (Appendix 1))
f. Global Vegetation Index
g. A nominal value only

and areal coverage of imagery from satellite-borne sensors are determined by the inflexible orbital characteristics of the satellite and consequently satellite sensors

Table 3. Economic Characteristics of Imagery from Selected Satellite-Borne Electro-Optical Imaging Systems[a]

	Area of Scene[b]	Cost Per Scene[c]	Cost Per 100km²	Cost of Receiver[d]
SPOT Panchromatic or Colour Mode (all channels)	60km²	10 300FF	28 600FF	$7x10^6$
Landsat 4 Thematic Mapper (all channels)	185km²	$3300	$964	$7x10^6$
Landsat 4 Multispectral Scanner (all channels)	185km²	$660	$193	$7x10^6$
NOAA 9 AVHRR/2 HRPT[b] (all channels)	3000km²	£40	£0.05	£42 000
Meteosat 2 (all channels)	12 250km²	£40	£0.003	£11 000
NOAA 9 AVHRR/2 GVI[b]	20 250km²	$6.88	$0.0002	

a. All prices are for November 1987 and are intended as a guide only

b. The area of scene for High Resolution Picture Transmission (HRPT) is approximately half the entire swath length which can be received by a single ground receiving station (i.e. 3000 x 2900km). The area of scene for Meteosat imagery is the area bounded by 60°N, 60°S, 60°W and 60°E (Amiran and Schick 1961). The area of scene for Global Vegetation Index (GVI) imagery is the area covered by one complete image (i.e. 75°N to 55°S (Amiran and Schick 1961))

c. Prices form Nigel Press Associates (SPOT), Eosat (Landsat), Dundee Satellite Receiving Station (High Resolution Picture Transmission and Meteosat) and the Satellite Data Services Division of NOAA (Global Vegetation Index). The price for High Resolution Picture Transmission is for all channels. The price for Meteosat is for either one 2.5km^2 visible image or four 5km^2 images (all full disk images). The price for the Global Vegetation Index is for polar-stereographic imagery stacked on 1600 bits-per-inch computer compatible tapes

d. A "receiver" is a ground receiving station able to decode the satellite data stream and load the imagery onto magnetic tape. The price given is a minimum price and does not include the cost of suitable housing (approximately $1.5x10^6 for Landsat and SPOT), the running costs (i.e. license to receive imagery, maintenance and staff (approximately $2-3x10^6 per annum for Landsat and SPOT)) or the hardware and software required for image preprocessing, processing, analysis and interpretation. The price of a receiver able to receive both SPOT and Landsat images was provided by Macdonald-Dettwiler. The price of the AVHRR High Resolution Picture Transmission receiver and the Meteosat receiver was provided by Dundee Satellite Data Receiving Station

produce imagery even when the target is obscured by cloud. In contrast, airborne sensors can produce imagery of precisely the location desired at precisely the time desired with finer spatial detail than the best satellite imagery.

High resolution imagery from any source is expensive[3] and voluminous. Consequently, multidate high resolution imagery of very large areas (e.g. Africa) is not easily obtained or processed unless some kind of spatial sampling framework is used (e.g. MacDonald and Hall 1980; Woodwell *et al.* 1984; Nelson *et al.* 1987a,1987b). In contrast, small scale radiometric imagery from satellite altitudes is relatively cheap and manageable (tables 1, 2 and 3). Furthermore, whereas large scale imagery can be made by either airborne or satellite-borne sensors, *only* satellite-borne sensors can provide frequent imagery of very large areas. A synoptic view of the Earth's surface is one of the unique scientific opportunities provided by satellite technology.

2. The NOAA AVHRR imaging system

Agronomists have been much slower to recognise the originality and potential of small scale radiometric imagery than meteorologists. In part this may be attributed to the absence during the 1970s of a satellite-borne sensor producing small scale data suitable for phytogeographical purposes. However, this situation changed in June 1979 when NOAA 6 was launched by the National Oceanic and Atmospheric Administration (NOAA).

NOAA satellites are the latest in a series of operational polar-orbiting meteorological satellites designed and built by Radio Corporation of America Electronics under the technical management of the United States National Aeronautics and Space Administration and procured and operated by the United States Department of Commerce (table 4). The two principal payload sensors aboard NOAA satellites are the Tiros Vertical Sounder, a three instrument system comprised of the High Resolution Infrared Radiation Sounder, the Stratospheric Sounding Unit and the Microwave Sounding Unit, and the Advanced Very High Resolution Radiometer (AVHRR), a four- or five-channel passive scanning radiometer (Allison and Schnapf 1983; Norwood and Lansing 1983).

The NOAA sensors were designed primarily for the operational collection of meteorological data to assist with cloud cover assessment, cloud classification and sea and land surface temperature monitoring (Hussey 1977; Schnapf 1985; Garcia 1985; Smith *et al.* 1986). However, in recent years, technological innovations have resulted in sensors capable of producing meteorological data at geostationary altitudes. Since data from geostationary satellites can be supplied more frequently and require less

3 Regional remote sensing centres can spread the cost of imagery among many users (e.g. Falconer 1985)

Table 4. Chronological Summary of United States Polar-Orbiting Meteorological Satellites
(sources: Schnapf 1982; Allison and Schnapf 1983; Dundee Satellite Receiving Station 1986; Fusco and Muirhead 1987; Fischer 1987)

Prelaunch Name	Postlaunch Name	Period of Operation[a]	Imaging Sensors
	TIROS I-X[b]	1960-5	VCS[c], APT[d]
	ESSA 1-9[e]	1966-9	VCS, APT
	ITOS 1[f]	1970	APT, AVCS[g]
ITOS 1	NOAA 1	1970	APT, AVCS
ITOS D, F-H	NOAA 2-5	1972-6	VHRR[h]
	TIROS-N[i]	19.10.78-30.1.80	AVHRR[j]
NOAA A	NOAA 6	27.6.79-30.6.86	AVHRR/1[j]
NOAA B		Failed	
NOAA C	NOAA 7	9.7.81-11.1.85	AVHRR/2[j]
NOAA D		Not launched	
NOAA E[k]	NOAA 8	3.5.83-6.3.86	AVHRR/1[j]
NOAA F	NOAA 9	8.1.85-present	AVHRR/2[j]
NOAA G	NOAA 10	20.9.86-present	AVHRR/1[j]
NOAA H-J		1988-1992	AVHRR/2[j]
NOAA K-M		1992-1995	AVHRR/3[j]
Polar Platform		1995 onwards	AMRIR[l]

a. Includes gaps due to temporary failure of sensor. Image quality may deteriorate towards the end of a sensor's lifetime
b. TIROS I-X belong to the Television and Infrared Observation Satellite series (semi-operational)
c. Half-inch Vidicon Camera System
d. Automatic Picture Transmission (realtime direct readout)
e. ESSA 1-9 belong to the Tiros Operational System series
f. ITOS 1 and NOAA 1-5 belong to the Improved Tiros Operational System series
g. One inch Advanced Vidicon Camera System
h. Very High Resolution Radiometer (one visible and one thermal infrared channel only)
i. TIROS-N and NOAA A-D belong to the Tiros-N series
j. Advanced Very High Resolution Radiometer (Appendix 1)
k. NOAA E-J belong to the Advanced Tiros-N series
l. Advanced Medium Resolution Imaging Radiometer (eleven channels, not confirmed)

preprocessing than data from the NOAA satellites (Greaves and Shenk 1985), generally they are used in preference to AVHRR data wherever possible[4]. Meanwhile, during the 1980s, AVHRR imagery has been used increasingly to describe a variety of terrestrial and oceanographic features (e.g. Hayes 1985; Hussey 1985; Yates *et al.* 1986; Dawe *et*

4 Geostationary satellites provide poor coverage of high latitudes (i.e. >60° N and S)

al. 1986; Gorman and Sadowsky 1986; Wiesnet and Tarpley 1987; Ali *et al.* 1987; Harrison and Lucas 1988).

It seems likely that there will be competition in the field of terrestrial and oceanographic studies between the AVHRR and sensors aboard both the second generation Meteosat satellite (Bizzarri 1986) and also SPOTs 4 and 5 (Colucci 1987). However, it is unlikely that AVHHR data will eclipsed by the new data. Hardware and software investment in AVHRR data is immense (Ellingsen *et al.* 1986; Popham 1987). Furthermore, a supply of AVHRR imagery is guaranteed for the foreseeable future (table 4). Four NOAA spacecraft with AVHRRs will fly aboard the Advanced Tiros-N sequence and three further spacecraft, also with AVHRRs, are planned for the follow-on NOAA "next-sequence" with provisional launching dates of December 1992, March 1994 and June 1995. The monitoring functions of the NOAA series will be continued into the twenty-first century by the Polar Platform of the Space Station Program due to be launched in 1995 (Fischer 1987; Curran and Plummer 1987).

3. Vegetation mapping using AVHRR NDVI imagery

Currently, the AVHRR is the only satellite-borne sensor producing small scale shortwave imagery suitable for phytogeographical studies. The phytogeographical potential of this imagery has been investigated principally using a variety of one-dimensional shortwave vegetation indices calculated from the red and near-infrared reflectance measurements provided by AVHRR channels 1 and 2 (Gray and McCrary 1981; Gatlin *et al.* 1981; Schneider and McGinnis 1982; Tucker *et al.* 1984a; Dijk *et al.* 1984; Yates *et al.* 1984; McGinnis and Tarpley 1985). The Normalised Difference Vegetation Index (NDVI) in particular has been widely used with AVHRR data (e.g. Justice 1986).

Multidate imagery describes primarily spatial variations in the timing, intensity and duration of photosynthetic activity. This interpretation, which is explained in Chapter Two, has provided the basis for a wide range of applications of AVHRR NDVI imagery. The relation between the AVHRR NDVI and the condition and productivity of rangelands has been the object of particular interest (Tucker *et al.* 1983,1985b; Taylor *et al.* 1985; Justice 1986). In addition, AVHRR NDVI imagery has been used to detect forest fires and agricultural burning (Malingreau *et al.* 1985; Matson and Holben 1987; Matson *et al.* 1987), to locate areas on the ground where conditions are liable to result in locust plagues (e.g. Hielkema *et al.* 1986), to elucidate

the role of terrestrial biota in the global carbon cycle (Tucker *et al.* 1986a) and even to determine the extent of volcanic dust deposition (Tucker and Matson 1985).

Relatively few attempts have been made to derive maps of vegetation cover from AVHRR NDVI imagery. In part this may be due to the fact that shortwave vegetation indices such as the NDVI are largely independent of vegetation canopy physiognomy or floristic composition (Tucker *et al.* 1983; Steven 1987). Thus, single date NDVI imagery has limited value for vegetation mapping since, on any particular day, several different cover types may have similar levels of photosynthetic activity and so be indistinguishable (e.g. Steiner 1969; Blümel and Tonn 1986). Studies by Tucker *et al.* (1984b) and Nelson and Holben (1986) demonstrate the degree of discrimination that may be achieved using single date AVHRR NDVI imagery. Although the power of shortwave vegetation index imagery to discriminate among physiognomic and agricultural vegetation cover classes may be increased using multitemporal data sets (e.g. Steiner 1969; Badhwar 1984a,1984b; Ajai *et al.* 1985; Hall and Badhwar 1987), a multitemporal approach to the production of vegetation cover maps from shortwave vegetation index imagery has been used only rarely with AVHRR NDVI imagery (Norwine and Greegor 1983; Tucker *et al.* 1985a; Townshend *et al.* 1987). Presumably, this is due primarily to the fact that, even with the enhanced discriminatory power provided by a multitemporal data set, there remains uncertainty over the meaning of AVHRR NDVI values on account of the large areas on the ground associated with individual AVHRR pixels.

AVHRR data is produced at several spatial scales (see Appendix 1 and Table 2). All of these data are small scale. For example, pixels in full resolution AVHRR imagery represent an area on the ground of at least 121 hectares while pixels in AVHRR Global Vegetation Index imagery represent an area on the ground of at least 12 800 hectares. Consequently, whereas the classes produced by classification of multidate large scale vegetation index imagery derived from the imagery produced by the sensors aboard Landsat and SPOT can be related usually to physiognomic and agricultural vegetation cover classes, the relation between vegetation classes that are recognisably distinct to an observer on the ground and the classes produced by classification of multidate AVHRR NDVI imagery is not always clear.

The interpretation of classified multidate AVHRR NDVI imagery in terms of vegetation cover is assessed in Chapter Three. At this stage it is worth remarking that all attempts to map vegetation using AVHRR NDVI imagery so far have aimed to use the satellite data to reproduce patterns of physiognomic and agricultural vegetation

cover classes. Given the fact that there seems to be no direct relation between NDVI values and either vegetation canopy physiognomy or floristic composition, it is unsurprising that many of the patterns in vegetation maps derived from small scale multidate vegetation index imagery do not appear to correspond with physiognomic or agricultural vegetation cover classes (Townshend *et al.* 1987). This lack of correspondence has lead Townshend *et al.* to suggest that vegetation classes derived from multidate AVHRR NDVI imagery may not have been described before. The implication here is that NDVI imagery provides a means to classify vegetation cover on the basis of variations in photosynthetic activity rather than, for example, physiognomy. Although this point is discussed further in Chapter Three, it should be noted that the research described in this thesis is the first to investigate vegetation classifications based on the timing, intensity and duration of vegetation photosynthetic activity derived from multidate AVHRR NDVI imagery.

The insensitivity of the NDVI to vegetation cover type and the smallness of the spatial scale of AVHRR NDVI imagery together are, perhaps, the major reasons why relatively few attempts have been made to derive vegetation cover maps from multidate AVHRR NDVI data. However, there are other factors also which help to explain the relative neglect of these data for purposes of vegetation mapping. Thus, full resolution AVHRR NDVI imagery requires substantial preparation before it may be used[5]. In addition, full resolution AVHRR NDVI imagery is not available for all parts of the Earth's surface on a regular basis[6]. Similarly, although spatially-degraded AVHRR NDVI imagery requires less preprocessing than full resolution AVHRR data, <u>all</u> of the various types of spatially-degraded AVHRR NDVI imagery are produced using a spatial and temporal subsampling procedure that tends to make the NDVI values too high (Townshend and Justice 1986). Nevertheless, in spite of the shortcomings of the small scale NDVI imagery that is available currently (i.e. AVHRR NDVI imagery), the motivation to pursue this research stems from my belief that the full potential of small scale NDVI imagery has not yet been demonstrated or appreciated. This sentiment is supported by the interest expressed already in the *next* generation of medium resolution imaging radiometers for purposes of mapping and monitoring vegetation (e.g. Justice *et al.* 1987; Townshend and Justice 1988).

---

5 Preprocessing of full resolution AVHRR imagery is discussed in Chapter Four Section 1

6 Note, however, that the cost of installing a receiver for full resolution AVHRR imagery is relatively low (table 3)

4. Aims of this research

In 1982 Dr. Eric Barrett proposed a research project to evaluate AVHRR Global Vegetation Index imagery for purposes of mapping and monitoring vegetation. At that time, the AVHRR was regarded as a meteorological sensor primarily and research evaluating AVHRR NDVI data for phytogeographical purposes was a novel idea. However, soon after the start of this research it became apparent that the phytogeographical potential of small scale NDVI imagery was of interest to several other scientists, and that an evaluation of Global Vegetation Index imagery for purposes of mapping *and* monitoring vegetation was too broad an aim for a project with limited resources. Consequently, this evaluation of AVHRR NDVI imagery is limited to an assessment of its potential for purposes of vegetation *mapping* only.

This research has two fundamental aims. The first of these is to demonstrate the extent to which full resolution AVHRR imagery may be used to map physiognomic and agricultural vegetation cover classes. The study presented here in Chapter Four is based on eighteen full resolution AVHRR images of northeastern and southern Spain for the Spring and Summer months of 1985 and 1986. Use has not been made before of so many full resolution AVHRR NDVI images for purposes of mapping vegetation cover either in Spain (Gonzalez Alonso 1987, personal communication; GTT 1987) or elsewhere.

The second fundamental aim of this research is to demonstrate and explain, for the first time, maps of vegetation cover derived from multidate AVHRR NDVI imagery in which the classes are distinguished by the timing, intensity and duration of their period of photosynthetic activity. The study presented here evaluates this classificatory approach at the two extreme spatial scales of AVHRR data. The results for full resolution AVHRR imagery of Spain are discussed in Chapter Four, while those derived from a set of twenty-four Global Vegetation Index monthly images of Africa for the period January 1985 to December 1986 are discussed in Chapter Five.

In the course of pursuing these two, fundamental aims, three subsidiary aims emerged. The first of these is the identification of the most suitable map projection for purposes of displaying small scale radiometric imagery. The map projection to which all the AVHRR imagery used in this study has been mapped is the equal area radial projection (Tissot 1881; Peters 1967,1979,1982,1983). Although this construction has not been used before to display radiometric imagery, it is well-suited for this purpose since it provides a rectilinear graticule and a constant areal scale. A rectilinear graticule

offers practical advantages for both digital image processing (i.e. digital imagery is stored in linear arrays) and also general map usage (i.e. orientation is easier with a rectilinear graticule than with a curvilinear graticule). A constant areal scale means that all parts of the map are displayed in the same detail. Since raw NOAA AVHRR imagery has nominally uniform spatial resolution (Appendix 1), clearly, a map projection that retains all the spatial detail is preferable to one, such as the Mercator, that does not. Of course, there are many types of equal area projection. The particular attraction of the equal area radial construction over other equal area projections is its flexibility. The equal area radial projection can be tailored so as to minimise shape distortion in a specified area of interest. The illustrations in Chapters Four and Five demonstrate this flexibility. A detailed discussion of the merits of equal area radial projections for the purpose of mapping small scale radiometric data is presented in Appendix 2.

The second subsidiary aim is a quantitative assessment of the effect of temporal and spatial subsampling on the NDVI values of Global Vegetation Index imagery. Unrealistically high NDVI values in spatially-degraded AVHRR NDVI imagery have been observed by several workers (e.g. Justice 1986). However, no attempt to measure the distortion has been made, even though some indication of the degree to which spatially-degraded AVHRR NDVI values are exaggerated is essential if these data are to be interpreted with any accuracy. The results of a study comparing the NDVI values in full resolution AVHRR NDVI imagery, simulated Global Vegetation Index imagery (produced *without* drastic spatial subsampling) and Global Vegetation Index imagery are presented and discussed in Chapter Five.

The third subsidiary aim is the derivation of imagery from basic Global Vegetation Index data which describes the distribution of vegetated and unvegetated land for all parts of the globe. This aim arose from the interest expressed by Professor Doctor Arno Peters in the possibility of using Global Vegetation Index imagery to assist with the depiction of vegetation in the regional plates of his forthcoming world atlas, the *Peters Equality Atlas of the World*[7]. The imagery derived from Global Vegetation Index data that has been used to assist with the production of Peters' atlas is presented and discussed in Chapter Five.

---

7 Scheduled for publication (German edition) in March 1989

Chapter Two

Physical and Physiological Bases of the Normalised Difference Vegetation Index

1. Introduction

The spectral response of plants and vegetation canopies has been studied in both the shortwave and the longwave wavelengths of the electromagnetic spectrum. The shortwave response corresponds to the spectrum of solar irradiance at the Earth's surface (i.e. 0.4-2.5μm) and is measured using passive sensing instruments. The longwave response (i.e. >2.5μm) is measured using either passive or active sensing instruments (Colwell 1963,1983). Although photographic shortwave imagery is perhaps the most familiar type of radiometric data having been available for many years (Neblette 1927,1928; Ives 1939; Colwell 1956; Simonett 1983; Hoffer 1984; Curran 1985), during the last twenty years there has been a steady increase in the availability of both shortwave and longwave imagery produced by electro-optical imaging systems.

The superior spatial resolution of photographic imagery compared with that of electro-optical imagery is irrefutable. However, electro-optical systems offer three distinct advantages over photographic systems. Firstly, they are sensitive to a wider range of radiometric frequencies than photographic emulsions. Secondly, their sensitivity to incident radiation can be controlled within predetermined wavelengths more precisely than can photographic emulsions. Thirdly, they produce digital imagery. The image produced in a single waveband of an electro-optical imaging system is made up of rows and columns of picture elements, pixels, each of which contains a radiance value corresponding to the instantaneous field of view of the sensor (Slater 1980; Norwood and Lansing 1983). The quantitative format of shortwave imagery produced by electro-optical sensors makes these data ideally-suited to analysis using computer-aided techniques which can enhance the information contained in large volumes of raw radiometric data rapidly, objectively and dramatically (Swain and Davis 1978; Pratt 1978; Moik 1980; Schowengerdt 1983; Richards 1986; Lillesand and Kiefer 1987).

Preliminary studies using microwave data produced by the sensors onboard Seasat and the Nimbus satellites (e.g. Allen 1983; Choudhury *et al.* 1987; Choudhury and Tucker 1987a, 1987b; Choudhury 1987b; Tucker and Choudhury 1987; Becker and

Choudhury 1988) and also the data produced by air-borne sensors (e.g. Sader and Joyce 1985; Sieber 1985) suggest that the European Remote Sensing Satellite, due for launch in 1990 (Duchossois 1985), will produce useful data for phytogeographical purposes. However, even when microwave imagery is more widely available and suitable data types have been defined, shortwave imagery seems likely to remain more important for phytogeographical purposes. This is because vegetation shortwave response is controlled by the *internal* structure and physiology of the plants in a canopy whereas vegetation microwave response is controlled by the *external* form of a canopy including ephemeral environmental conditions such as wetness (Sieber 1985; Paris 1986).

This chapter describes why and how certain digital shortwave reflectance measurements may be combined to produce the Normalised Difference Vegetation Index.

2. Leaf spectral response to solar irradiance

2.1 Introduction

The solar irradiance arriving at a plant growing on the surface of the Earth is essentially the spectrum of a black body at around 6000 K modified by absorption and scattering processes. Absorption is due mainly to molecular gases in the atmosphere, especially ozone, oxygen, carbon dioxide and water vapour, while scattering is due mainly to aerosols and water droplets in the atmosphere. Atmospheric absorption restricts shortwave remote sensing of the surface, except through short atmospheric path lengths, to "windows" between the absorption wavebands (Smith and Morgan 1981; Horler and Barber 1981).

The interaction of solar irradiance with plant tissue is a complicated subject best approached with a specific purpose in mind (Fukshansky 1981). For purposes of satellite remote sensing of vegetation the fate of solar energy incident on a plant leaf, I, may be expressed in terms of reflectance, ρ, absorptance, α, and transmittance, τ

$$\text{i.e.} \qquad I = \rho + \alpha + \tau \qquad (1)$$

Although some solar irradiance is reflected at the leaf surface (Woolley 1971), by far the greater part passes through the cuticle to the epidermis, palisade cells, mesophyll cells and air cavities of the leaf interior.

The shortwave region of the spectrum may be divided into many separate wavebands for purposes of discriminating among plant types (e.g. Kumar and Silva 1977). However, physiologically and structurally, just three waveband regions of distinct spectral response may be identified. These are the visible, the near-infrared and the middle-infrared.

2.2 0.3-0.7μm (visible)

Plant spectral response in this waveband is complicated by the range of pigments which may be present. In addition to chlorophylls a and b, which are present in a number of spectral forms and which together comprise about 70% of all leaf pigments in a ratio of 3:1 (a:b), there are also carotenoids (accessory pigments in photosynthesis absorbing 0.4-0.5μm wavelengths) which comprise the bulk of remaining pigments, chlorophyll and carotenoid precursors, variable amounts of non-photosynthetic anthocyanin pigments, polyphenols and various secondary plant products. Typically, there is high absorption in this waveband with an absorption minimum at 0.55μm, the green part of the spectrum (Coblentz 1912; Shull 1929; Seybold and Weissweiller 1943; Rabideau *et al.* 1946; Billings and Morris 1951; Gates and Tantraporn 1952; Moss and Loomis 1952; Gates *et al.* 1965; Wong and Blevin 1967; Allen and Richardson 1968; Scott *et al.* 1969).

2.3 0.7-1.3μm (near-infrared)

There is only slight absorption of radiation in this waveband resulting in high reflection and transmission. The amount of radiation reflected and transmitted from a healthy leaf is approximately the same due to scattering processes within the leaf which randomise the direction of the radiation (Knipling 1970; Tucker and Garratt 1977). Scattering processes increase the path length of radiation through a leaf and thereby promote high absorption in the pigment and water absorbing wavebands.

The main cause of scattering within a leaf is refraction due to differences in the refractive indices of intercellular air space (1.0) and hydrated cellulose cell walls (1.4) (Willstäter and Stoll 1918; Mestre 1935; Gausman *et al.* 1970; Woolley 1971; Allen *et al.* 1973). Reflection due to the surface roughness of cell walls causes some additional scattering (Sinclair *et al.* 1973) as must certain cell structures such as lysosomes and macromolecules (e.g. proteins, lipids and carbohydrates) which can be smaller than 1μm and so cause Rayleigh and Mie scattering. Although hard to quantify (Kumar and Silva 1973), as much as 10% of the internal leaf scattering may be due to Rayleigh scattering (Tucker and Sellers 1986).

The parameter controlling the levels of reflectance and transmittance from a leaf is the number or total area of air-wall interfaces (Knipling 1970). As a result, the 0.7-1.3μm reflectance of dehydrating and senescing leaves may *increase* during the early stages of dehydration or senescence (Thomas *et al.* 1966; Knipling 1969) even though the leaf volume decreases. This is because microcavities remain between walls and the number of air-wall interfaces may actually increase as adjacent cells split apart and as the living cell contents shrink away from interior cell walls. In advanced stages of dehydration and senescence the 0.7-1.3μm reflectance decreases and transmission increases probably due to the breakdown of cell walls (Knipling 1970).

2.4 1.3-2.5μm (middle-infrared)

High absorption in this waveband is due to leaf water. There is an absorption minimum at 1.7μm (Curcio and Petty 1951; Allen and Richardson 1968; Gausman *et al.* 1970; Knipling 1970; Carlson *et al.* 1971).

3. Factors controlling vegetation canopy spectral response to solar irradiance

3.1 Introduction

The spectral response of vegetation canopies is more relevant to satellite image analysis than is the spectral response of green leaves. Unfortunately, although green leaves have a particularly distinctive reflectance spectrum it is not possible to extrapolate directly from hemispherical leaf reflectance measurements made in the laboratory to reflectance measurements of natural canopies made by satellite-borne sensors. A variety of factors besides the spectral response of the leaf itself alter qualitatively and quantitatively the radiance from a canopy measured by a satellite-borne sensor such as the NOAA-AVHRR (Knipling 1970; Colwell 1974; Horler and Barber 1981; Tucker and Sellers 1986).

Mathematical models have been developed to assist understanding of the interception, scattering and absorption of solar irradiance by various plant forms and plant structures within canopies (Milton and Wardley 1987). These may be realistic (e.g. Kubelka and Munk 1931; Suits 1972a; 1972b; Smith and Oliver 1974; Goudriaan 1977; Bunnik 1977; Chance 1977; Kimes 1984; Badhwar *et al.* 1985) or relatively simplistic (e.g. Meador and Weaver 1980; Dickinson 1983; Sellers 1985; Choudhury 1987a). In either case their principal purpose is to permit some control by the investigator of selected system variables thus allowing the effects of other system parameters to be monitored. These variables are described here under seven headings.

3.2 The spectral response of the vegetation target

The spectral response of different types of vegetation is a function of not only the constituent plant types but also their phenological stage and condition or "stress" (Wiegand and Richardson 1987; Steven and Demetriades-Shah 1987).

3.3 The spectral response of the background

All the components of an instantaneous field of view except vegetation are described as background. Background refers particularly to soil surfaces which can be highly variable (Bowers and Hanks 1965). If the ground coverage provided by a vegetation canopy is continuous the importance of background is minimal and the spectral response recorded for that area is dominated by the vegetation canopy. However, if the vegetation canopy is sparse or discontinuous then the spectral response of the background becomes an important part of the overall "canopy" response (Colwell 1974; Curran 1983; Ezra *et al.* 1984; Huete *et al.* 1984; Elvidge and Lyon 1985). Thus background influences the spectral response of many types of "cultural" vegetation since this is often planted in rows (Tucker and Miller 1977; Rao *et al.* 1979; Kollenkark *et al.* 1982a).

Vegetation indices have been developed which transform multispectral data in such a way as to reduce the influence of background reflectance (Kauth and Thomas 1976; Richardson and Wiegand 1977; Crist and Kauth 1986). Nevertheless, the soil spectral response within a study area should be known if high radiometric and spatial resolution data are being used (Huete *et al.* 1984,1985).

3.4 The spectral resolution of the sensor

Data from sensors with narrow bandwidths corresponding to specific absorption or reflection properties of plant canopies provide the best results for vegetation studies (Tucker and Maxwell 1976; Tucker 1978; Jackson 1983; Mack *et al.* 1984; Stevens and Demetriades-Shah 1987). Since satellite-borne sensors often have to satisfy a variety of different user requirements the spectral specifications of a sensor may represent a compromise that serves specific applications imperfectly (e.g. Barrett and Herschy 1986). For example, four different AVHRR sensors have been designed. The AVHRR aboard Tiros-N (AVHRR) was unsuitable for vegetation monitoring purposes due to an overlap between the red (channel 1) and the near-infrared (channel 2) wavebands. However, once the phytogeographical potential of AVHRR data was realised, the spectral response of channels 1 and 2 was changed and the spectral response curves on AVHRR/1, AVHRR/2 and AVHRR/3 do not overlap.

It is important to realise that "visible" and "near-infrared" are imprecise spectral labels. Price (1987a) has shown how vegetation index values for a target canopy calculated from calibrated "visible" and "near-infrared" reflectances measured by the Landsat Thematic Mapper, SPOT and the AVHRR are different. The difference is due partly to the slightly different bandwidths of the shortwave bands of each sensor and partly to calibration errors. Although Jackson (1983) demonstrated that AVHRR/1 and AVHRR/2 channel 1 and channel 2 data are less sensitive to vegetation than the shortwave channels of the sensors aboard Landsat and SPOT, Gallo *et al.* (1987) suggest that for practical purposes the inferior sensitivity of AVHRR shortwave data does not reduce significantly the extent to which these data may be used to estimate agronomic variables.

Several changes are planned for AVHRR/3 which will enhance the phytogeographical value of AVHRR data. These changes are described in Appendix 1.

3.5 The radiometric accuracy of the sensor

Radiometric accuracy is a feature of satellite remotely-sensed data that has become increasingly important as the number of different sensors producing radiometric data suitable for vegetation studies has increased (Price 1987b, 1987c). Although radiometric imagery may be calibrated to *relative* radiance scales using only radiance values within the image(s) to be calibrated (e.g. Ahern *et al.* 1987), the fundamental approach to radiometric calibration involves calibration to an *absolute* scale. Currently, AVHRR shortwave data are calibrated in this way only before the satellite is launched. There is no inflight correction. Consequently AVHRR imagery made at different times may not be compatible, although preliminary results from investigations into the calibration accuracy of AVHRRs suggest that inter- and intra-sensor variations in the calibration accuracy of the AVHRR do not affect significantly phytogeographical applications of AVHRR data (Tucker 1986).

3.6 The instantaneous field of view of the sensor

The instantaneous field of view is one measure of the maximum spatial resolving power of a sensor (Townshend 1981; Townshend and Justice 1981). It is determined by the size and shape of the aperture and the sensor scan angle (Slater 1980; Norwood and Lansing 1983). The radiance recorded for a particular instantaneous field of view represents an areal integration of the radiance of everything "seen" by the sensor at that point in the scan line. Clearly, as the size of the instantaneous field of view increases so too does the likelihood that the spectral response recorded will be the

area-integrated response from a *heterogeneous* surface including different plant species and a variety of non-vegetation components such as soil, shadow and cloud (Duggin *et al.* 1982b,1984; Townshend and Justice 1988).

The geometric characteristics of AVHRR data are described in Appendix 1.

3.7 The viewing and illumination geometry

The viewing and illumination geometry are determined by the solar zenith angle, the look zenith angle and the look azimuth angle which are themselves dependent upon the latitude and longitude of the target, the time of year and day and the scan angle. Variations in the viewing and illumination geometry greatly influence the radiance value recorded by a satellite-borne sensor, particularly sensors with wide scan angles such as the AVHRR. This has been amply demonstrated by ground measurements (e.g. Egbert and Ulaby 1972; Kollenkark *et al.* 1982b), digital analyses of actual and simulated satellite multispectral scanner imagery (e.g. Duggin *et al.* 1982a; Holben and Fraser 1984; Taylor *et al.* 1985; Holben *et al.* 1986; Blümel and Tonn 1986) and modelling studies (e.g. Suits and Safir 1972; Kimes and Kirchener 1982).

The importance of variations in recorded radiance due to variations in viewing and illumination geometry are least when the sun is high in the sky and the measurements are made near nadir. Consequently, one method of obtaining NDVI imagery relatively free of distortions due to viewing and illumination angle involves using only data recorded at low scan angles at midday. For example, Duggin *et al.* (1982a) and Tucker *et al.* (1983) use a ±20° off-nadir limit. Although this method is attractively simple it reduces drastically the amount of usable imagery. Consequently, corrections have been devised for the systematic errors in radiance values introduced by variations in viewing and illumination geometry (e.g. Duggin and Schoch 1984; Holben and Fraser 1984; Duggin 1985; Taylor *et al.* 1985; Blümel and Tonn 1986; Singh 1987b). These corrections are especially necessary for studies involving intercomparison between AVHRR images made at different times of day and year.

3.8 Atmospheric conditions

The reduction in vegetation canopy radiance measured by a satellite-borne sensor due to attenuation as a result of Rayleigh, Mie and non-selective scattering and absorption by molecular gases in the atmosphere is largely random and unpredictable. This is because the turbidity and the aerosol and water content of the atmosphere are constantly changing. However, atmospheric attenuation of solar irradiance and reflected radiance generally increases with optical path length (Smith and Morgan 1981; Horler

and Barber 1981; Duggin and Schoch 1984; Fraser and Kaufman 1985). Consequently, quantitative methods to predict atmospheric attenuation and adjust recorded radiance values accordingly have been devised (e.g. Duggin and Piwinski 1984; Lagouarde and Kerr 1986) although their reliability is not easily tested.

4. Shortwave vegetation indices

4.1 Introduction

Multispectral data provided by electro-optical imaging sensors have been widely used for phytogeographical purposes (e.g. Maxwell 1976; Bauer *et al.* 1979; Talbot and Markon 1986; Lacaze and Joffre 1987; Belward and Hoyos 1987; Donoghue and Shennan 1987). They have also been used to make one-dimensional indices. A good radiometric index has two important advantages over the multispectral data from which it is derived. Firstly, it is easy to interpret since, ideally, it contains only the information contained in the original multispectral data that is relevant to the study in hand. Secondly, it provides imagery that is relatively cheap and easy to handle once transformation of the raw multispectral data has been performed.

A vegetation index is a one-dimensional numerical scale derived from multispectral radiance data whose sensitivity to variations in vegetation type and condition is a function of the wavelength intervals used (Jackson 1983; Mack *et al.* 1984) and the mathematical transformations performed on the raw data (Perry and Lautenschlager 1984; Crist and Kauth 1986). A large number of shortwave vegetation indices have been proposed based on ratios and differences of bands, principal component analysis and other linear combinations of multispectral data. Some of these indices are computationally-complex. For example, The Tasselled Cap transformation (Kauth and Thomas 1976; Crist and Cicone 1984) uses the Gram-Schmidt sequential orthogonalisation procedure in order to find the desired data structures inherent to a particular sensor and set of scene classes and to adjust the viewing perspective such that these structures can be most easily and completely observed (Crist and Kauth 1986). Other indices based on waveband ratios and differences between wavebands, are relatively simple (Jordan 1969; Tucker 1979; Jackson *et al.* 1983; Perry and Lautenschlager 1984). Several shortwave vegetation indices are *functionally-equivalent*, that is, decisions made on the basis of one index could have been made equally well on the basis of one of several others (Perry and Lautenschlager 1984).

4.2 The Normalised Difference Vegetation Index

The Normalised Difference Vegetation Index (NDVI) is calculated as

$$NDVI = (NIR - R)/(NIR + R) \quad (2)$$

where **NIR** and **R** are the radiances from the near-infrared and the red regions of the electromagnetic spectrum respectively (Rouse *et al.* 1973,1974). Figure 1 illustrates how the NDVI simplifies the two-dimensional red/near-infrared feature space. While it is possible to re-introduce to NDVI data some of the information that is lost as a result of the normalisation transformation (e.g. Ambroziak's (1984) Colour Co-ordinate System), most users of NDVI imagery have preferred to keep the index's simplicity and exploit instead the information contained in multitemporal NDVI data.

Figure 1. The Red/Near-Infrared Feature Space Showing Lines of Equal NDVI.

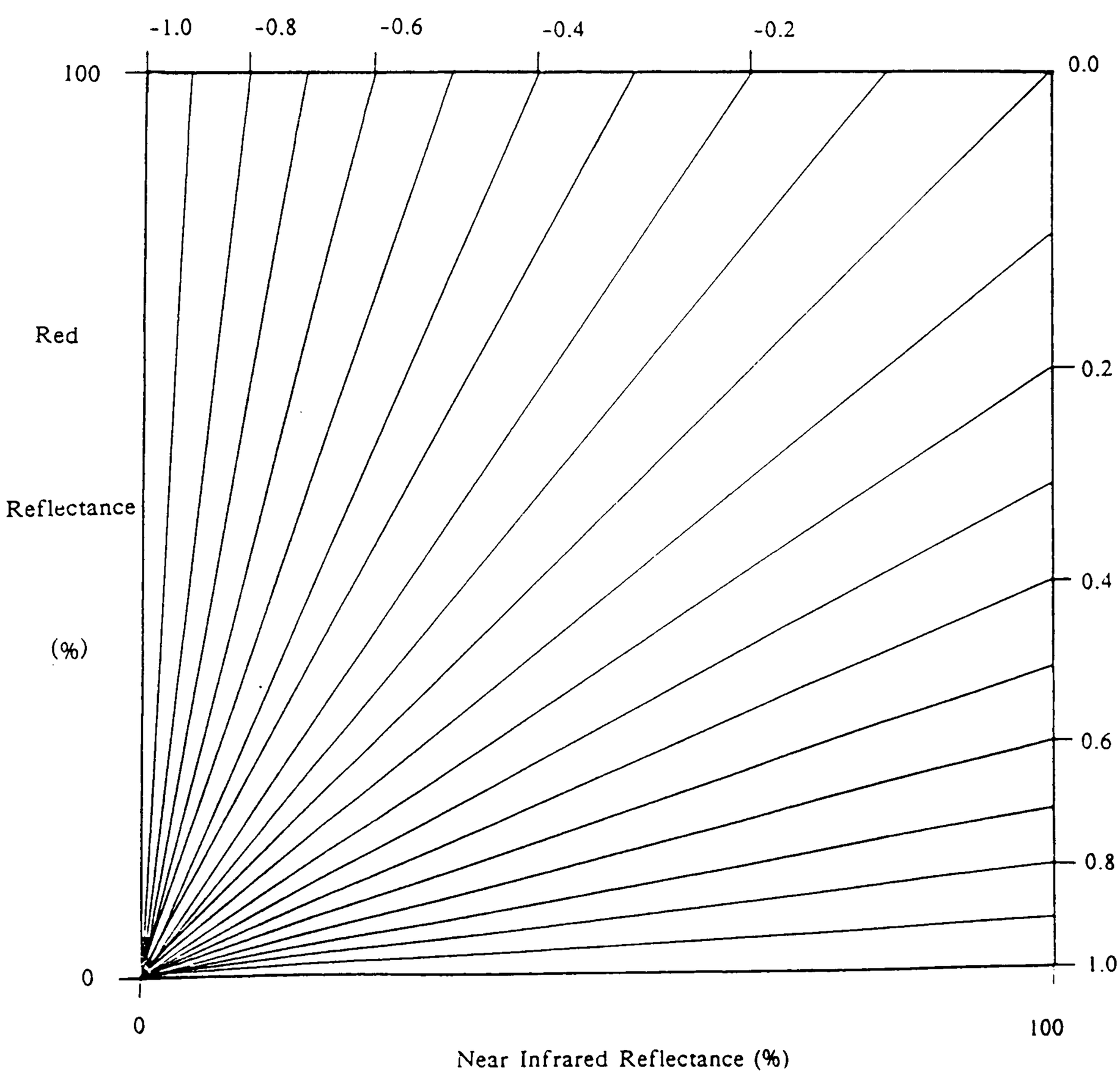

The NDVI and other functionally-equivalent indices provide a measure of the amount of solar irradiance absorbed by leaf pigments[1] intercepted by vegetation canopies (Kumar and Monteith 1981; Hipps *et al.* 1983; Daughtry *et al.* 1983; Hatfield *et al.* 1984; Asrar *et al.* 1984; Gallo *et al.* 1985; Sellers 1985; Tucker and Sellers 1986; Steven and Demetriades-Shah 1987), the percentage vegetation cover (Celis-Ceusters 1980; Steven *et al.* 1986; Steven and Demetriades-Shah 1987) and the chlorophyll density (Curran and Milton 1983; Steven 1983; Steven and Demetriades-Shah 1987). In each case the relation between the NDVI and the biophysical variable is approximately linear, with correlation coefficients as high as 0.98 (absorbed solar irradiance), 0.98 (chlorophyll density) and 0.96 (percentage vegetation cover). In each case also the strength of the relation weakens as the proportion of yellow leaves in the canopy increases and also as the canopy suffers increasingly from drought stress. Thus, green, photosynthesising vegetation has positive NDVI values whereas snow, water and ice usually have negative NDVI values due to their reflectance being higher in the red waveband than in the near-infrared waveband. Soils and rock usually have NDVI values around zero because their reflectance is similar in both wavebands.

The magnitude of many shortwave indices is greatly influenced by day-to-day variations in atmospheric absorption of solar irradiance and also the viewing and illumination geometry. In such circumstances meaningful comparisons between images made on different days and images made at different times of year cannot be made without first correcting the data. A particularly attractive feature of the NDVI is that normalisation partially compensates for all these variations. Differential absorption by the atmosphere of red and near-infrared radiation is not usually noticeable under daylight conditions at mid- and low-latitudes and variations which affect the red and the near-infrared wavelengths equally do not affect the normalised difference vegetation index values (Wardley 1984; Holben *et al.* 1986; Gallo *et al.* 1987)[2].

A further attraction of the NDVI is that the quality of NDVI imagery may be improved simply using a technique called maximum NDVI value compositing. This technique involves the retention at each array location of the highest NDVI value to occur at that pixel during a selected time period (Justus 1985; Holben 1986; Gutman 1987). Maximum NDVI value compositing is based on the fact that high positive NDVI

---

1 i.e. photosynthetically-active radiation

2 Differential absorption by the atmosphere of red and near-infrared radiation under conditions of low illumination have a marked deleterious effect on NDVI values. For example, the "terminator" is an area of spuriously high NDVI values visible at high latitudes on Global Vegetation Index imagery which occurs because of a combination of low winter sun illumination levels and differences in the atmospheric tranmissivities of red and near-infrared radiation (i.e. the atmosphere absorbs more red than near-infrared radiation) (Justice et al. 1985)

values are caused only by vegetation. Thus, it is assumed that the highest NDVI value recorded for a particular location in a given time period will be also the most accurate value and that lower NDVI values occur either because of atmospheric scattering due to aerosols and clouds or because the NDVI value is calculated from red and near-infrared values measured at high scan angles. This technique presents the image analyst with a choice between temporal precision and image quality. If the compositing period is too long, important changes in the NDVI value of the vegetation target will be missed. Conversely, if the compositing period is too short an unacceptably high proportion of the data may be cloud contaminated (Duggin *et al.* 1982b,1984).

4.3 Estimating net primary productivity

Monteith (1977) proposed that the rate of growth of many plants, at least during vegetative development, is almost proportional to the rate at which radiant energy is intercepted by the foliage and that net primary productivity, **dw/dt**, defined as the rate of increase with time **t** of phytomass **w** per unit area of ground, may be calculated using the relation

$$dw/dt = \epsilon \cdot f \cdot S \qquad (3)$$

In this relation, **S** is the total solar irradiance incident on the canopy, ϵ, is the net efficiency of conversion of absorbed photosynthetically active radiation into phytomass and f is the fraction of incident solar radiation absorbed by a vegetation canopy.

For a variety of healthy, unstressed arable and orchard crops in Britain ϵ is almost constant (Monteith 1977). Therefore the primary control on net primary productivity is f. Since f is highly correlated to various shortwave vegetation indices, time-integrated shortwave vegetation index data have been used widely to estimate net primary production (i.e. kg ha^{-1}) (MacDonald and Hall 1980; Tucker *et al.* 1981,1983,1985b,1986b; Aase and Siddoway 1981; Pinter *et al.* 1981; Hatfield 1983; Kamat *et al.* 1983; Barnett and Thompson 1983; Steven *et al.* 1983; Hatfield 1983; Bauer 1984; Goward *et al.* 1985; Asrar *et al.* 1985; Taylor *et al.* 1985; Hogg 1986; Taylor *et al.* 1986; Wiegand *et al.* 1986; Justice and Hiernaux 1986; Hiernaux and Justice 1986; Hielkema *et al.* 1986; Prince and Astle 1986; Prince and Tucker 1986). This "spectral components" approach to shortwave vegetation index interpretation (Wiegand and Richardson 1987) has now superseded approaches which sought to establish direct relationships between shortwave vegetation indices and canopy variables such as leaf phytomass (Tucker 1979; Kimes *et al.* 1981), leaf area index (Wiegand *et*

al. 1979; Holben *et al.* 1980; Curran 1981,1982,1983), and total canopy phytomass (Tucker 1980; Curran 1983).

The relation between time-integrated vegetation index data and net primary production has been investigated principally for rangeland and agricultural vegetation cover types. Work by Steven and Demetriades-Shah (1987) using high resolution radiometric data of agricultural crops suggests that reductions in the value of ϵ during periods of stress may not always be accompanied by reductions in canopy chlorophyll concentration and that, conversely, reductions in the value of f may not always be accompanied by reductions in ϵ. Consequently spectral indices which can separate the effects of leaf cover from leaf colour on the reflected radiance from a vegetation canopy will probably give a more reliable estimation of net primary productivity than the NDVI and functionally equivalent vegetation indices. A vegetation index based on the ratio of vegetation canopy reflectance at 0.8μm and 0.974μm has shown promise in this respect[3].

Investigations into the relation between time-integrated vegetation index data and net primary production using both large and small scale data produced by satellite-borne sensors suggest that the relation is quite weak in areas of low productivity and that an alternative approach relating the maximum NDVI value during the growing season to net primary production may be more successful (e.g. Tucker *et al.* 1985b; Hiernaux and Justice 1986). It would also appear that the relationship changes when the canopy comprises a significant woody fraction (Prince and Tucker 1986).

Alternative approaches to the use of multidate NDVI imagery for the prediction of net primary productivity, particularly the net productivity of cereal crops, use the satellite data to identify the time of heading[4]. Since heading is the time in a crop's growth cycle when NDVI values are highest, it may be estimated with reasonable accuracy from multidate NDVI imagery (Gallo and Flesch 1987). The basis for this approach is the fact that weather conditions at heading are critical to the grain yield of cereal crops (Claassen and Shaw 1970). Indeed, Comte *et al.* (1988) have demonstrated that reasonably accurate estimates of the yield of sorghum and millet in Burkina Faso may be obtained using a model which relates final yield *directly* to NDVI values at the time of heading.

---

3 N.B. Currently, satellite imagery in these wavebands is not available

4 i.e. the moment when plant growth shifts from the vegetative to the reproductive phase

An improvement in the accuracy and precision of estimates of net primary production and related biophysical variables from shortwave vegetation index imagery is one of the primary research goals of the Surface Radiation and Biology Group of the First International Satellite Land Surface Climatology Project Field Experiment (FIFE) (Sellers and Hall 1987).

4.4 Estimating the duration of the growing season

The growing season is a period of active vegetative growth. The duration of the growing season may be estimated phytophenologically as the difference between the mean date of leaf coloration (i.e. senescence) and leaf emergence of indicator species (e.g. Reader *et al.* 1974). Alternatively, it may be estimated climatologically as the period during which soil moisture from precipitation is freely available to vegetation cover and the air temperature is high enough to permit normal physiological activity. Thus FAO (1984) defines the growing season as the period when rainfall is greater than half the rate of potential evapotranspiration. A third method of expressing the duration of the growing season is in terms of the number of daylight hours per year (Leith 1974b).

Henrickson and Durkin (1986) demonstrated that estimates of the start and end of the growing season made using climatological data and estimates based on the rate of change of multidate NDVI values were very highly correlated. They found that a climatologically-defined growing season was unlikely to occur if the (AVHRR Global Area Coverage) NDVI value was below 0.10 NDVI. This is a similar value to the maximum (AVHRR Global Area Coverage) NDVI value reported by Justice *et al.* (1986) for Kenyan bushland in the period immediately before the growing season.

4.5 Estimating the timing of the growing season

The growing season is a period of time not a specific date. Nevertheless, it is useful to assign a date to photosynthetic activity for purposes of vegetation cover classification. A variety of dates are possible although the ones that may be defined most reliably using multidate NDVI data are probably the time of maximum photosynthetic activity (i.e. the maximum NDVI recorded during the growing season) and the start of the growing season (i.e. the date when the NDVI rises above a threshold "no-growth" NDVI value (Henrickson and Durkin 1986)).

4.6 Phytophenological variables

Phenology is the study of the timing of recurring biological events, the causes of their timing with regard to biotic and abiotic forces, and the interrelation among

phases of the same or different species (Leith 1974b). Thus plant phenological studies are concerned with the influence of seasonally varying environmental conditions such as daylength, air temperature and water availability on the timing of plant development stages, or phenophases, including germination, flowering and senescence (Flint 1974). Although phytophenological observations are usually made by a network of observers on the ground (Hopp 1974; Caprio *et al.* 1974), analysis of multidate shortwave vegetation index imagery has shown the sensitivity of these data to phenological variations in the timing, intensity and duration of photosynthetic activity (e.g. Rouse *et al.* 1973,1974; Badhwar 1980; Badhwar and Henderson 1981; Henderson and Badhwar 1984; Justice *et al.* 1985; Goward *et al.* 1985,1987; Townshend *et al.* 1985; Malingreau 1986; Townshend and Justice 1986; Lloyd 1988).

The time-integrated NDVI, the maximum NDVI to occur within a selected time period, the timing of the maximum NDVI and the period of time for which the NDVI at any particular pixel has exceeded 0.099 NDVI are called phytophenological variables in this study. This description implies that these variables describe attributes of vegetation photosynthetic activity that vary from year to year due primarily to the seasons. Of course, a variety of factors unrelated to phenology also affect the numerical values of these variables at any particular location. These other factors include changes in landuse, changes in farming practices, the precise dates of the imagery used to make the phytophenological variables and the quality of the imagery used to make the phytophenological variables. Generally, however, it seems reasonable to suppose that these other factors assume less and less importance compared with phenological factors as the spatial scale of the data decreases.

Chapter Three

The Definition of Vegetation Cover Classes For Use With Multidate AVHRR NDVI Imagery

1. Introduction

The synoptic coverage, temporal frequency and cheapness of multidate AVHRR imagery[1] are compelling reasons to use multidate AVHRR NDVI imagery to map vegetation. Surprisingly, however, the nature of vegetation cover classes that may be mapped using multidate AVHRR NDVI imagery has received little attention. Just three studies, by Norwine and Greegor (1983), Tucker *et al.* (1985a) and Townshend *et al.* (1987), have investigated the extent to which multidate AVHRR NDVI data may be used to map comprehensively the vegetation cover of large areas. Furthermore, although these three studies provide interesting information relating to the potential of certain multidate AVHRR NDVI data to map physiognomic and agricultural vegetation cover classes, they provide incomplete evaluations of the phytogeographical potential of AVHRR NDVI data for purposes of mapping vegetation since they do not investigate the potential of AVHRR NDVI data to map *phytophenology*[2] and they do not evaluate fully the potential of full resolution AVHRR NDVI data[3].

This chapter describes the problems associated with the use of both full resolution AVHRR NDVI data and Global Vegetation Index data to map phenological, physiognomic and agricultural vegetation cover classes. Section 2 describes an original phytophenological approach to vegetation cover classification for use with both full and spatially degraded AVHRR NDVI data. Section 3 explains the limitations of AVHRR NDVI data for purposes of mapping physiognomic and agricultural vegetation cover classes and presents a physiognomic and agricultural vegetation cover classification for use with multidate full resolution AVHRR NDVI imagery of Spain that was devised with these limitations in mind.

---

1 Described in tables 1, 2, 3

2 A map of the length of the growing season in an area of bushland in Kenya derived from AVHRR Global Area Coverage data produced by Justice et al. (1986) is the only example of phytophenological mapping using multidate NDVI data (see Chapter Two Section 4.4)

3 Norwine and Greegor (1983) used full resolution AVHRR images recorded on just three separate dates. Both Tucker et al. (1985a) and Townshend et al. (1987) used Global Vegetation Index imagery

2. Phytophenological mapping using AVHRR NDVI imagery

Multidate NDVI data record primarily temporal and spatial variations in the intensity of photosynthetic activity. Four phytophenological variables were defined in Chapter Two Section 4.6. Imagery of *time-integrated NDVI* shows spatial variations in vegetation net primary production, imagery of *the maximum NDVI to occur within a selected time period* shows spatial variations in the maximum intensity of photosynthetic activity, imagery of *the timing of the maximum NDVI* shows spatial variations in the timing of the maximum intensity of photosynthetic activity and imagery of *the period of time for which the NDVI has exceeded 0.099 NDVI* shows spatial variations in the length of the period of active vegetative growth. While it is true that the interpretation of time-integrated NDVI values in terms of kilograms of phytomass per hectare, and the accuracy of the 0.099 NDVI threshold for purposes of defining active vegetative growth, require further study, nevertheless, the research reviewed in Chapter Two indicates that, qualitatively at least, imagery of the phytophenological variables provides valid, spatially-comprehensive information with which to map vegetation classes defined by the timing, intensity and duration of their photosynthetic activity.

Imagery of the four phytophenological variables may be derived from both full resolution AVHRR NDVI data and spatially-degraded AVHRR NDVI data. Imagery of each of these variables is of interest in its own right. For example, time-integrated NDVI imagery has been used to assist with the depiction of vegetation in the plates of a major new world atlas[4]. In addition, the information provided by the phytophenological variables may be integrated into a single classification scheme using a supervised binary decision tree classifier. This classifier, which is simple, flexible and computationally-efficient (Swain and Hauska 1977; Qing-Yun and Fu 1983; Belward and Hoyos 1987), is used in this study to produce vegetation maps from imagery of the timing of maximum NDVI, the duration above 0.099 NDVI and the mean daily NDVI[5].

Supervised binary decision tree classifiers are used in this study to classify both full resolution AVHRR NDVI data (of Spain) and Global Vegetation Index data (of Africa). The classifiers that are used for these data are shown in figure 2. In each case the classes are distinguished by the timing, intensity and duration of their period of

---

4 Described in Chapter Five Section 5.2

5 The time-integrated NDVI value divided by the number of days in the time period gives the mean daily NDVI

Figure 2. Supervised Binary Decision Tree Classifiers.
A) Northeastern Spain, B) Southern Spain, C) Africa

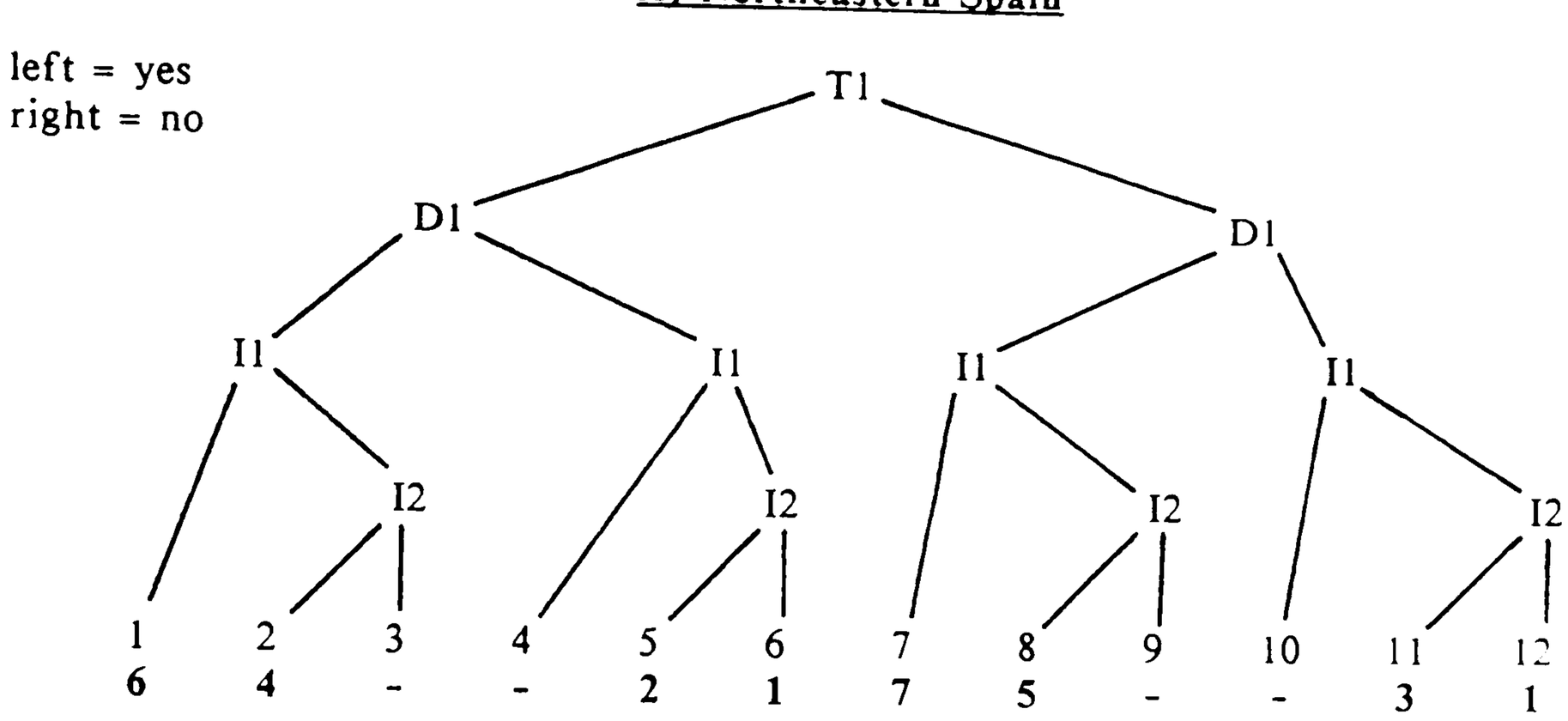

T1, T2 and T3 represent the timing of maximum NDVI
D1 and D2 represent the duration above 0.099 NDVI
I1, I2 and I3 represent the mean daily NDVI
Numbers in **bold** type face correspond to the classes in figures 10 and 11

T1 (Northeastern Spain, 1986): 27th March, 15th May
T1 (Southern Spain, 1985): 2nd April
T2 (Northeastern Spain, 1986): 16th July, 2nd and 27th August, 28th September
T2 (Southern Spain, 1985): 3rd May
T3 (Southern Spain, 1985): 5th and 24th July, 25th August, 3rd October
D1 (Northeastern and southern Spain): 4-6 dates
D2 (Northeastern and southern Spain): < 4 dates
I1 (Northeastern and southern Spain): > 0.199 NDVI
I2 (Northeastern and southern Spain): 0.1-0.199 NDVI
I3 (Northeastern and southern Spain): < 0.1 NDVI

C) Africa

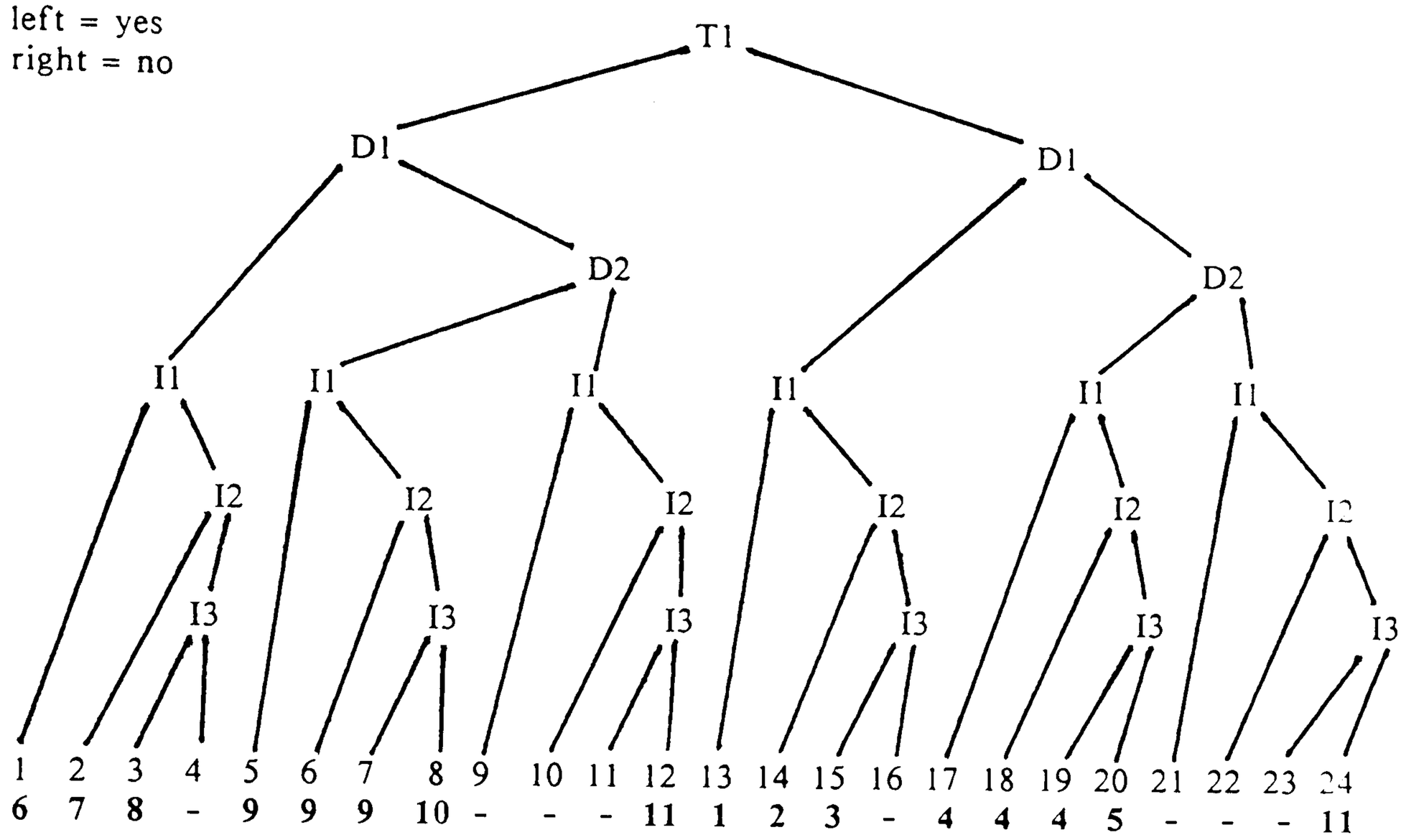

T1 and T2 represent the timing of maximum NDVI
D1, D2 and D3 represent the duration above 0.099 NDVI
I1, I2, I3 and I4 represent the mean daily NDVI
Numbers in **bold** type face correspond to the classes in figure 19

T1 is November to April
T2 is May to October
D1 is greater than eight months
D2 is one to eight months
D3 is no months
I1 is greater than 0.27 NDVI
I2 is 0.2-0.269 NDVI
I3 is 0.1-0.199 NDVI
I4 is less than 0.1 NDVI

photosynthetic activity. It is important to realise that although the phenological characteristics of the classes produced by these classifiers are constant form year to year, the *pattern* of phytophenological vegetation classes produced by this approach will vary from year to year because the precise timing, intensity and duration of photosynthetic activity at a particular location is governed by environmental conditions which vary interannually: Seasonality[6] is expressed in terms of probability.

A supervised binary decision tree classification of phytophenological variables has not been tried before. Although the classified images produced by this approach

6 i.e. the occurrence of certain biotic and abiotic events within a definite limited period or periods of the solar year (Leith 1974)

are discussed in Chapter Four (Spain) and Chapter Five (Africa), it is worth noting at this stage that the threshold values at the non-terminal nodes of the decision trees were chosen on the basis of interactive image inspection with a view to bringing out the major phytophenological patterns contained in the multidate NDVI data. Thus, although the extent to which these expressly phenological classes correspond with physiognomic and agricultural classes *is* assessed for the full resolution AVHRR NDVI imagery of Spain, it must be stressed that a poor correspondence should be interpreted not only as an indication that the particular physiognomic or agricultural vegetation cover class in question may not occupy discrete parts of the multidate NDVI feature space but also as a measure of the originality of the phytophenological classification.

3. Physiognomic and agricultural vegetation cover mapping using AVHRR NDVI imagery

3.1 Review

NDVI values are largely independent of vegetation cover floristic composition or physiognomy (Steven 1987). However, insofar as physiognomic and agricultural vegetation cover classes have distinctive phenological characteristics, it should be possible to use multidate NDVI imagery to map physiognomic and agricultural vegetation cover classes. Although physiognomic and agricultural vegetation cover mapping has been performed successfully using large scale shortwave vegetation index data (e.g. Steiner 1969; Hall and Badhwar 1987), very few studies have investigated the potential of AVHRR NDVI imagery in this respect (e.g. Norwine and Greegor 1983; Tucker *et al.* 1985a; Townshend *et al.* 1987).

The nature of physiognomic and agricultural vegetation classes that may be mapped using Global Vegetation Index imagery has been investigated by Tucker *et al.* (1985a) and Townshend *et al.* (1987). The study by Tucker *et al.* (1985a) includes a vegetation map derived from eight, twenty-one-day maximum NDVI value composite images between April 1982 and February 1983 which purports to show the distribution of desert, semi-arid seasonal grasslands, dry savannas, wet savannas and tropical forest in Africa. The study by Townshend *et al.* (1987) aimed to assess the extent to which three classificatory approaches, applied to thirteen, twenty-eight-day maximum (Global Vegetation Index) NDVI value composite images of South America[7], are able to reproduce the patterns of vegetation cover found in small scale physiognomically-based vegetation maps. In both of these studies, the classifications of the multidate NDVI

7 The imagery in this study is undated

data were produced and verified using training areas[8] of physiognomic and agricultural vegetation cover classes which were chosen using cartographic sources supplemented by field observations.

The studies by Tucker *et al.* (1985a) and Townshend *et al.* (1987) provide tantalising evidence of the potential of very small scale multidate NDVI imagery for purposes of mapping vegetation. However, the use of Global Vegetation Index data in both studies to map physiognomic and agricultural vegetation cover classes is surprising. Global Vegetation Index data are extremely small scale (i.e. a single pixel represents an area of at least 12 800 hectares), they are the product of an unrepresentative spatial and temporal subsampling process which tends to make all Global Vegetation Index values unrealistically high, and they have poor geodetic registration accuracy[9]. Consequently, it seems unwise to place too much confidence in interpretations of Global Vegetation Index NDVI data which stray too far from their primary, phytophenological meaning.

Full resolution multidate AVHRR NDVI data are far more promising data with which to produce physiognomic and agricultural vegetation maps than the Global Vegetation Index. A full resolution AVHRR pixel covers an area between 121 and 1750 hectares (i.e. 1.1x1.1km and 2.5x7.0km, see table 30). Although the spatial resolving power of these data will be reduced due to geodetic misregistration[10], clearly they are substantially larger scale than Global Vegetation Index data. In addition, full resolution AVHRR data are not the product of either spatial or temporal subsampling.

The nature and accuracy of landcover classifications that are produced using full resolution AVHRR data have been investigated primarily with reference to Landsat Multispectral Scanner data (Townshend and Tucker 1981,1983; Ormsby 1982; Hayes and Cracknell 1984a,1985; Gervin *et al.* 1985; Prince and Tucker 1986). In these studies, Landsat Multispectral Scanner and AVHRR data are co-registered and the relationship between the two data types is measured. One method of assessing AVHRR landcover classification accuracy uses an averaged Multispectral Scanner response derived for each AVHRR pixel to establish the extent to which the AVHRR data represent the areally-integrated response of the Multispectral Scanner data. Very high correlations have been found using this approach (e.g. 0.96 (Hayes and Cracknell 1984a)) suggesting that the AVHRR pixel value does indeed represent the areally

---

8 Training areas are discussed in Section 3.2

9 The characteristics of Global Vegetation Index are described in Appendix 1 and discussed in Chapter Five

10 Geodetic registration of full resolution AVHRR data is discussed in Chapter Four Section 1

integrated response of the Multispectral Scanner data. A second method of assessing AVHRR landcover classification accuracy involves the determination of an AVHRR value for each Multispectral Scanner pixel in order to establish how well the AVHRR data record the spatial variability of the ground surface as represented by the Multispectral Scanner data. Inevitably the correlation coefficients between the two types of data from this approach are lower (e.g. 0.76 (Hayes and Cracknell 1984a)) because the broad instantaneous field of view of the AVHRR produces a general smoothing of the surface.

Comparative studies of AVHRR and Multispectral Scanner data provide a valuable indication of the spatial and spectral detail contained in AVHRR imagery. The results of these comparative studies are also much easier to interpret than classified AVHRR imagery on its own. Perhaps for this reason, very few attempts have been made to classify multidate full resolution AVHRR NDVI imagery *without* reference to Multispectral Scanner data, or other collateral data types. For example, although Norwine and Greegor (1983) describe a very rare example of a study to map a wide variety of vegetation cover classes using multidate full resolution AVHRR NDVI data, their approach involved a climatological moisture variable in addition to the satellite data.

3.2 Methodology

A variety of classification methods have been proposed for the production of physiognomic and agricultural vegetation maps from AVHRR NDVI imagery (Townshend *et al.* 1986). The classification techniques used in this study to reduce multidimensional (i.e. multidate) full resolution AVHRR NDVI imagery to a single band image of discrete classes are cluster analysis, a supervised binary decision tree classifier and a minimum distance classifier.

The cluster analysis algorithm used in this study, "*Cluster*" (IIS 1984), is an unsupervised classification technique whereas the supervised binary decision tree[11] and the minimum distance classifier, "*Classify*" (IIS 1984), are supervised classification techniques (Swain and Davis 1978; Schowengerdt 1983; Lillesand and Kiefer 1987). The essential difference between supervised and unsupervised classifiers is that supervised classifiers permit the image analyst to impose his or her knowledge of the area on the

11 Described in Section 2

analysis whereas unsupervised classifiers are designed to determine the inherent structure of the data, unconstrained by external knowledge about the area[12].

Classify is one of several supervised classifiers which compare the multidimensional radiometric characteristics of an unknown pixel against a set of training statistics. The training statistics for each class in a classification scheme are derived from pixels corresponding exclusively to that class. These pixels are located in a training area which is defined as an homogeneous sample of a particular class that contains within it the full range of variability for that class (Schowengerdt 1983)[13]. *Classify* assigns an unknown pixel to the class whose training statistics it resembles most. If an unknown pixel does not correspond closely to any of the classes defined by the image analyst it may be "unclassified". The threshold value used in this study to mark the boundary between classified and unclassified pixels is one standard deviation from the training class means (i.e. the default value for *Classify*).

Ideally, the results of supervised and unsupervised classifications should be similar, since this would imply that the classes of interest to the image analyst occupied discrete areas of the multidimensional feature space. However, generally, the patterns of classes produced by supervised and unsupervised classifiers are not the same. The reason for this is that, generally, image analysts attempt to map classes that are related only indirectly to the factors controlling the digital values in radiometric imagery (Steven 1987).

3.3 The definition of physiognomic and agricultural classes

There are two preconditions for successful classification of multidimensional data according to a particular classification scheme. The first is that the classes occupy discrete parts of the multidimensional feature space and the second is that the majority of the pixels in the data correspond with areas that are covered by just one of these classes. The main problem associated with the definition of physiognomic and agricultural vegetation classes for use with AVHRR NDVI imagery is "mixed" pixels. For purposes of this study a mixed pixel may be defined as an area on the ground, with dimensions the same as those of the instantaneous field of view of the sensor, for

---

12 Note, however, that, in common with most unsupervised classifiers, there is some supervision by the image analyst of "Cluster". Thus "Cluster" requires the analyst to specify the number of iterations, the improvement threshold, the total number of classes to be found and the threshold beyond which a pixel no longer belongs to one class. The values that were used for each of these options in this study were sixteen, default value, sixteen and default value respectively

13 The training areas used in this study are described in detail in Section 3.5.

which the NDVI value is determined by two or more contrasting vegetation cover classes.

There are two distinct causes of mixed pixels in the context of physiognomic and agricultural vegetation cover mapping using AVHRR NDVI data. The first is the fundamental "mixedness" of physiognomic and agricultural vegetation cover classes in terms of their NDVI response and the second is the spatial scale of the data. Although many physiognomic and agricultural vegetation classes are distinctive in some or all of the timing, the intensity or the duration of their period of photosynthetic activity, typically, an area of vegetation that is homogeneous with respect to physiognomic or agricultural vegetation type is heterogeneous with respect to NDVI response. Consequently, *all AVHRR NDVI pixels are mixed pixels for purposes of mapping physiognomic and agricultural vegetation cover classes, even when the pixels correspond to areas covered entirely by a single agricultural or physiognomic class*. The reason for this is that the bases for agricultural and physiognomic vegetation classes are not the same as the physical and physiological bases of the NDVI. For example, a field of potatoes may be one class of agricultural crop, but it contains at least two distinct NDVI classes (i.e. the green potato plant and the bare soil between the rows).

The fundamental "mixedness" of physiognomic and agricultural vegetation cover classes in terms of their NDVI response limits the extent to which all NDVI data may be used to map physiognomic and agricultural vegetation classes. However, an even greater limitation to the success with which AVHRR NDVI data may be used to map physiognomic and agricultural vegetation cover classes is the spatial scale of these data[14]. Since even the most broadly defined vegetation cover classes rarely cover uninterruptedly areas as large as individual AVHRR pixels, most full resolution AVHRR pixels and practically all Global Vegetation Index pixels will contain the area integrated NDVI of at least two vegetation cover classes. For example, an extensive area of vineyards will include not only rows of vines, with rows of bare soil between them, but also stretches of road, occasional houses with gardens, hedges, rows of trees and so on. Mixed pixels due to the spatial scale of the data are a problem associated particularly with Global Vegetation Index pixels. Indeed, the high proportion of Global Vegetation Index pixels that are mixed in this way is the reason why many physiognomic and agricultural vegetation classes have similar (Global Vegetation Index) NDVI temporal profiles (e.g. Justice *et al.* 1985; Townshend *et al.* 1987).

---

14 A full resolution AVHRR pixel represents an area on the ground of at least 121 hectares while a Global Vegetation Index pixel represents an area of at least 12 800 hectares (Appendix 1)

Mixed pixels affect the extent to which physiognomic and agricultural vegetation classes may be mapped using multidate full resolution AVHRR NDVI data. So too does the temporal resolution of the data. The reason for this is that the ability to discriminate among physiognomic and agricultural vegetation cover classes is based on phenological contrast between the classes. Clearly, the fewer multidate NDVI images there are, the more marked will need to be the differences in the timing, intensity and duration of photosynthetic activity among a set of vegetation cover classes if they are to be mapped successfully.

The foregoing discussion indicates that only the most extensive, phenologically-contrasting classes of vegetation cover will be discernible using full resolution AVHRR NDVI imagery. The problem here is that these two requirements are usually contradictory. Broadly-defined vegetation cover classes that are defined in order to fulfil the requirement of spatial extensivity run the risk of having indistinct multidate NDVI characteristics, whilst narrowly-defined vegetation cover classes that are defined in order to maximise their phenological distinctiveness will cover contiguous areas too small to be resolved by AVHRR data. Presumably these are the reasons why large scale multidate shortwave vegetation index data have been used successfully to map physiognomic and agricultural vegetation cover classes (e.g. Steiner 1969; Morain 1974; Park 1984; Badhwar 1984a,1984b; Odenwaller and Johnson 1984; Ajai *et al.* 1985; Lo *et al.* 1986; Hall and Badhwar 1987), whereas just one map purporting to show physiognomic and agricultural vegetation cover classes derived from multidate AVHRR NDVI imagery has been published (Townshend *et al.* 1987)[15].

3.4 Spanish physiognomic and agricultural classes

The Iberian Peninsula is a region of exceptional floristic diversity (Polunin and Smythies 1973; Terán and Solé Sabarís 1978). This has been attributed to a combination of factors including the wide range of bioclimatic, lithological and topographic environments, the relative geographic position of the peninsula between Africa and the rest of Europe, and the lack of a permanent ice cap in the south-west part of the peninsula during the last ice age.

The wide variety of vegetation cover classes found in Spain range from the semi-desert areas of the south-east and the Ebro Depression to the densely populated deciduous forests of the northern coastal fringe and the western end of the Pyrenees. Although, at the smallest scale, many of the patterns of vegetation cover may be

15 This study used Global Vegetation Index imagery

related to variations in climatic conditions[16], locally, the pattern of vegetation cover can be very intricate. This was apparent from both field observation and also 1:200 000 landuse maps (MAPA 1988)[17] and national inventories of coniferous and broadleaf woodlands (MAPA 1979,1980) produced by the Spanish ministry of agriculture.

A physiognomic and agricultural vegetation cover classification for Spain was devised on the basis of four, three-week field excursions of approximately 3000km each. The areas visited during these excursions, which were made in August 1984 and March, July and September 1985, are shown in figure 3. First-hand observations of the physiognomic and phenological characteristics of Spanish vegetation cover made in the course of the field excursions provided the bases for simplifying natural diversity into a few, physiognomic and agricultural vegetation cover classes. These classes are summarised in table 5. It is important to emphasise that although the Generic Classes in table 5 may be helpful for purposes of defining a similar classification scheme for other areas, the Specific Classes apply only to Spain. These Specific Classes stand a reasonable chance of being detected and mapped using multidate AVHRR NDVI data due to their phenological contrast and spatial extensivity. They are described below.

Woodland is defined as areas in which trees greater than 1.5m high cover more than 20% of the ground surface. This is the same definition as that implied by the 1:200 000 landuse maps (MAPA 1988). There are three classes of Woodland. The principal difference between Deciduous and Coniferous Woodland is phenological. Conifer trees are in leaf throughout the year whereas deciduous trees are not. The principal difference between Coniferous and Evergreen Oak Woodland is physiognomic. Field observations indicated that *Quercus suber* and *Quercus ilex* have a denser canopy than conifers.

Parkland is a very typical Iberian vegetation cover class. The distinction between Woodland and Parkland is that the density of trees in Parkland is less than 20%. The inclusion of orchard crops as types of Parkland may seem surprising. However, all Parkland classes are similar from the point of view of the satellite-borne AVHRR. Their unifying characteristic is a broken tree canopy which results in other

16 The northern coastal fringe has significant rainfall throughout the year and a mean annual rainfall of at least 1000mm. Elsewhere the climate is fiercely continental (i.e. a high mean annual amplitude of temperature) with hot dry summers and winters whose dryness and coldness increases from west to east. The dryest part of Spain, the south-east, has less than 300mm rainfall, fewer than forty raindays and over 3000 hours sunshine per year (MTTC 1982,1983)

17 Derived from a 1:50 000 landuse series compiled between 1974 and 1978

Figure 3. Northeastern and Southern Spain: Map Showing the Major Physiographic Features, the Field Excursion Routes and the Location of the Field Sites.

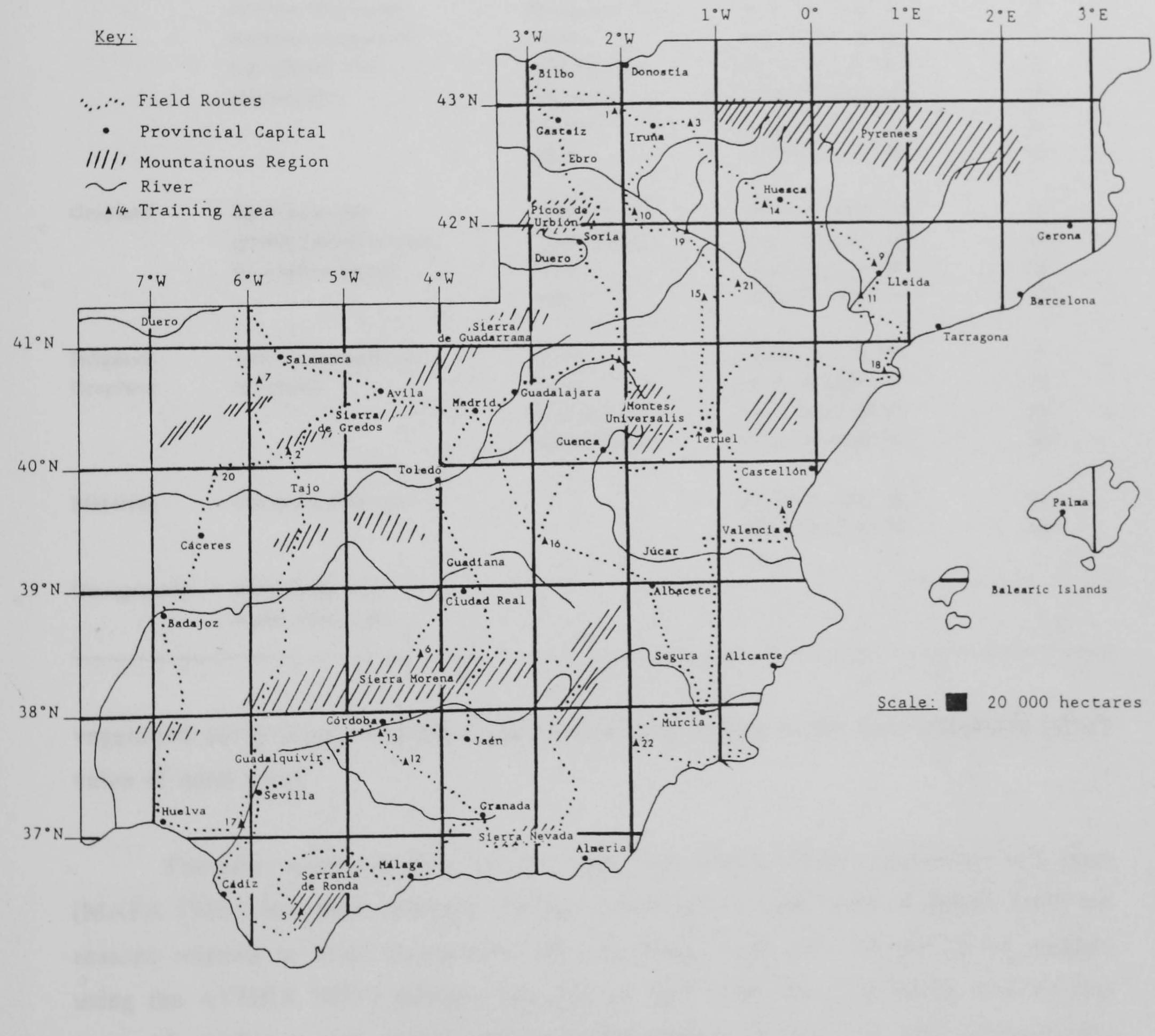

Table 5. Iberian Vegetation Cover Classes

Generic Class	Characteristics	Specific Class	Location of Field sites	Field site Number
Woodland	Continuous cover of trees	Deciduous	42.83 ° N, 2.08 ° W	1
		Deciduous	40.07 ° N, 5.88 ° W	2
		Coniferous	42.78 ° N, 0.98 ° W	3
		Coniferous	40.72 ° N, 2.08 ° W	4
		Evergreen Oak	36.47 ° N, 5.55 ° W	5
Parkland	Discontinuous cover of trees. May have seasonal undercover e.g. cereals, vine, grasses, etc.	Evergreen Oak	38.53 ° N, 4.03 ° W	6
		Evergreen Oak	40.77 ° N, 6.03 ° W	7
		Citrus	39.57 ° N, 0.38 ° W	8
		Soft Fruit	41.78 ° N, 0.70 ° E	9
		Almond	42.20 ° N, 2.08 ° W	10
		Olive	41.38 ° N, 0.47 ° E	11
		Olive	37.30 ° N, 4.65 ° W	12
Cropland	Short,intensive growth period followed by a fallow period	Cereals and Sunflowers	37.78 ° N, 4.63 ° W	13
			42.17 ° N, 0.57 ° W	14
		Vine	41.33 ° N, 1.22 ° W	15
		Vine	39.23 ° N, 2.87 ° W	16
Irrigated Cropland	Growth independent of rainfall	Rice	37.08 ° N, 6.17 ° W	17
		Rice	40.70 ° N, 0.67 ° E	18
		Mixed Crops	41.92 ° N, 1.28 ° W	19
		Mixed Crops	39.97 ° N, 6.33 ° W	20
Matorral	Grasses and shrubs	-	41.53 ° N, 0.87 ° W	21
			37.77 ° N, 1.83 ° W	22
Unvegetated	Bare earth, rock water, urban, etc.	-	-	-

vegetation cover classes making a significant contribution to the area-integrated NDVI value of each pixel.

The most extensive field crops in Spain are wheat, barley, sunflowers and vines (MAPA 1986). However, although all four classes cover large areas of Spain, there are reasons relating to their distribution and phenology why they cannot all be mapped using the AVHRR NDVI imagery available in this study. Thus, it seems unlikely that areas of sunflower and cereal can be distinguished, in spite of their phenological dissimilarity (MAPA 1982), because sunflowers are frequently grown in a "chequer-board" pattern with cereals in fields that are similar in size to the area represented by individual AVHRR pixels. On the other hand, it seems unlikely that fields of barley and wheat can be distinguished because phenologically they are practically identical (MAPA 1982).

Irrigated Cropland is extremely important over much of Spain. The common characteristic of all irrigated crops is that growth is independent of rainfall. While it is true that many of the wide variety of irrigated crops that are grown are different phenologically, usually it is not possible to distinguish between most of them using AVHRR NDVI imagery because of the small size of the plots on which they are grown.

There are many different types of Matorral in Spain (Polunin and Smythies 1973). The essential features of this class for purposes of this classification are that trees greater than 1.5m cover less than 20% of the ground surface and that the vegetation cover of the remaining 80% consists mainly of shrubs and grasses with areas of bare rock and soil.

3.5 Field sites in Spain

Field sites are used for three purposes in this study. They are the basis for describing the multidate NDVI characteristics of the physiognomic and agricultural vegetation classes described in the previous section. They are used to provide training statistics for a minimum distance classification (i.e. they act as training areas[18]). They are used to interpret classified images derived from multidate full resolution AVHRR NDVI data.

Schowengerdt (1983) states that between ten and one hundred training pixels per class *per NDVI image*[19] are needed in order to obtain reliable training statistics. The multidate full resolution AVHRR NDVI data sets used in this study consist of six NDVI images for each year[20]. Therefore, according to Schowengerdt, between sixty and six hundred full resolution AVHRR NDVI pixels are required for each field site (i.e. training area). Since an individual mapped full resolution AVHRR pixel in this study represents an area of 156.25 hectares, this means that, according to Schowengerdt, each field site should cover areas of between 9375 hectares ($\approx$10km^2) and 93 750 hectares ($\approx$31km^2). Although each of the thirteen vegetation cover classes listed in table 5 covers thousands of hectares in Spain, areas covered exclusively by one class as large as 9375 hectares are extremely rare. For this reason, the field sites in this study cover a six by six pixel area (i.e. 5625 hectares ($\approx$7.5km^2)).

---

18 See Section 3.2

19 i.e. a single NDVI image is a "feature" (Schowengerdt 1983)

20 The characteristics of the full resolution AVHRR NDVI imagery used in this study are described in Chapter Four Section 1

The field sites that are used in this study are the most homogeneous examples of the vegetation classes described in table 5 that I encountered in the course of the four field excursions. The location of each field site is given in table 5 and illustrated in figure 3. Where a field site for a particular vegetation cover class has patches of other vegetation cover classes (i.e. not the training class) sufficiently extensive to appear on the 1:200 000 landuse maps, the existence of these other classes is noted and an approximate measure of the area they cover is provided in the description of each field site that follows. If no other vegetation class is mentioned, it may be assumed that a field site is covered exclusively by just one of the vegetation cover classes in table 5 and that the occurrence of other vegetation cover classes is limited to occasional roads, streams, rivers, houses, gardens, trees lining roads and rivers, clearings in woodlands and so on (i.e. the vegetation cover heterogeneity that is practically unavoidable at the spatial scale of full resolution AVHRR data).

There are two Deciduous Woodland field sites (i.e. 1 and 2). Field site 1 is located in the Sierra de Urbasa in western Navarra. It is covered by a dense, deciduous forest which is made up mostly of mature beech trees. Although there are patches of grass pasture (i.e. Matorral) within the field site, these cover no more than approximately 6% of the total area[21]. Field site 2 is located at the western end of the Sierra de Gredos in northeast Cáceres. Although there are patches of rough grassland (i.e. Matorral), Evergreen Oak Parkland, Olive Parkland, Almond Parkland and irrigated and unirrigated market gardening (i.e. Mixed Irrigated Cropland and Cropland) within this field site, these cover no more than 6%, 8%, 6%, 3%, 3% respectively of the total area.

There are two Coniferous Woodland field sites (i.e. 3 and 4). Field site 3 is in northeastern Navarra in the valley of the river Esca. It is covered by conifer trees. Although there are patches of ericaceous moorland (i.e. Matorral) and arable farmland (i.e. Cropland) within the field site, these cover no more than approximately 3% each of the total area. Field site 4 is located in the La Sierra region Guadalajara, close to the source of the Tajo. It is covered completely by conifer trees.

There is one Evergreen Oak Woodland field site (i.e. 5). It is located in the Sierra del Aljibe in eastern Cádiz. Most of the trees are *Quercus suber*. Although there patches of unwooded matorral, these cover no more than 6% of the total area.

---

21 Each field site covers 5625 hectares. Percentages are the proportion of each field site covered by classes other than the training class as depicted on the 1:200 000 landuse maps (MAPA 1988).

There are two Evergreen Oak Parkland field sites (i.e. 6 and 7). Field site 6 is located at the eastern end of the Valle de Alcudia in south-western Ciudad Real. The seasonal undercover for this field site is mostly rough grass pasture. Although there are small unwooded patches of both rough pasture (i.e. Matorral) and Cropland within this field site, these do not cover more than approximately 6% each of the total area. Field site 7 is located in the western part of the Campo de Salamanca in Salamanca. The seasonal undercover for this field site is mostly rough pasture. Although there are patches of unwooded grassland (i.e. Matorral), unwooded irrigated grassland (i.e. Mixed Irrigated Crops) and unwooded Cropland within this field site, these do not cover more than approximately 8%, 6% and 3% respectively of the total area.

There is one Citrus Parkland field site (i.e. 8). It is located on the coastal plain in northeast Valencia. Although there are patches of urban landuse (i.e. Unvegetated) and Almond Parkland within this field site, these cover no more than approximately 3% and 11% respectively of the total area.

There is one Soft Fruit Parkland field site (i.e. 9). It is located in southern Lleida. Most of the fruit trees are irrigated apple and pear trees. Although there are patches of Matorral and Cropland, these cover no more than approximately 8% and 6% respectively of the total area.

There is one Almond Parkland field site (i.e. 10). It is located in eastern La Rioja. Although there are patches of Mixed Irrigated Cropland, Vine and Matorral these cover no more than approximately 6%, 3% and 3% respectively of the total area.

There are two Olive Parkland field sites (i.e. 11 and 12). Field site 11 is located in southern Lleida. Although there are patches of Matorral these cover no more than approximately 6% of the total area. Field site 12 is located in southern Córdoba. Although there are patches of arable farmland (Cropland) and Matorral these cover no more than approximately 6%, and 3% respectively of the total area.

There are two Cereals and Sunflowers Cropland field sites (i.e. 13 and 14). Field site 13 is located in central Córdoba. The arable crops grown in this field site are wheat, barley and sunflower. Although there are small patches of Olive Parkland within this field site, these cover no more than approximately 3% of the total area. Field site 14 is located in the Hoya de Huesca in western Huesca. The arable crops grown in this field site are wheat and barley. Although there are small patches of

Matorral and Evergreen Oak Woodland within this field site, these cover no more than approximately 6% each of the total area.

There are two Vine Cropland field sites (i.e. 15 and 16). In both cases the vines are grown in rows with strips of bare earth between the rows. Field site 15 is located in the Campo de Cariñena in southern Zaragoza. Although there are small patches of Mixed Irrigated Cropland and Matorral within this field site, these cover no more than approximately 3% and 8% respectively of the total area. Field site 16 is located northeast of Tomelloso in northeastern Ciudad Real. Although there are patches of Mixed Irrigated Cropland and Cropland within this field sites, these cover no more than approximately 3% and 6% respectively of the total area.

There area two areas of Rice Irrigated Cropland (i.e. 17 and 18). Field site 17 is located in the delta of the river Guadalquivir in Sevilla. Although there are patches of Mixed Irrigated Cropland, marshland (i.e. Matorral) and open water (i.e. Unvegetated) within this field site, these cover no more than approximately 8%, 6% and 3% respectively of the total area. Training are 18 is located in the delta of the Ebro in Tarragona. Although there are patches of Mixed Irrigated Cropland within this field site, these cover no more than approximately 11% of the total area.

There area two Mixed Irrigated Cropland field sites (i.e. 19 and 20). Field site 19 is located just north of the river Ebro in western Zaragoza. The main crops grown in this field site are maize, root vegetables and alfalfa. Although there are patches of (unirrigated) Cropland and Matorral within this pixel, these cover no more than approximately 6% each of the total area. Field site 20 is located close to the river Alagón in central Cáceres. The main crops grown in this field site are tobacco, maize and alfalfa. Although there are patches of Matorral and Evergreen Oak Parkland within this pixel, these cover no more than approximately 3% each of the total area.

No attempt is made to discriminate among the many different type of Matorral that are found in Spain. The two Matorral field sites used in this study are areas of extremely sparse, xerophytic vegetation cover. Field site 21 is located south of the river Ebro in southern Zaragoza and field site 22 is located close to the Embalse de Puentes in western Murcia. Although there are small patches of arable farmland (i.e. Cropland) within field site 21 (i.e. approximately 8% of the total area) and small patches of Coniferous Woodland Cropland and Cropland in field site 22 (i.e. approximately 6% and 14% respectively of the total area), these two areas were chosen for the sparseness of their vegetation cover. Once the green flush associated with Spring growth has died

back, the NDVI values for these two areas will provide an indication of NDVI values for land where levels of photosynthetic activity are near zero.

4. Summary

The nature of vegetation cover classes that may be mapped using multidate small-scale NDVI imagery is discussed. An original method whereby imagery of phytophenological variables may be integrated to produce a phytophenological classification is proposed and phytophenological classifiers of this type for full resolution AVHRR NDVI imagery of Spain and Global Vegetation Index imagery of Africa are presented. The classifications produced by these classifiers are presented and discussed in Chapters Four (Spain) and Five (Africa).

The use that has been made of Global Vegetation Index and full resolution AVHRR NDVI imagery to map physiognomic and agricultural vegetation cover classes is reviewed and the greater potential of full resolution AVHRR NDVI data over Global Vegetation Index data in this respect is explained. The preconditions for successful classification of multidate data are explained and the shortcomings of full resolution AVHRR NDVI data in this respect are described. The approach used in this study to assess the extent to which full resolution AVHRR NDVI imagery may be used to map physiognomic and agricultural vegetation cover classes in Spain is described.

A physiognomic and agricultural vegetation cover classification for Spain for use with full resolution AVHRR NDVI imagery is presented. The problems associated with the identification of field sites for each of the classes in this classification are explained. A description of each of the field sites that are used in this study is given including details of the extent to which they are covered significantly by vegetation classes other than the training class. The success with which full resolution AVHRR NDVI imagery may be used to map the vegetation classes in this physiognomic and agricultural vegetation cover classification is assessed in Chapter Four.

Chapter Four

Vegetation Mapping Using Full Resolution AVHRR NDVI Imagery

1. Preparation of full resolution AVHRR NDVI imagery[1]

Full resolution AVHRR NDVI imagery is evaluated for purposes of vegetation mapping using High Resolution Picture Transmission imagery of Spain. Spain was chosen as the study area for four main reasons. It contains a wide variety of vegetation cover types, it is within the catchment of the AVHRR receiver at the Satellite Data Receiving Station at Dundee, it is well documented with ancillary data pertinent to the aims of this study and it is within easy reach of Bristol. Eighteen High Resolution Picture Transmission images of the Iberian Peninsula were obtained from the archive of NOAA-AVHRR imagery at Dundee Satellite Receiving Station (table 6). The images were chosen to provide the best cloudfree coverage of Spain with a frequency of approximately one image per month between April and September for the years 1985 and 1986. All the images were made by the NOAA 9 AVHRR/2 between 13:42 and 15:03 hours Greenwich Mean Time.

Table 6. NOAA 9 AVHRR/2 High Resolution Picture Transmission of the Iberian Peninsula Obtained from Dundee Satellite Receiving Station

Date (1985)	Julian Day	Time	Date (1986)	Julian Day	Time
2nd April	92	14:13	27th March	86	14:06
29th April	119	14:27	9th May	129	14:56
8th May	128	14:32	21st May	141	14:21
5th July	186	14:16	16th July	197	14:25
21st July	202	14:49	2nd August	214	14:44
26th July	207	13:55	21st August	233	14:42
17th August	229	15:03	2nd September	245	14:13
3rd September	246	13:42	28th September	271	14:36
29th September	272	14:07			
7th October	280	14:22			

1 The satellite data were processed using a Systime 8750 running the UNIX operating system and an International Imaging Systems Model 75 image processor with system 575 software hosted by a Digital Equipment Vax 11/750 running the VMS operating system

Channel 1 and channel 2 data were extracted from each image and calibrated using the preflight gain and intercept coefficients for NOAA 9 AVHRR imagery supplied by NOAA[2]. No attempt was made to correct the radiance values for the effect of scan angle. However, since all the images were recorded at midday and nearly all the images were recorded between the vernal and autumnal equinoxes, the distortion in NDVI values due to variations in viewing and illumination geometry should be small.

The calibrated channel 1 and channel 2 data for all pixels with a visible (i.e. channel 1) radiance less than 400 digital counts[3] were used to calculate NDVI values according to equation 2. Pixels with visible radiances greater than 400 digital counts were deemed cloud-contaminated and assigned an NDVI value of zero[4].

Geodetic registration of the AVHRR NDVI data was performed to enable easy, quantitative intercomparison between images made on different dates. The geodetic registration algorithm used in this study was developed by Brush (1988) and is described in Appendix 3. Following geodetic registration, the eighteen NDVI images were mapped to an equal area radial projection of the Iberian Peninsula with standard parallels at 40°N (and S), latitudinal and longitudinal limits of 35.4°-44.17°N and 10.03°W-4.98°E and a spatial resolution of 156.25 hectares per pixel. The spatial resolution of 156.25 hectares[5] is approximately the area represented by a single High Resolution Picture Transmission pixel twenty degrees from nadir (Saull 1985). It is thus a reasonable compromise size between the largest and the mean spatial resolution of High Resolution Picture Transmission pixels. The standard parallel at 40°N minimises shape distortion between 36° and 44°N. The spatial scale and 40° standard parallels together create an array with dimensions 1024x784 in which a square on the ground covering 100 hectares has dimensions 1.06x0.94km at 36°N, 1.0x1.0km at 40°N and 0.94x1.06km at 44°N.

The full resolution mapped AVHRR NDVI images were compared with an image of control points digitised from Spanish landuse maps (MAPA 1988)[6]. Only one of the eighteen images, the 2nd April 1985, fitted the ground control points perfectly.

---

2 i.e. A = GX + I, where A is the calibrated radiance value, X is the uncalibrated radiance value, G (channel 1 gain) = 0.1063400366, G (channel 2 gain) = 0.107491067, I (channel 1 intercept) = -3.846375952, I (channel 2 intercept) = -3.877005621

3 The maximum value is 1024

4 This threshold value was chosen on the basis of interactive analysis of all eighteen images

5 i.e. equivalent to a square 1.25x1.25km

6 The 1:200 000 landuse maps (MAPA 1988) were digitised using a forty-eight inch Terminal Display Systems LC-20 high resolution digitiser and GINGA computer aided design software by Design Computing (Bristol, England) hosted by an Opus XT-compatible personal computer

This is disappointing but not surprising. It is quite common for AVHRR images to be imperfectly registered at the end of a geodetic registration algorithm (Cracknell and Paithoonwattanakij 1987). Lack of fit may be attributed to either incorrect satellite altitude or incorrect equatorial crossing longitude (both of which result in a lack of fit in an east-west direction) or incorrect timing of the equatorial crossing or the first line (both of which result in a lack of fit in a north-south direction).

The registration accuracy of the seventeen misregistered images in this study was improved using "*Warp*" (IIS 1984). However, since this nearest neighbour interpolation algorithm is designed for images no larger than 512x512, two 512x512 areas within the base map array were selected. These areas, described hereafter as northeastern and southern Spain, were extracted from all eighteen images and "warped" to fit the image made on the 2nd April 1985. Coastal headlands and reservoirs provided most of the control points. Table 7 shows the registration accuracy that was achieved.

Table 7. Registration Accuracy of NOAA 9 AVHRR/2 High Resolution Picture Transmission NDVI Imagery of Northeastern and Southern Spain[a]

Image	Northeastern Spain		Southern Spain	
	Goodness of fit[b]	Control Points	Goodness of fit[b]	Control Points
29.4.1985	0.66	9	0.36	8
8.5.1985	0.56	11	0.60	10
5.7.1985	0.72	12	0.19	8
21.7.1985	1.38	11	0.30	5
26.7.1985	0.40	12	0.42	9
17.8.1985	1.34	11	0.57	7
3.9.1985	0.66	9	0.43	8
29.9.1985	0.40	12	0.38	8
7.10.1985	0.90	11	0.44	9
27.3.1986	0.57	11	0.42	9
9.5.1986	0.58	12	0.39	9
21.5.1986	0.53	14	0.40	9
16.7.1986	0.57	14	0.36	9
2.8.1986	0.52	13	0.27	7
21.8.1986	0.38	12	0.47	8
2.9.1986	0.55	11	0.46	8
28.9.1986	0.38	10	0.40	9
mean	**0.65**	**12**	**0.40**	**8**

a. All images registered to the mapped 2nd April 1985 image using a nearest neighbour interpolation algorithm ("Warp" (IIS 1984))

b. Measured in pixels. One pixel represents an area on the ground of 156.25 hectares

Some of the eighteen mapped NDVI images contained large areas of cloud. The final part of the AVHRR NDVI data preparation process involved making maximum value NDVI composites from selected images to reduce the amount of cloud contamination. The result was six images each for 1985 and 1986 (table 8). The mean time interval between the six composite images for each year is thirty-seven days.

Table 8. NOAA 9 AVHRR/2 High Resolution Picture Transmission NDVI Imagery of Northeastern and Southern Spain: Image Dates after Maximum NDVI Value Compositing

Image Date[a]	Julian day	Images Used	Number of Days to Previous Image
2.4.1985	92	-	-
3.5.1985	123	29.4 and 8.5.1985	31
5.7.1985	186	-	63
24.7.1985	205	21 and 26.7.1985	19
25.8.1985	237[b]	17.8 and 3.9.1985	32
3.10.1985	276	29.9 and 7.10.1985	39[c]
27.3.1986	86	-	-
15.5.1986	135	9 and 21.5.1986	49
16.7.1986	197	-	62
2.8.1986	214	-	17
27.8.86	239	21.8 and 2.9.1986	25
28.9.1986	271	-	32

a. For composite images, the image date is defined as the midpoint between the two images
b. The northeastern area image for this date is not a maximum NDVI value composite. It is the image for 3.9.1985 only. The number of days to the previous northeastern area image is 41 days (i.e. 3.9.1985 is Julian day 246)
c. The number of days to the previous northeastern area image is 30

2. Single-date full resolution AVHRR NDVI imagery of northeastern and southern Spain

2.1 General description

Figure 4 shows full resolution AVHRR NDVI imagery of northeastern and southern Spain for 2nd April 1985, 15th May 1986, 16th July 1986 and 3rd October 1985 mapped to an equal area radial projection. Bright grey tones are associated with high NDVI values and most areas of dark grey may be interpreted as surfaces with low densities of photosynthesising vegetation. Black areas correspond mostly to surfaces devoid of significant amounts of photosynthesising vegetation such as water bodies (e.g. lakes and rivers) and areas covered by snow (e.g. the Pyrenees and the Sierra de Urbion). The images contain very little cloud contamination. Where this does occur the

Figure 4. Northeastern and Southern Spain: Full Resolution AVHRR NDVI.
A) 2nd April 1985, B) 15th May 1986 (continued on next page)

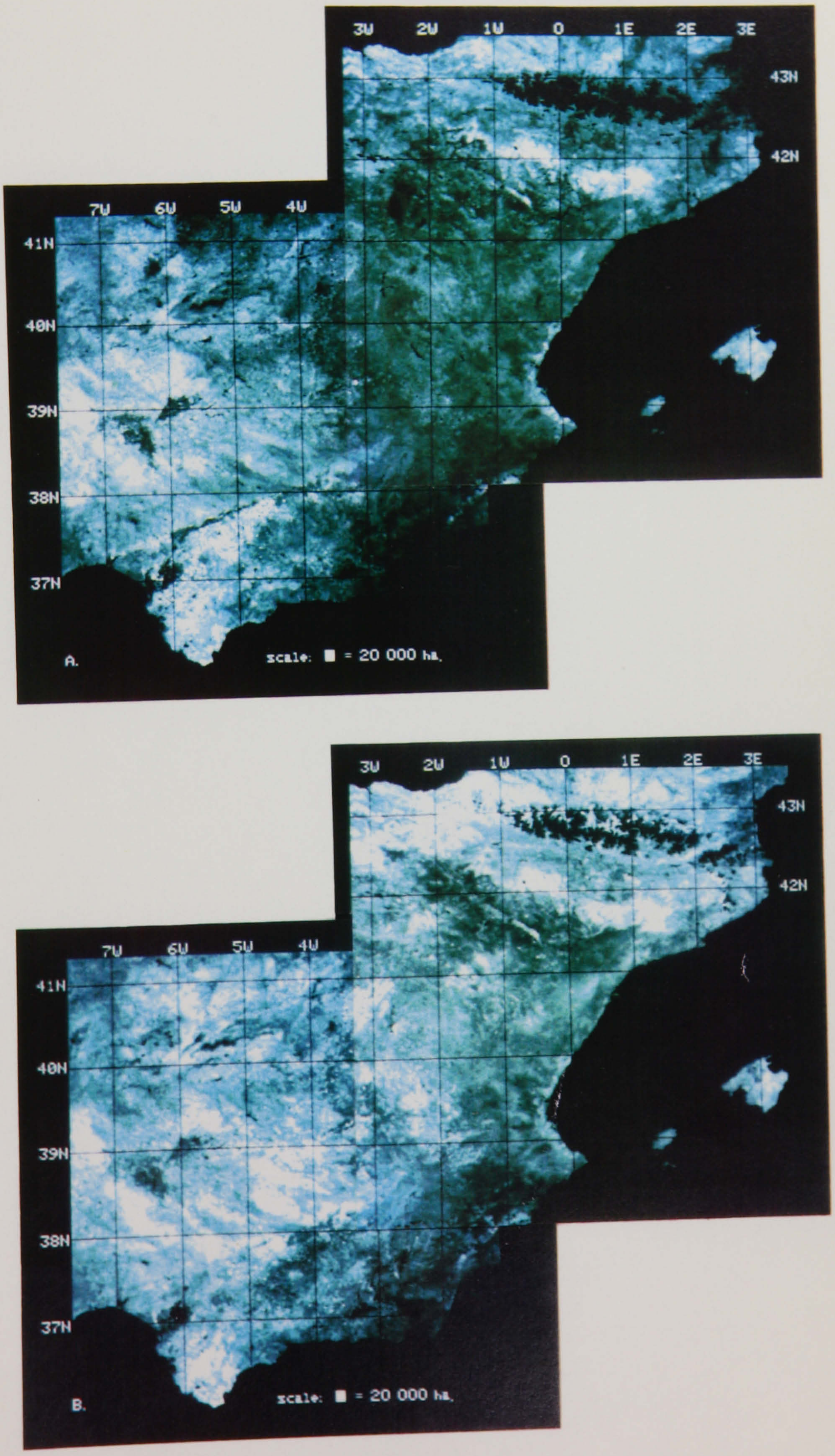

Figure 4. (conclusion) C) 16th July 1986, D) 3rd October 1985

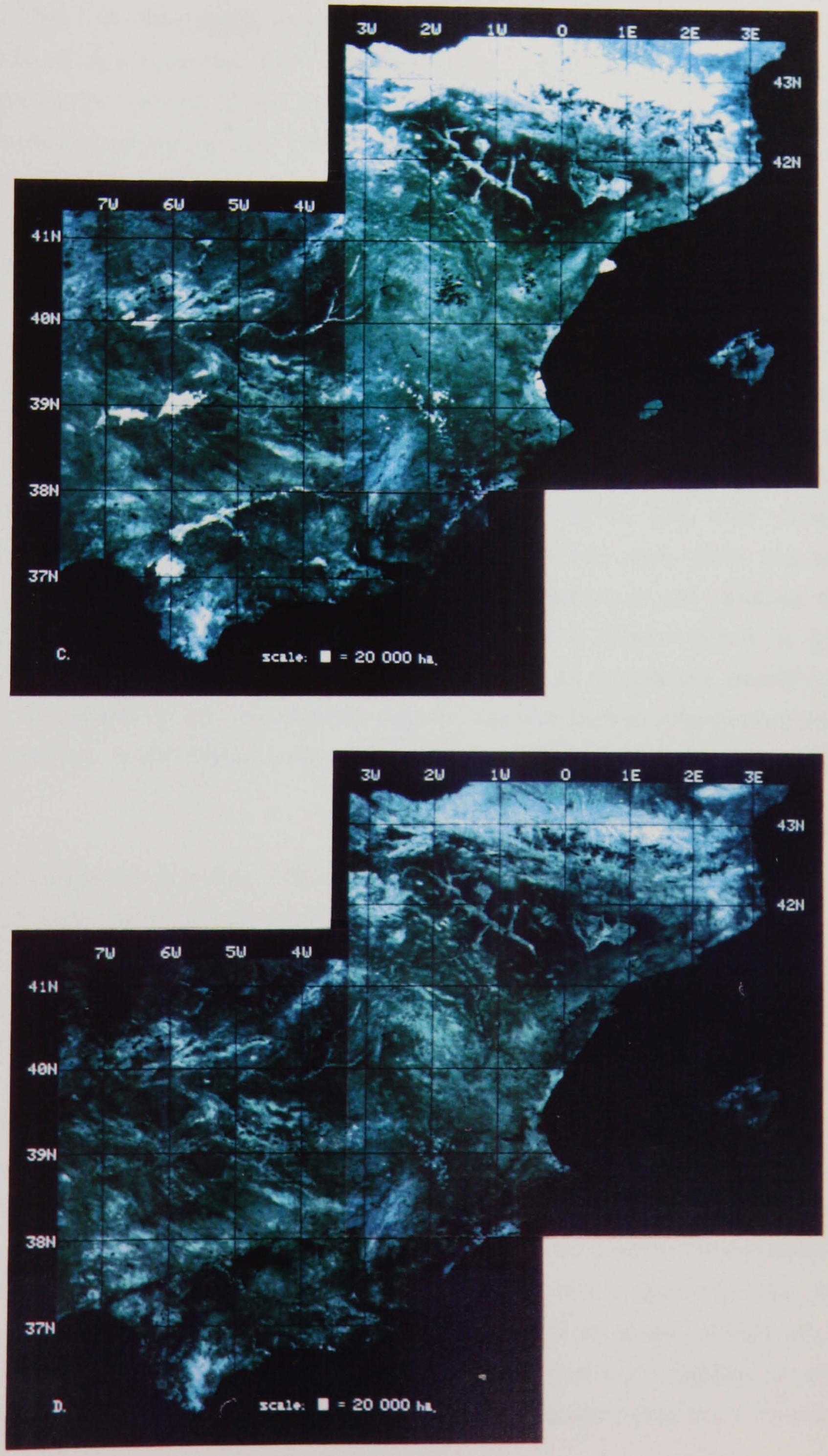

imagery appears either black or dark grey tones depending upon whether they were detected by the cloud screening process or not. Thus, the 2nd April image contains cloud contamination around Almeria, south of Soria and in the central and eastern Pyrenees. The 15th May image contains small patches of cloud contamination at the eastern end of the Pyrenees. The 16th July image contains small patches of cloud contamination over several of the mountainous areas including the Pyrenees, the Sierra de Guadarrama and the Montes Universales. The 3rd October image contains small patches of cloud contamination over the Pyrenees.

The image for early April, figure 4(A), shows Spring growth (the green wave) covering over half of northeastern and southern Spain including the Balearic Islands. The highest levels of photosynthetic activity are associated principally with cereal-growing areas (including the north side of the Ebro valley) and the extreme northern part of the study area. In several of the cereal-growing areas the image appears speckled (e.g. the south side of the Guadalquivir valley). This may be attributed to the fact that fields of wheat and barley are frequently side-by-side with fields of sunflower or maize. Since sunflower and maize are sown later than wheat and barley (MAPA 1982) a "chequerboard" pattern of vegetation (cereal) and soil (seedling maize or sunflower) results. In central and eastern Spain there is little evidence of Spring growth. The brighter grey tones in this part of the image correspond mostly to the evergreen woodlands of the mountainous regions (e.g. the Montes Universales) and to the citrus groves in the Segura valley and along the coast to the north and south of Valencia.

The image for mid-May, figure 4(B), shows Spring growth covering almost the entire study area. Although the south-east and the Ebro valley have the lowest NDVI values of this image, even these values are relatively high compared to the values for these areas later in the year. The generally high levels of photosynthetic activity make it difficult to discriminate among vegetation cover types at this time.

By mid-July, figure 4(C), the pattern of photosynthetic activity has changed dramatically. Although intermediate levels of photosynthetic activity may be found, associated particularly with areas of evergreen woodland, the overriding impression given by this image is one of contrast. The boundary between humid "Green" Spain and dry "Brown" Spain (MTTC 1983) is particularly clear in this image, especially at the western end of the Pyrenees. High NDVI values are associated almost exclusively with either woodland or irrigated cropland. The extent of riparian irrigation is clearly depicted in this image. It is not confined simply to the biggest rivers but is found also

along the banks of many smaller rivers and canals. For example, the high NDVI values west of Albacete correspond to irrigated agriculture beside the Tajo-Segura canal.

By early October, figure 4(D), levels of photosynthetic activity are lower than they were in July almost everywhere. The main exceptions to this are the evergreen woodlands of the central, southern and eastern mountain regions. Other exceptions occur locally. For example, a small area of sugar cane on the south coast, south of Granada, has much higher NDVI values than the surrounding vegetation.

2.2 Discussion

Figure 4 illustrates the spatial and temporal variations in photosynthetic activity over northeastern and southern Spain that may be detected by full resolution AVHRR NDVI imagery. It is clear from these images that the timing of imaging can influence greatly the extent to which these AVHRR NDVI data may be used to discriminate among vegetation cover classes. Clearly, there are times of year when fine temporal resolution[7] can provide useful additional information with which to discriminate among vegetation cover classes (e.g. during the months of widespread, rapid vegetative growth) and times of year when fine temporal resolution is of little value (e.g. during the months of widespread senescence and dormancy).

Two of the images in figure 4 were recorded in 1985 and two were recorded in 1986. While this is acceptable for purposes of describing the basic phytophenological characteristics of the study area, clearly there may be substantial phenological variations from year to year. Consequently, for purposes of vegetation mapping, NDVI imagery from different years should not be mixed. In fact, although the dates of the images for 1985 and 1986 are different (see table 8) and the images for 1985 and 1986 are treated separately in the following sections, the similarity of the patterns and colours in the images for 1985 and 1986 in figure 5 suggests that between April and October 1985 and 1986 northeastern and southern Spain were quite similar phytophenologically[8].

An obvious difference between figure 5 and the images in figure 4 is that some of the images in figure 5 contain black patches whereas the images in figure 4 do not.

---

7 i.e. imagery at frequent intervals

8 The images in figure 5 were made by displaying the first three dates and last three dates for each year (see table 8) simultaneously through the red, green and blue guns of a colour monitor. The result is an image in which colours describe the timing and duration of photosynthetic activity (e.g. red and green make yellow, green and blue make cyan etc.) and brightness describes the intensity of photosynthetic activity (e.g. dark tones are associated with low levels of photosynthetic activity)

Figure 5. Northeastern and Southern Spain: Full Resolution AVHRR NDVI
A) Spring 1985 (2nd April (red), 3rd May (green), 5th July (blue),
B) Summer 1985 (24th July (red), 25th August (green), 3rd October (blue)
(continued on next page)

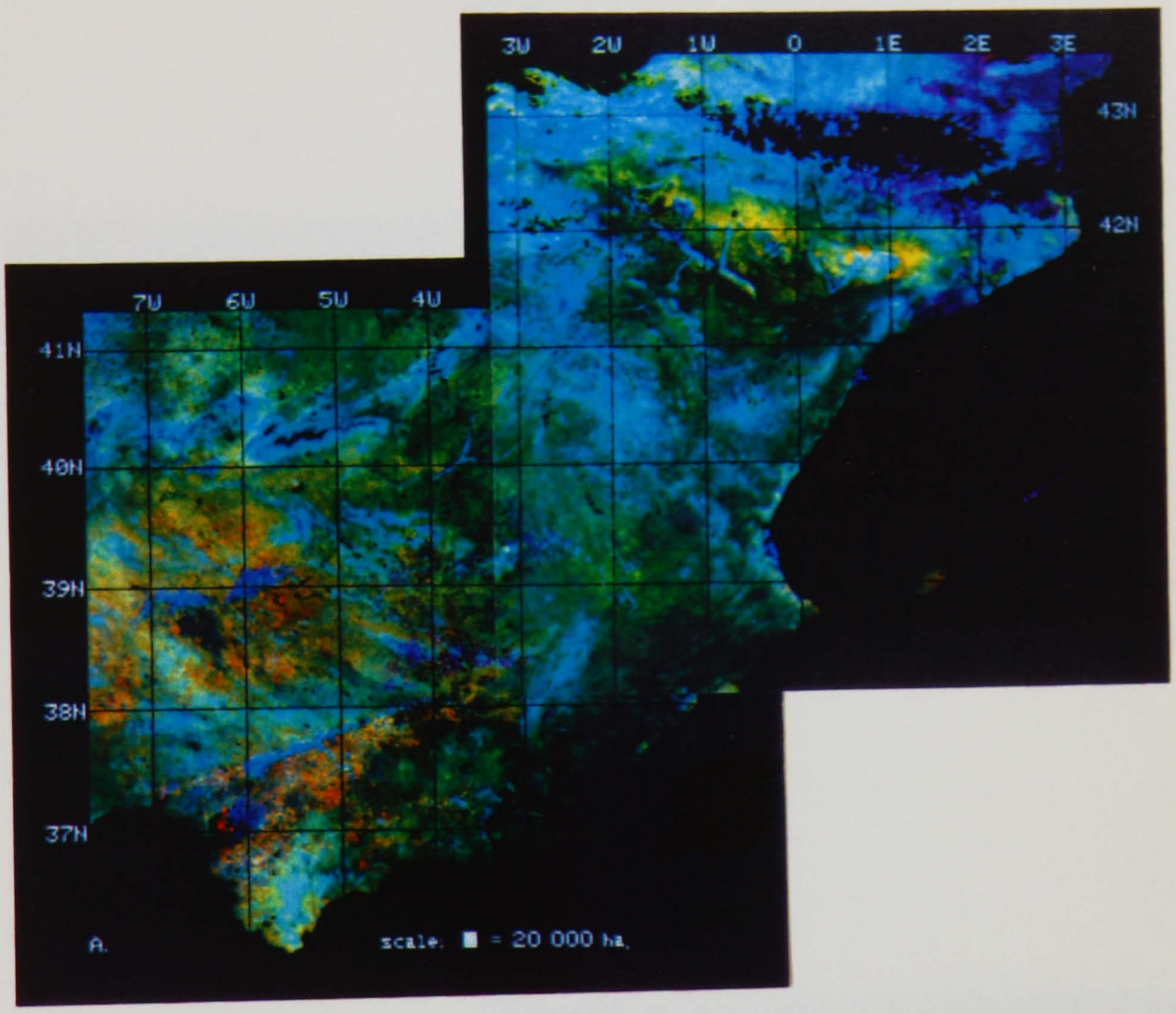

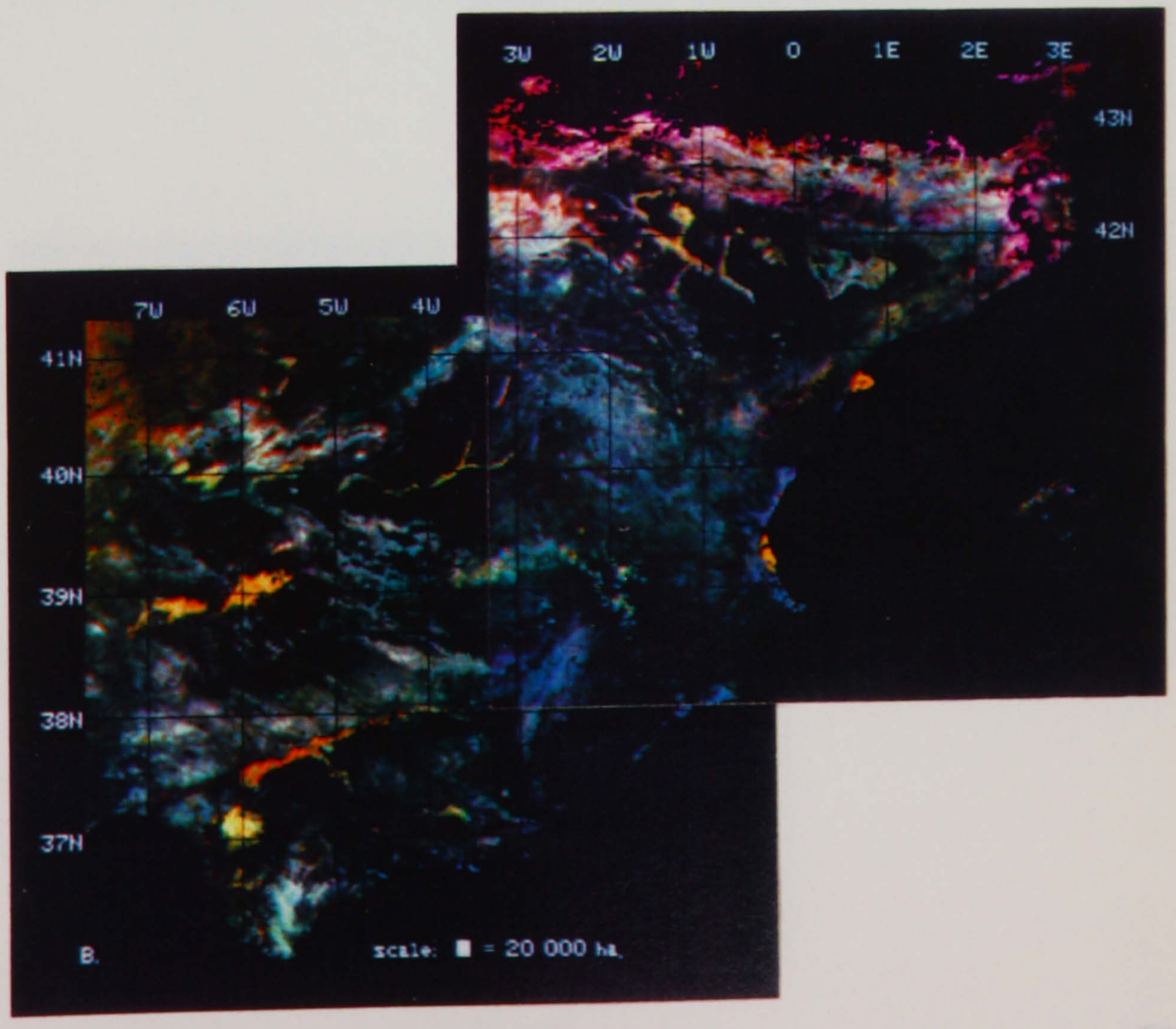

Figure 5. (conclusion) C) Spring 1986 (27th March (red), 15th May (green), 16th July (blue), D) Summer 1986 (2nd August (red), 27th August (green), 28th September (blue)

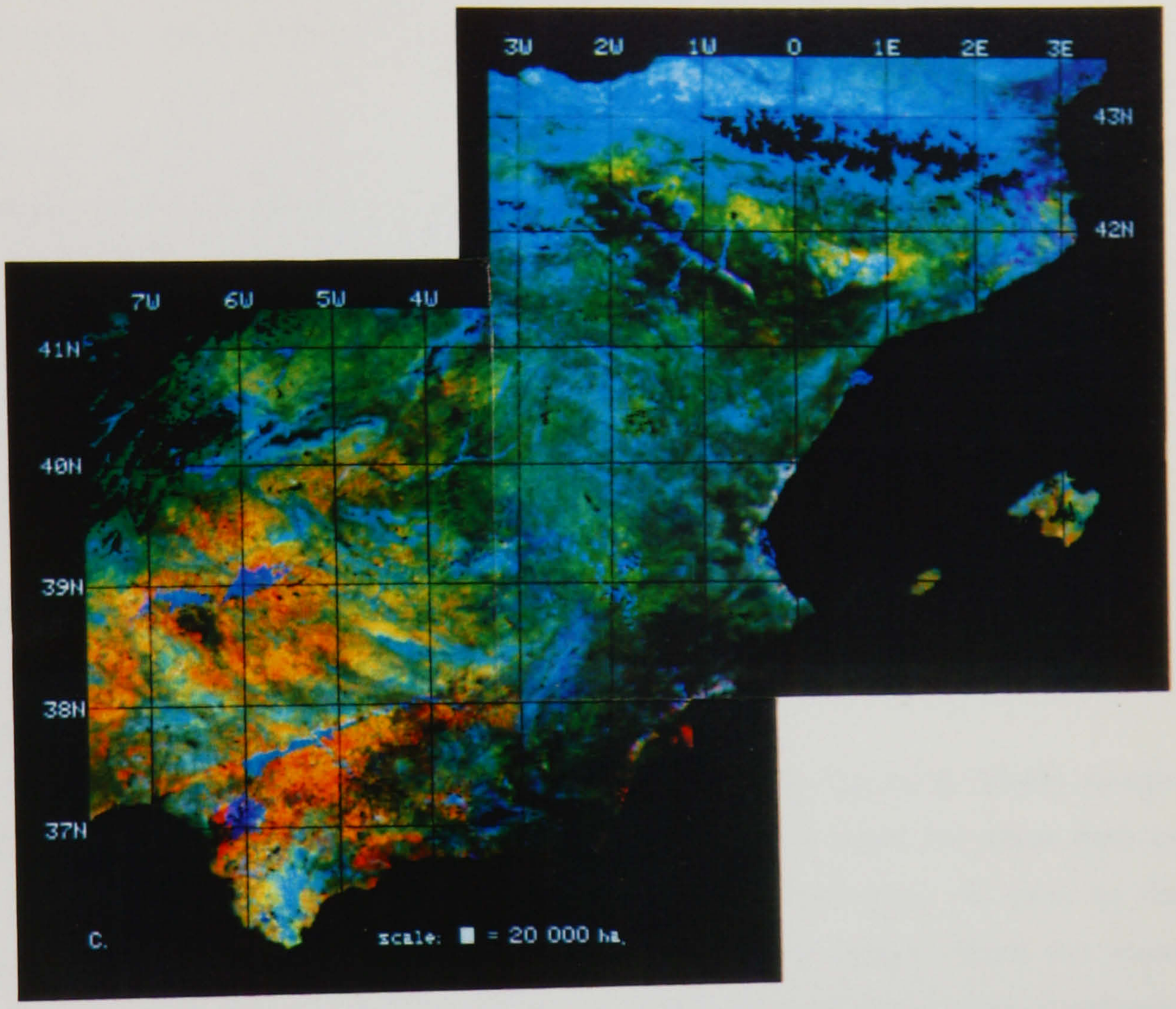

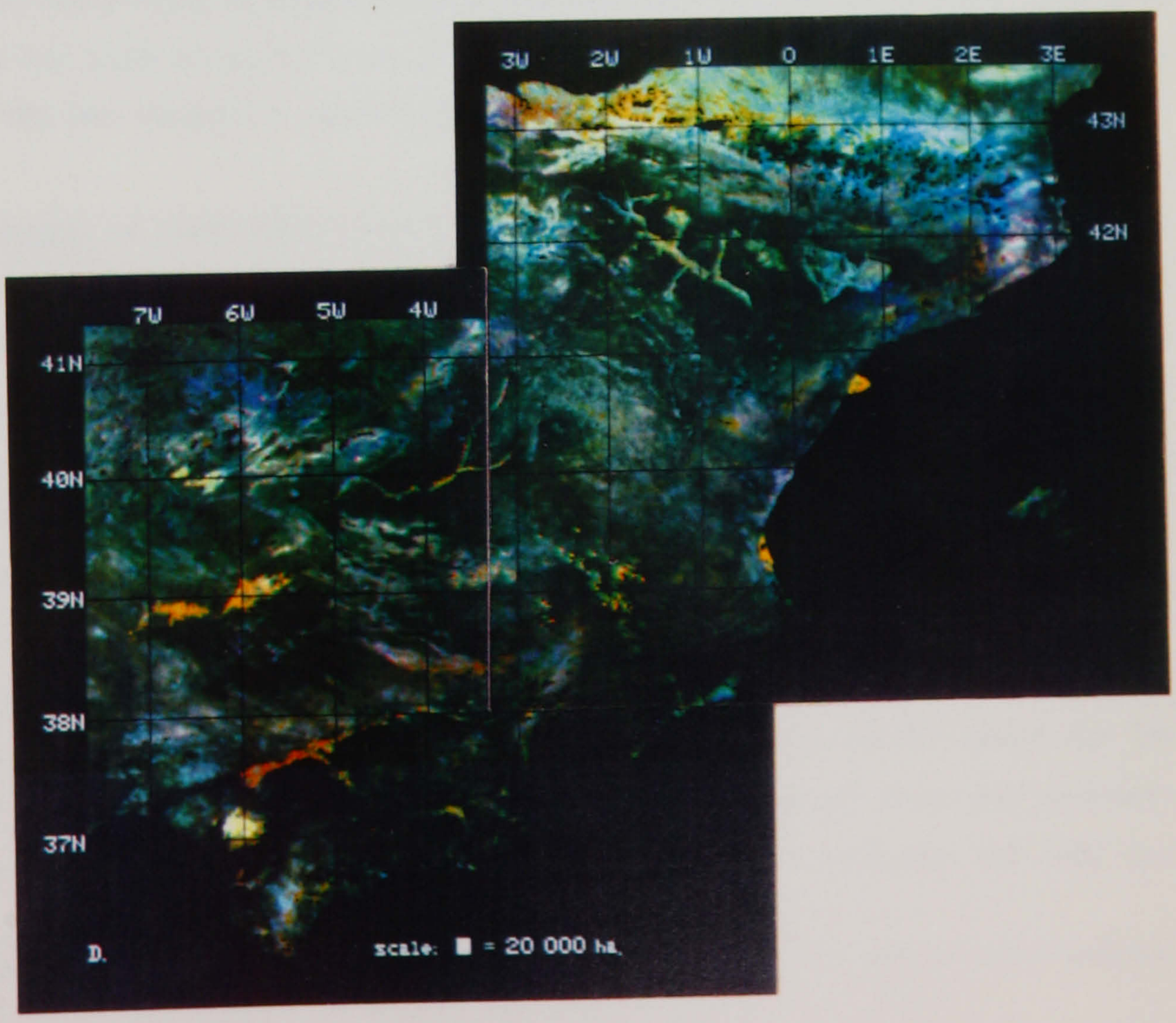

Although a few of the black pixels in figure 5 correspond to pixels that were devoid of significant vegetation, most correspond to pixels that contained visible radiance values greater than the cloud-mask threshold in at least one of the three images that make up the colour composite image. Thus, the red colour around the black area in the summer 1985 image of the Pyrenees is due to undetected cloud contamination in the 25th August image (i.e. the green band). Similarly, the blue and yellow areas at the western and eastern ends of the Pyrenees in the summer 1986 image are due to undetected cloud in the 2nd August and 28th September images respectively. Small red speckles south of Ciudad Real and in northeast Spain in Spring 1985 are due to undetected cloud in the 3rd May image. It is clear from these images that the simple monospectral thresholding method used to make the cloud masks was only partially successful[9].

3. A phytophenological description of northeastern and southern Spain

3.1 Mean daily NDVI

The mean daily NDVI for 1985 and 1986 is shown in figure 6. These images are produced as follows. First a time-integrated NDVI image is made for each date by multiplying the NDVI at each pixel by the sum of half the number of days to the previous image and half the number of days to the subsequent image. Then the mean daily NDVI for each pixel is calculated as the sum of the six individual time-integrated NDVI images for each six month period divided by the total number of days between the first and the last image (i.e. approximately two-hundred-and-twenty-three days).

The images of mean daily NDVI provide a qualitative measure of net primary production over northeastern and southern Spain. The highest values are located along the north coast and the northern side of the Pyrenees. Elsewhere, values are remarkably uniform over much of the study area with "islands" of higher mean daily NDVI associated usually with wooded mountain regions. The lowest levels of photosynthetic activity are found in the Ebro valley and the south-east although mean daily NDVI values are lower generally in the east than in the west.

The most obvious differences between the mean daily NDVI images for 1985 and 1986 are due to cloud contamination. Thus, the mean daily NDVI values for the north side of the Pyrenees are lower in 1985 than in 1986 because there was extensive and complete cloud contamination over much of this area on both the 3rd May and

9 Cloud masks produced by either bispectral thresholding (e.g. Barrett and D'Souza 1986) or trispectral cluster analysis (e.g. Harrison and Lucas 1988) might have been more successful

Figure 6. Northeastern and Southern Spain: Mean Daily NDVI.
A) 1985, B) 1986

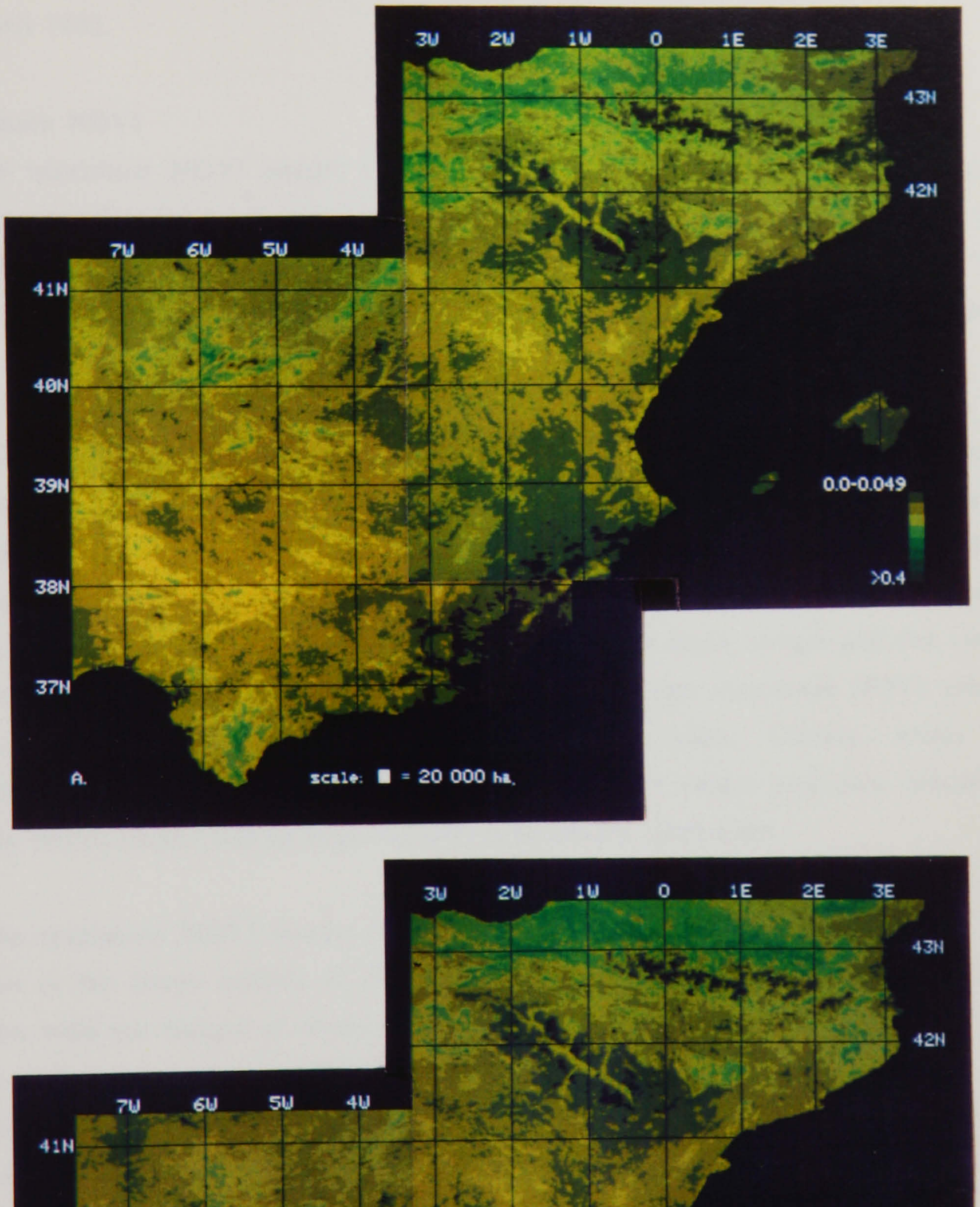

25th August 1985[10]. Similarly, the mean daily NDVI values for the south-east of Spain are lower in 1985 than in 1986 because this region was completely cloud contaminated on 2nd April 1985.

3.2 Maximum NDVI

The maximum NDVI images for 1985 and 1986 are shown in figure 7. These images were produced by retaining at each pixel the highest NDVI value of all six images. The only major difference between the images for 1985 and 1986 is in the south-east. This may be attributed to cloud contamination in the image for 2nd April 1985.

The images of maximum NDVI show spatial variations in the maximum intensity of photosynthetic activity between April and October over northeastern and southern Spain. The highest maximum NDVI values are located over the northern and western parts of the study area and the lowest values are located over the eastern and southeastern parts of the study area. A comparison between these images and the mean daily NDVI images reveals that there are more areas with high maximum NDVI values than there are areas with high mean daily NDVI values. Clearly, levels of photosynthetic activity in areas with high maximum NDVI values and only moderate mean daily NDVI values will be high for only a relatively short time.

The maximum NDVI images indicate that levels of photosynthetic activity are always low in the lower reaches of the Ebro valley and the south-east. Once again, a comparison with the images of mean daily NDVI is instructive. Figures 6 and 7 show that areas with low mean daily NDVI values are associated with areas of both high and low maximum NDVI values. Therefore it would seem that the imagery of maximum NDVI is better than imagery of mean daily NDVI for purposes of identifying areas of extremely sparse vegetation cover: An area with high NDVI values, even if they last only a short time, must be considered more densely vegetated than an area with perpetually low NDVI values.

3.3 Timing of maximum NDVI

The date on which the maximum NDVI values in figure 7 were recorded is shown in figure 8. The dates associated with the different colours in figure 8 are given in table 8.

---

10 Figure 5 shows the main areas of cloud contamination

Figure 7. Northeastern and Southern Spain: Maximum NDVI.
A) 1985, B) 1986

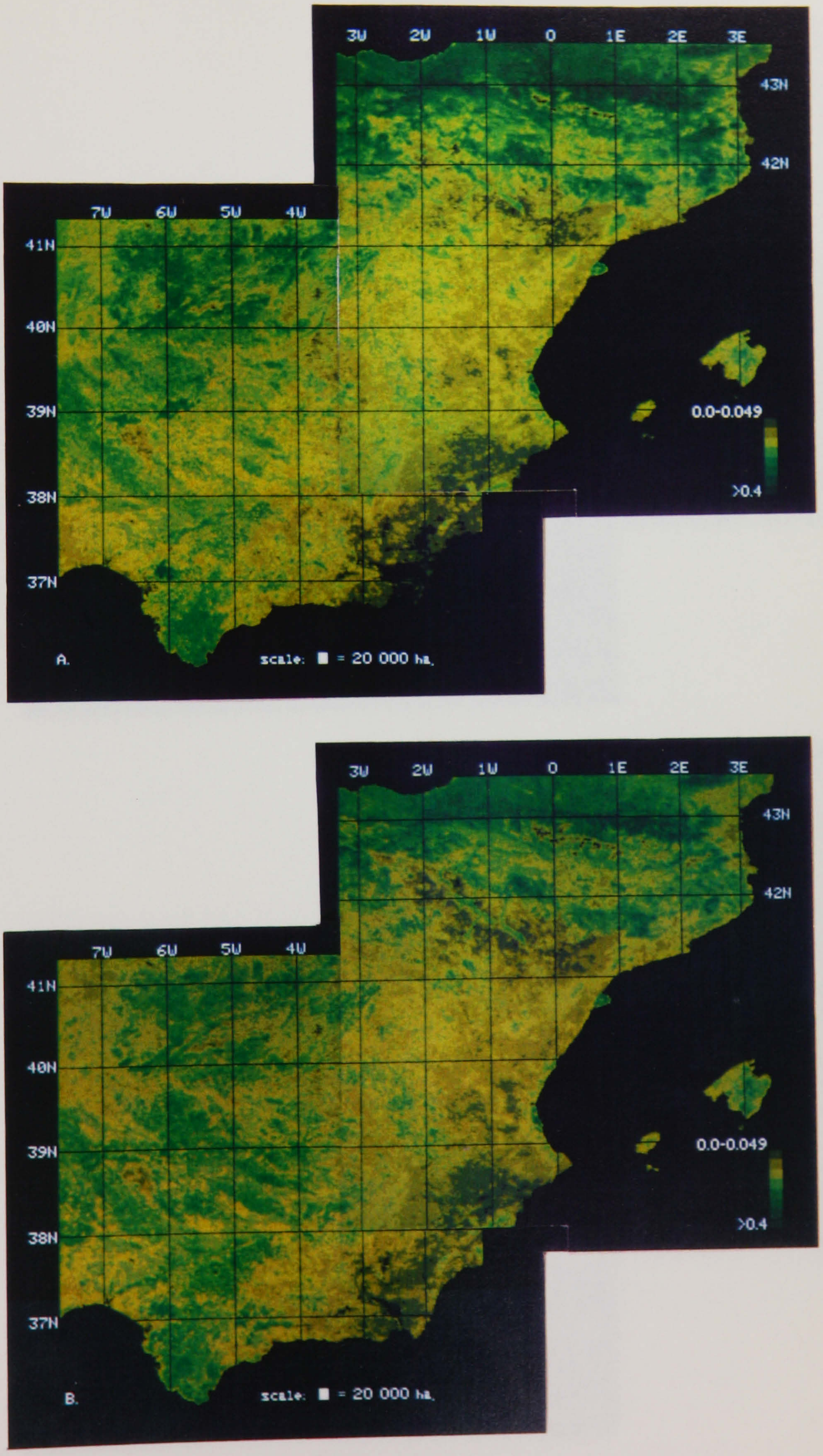

Figure 8. Northeastern and Southern Spain: Timing of Maximum NDVI.
A) 1985, B) 1986

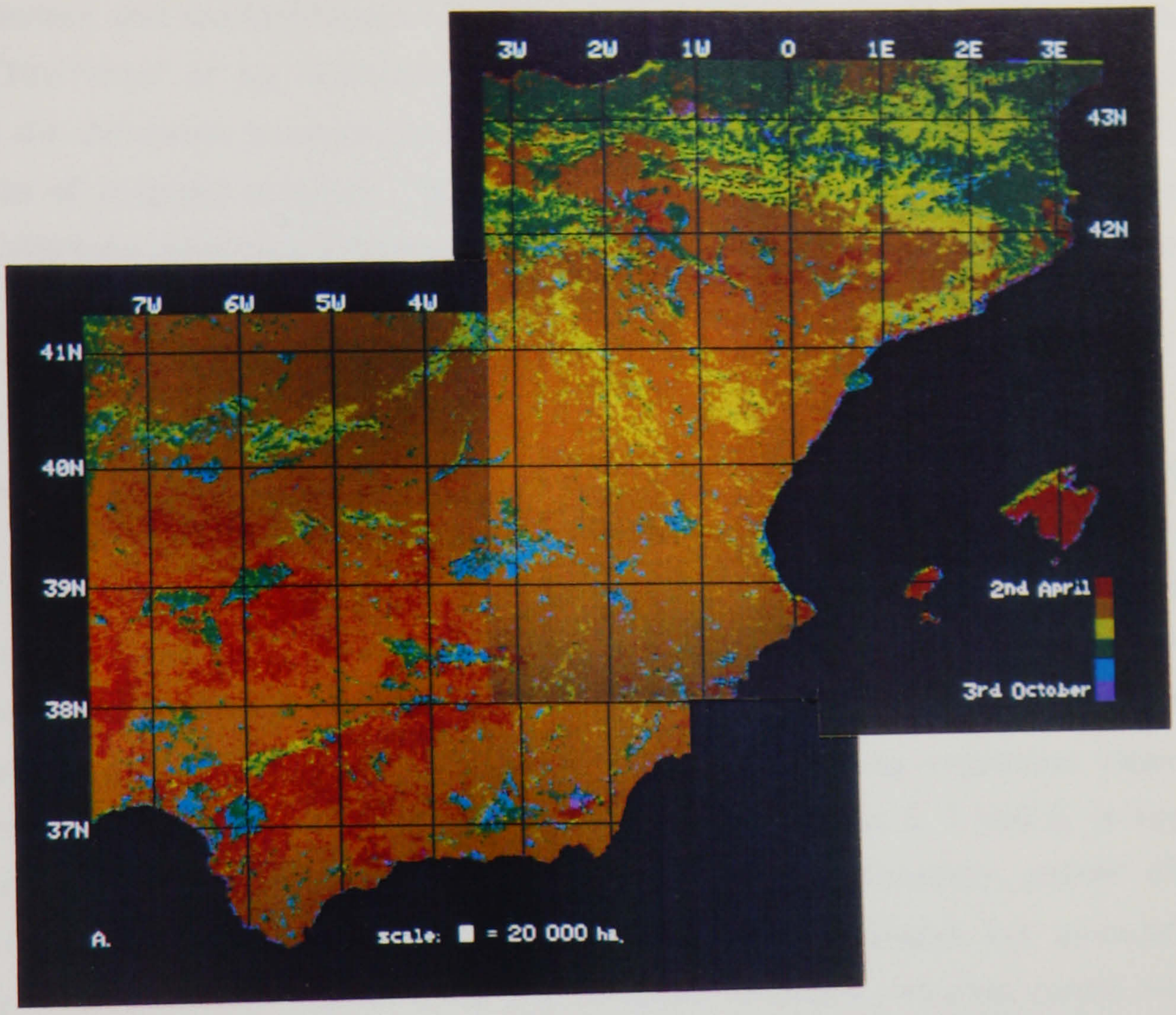

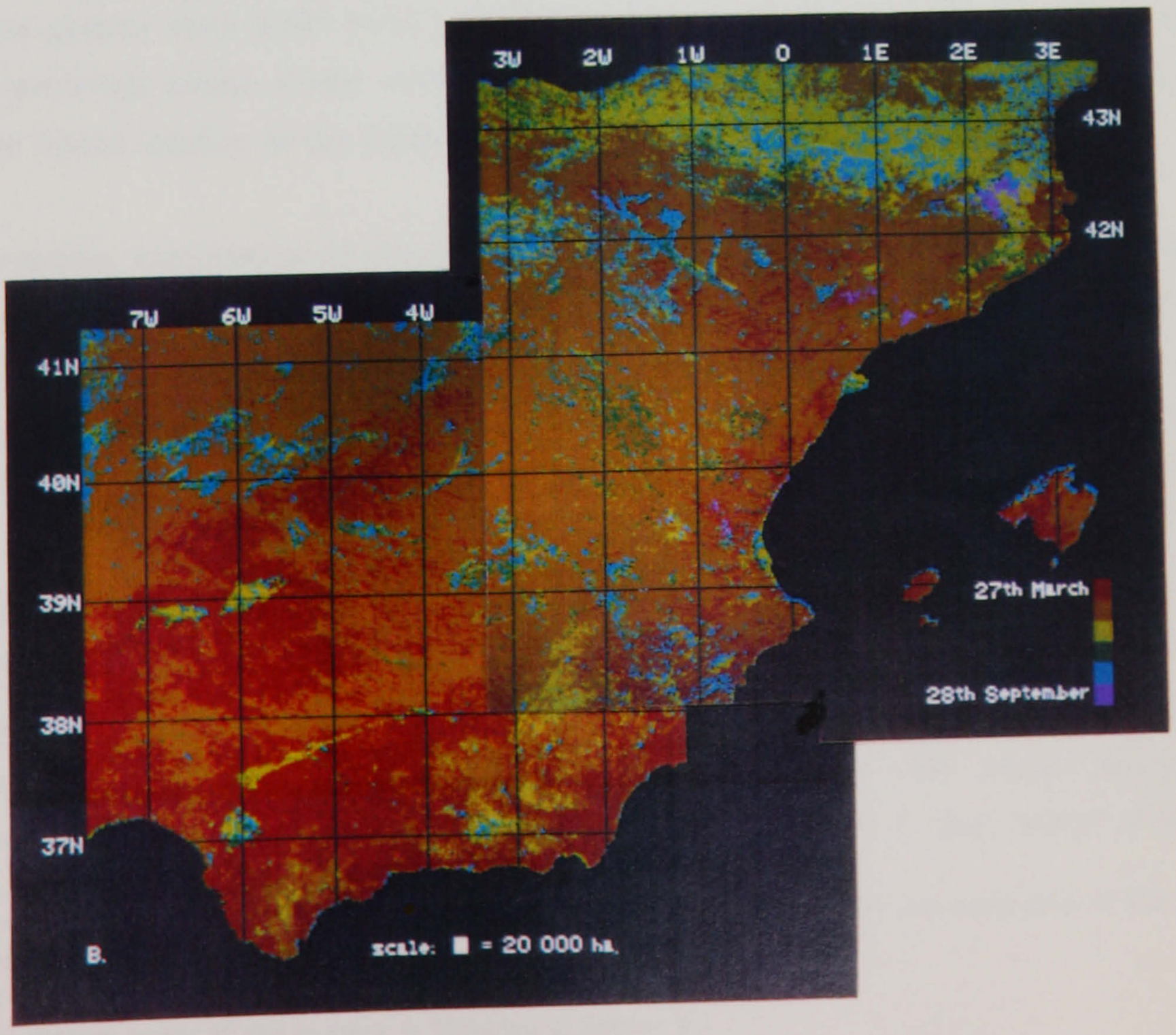

The images of the timing of maximum NDVI show spatial variations in the timing of the maximum intensity of photosynthetic activity between April and October over northeastern and southern Spain. The earliest peak NDVI values are found in the southwest. The "crest" of the "green wave"[11] occurs during May for most of the study area except the deciduous northern parts, where maximum NDVI values occur in July, and the areas of irrigated cropland. The timing of maximum NDVI values for irrigated areas vary although generally they are asynchronous with the surrounding vegetation cover.

3.4 Duration above 0.099 NDVI

Images showing the number of dates out of the total of six on which NDVI values over northeastern and southern Spain exceeded 0.099 between April and October 1985 and 1986 are shown in figure 9. 0.099 NDVI has been described as the threshold NDVI value that separates dormant vegetation from vegetation that is actively photosynthesising[12]. Whether or not this is true, figure 9 illustrates that the 0.099 NDVI threshold provides an effective means to discriminate among vegetation classes. Although many of the patterns in figure 9 are suggested in figures 6, 7 and 8, in none of these other images are these patterns so sharply defined. Generally, pixels with NDVI values greater than 0.099 NDVI in most of the six images are associated particularly with (wooded) upland areas and irrigated cropland, whereas pixels with NDVI values greater than 0.099 NDVI on just two or three dates are found mostly on the (cereal-growing) plains. Pixels with NDVI values that exceed 0.099 NDVI just once or never are found mainly in the Ebro valley and the south-east[13].

Interactive exploration of the original multidate imagery suggested that raising or lowering the threshold between approximately 0.06 and 0.12 NDVI does not alter significantly the number or the pattern of the classes, simply the number of dates on which a particular class exceeded the threshold. Clearly, raising or lowering the threshold NDVI by a very large amount will result in a loss of detail.

3.5 Discussion

The appeal of a phytophenological approach to the analysis of multidate NDVI data is that vast amounts of digital data are reduced to a few, relatively simple images with a minimum of interference from or interpretation by the image analyst. Furthermore, although it is apparent from figures 6, 7, 8 and 9 that some of the

---

11 i.e. the polewards movement of photosynthetic activity associated with the polewards movement of the sun during Spring

12 Chapter Two Section 4.4

13 The discriminatory power of this imagery is discussed in Section 3.2

Figure 9. Northeastern and Southern Spain: Period Above 0.099 NDVI.
A) 1985, B) 1986

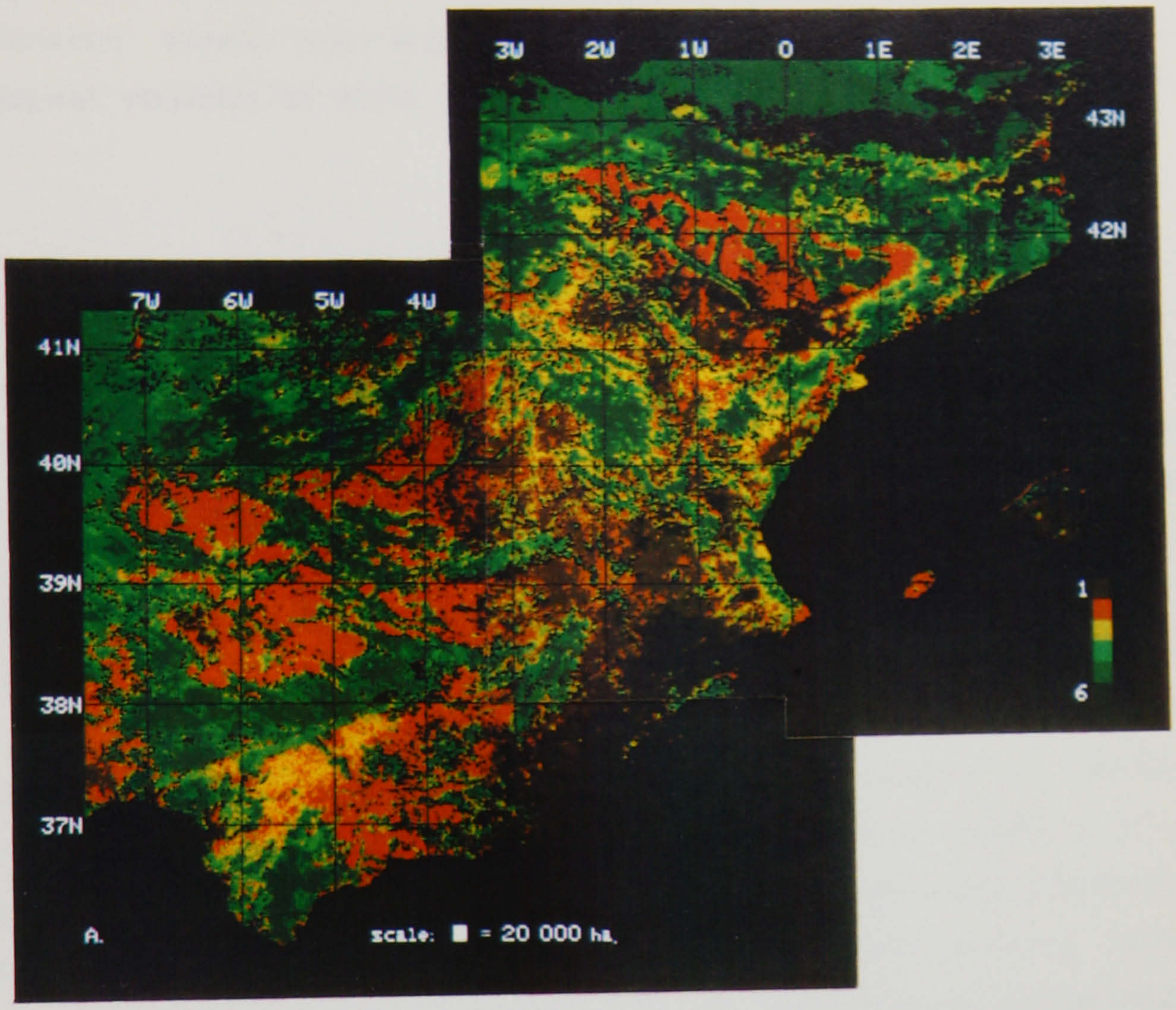

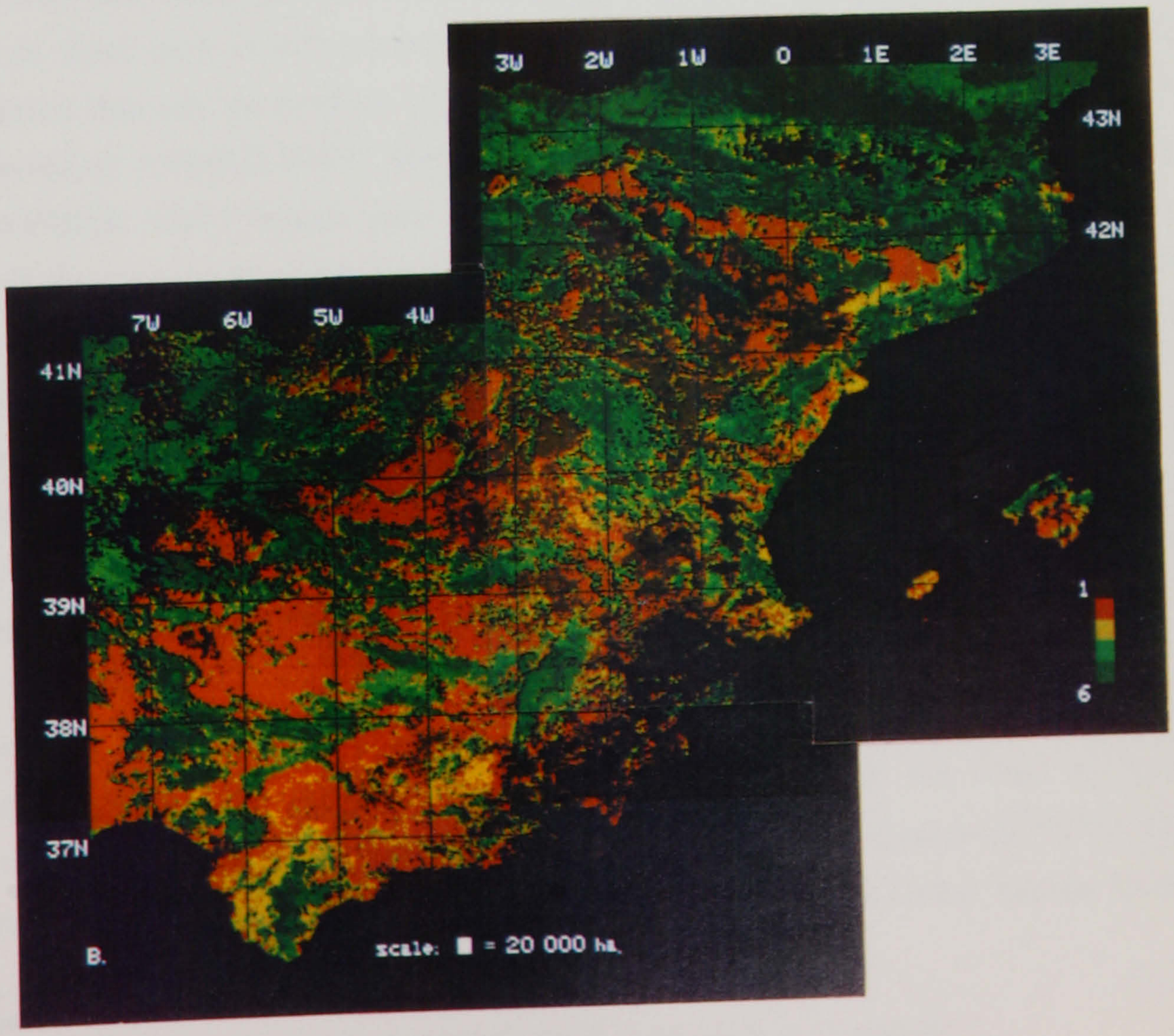

patterns found in imagery of one of the four phytophenological variables are found also in imagery of the other variables, this similarity between the images of the different variables should not disguise the fact that the meaning of the phytophenological variables in terms of vegetation photosynthetic activity is quite distinct.

1985 and 1986 were both years in which weather conditions in Spain were generally average. Carrillo Suárez (1988) states that the recent period of drought in Spain ended in 1984, while maps of monthly rainfall anomaly produced by the Royal Meteorological Office indicate that, although January and February received more rain in 1985 than 1986 especially in the South, March and April received more rain in 1986 than 1985. The occurrence of near-average meteorological conditions before and during the dates of the imagery in this study suggests that figures 6, 7, 8, and 9 describe average phytophenological conditions over northeastern and southern Spain.

Perhaps the most striking feature of the pairs of images of individual phytophenological variables for 1985 and 1986 is the interannual similarity of the patterns and NDVI values they reveal. However, although this interannual similarity is remarkable considering the uneven temporal resolution of the data and their variable quality, clearly, the main problem associated with the interpretation of interannual differences in these data is distinguishing between truly phytophenological differences and differences that are an artefact of image production. In spite of being among the best full resolution AVHRR NDVI data sets of Spain[14] that has been produced, the full resolution AVHRR NDVI images used in this study have three important shortcomings. They contain large areas of cloud contamination, their quality is uneven (i.e. the extent to which individual NDVI values are affected by scan angle and haze is not measured) and their temporal resolution is both coarse and uneven (i.e. the time interval between images is both too long and too variable). While these failings can be rectified easily by using many more single-date images[15], they limit the extent to which relatively minor interannual variations in the timing, intensity and duration of photosynthetic activity may be interpreted reliably.

The most that can be said of the interannual variations apparent in the images of the four phytophenological variables relates to the timing of the onset of Spring growth in 1985 and 1986. There is a larger area in 1986 with a maximum NDVI value on the first date of the six compared with 1985. This suggests that Spring growth

---

14 Or anywhere else

15 A suggestion for improving the quality of multidate NDVI data is made in Chapter Six

occurred sooner, in the south of Spain particularly, in 1986 than in 1985. Although ancillary information to support this interpretation is scarce, monthly rainfall anomaly maps for 1985 and 1986[16] suggest that southern Spain received considerably more rainfall in January and February 1985 than in the same months in 1986. Thus, it may be that the relatively clear skies during January and February 1986 resulted in a relatively early Spring in that year compared to 1985.

4. A phenological description of Iberian physiognomic and agricultural classes

4.1 Multidate NDVI characteristics of classes

In view of the shortcomings of the full resolution AVHRR NDVI data set described in the previous section, the analyses that follow relate primarily to the field sites described in Chapter Three Section 3.5. The NDVI temporal profile for each field site listed in table 5 is shown in table 9. All the Woodland and Parkland classes except Almond and Olive (1-9) have relatively high NDVI values throughout the period April to October. Deciduous Woodland (i.e. field site number 1) has the highest NDVI values of all the vegetation cover classes measured in this study. There is also a suggestion that the Coniferous Woodlands of Green Spain (3) are more photosynthetically-active than the Coniferous Woodlands of Brown Spain (4). The Evergreen Oak Woodlands of Cádiz (5) have NDVI values that are quite similar to those of the Deciduous Woodland of the Sierra de Gredos (2). The values for Evergreen Oak Parkland (6 and 7) are similar to those for Evergreen Oak Woodland except they are lower. The NDVI values for both Citrus (8) and Soft Fruit (9) are similar to the values for the Coniferous Woodland of Brown Spain (4) and Green Spain (3) respectively. Although there is an increase in NDVI values during the Spring months for both Woodland and Parkland classes, the Parkland classes' maximum NDVI value is earlier, lower and of shorter duration than it is for most of the Woodland classes. The relative lowness of the Parkland values may be attributed to the relative sparseness of Parkland tree cover. The relative earliness and short duration of the Parkland classes maximum NDVI value may be attributed to groundcover which forms an important part of the area-integrated response of Parkland and which is at its most photosynthetically-active for only a short period during Spring.

The NDVI values for Almond (10) and Olives (11 and 12) are particularly low. Indeed, the NDVI values for these classes for the Summer months are scarcely higher

16 Extractions from the Northern Hemisphere Rainfall Anomaly maps produced by the Royal Meteorological Office at Bracknell

Table 9. NDVI Temporal Profiles of Iberian Vegetation Cover Classes[a] (NDVI values in thousandths) (continued on next page)

Field Site	Year	2.4.1985 27.3.1986	3.5.1985 15.5.1986	5.7.1985 16.7.1986	24.7.1985 2.8.1986	25.8.1985 27.8.1986	3.10.1985 28.9.1986
1	1985	165	227	396	400	cloudy	196
	1986	75	290	333	298	282[b]	188
2	1985	141	251	259	259	208[c]	165
	1986	133	231	200	173[d]	212[b]	122
3	1985	173	224	251	255	153	165
	1986	137	212	212	200	208	149
4	1985	125	180	196	169	161	137
	1986	114	173	157	173	153	125
5	1985	224	314	243	286	290	200
	1986	200	247	251	208	192	188
6	1985	133	157	216	239	204	180
	1986	153	235	196	192	157	141
7	1985	235	318	129	133	110	86
	1986	247	295	125	114	133	149
8	1985	173	216	161	137	114	145
	1986	188	192	141	145	125	141
9	1985	200	271	255[c]	216	188[e]	176
	1986	180	263	235	200	220	196
10	1985	75	114	137	145	67	86
	1986	82	98	98	94	94	78
11	1985	98	114	78	67	47	59
	1986	102	102	55	55	71	94
12	1985	118	125	67	78	63	67
	1986	141	110	75	63	63	39

a. All field sites cover a 6x6 pixel area. One standard deviation from the mean value (1σ) is less than 0.040 NDVI (i.e. 40 thousandths) unless indicated

b. $1\sigma = 0.047$ NDVI c. $1\sigma = 0.043$ NDVI d. $1\sigma = 0.055$ NDVI e. $1\sigma = 0.051$ NDVI

than those for Matorral (21 and 22, discussed below). This is not surprising. Field observation suggests that there are usually large gaps between almond and olive trees and that, in addition, the canopies of both these trees are frequently sparse. The only surprise is that the northern (11) and southern (12) Olive classes have very similar NDVI values. Field observation suggests that olive trees in the south of Spain are frequently bigger and bushier than olive trees in the northeast.

Table 9. (conclusion)

Field Site	Year	2.4.1985 27.3.1986	3.5.1985 15.5.1986	5.7.1985 16.7.1986	24.7.1985 2.8.1986	25.8.1985 27.8.1986	3.10.1985 28.9.1986
13	1985	224[f]	208	106	67	35	20
	1986	282[d]	220	47	24	24	8
14	1985	282[b]	388	63	63	24	27
	1986	267	376	47	27	59	63
15	1985	55	86	75	106	86	86
	1986	75	86	78	67	82	71
16	1985	63	94	122	125	133	106
	1986	63	102	125	118	114	106
17	1985	47	24	271[c]	431	376	106
	1986	184	24	373	329	310	157
18	1985	0	0	247[g]	310[g]	184[h]	47
	1986	12	24	329[b]	290[i]	255[d]	47
19	1985	71	98	184	275[c]	176[b]	110
	1986	86	114	200	243[b]	227	125
20	1985	118	153	188	298	278	133
	1986	55	153	259	278	282	157
21	1985	55	82	27	24	16	20
	1986	43	67	27	12	35	39
22	1985	31	75	27	24	27	20
	1986	78	78	47	27	47	0

f. $1\sigma = 0.071$ NDVI g. $1\sigma = 0.067$ NDVI h. $1\sigma = 0.063$ NDVI i. $1\sigma = 0.078$ NDVI

Cropland (13 and 14) and Rice (17 and 18) have a particularly distinctive NDVI temporal profiles. The NDVI values for Cropland are in the Spring and very low values in the Summer while those for Rice are low in Spring, high in Summer and low again in Autumn. Irrigated Mixed Cropland (19 and 20) has a Summer maximum NDVI also. Although this class has a different NDVI profile to Rice, high NDVI values being neither as high nor as short-lived as they are for Rice, it has a similar NDVI profile to several of the Woodland classes. Vine (15 and 16) has quite low NDVI values on all dates although there is a clear Summer maximum. The lowness of the Vine NDVI values may be attributed to the large areas of bare earth between rows of vines.

The NDVI values for both Matorral field sites (21 and 22) are generally low. These are values one would expect for areas where the vegetation cover is extremely sparse except for a short period in the Spring.

4.2 Phytophenological characteristics of classes

The phytophenological characteristics of the physiognomic and agricultural vegetation cover classes in table 5 are shown in tables 10, 11, 12 and 13. Table 10 shows that the mean daily NDVI of most classes for the period April to September is between 0.05 and 0.25 NDVI. The highest values are for Deciduous and Evergreen Oak Woodland (i.e. field sites 1 and 5) and Soft Fruit Parkland (9) while the lowest values are for Almond and Olive Parkland (10, 11 and 12), Vine (15) and Matorral (21 and 22).

Table 11 shows that the maximum NDVI of Iberian vegetation cover classes varies from less than 0.05 to greater than 0.349. There are more classes with high maximum NDVI values than with high mean daily NDVI values. In addition to Deciduous and Evergreen Oak Woodland (1 and 5) and Soft Fruit Parkland (9), Evergreen Oak Parkland (7), Cereals and Sunflowers (14) and Rice (17)) also have high Maximum NDVI values. The classes with low maximum NDVI values are Almond and Olive Parkland (10, 11 and 12), Vine (15) and Matorral (21 and 22).

Table 12 shows that the maximum NDVI for most Iberian Vegetation Cover Classes appears to occur during the Spring months. Only Deciduous and Coniferous Woodland (1 and 3), Vine (16), Rice (17 and 18) and Mixed Irrigated Cropland (19 and 20) have maximum NDVI values later than mid-May in both years.

Table 13 shows that the 0.099 NDVI threshold divides Iberian Vegetation Cover Classes into four groups. These are classes that exceed 0.099 NDVI throughout most of the period from April to September (i.e. all classes of Woodland and Parkland except Almond and Olive Parkland (i.e. 1 to 9) and also some areas of Mixed Irrigated Cropland (20)), classes that exceed 0.099 NDVI for three to five months (i.e. Vine (16), Rice (17 and 18), some areas of Mixed Irrigated Crops (19), classes that exceed 0.099 NDVI for a two month period (i.e. Cereals and Sunflowers (13 and 14) and classes that exceed 0.099 NDVI for fewer than two months (i.e. Almond and Olive Parkland (10, 11 and 12), Vine (15) and Matorral (21 and 22)).

Table 10. Mean Daily NDVI of Iberian Vegetation Cover Classes

Field Site	NDVI (thousandths)						
	<50	50-99	100-149	150-199	200-249	250-299	>299
1[a]	-	-	-	-	29	7	
1[b]		-	-	-	3	30	3
2	-	-	-	12	24		
	-	-	4	13	19		
3	-	-	-	17	19		
	-	-	-	25	11		
4	-	2	26	8			
	-	-	34	2			
5	-	-	-	-	6	30	
	-	-	-	4	32		
6	-	-	8	28			
	-	-	3	31	2		
7	-	-	-	35	1		
	-	-	-	7	29		
8	-	-	10	26			
	-	-	8	28			
9	-	-	-	4	32		
	-	-	-	3	33		
10	-	35	1				
	1	33	2				
11	1	35					
	2	34					
12	-	26	10				
	-	27	9				
13		1	31	4			
	-	-	23	13			
14	-	-	22	14			
	-	-	12	24			
15	-	35	1				
	-	36					
16	-	-	36				
	-	-	36				
17	-	-	-	20	16		
	-	-	-	11	25		
18	-	6	20	10			
	-	-	16	20			
19	-	-	16	20			
	-	-	10	26			
20	-	-	-	32	4		
	-	-	3	31	2		
21	26	10					
	20	16					
22	33	3					
	2	34					

a. 1985

b. 1986

Table 11. Maximum NDVI of Iberian Vegetation Cover Classes

Field Site	NDVI (thousandths)						
	50-99	100-149	150-199	200-249	250-299	300-349	>349
1[a]	-	-	-	-	-	-	36
1[b]	-	-	-	-	-	-	36
2	-	-	-	8	22	6	
	-	-	4	14	18		
3	-	-	-	9	24	3	
	-	-	-	34	2		
4	-	6	27	3			
	-	8	28				
5	-	-	-	-	11	25	
	-	-	-	16	19	1	
6	-	-	6	20	10		
	-	-	8	24	4		
7	-	-	-	1	5	26	4
	-	-	-	2	20	14	
8	-	-	10	26			
	-	-	10	26			
9	-	-	-	-	32	4	
	-	-	-	3	33		
10	2	29	5				
	23	13					
11	20	16					
	34	2					
12	-	34	2				
	-	8	26	2			
13	-	-	1	8	8	16	3
	-	-	1	8	15	9	3
14	-	-	-	-	-	3	33
	-	-	-	-	8	24	4
15	16	20					
	27	8					
16	-	25	11				
	-	26	10				
17	-	-	-	-	-	-	36
	-	-	-	-	3	9	24
18	-	2	4	7	1	12	10
	-	-	2	3	8	13	10
19	-	-	2	10	10	13	
	-	-	2	10	20	4	
20	-	-	-	-	14	20	2
	-	-	1	3	16	16	
21	25	11					
	1	35					
22	36						
	22	14					

a. 1985

b. 1986

Table 12. Timing of Maximum NDVI for Iberian Vegetation Cover Classes

Field Sites	27.3 1986 2.4.1985	15.5.1986 3.5.1985	16.7.1986 5.7.1985	2.8.1986 24.7.1985	27.8.1986 25.8.1985	28.9.1986 3.10.1985
1[a]	-	-	-	36		
1[b]	-	13	20	3		
2	-	22	9	5		
	-	20	-	5	11	
3	-	1	11	24		
	-	14	18	2	2	
4	-	13	20	3		
	6	19	2	5	4	
5	-	26	-	8	2	
	-	16	20			
6	-	-	5	29	2	
	-	31	3	1	1	
7	-	36				
	2	34				
8	1	34	1			
	20	13	3			
9	-	24	12			
	-	32	3	-	1	
10	7	25	3	1		
	5	24	1	4	1	1
11	2	34				
	13	20				
12	13	23				
	36					
13	20	14	2			
	23	13				
14	2	34				
	-	36				
15	-	20	-	12	4	
	9	19	-	-	8	
16	-	3	8	10	13	2
	-	7	20	1	8	
17	-	-	-	36		
	-	-	32	3	1	
18	-	-	4	27	5	
	-	-	24	6	6	
19	-	-	2	33	1	
	-	-	2	26	8	
20	-	-	-	31	5	
	-	2	11	9	14	
21	5	31				
	1	35				
22	-	36				
	17	17	2			

a. 1985

b. 1986

Table 13. Period Above 0.099 for Iberian Vegetation Cover Classes[a]

Field Sites	Number of images						
	0	1	2	3	4	5	6
1[a]	7	-	-	-	-	27	2
1[b]	-	-	-	-	2	31	3
2	-	-	-	-	1	3	32
	1	-	-	-	5	4	26
3	-	-	-	-	-	11	25
	-	-	-	-	-	-	36
4	4	-	1	2	8	20	2
	3	-	-	2	10	16	5
5	-	-	-	-	-	-	36
	-	-	-	-	-	4	32
6	-	-	-	-	-	12	24
	1	-	-	-	-	8	27
7	-	-	-	-	6	22	8
	1	-	-	-	-	13	22
8	1	-	-	-	2	9	24
	-	-	-	-	-	4	32
9	-	-	-	-	-	3	33
	1	-	-	-	-	6	29
10	2	18	13	2	1		
	22	12	2				
11	21	11	4				
	34	2					
12	3	4	28	1			
	-	32	4				
13	2	-	11	20	3		
	-	-	35	-	1		
14	-	-	36				
	-	-	35	1			
15	17	16	1	2			
	22	14					
16	-	-	-	3	19	12	2
	3	-	-	2	20	11	
17	1	-	-	13	20	2	
	1	-	-	-	2	33	
18	3	1	3	27	2		
	1	-	5	25	4	1	
19	1	-	-	10	20	5	
	2	-	-	5	11	12	7
20	2	-	-	-	-	14	20
	4	-	-	-	1	27	4
21	25	8	3				
	36						
22	36						
	23	11	2				

a. 1985

b. 1986

4.3 Discussion

Two points emerge from examination of tables 9 to 13. The first is that no vegetation class in either year's data is associated with a single value for all the phytophenological variables. Although several vegetation classes are associated overwhelmingly with one mean daily NDVI value range and one timing of maximum NDVI date, many of the vegetation classes are associated with several ranges of maximum NDVI and several period above 0.099 NDVI classes. Furthermore, phytophenological differences between field sites of the same physiognomic or agricultural vegetation class (e.g. Deciduous Woodland (1 and 2) and Vine (15 and 16)) may be observed. These within-class differences are due to the differences between the two field sites described in Chapter Three Section 5. For example, Field Site 1 is covered almost entirely by a dense, deciduous forest whereas Field Site 2 includes areas of Matorral, Evergreen Oak Parkland, Olive Parkland, Almond Parkland, Mixed Irrigated Cropland and Cropland in addition to Deciduous Woodland.

The within-class variability of a multidate NDVI class may be expressed in terms of the variance and standard deviation from a mean NDVI value. However, the data in tables 10 to 13, which express within-class variability using phytophenological variables rather than NDVI values, reveal that some within-class variability is associated clearly with phenological differences among the field site pixels of individual field sites. For example, the pixels which make up the Tarragona Rice field site (18) have similar timing of maximum NDVIs and mean daily NDVIs but quite variable seasonal maximum NDVIs and periods of time above 0.099 NDVI. Within-class variation of this type is apparent for almost every vegetation cover class. It indicates that the vegetation cover of nearly all the field sites selected for this study is sufficiently heterogeneous for the differences to be detectable in full resolution AVHRR NDVI imagery.

The second point that emerges from tables 9 to 13 is that similar phytophenological characteristics are shared by vegetation classes that are distinct, physiognomically or agriculturally, almost as often as they are by vegetation classes that are similar, physiognomically or agriculturally. A variety of measures of class separability have been devised (e.g. Singh 1984,1987). An advantage of the data in tables 10 to 13 is that they reveal the phytophenological bases of between-class similarity. For example, Coniferous Woodland (3) has a similar mean daily NDVI to Rice (17), the maximum NDVI for Olive (11) is similar to that for Vine (15), the timing of maximum NDVI for Matorral (21) is similar to that for Cropland (14) and

the period above 0.099 NDVI for Deciduous Woodland (1) is similar to that for Irrigated Mixed Crops (20).

The data in tables 10 to 13 relate to field sites that were selected for their vegetation cover uniformity. However, it is apparent from tables 9 to 13 that not only do several of the field sites not represent areas of homogeneous vegetation cover, but that, even when they do, several of the classes have very similar phytophenological (i.e. multidate NDVI) characteristics. This does not bode well for the derivation of physiognomically-based vegetation maps from multidate full resolution AVHRR NDVI imagery, particularly when one remembers that most pixels in such imagery represent areas of vegetation cover that are less homogeneous than the field sites.

5. Mapping the vegetation of northeastern and southern Spain

5.1 Introduction

An indication of the vegetation mapping potential of multidate full resolution AVHRR NDVI data is provided by the frontispiece. In this image, figure 4(A), 4(B) and 4(C) have been displayed simultaneously through the red, green and blue guns respectively of a colour monitor. The result is an image in which colours describe the timing and duration of photosynthetic activity (e.g. red and green make yellow, green and blue make cyan etc.) and brightness describes the intensity of photosynthetic activity (e.g. dark tones are associated with low levels of photosynthetic activity). In this section an attempt is made to simplify and reduce the patterns and shades in the frontispiece to vegetation maps in which the classes are defined precisely.

Classified multidate full resolution AVHRR NDVI imagery of northeastern Spain is shown in figure 10. These images are derived from the images for 1986. Classified multidate full resolution AVHRR NDVI imagery of southern Spain is shown in figure 11. These images are derived from the full resolution AVHRR NDVI images for 1985. The minimum distance classification and the binary tree classification use all six images for each year (see table 8). Since *Cluster* is limited to a maximum of five single-band images, the first five images only of northeastern and southern Spain for each year were used (i.e. all images except those for 3rd October 1985 and 28th September 1986). The 1985 images of northeastern Spain and the 1986 images of southern Spain were not classified because they are too cloud contaminated (figure 5).

Figure 10. Northeastern Spain (1986): Classified Multidate Full Resolution AVHRR NDVI Imagery. A) Cluster Analysis, B) Minimum Distance Classification, C) Supervised Binary Decision Tree Classification

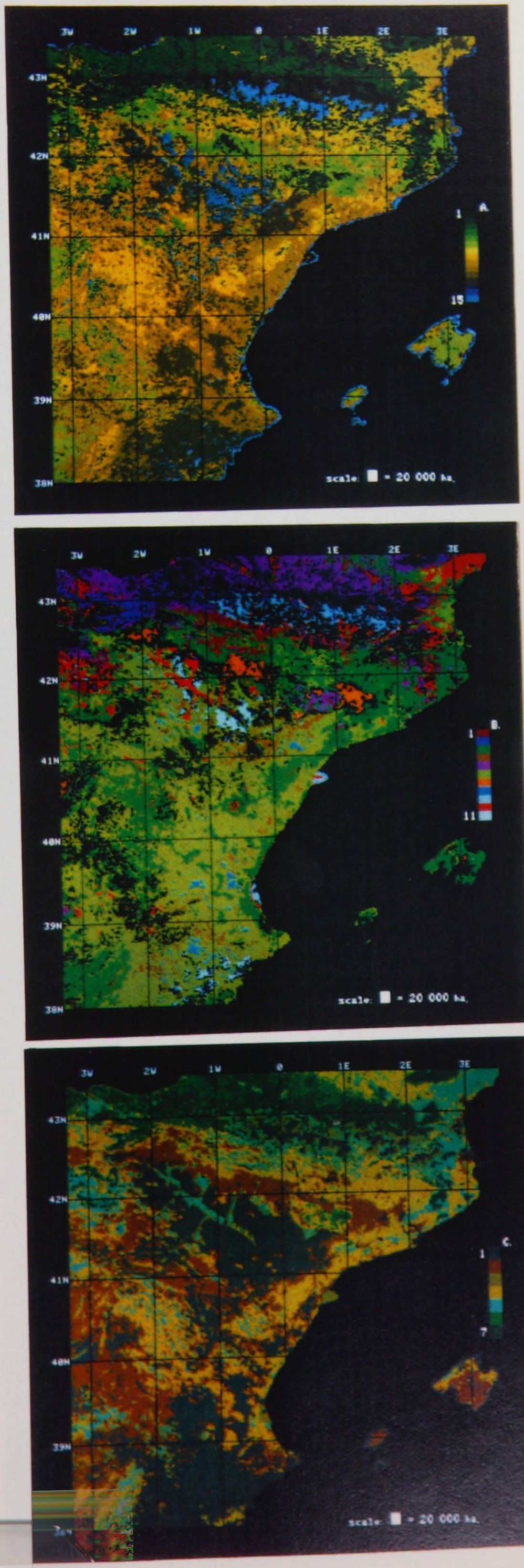

Figure 11. Southern Spain (1985): Classified Multidate Full Resolution AVHRR NDVI Imagery. A) Cluster Analysis, B) Minimum Distance Classification, C) Supervised Binary Decision Tree Classification

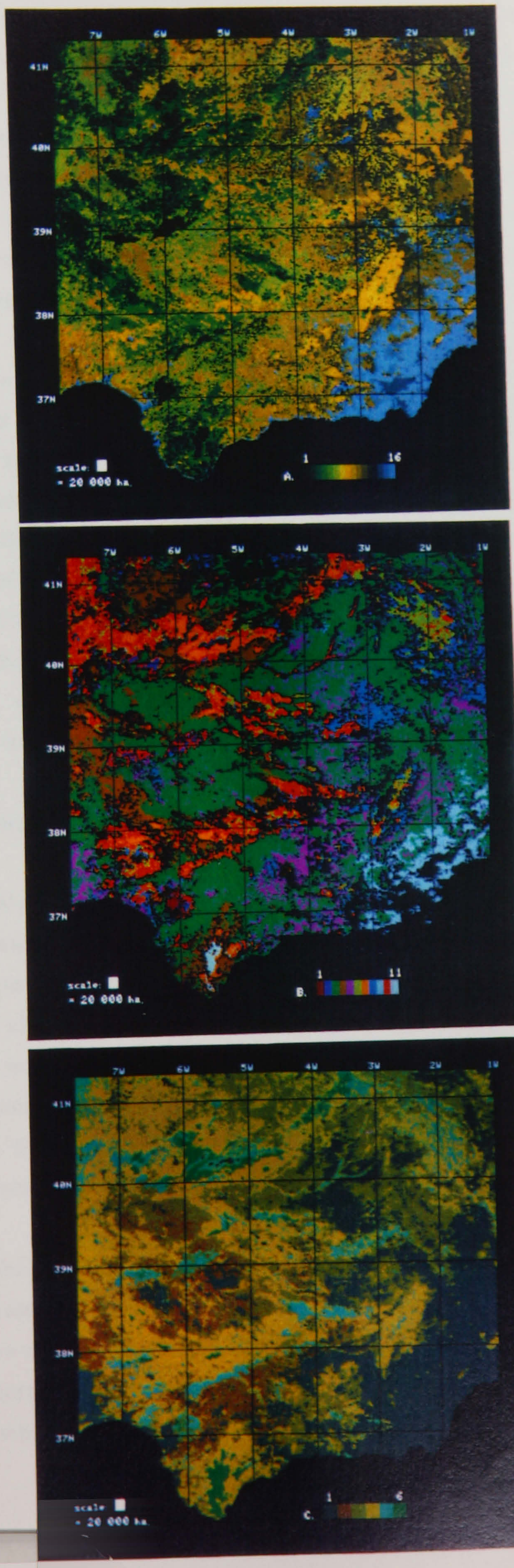

5.2. Cluster analysis

The pattern of classes in northeastern and southern Spain produced by the three classification algorithms is quite similar although the total number of classes in each image ranges from six to sixteen. The larger number of classes in the images produced by cluster analysis is a clear indication of the superior sensitivity of this classifier to the intrinsic variations within the multidate NDVI feature space. Tables 14 and 15 show that several of the cluster analysis classes do not appear to correspond with any of the vegetation cover classes in table 5. The location of these classes suggests that they are associated primarily with pixels that were either cloud contaminated or misregistered in one or more of the images.

The relation between the *Cluster* classes and the physiognomic and agricultural classes is generally ambiguous. Most *Cluster* classes are associated with at least two physiognomic or agricultural classes. Similarly, most physiognomic and agricultural classes are associated with at least two *Cluster* classes. However, a pseudo-natural colour scheme is used for the two maps derived from cluster analysis. Low-numbered classes are coloured shades of green and high-numbered classes are coloured shades of brown and grey. The basis for this simple colour coding is the association suggested by tables 14 and 15 between low-numbered classes and vegetation cover types with high NDVI values (e.g. woodland and parkland) and high-numbered classes and vegetation cover types with low NDVI values (e.g. Olive and Matorral). In fact, several of the "greenest" classes in both northeastern and southern Spain (e.g. Deciduous and Evergreen Oak Woodland, Cropland and Irrigated Cropland) are unclassified by *Cluster*.

5.3 The minimum distance classifier

The minimum distance classifier used training statistics derived from the field sites. This is the reason for the strong correlation between field site pixels and classes produced by this classifier shown in tables 16 and 17. Of course, the veracity of the classified images would have been tested more rigourously if different field sites for each class had been used for verification purposes than those used to produce the training statistics. Unfortunately, extensive areas of the vegetation cover classes listed in table 5 are uncommon (Chapter Three Section 3.5).

The distribution of some minimum distance classes such as Rice, Deciduous Woodland (northeastern Spain) and Cropland (southern Spain) seems to be correspond with reality. However, the distribution of others, notably Citrus and Deciduous Woodland (southern Spain), is clearly wrong. The problem here is one of misclassification which is due to the fact that the training statistics for the different

Table 14. Northeastern Spain: Confusion Matrix Showing the Occurrence of Field Site Pixels within Classes Produced by Cluster Analysis

	Field Site										
Class	1	3	8	9	10	11	14	15	18	19	21
1[a]	-	10	22	1							
1[b]	-	4	-	3	-	-	-	-	1		
2	-	18	-	26							
	-	10	20	14	-	-	-	-	-	1	
3	-	7	-	5							
	13	-	-	4							
4	28	1									
	-	13	-	13	-	-	-	-	-	13	
5	-	-	12	1							
	-	-	-	-	-	-	3				
6	-	-	2	-	-	-	-	4	5	3	
	-	-	8	1	-	-	1				
7	-	-	-	-	-	-	22				
	-	6	-	-	-	-	-	-	1		
8	1	-	-	-	-	-	-	-	2	1	
	-	2	2	-	-	-	-	-	-	6	
9	-	-	-	-	14	6	-	28			
	-	-	1	-	2						
10	-	-	-	-	-	-	-	-	13	31	
	-	-	1	-	-	-	-	2			
11	-	-	-	-	4						
	-	-	-	-	-	-	-	-	9	7	
12	-	-	-	-	1	-	-	-	-	1	
	-	-	-	-	28	35	-	34	-	-	11
13	-	-	-	-	-	-	-	3	1		
	-										
14	-	-	-	-	-	-	-	-	3		
	-										
15	-	-	-	-	16	29	-	-	-	-	36
	-	-	-	-	5	1	-	-	-	-	25
Unclassified	7	-	-	3	1	1	14	1	12		
	23	1	4	1	1	-	32	-	25		

a. 1985 b. 1986

Table 15. Southern Spain: Confusion Matrix Showing the Occurrence of Field Site Pixels within Classes Produced by Cluster Analysis

	Field Site										
Class	2	4	5	6	7	12	13	16	17	20	22
1[a]	-	-	-	-	22	-	10				
1[b]	1	-	-	11	5						
2	3	-	-	20	-	-	-	-	-	4	
	26	5	22	20	-	-	-	-	-	2	
3	-	-	-	-	13	-	2				
	-	-	-	-	31	-	13				
4	22	5	1	4	-	-	-	-	-	1	
	-	-	-	-	-	-	13				
5	-	-	-	-	-	-	6				
	-	-	-	-	-	-	1				
6	-	3	-	3	-	-	-	2			
	4	27	-	4	-	-	-	17	-	1	
7	-	-	-	-	-	-	1				
	-	-	-	-	-	-	6				
8	-	24	-	-	-	-	-	19			
	-	1	-	-	-	3	1				
9	-	-	-	-	-	18	2				
	-	1	-	-	-	-	-	2	-	2	
10	-	2	-	-	-	16	-	14	-	-	1
	-	1	-	-	-	-	-	17	-	-	1
11	-	-	-	-	-	-	1				
	-										
12	-	2	-	-	-	2	1				
	-	-	-	-	-	33	-	-	-	-	13
13	-										
	-										
14	-										
	-	-	-	-	-	-	-	-	-	-	4
15	-	-	-	-	-	-	-	-	-	-	1
	-	-	-	-	-	-	-	-	-	-	17
16	-	-	-	-	-	-	-	-	-	-	34
	-										
Unclassified	11	-	35	9	1	-	13	1	36	31	
	5	1	14	1	-	-	2	-	36	31	1

a. 1985 b. 1986

Table 16. Northeastern Spain: Confusion Matrix Showing the Occurrence of Field Site Pixels within Classes Produced by the Minimum Distance Classifier

	Field Site										
Class	1	3	8	9	10	11	14	15	18	19	21
1[a]	-	13									
1[b]	-	32									
2	36										
	36										
3	-	2	35								
	-	2	36	1							
4	-	-	-	-	24	26	-	-	-	-	1
	-	-	-	-	5	19	-	2			
5	-	18	-	36							
	-	2	-	35							
6	-	-	1	-	3	-	-	7			
	-	-	-	-	25	9	-	10	-	-	2
7	-	-	-	-	-	-	36				
	-	-	-	-	-	-	36				
8	-	-	-	-	-	-	-	26	1		
	-	-	-	-	2	-	-	24			
9	-										
	-	-	-	-	-	-	-	-	22	1	
10	-	-	-	-	-	-	-	1	4	36	
	-	-	-	-	-	-	-	-	12	35	
11	-	-	-	-	-	2	-	-	-	-	27
	-	-	-	-	4	5	-	-	-	-	34
Unclassified	-	3	-	-	9	8	-	2	31	-	8
	-	-	-	-	-	3	-	-	2		

a. 1985

b. 1986

classes are not sufficiently distinctive. Field experience and ancillary information sources may enable an experienced analyst to reinterpret misclassified pixels. Thus, it seems reasonable to assert that many of the pixels classified as Citrus correspond to areas of Coniferous Woodland. However, reinterpretation is clearly an undesirable, subjective process. For example, the true nature of the vegetation cover represented by

Table 17. Southern Spain: Confusion Matrix Showing the Occurrence of Field Site Pixels within Classes Produced by the Minimum Distance Classifier

	Field Site										
Class	2	4	5	6	7	12	13	16	17	20	22
1[a]	-	-	-	-	-	-	-	-	36		
1[b]	-	-	-	-	-	-	-	-	36		
2	-	-	-	-	-	-	-	-	-	34	
	-	-	-	-	-	-	-	-	-	29	
3	-	-	-	-	-	-	33				
	-	-	-	-	-	-	31				
4	-	-	-	-	35						
	-	-	-	-	29						
5	-	-	-	-	-	36					
	-	-	-	-	-	36	-	-	-	-	3
6	-	5									
	-	14	-	2							
7	31	-	-	-	-	-	-	-	-	2	
	35	13	7	18	1	-	-	2	-	4	
8	-	13	-	-	-	-	-	34			
	-	8	-	-	-	-	-	34			
9	-	-	-	-	-	-	-	-	-	-	34
	-	-	-	-	-	-	-	-	-	-	32
10	5	3	-	36	-	-	-	2			
	1	-	1	16							
11	-	-	36								
	-	-	27								
Unclassified	-	15	-	-	1	-	3	-	-	-	2
	-	1	1	-	6	-	5	-	-	3	1

a. 1985

b. 1986

class 6 (northeastern Spain), apparently a class representing Almond, Olive and Vine according to table 16, is far less obvious.

There are large numbers of unclassified pixels in the minimum distance classified images of both northeastern and southern Spain. This suggests that the training statistics described incompletely the variability within the multidate NDVI

feature space. There are two ways in which the number of unclassified pixels might have been reduced. The first involves using more field sites for each class while the second involves relaxing the threshold decision boundary value for each class (set at two standard deviations from the mean). The danger associated with both of these "solutions" is that they would reduce classification accuracy. Thus, although the use of more field sites would increase the proportion of the total variability of the vegetation cover class that is contained in the training statistics, probably it would be associated also with some loss of the distinctive NDVI characteristics of each class. Similarly, although relaxing the threshold decision boundary value for each class would reduce the number of unclassified pixels, probably it would increase the number of misclassified pixels.

5.4 The supervised binary decision tree

The supervised binary decision tree classifiers used to classify the multidate full resolution AVHRR NDVI imagery of northeastern and southern Spain are shown in figure 2 (A) and (B). Although, nominally, there are twelve classes for northeastern Spain and eighteen classes for southern Spain, fewer classes are displayed in figures 10 and 11. The reason for this is that several of the binary tree classes are either impossible or else represented by so few pixels that they were merged with other, closely related classes.

Tables 18 and 19 show that, in common with cluster analysis and the minimum distance classifier, the classes produced by the binary tree classifier correspond only partially with agricultural and physiognomic vegetation classes. However, unlike the classes produced by *Cluster* and *Classify*, the classes produced by the supervised binary decision tree classifier have a precise, phytophenological meaning.

The definition of the various binary tree classes is as follows. Class 1 (northeastern and southern Spain) has mean daily NDVI values (April to September) less than 0.1. Classes 2 and 3 (northeastern Spain) have mean daily NDVI values between 0.1 and 0.199 and NDVI values greater than 0.099 on fewer than four dates. Classes 4 and 5 (northeastern Spain) have mean daily NDVI values between 0.1 and 0.199 and NDVI values greater than 0.099 on four dates or more. Classes 6 and 7 (northeastern Spain) have mean daily NDVI values greater than 0.199 and NDVI values greater than 0.099 on more than four dates. The difference between classes 2 and 3, 4 and 5, and 6 and 7 (northeastern Spain) is that the maximum NDVI for classes 2, 4 and 6 was on or before 15th May 1986 whereas the maximum NDVI for classes 3, 5 and 7 was after the 15th May 1986. Classes 2 and 3 (southern Spain) have mean daily NDVI

Table 18. Northeastern Spain: Confusion Matrix Showing the Occurrence of Field Site Pixels within Classes Produced by the Binary Decision Tree Classifier

Class	Field Site										
	1	3	8	9	10	11	14	15	18	19	21
1[a]	-	-	-	-	34	36	-	35	6	-	36
1[b]	-	-	-	-	34	36	-	36	-	-	36
2	-	-	-	-	1	-	36				
	-	-	-	-	1	-	36				
3	1	-	1	-	-	-	-	1	27	11	
	-	-	-	-	-	-	-	-	31	6	
4	-	-	35	3							
	-	10	34	3							
5	-	17	-	1	-	-	-	-	2	25	
	-	14	2	-	-	-	-	-	5	29	
6	-	1	-	19							
	12	5	-	28							
7	29	18	-	13							
	24	6	-	4							
Unclassified	6	-	-	-	1	-	-	-	1		
	-	1	-	1	1	-	-	-	-	1	

a. 1985
b. 1986

values between 0.1 and 0.199 and NDVI values greater than 0.099 on fewer than four dates. The difference between them is that class 2 had a maximum NDVI on the 2nd April 1985 whereas class 3 had a maximum NDVI on the 3rd May 1985. Classes 4 and 5 have mean daily NDVI values between 0.1 and 0.199 and NDVI values greater than 0.099 on four dates or more. The difference between them is that class 4 had a maximum NDVI on or before the 3rd May 1985 whereas class 5 had a maximum NDVI after 3rd May 1985. Class 6 (southern Spain) has mean daily NDVI values greater than 0.199.

A pseudo-natural colour scheme is used for the binary tree classifications. Classes associated with high NDVI values appear shades of green and classes associated with low NDVI values appear shades of brown and grey. This colour scheme emphasises the particularly strong similarity between the binary tree classification and the cluster analysis classification. Since classes produced by cluster analysis correspond

Table 19. Southern Spain: Confusion Matrix Showing the Occurrence of Field Site Pixels within Classes Produced by the Binary Decision Tree Classifier

	Field Site										
Class	2	4	5	6	7	12	13	16	17	20	22
1[a]	-	1	-	-	-	26	1	-	-	-	36
1[b]	-	-	-	-	-	27	-	-	-	-	36
2	-	-	-	-	-	4	27				
	-	-	-	-	-	8	22				
3	-	5	-	-	-	6	14	3	10		
	-	5	-	-	-	-	12	4	1	3	
4	1	10	-	-	35	-	3	3			
	7	20	3	28	6	-	1	6			
5	11	20	-	36	-	-	-	29	10	32	
	10	10	1	5	-	-	-	26	10	31	
6	24	-	36	-	1	-	-	-	13	4	
	19	-	32	2	29	-	-	-	25	2	
Unclassified	-	-	-	-	-	-	1	1	3		
	-	1	-	1	1	1	1				

a. 1985
b. 1986

to natural groupings of the raw data[17], the similarity between the pattern of classes produced by the two classifiers lends support to the argument that the most appropriate classification schemes for multidate NDVI imagery are phenologically-based.

5.5 Discussion

It seems reasonable to presume that the classification produced by all three classifiers would be improved if more frequent and better quality imagery were available. However, on the basis of the results presented here it appears that a supervised binary decision tree classifier is particularly well-suited to classify small scale multidate NDVI imagery on account of its combining important features of cluster analysis and the minimum distance classifier. The supervised binary decision tree classifier defines classes solely in terms of their multidate NDVI characteristics (i.e. like *Cluster*), yet these classes have a (phytophenological) meaning in terms other than the NDVI (like *Classify*). Furthermore, the meaning of the phytophenological classes produced by the supervised binary decision tree classifier is unequivocal

17 Section 5.2

whereas the reliability of the physiognomic and agricultural classes produced by *Classify* is not. Of course, the phytophenological meaning of the supervised binary decision tree classes in figures 10 and 11 is strictly qualitative due primarily to the shortcomings of the satellite data. However, successful quantitative interpretation of imagery of phytophenological variables presented elsewhere[18] indicates the potential of this approach.

It may be that supervised binary decision tree classifiers provide also the best way to map physiognomic and agricultural vegetation classes. Although the binary tree classifications presented in figures 10 and 11 are expressly phenological with classes defined in terms of the timing, intensity and duration of photosynthetic activity, clearly, the values at the non-terminal nodes of the decision tree could be set so as to discriminate between physiognomic and agricultural vegetation classes insofar as these are phenologically-distinct.

6. Summary

Twelve NDVI images derived from eighteen High Resolution Picture Transmission images of the Iberian Peninsula are used to describe and classify the vegetation cover of northeastern and southern Spain. The general phytophenological characteristics of the study area are described using four, single-date images and the phytophenological characteristics of 1985 and 1986 are compared using images of phytophenological variables which provide a concise and readily interpretable summary of multidate NDVI imagery. Thirteen Iberian vegetation cover classes are defined. The multidate NDVI and phytophenological characteristics of these classes are described and the implications for image classification of within-class spectral variability and between-class spectral similarity of these classes are discussed. Vegetation cover maps produced by cluster analysis, the minimum distance classifier and the supervised binary decision tree classifier are described. Although each classificatory approach has its merits, the analysis presented here suggests that the binary tree classifier is particularly well-suited to create classifications from multidate NDVI imagery.

---

18 See Chapter Two Section 4

Chapter Five

Vegetation Mapping Using Spatially-Degraded AVHRR NDVI imagery

1. Spatially-degraded AVHRR NDVI imagery

Two types of small scale NDVI imagery are produced routinely by NOAA from full resolution AVHRR data. These are Global Area Coverage NDVI imagery and the Global Vegetation Index. In addition, a special 8km spatial resolution NDVI product derived from AVHRR Global Area Coverage and covering Africa only is produced jointly by the Global Inventory Monitoring and Modeling Studies programme at the National Aeronautics and Space Administration Goddard Space Flight Center and the Food Securities Group at the United Nations Food and Agricultural Organization. Global Vegetation Index imagery is the most readily available and cheapest of these three types of spatially-degraded AVHRR NDVI imagery (tables 2 and 3).

The Global Vegetation Index is available currently on three different map projections (Appendix 2). In each case, each Global Vegetation Index pixel is assigned the NDVI value of just one Global Area Coverage pixel. Since a single Global Area Coverage pixel value is the area-integrated response of an area of approximately 350 hectares whereas individual Global Vegetation Index pixels represent an area on the ground of at least 12 800 hectares (Appendix 1), clearly, all Global Vegetation Index imagery is the product of drastic spatial subsampling.

The production of NDVI values for Global Vegetation Index imagery involves temporal subsampling also. Each Global Vegetation Index image is a seven-day maximum NDVI value composite. Although this compositing period was designed to remove cloud contaminated pixels from the imagery, it is too short for areas of persistent cloudiness (e.g. midlatitudes and tropical areas). Consequently, most users of Global Vegetation Index imagery have opted to sacrifice temporal precision in order to reduce the amount of cloud contamination. For example, Tucker *et al.* (1985a), Townshend *et al.* (1985), Goward *et al.* (1985) and Malingreau (1986) used twenty-one date composting periods, while Justice *et al.* (1985), Tucker *et al.* (1986a) and Townshend *et al.* (1987) used twenty-eight day compositing periods.

This chapter describes an evaluation of polar-stereographic format Global Vegetation Index imagery for the period January 1985 to December 1986 for purposes of mapping vegetation. The evaluation is presented in three parts. Section 3 describes an attempt to quantify the effects of spatial and temporal subsampling techniques on the NDVI values in Global Vegetation Index imagery. Although several workers have noted that Global Area Coverage and Global Vegetation Index NDVI values are frequently unrealistically high NDVI (e.g. Malingreau 1986; Townshend and Justice 1986), this study presents the first attempt to measure this distortion. Section 4 contains a phytophenological description of Africa and Section 5 describes how imagery of phytophenological variables derived from Global Vegetation Index imagery may be used to map vegetation cover.

2. Preparation of spatially-degraded AVHRR NDVI imagery

One-hundred-and-four weekly Global Vegetation Index images produced by the NOAA 9 AVHRR/2 between January 1985 to December 1986 were taken from the archive of Global Vegetation Index imagery at Bristol. These images were processed to make twenty-four twenty-eight- and thirty-five-day maximum NDVI value composites corresponding as closely as possible to calendar months (table 20).

Interactive investigation of the data revealed a lack of fit between first and second generation polar-stereographic Global Vegetation Index imagery[1]. Since first generation polar-stereographic imagery was produced directly from the Global Area Coverage data whereas second generation polar-stereographic imagery was remapped from the Global Vegetation Index plate carrée array, it seems reasonable to presume that the first generation polar-stereographic world map is the more accurate of the two. Misregistration between the two data types is worse for some areas than for others. For example, first and second generation imagery of the continent of Africa and the Iberian Peninsula are not badly misregistered. Indeed, the lack of fit between the first and second generation imagery of the Iberian Peninsula could be rectified by a simple translation

i.e. 1st sample = 2nd sample - 1 (4)

1 The imagery for January, February and March 1985 is first generation imagery (Appendix 1)

Table 20. Global Vegetation Index Monthly Maximum NDVI Value Composites

Image	Start and End Dates of "Month"	Number of Days per "Month"
January 1985	31st December-27th January[a]	35
January 1986	3rd-28th January	28
February 1985	4th February-3rd March	28
February 1986	29th January-25th February	28
March 1985	4th-30th March	28
March 1986	26th February-1st April	35
April 1985	1st-29th April[b]	28
April 1986	2nd-29th April	28
May	30th April-3rd June	35
June	4th June-1st July	28
July	2nd-29th July	28
August	30th July-2nd September	35
September	3rd-30th September	28
October	1st-28th October	28
November	29th October-2nd December	35
December	3rd-30th December	28

a. Two weeks missing
b. 8th April (Julian day 98) not used

where **1st sample** is the x-co-ordinate of the first generation image and **2nd sample** is the x co-ordinate of the second generation image. On the other hand, first and second generation polar-stereographic format images of South-East Asia may be adrift by as many as three pixels in both the x and the y directions. This misregistration has not been reported elsewhere.

Monthly maximum NDVI value Global Vegetation Index composites of Spain and Africa for 1985 and 1986 were extracted from the Global data set and remapped to equal area radial projections using the algorithm provided by Kidwell (1986). The Global Vegetation Index images of the Iberian Peninsula were remapped to the equal area radial array described in Chapter Four Section 1. The monthly Global Vegetation Index images of Africa were remapped to an equal area radial projection with standard parallels at 25°N and S, latitudinal limits from 37.6°N-35.1°S, longitudinal limits from

20°W to 55°E, and a spatial resolution of 27 500 hectares per pixel. The spatial resolution is approximately the mean area represented by polar-stereographic Global Vegetation Index pixels over Africa. The latitudinal limits produce minimal shape distortion between 35°N and 35°S. For example, a square area equivalent to 100 hectares in the image has dimensions on the ground of 1.10x0.91km at 35°N and S, 1.0x1.0km at 25°N and S and 0.91x1.10km at the Equator.

3. Comparison between real and simulated Global Vegetation Index imagery

3.1 Characteristics of the contemporaneous data sets

This comparison uses full resolution AVHRR NDVI imagery and Global Vegetation Index imagery of northeastern and southern Spain. Maximum NDVI value composites were made for the months of April and July 1985 and May and August 1986 and time-integrated NDVI images for the period April to September were made for 1985 (southern Spain) and 1986 (northeastern Spain). The dates of the individual NDVI images used to make each maximum NDVI value composite image are given in table 21. Although the High Resolution Picture Transmission and Global Vegetation Index images are contemporaneous, table 21 shows that the composite Global Vegetation Index NDVI values may be derived from as many as thirty-five separate measurements, whereas the composite full resolution AVHRR NDVI values are derived from no more than three measurements. While this is clearly less than ideal, a comparison between the two data sets is meaningful because full resolution AVHRR imagery from both the beginning and the end of the month is used. Thus significant phytophenological changes during the month will be present in both data sets.

The method used to make the time-integrated full resolution AVHRR NDVI images has been described already[2]. The method used to make the time-integrated Global Vegetation Index images is very similar. First a time-integrated NDVI image was made for each month by multiplying the NDVI at each pixel by the number of days in the month (i.e. twenty-eight or thirty-five). Then the mean annual daily NDVI for each pixel was calculated as the sum of the twelve individual time-integrated NDVI images for each year divided by the total number of days in the year.

The monthly and the time-integrated full resolution AVHRR NDVI images of northeastern and southern Spain were spatially-degraded to make imagery in which individual pixels represent areas on the ground of 40 000 hectares. These spatially-

2 Chapter Four Section 3.1

Table 21. Imagery Used for Evaluation of Preparation Methods on Global Vegetation Index Values

Image Date (Location)	High Resolution Picture Transmission	Global Vegetation Index
April, 1985 (Southern Spain)	2nd April 29th April 8th May	1-29th April
July, 1985 (Southern Spain)	5th July 21st July 26th July	2-29th July
May, 1986 (Northeastern Spain)	9th May 21st May	30th April-3rd June
August, 1986 (Northeastern Spain)	2nd August 21st August 2nd September	30th July-2nd September

degraded full resolution AVHRR-NDVI images are called x16 imagery. A single pixel in the x16 imagery represents the same area as a single (remapped) Global Vegetation Index pixel. However, the Global Vegetation Index pixel is assigned the NDVI value from just one Global Area Coverage pixel, whereas the x16 imagery produced for this study has pixels whose NDVI value is based on the mean area-integrated NDVI value of all two-hundred-and-fifty-six full resolution base map array pixels contained within a single x16 pixel (i.e. there is no spatial subsampling).

The full resolution monthly AVHRR NDVI images contain small patches of cloud cover. Therefore a simple cloud mask was made for each area consisting of all full resolution AVHRR pixels with an NDVI value of zero at any time during the two monthly compositing periods. Cloud mask pixels are ignored in the comparison between the three data sets discussed below. The areas of images that are compared, excluding the cloud masks, are shown in table 22.

3.2 Results and discussion

The mean NDVI values of all pixels in the monthly and time-integrated NDVI images are shown in table 23. The figures in this table show that, whereas the mean NDVI values for the full resolution and the x16 imagery are very similar, the mean NDVI values for Global Vegetation Index imagery is consistently higher. The standard deviation for the Global Vegetation Index mean values is higher also than it is for either the full resolution AVHRR or the x16 imagery.

Table 22. Area of Imagery Used for Evaluation of Preparation Methods on Global Vegetation Index Values[a]

	Northeastern Area	Southern Area
Number of Full Resolution Pixels	151 289	188 959
Area in Hectares	23 638 906	29 524 844
Area in km²	486	543
Number of Global Vegetation Index Pixels[b]	591	738

a. Excluding areas covered by cloud in full resolution AVHRR NDVI imagery

b. One (remapped) Global Vegetation Index pixel covers an area of 40 000 hectares

Table 23. Mean NDVI Values for Full Resolution and Spatially-Degraded AVHRR NDVI Imagery of Northeastern and Southern Spain

	NDVI Values (thousandsths)				
Image (Location)	FR[a]	x16[b]	GVI[c]	x16-FR	GVI-x16
April (Southern)	187 (56)[d]	182 (45)	237 (68)	-5	+55
July (Southern)	121 (54)	117 (42)	171 (63)	-4	+54
May (Northeast)	179 (65)	175 (53)	264 (83)	-4	+89
August (Northeast)	138 (73)	134 (62)	206 (92)	-4	+72
Integrated[e] 1985 (Southern)	121 (36)	121 (31)	192 (50)	0	+71
Integrated[e] 1986 (Northeastern)	135 (49)	139 (45)	220 (71)	+4	+81

a. Full resolution AVHRR NDVI imagery

b. Spatially-degraded full resolution AVHRR NDVI imagery

c. Global Vegetation Index imagery

d. One standard deviation from the mean (1σ)

e. Presented as mean daily NDVI. The integration period for full resolution AVHRR NDVI imagery is 223 days. The integration period for Global Vegetation Index imagery is 182 days

The areal extent of selected NDVI-value ranges is shown in table 24. The figures in this table show that the Global Vegetation Index imagery has more higher NDVI values and fewer lower NDVI values than the full resolution imagery, whereas the x16 imagery has fewer extreme values, both high and low, than the full resolution imagery. These differences are illustrated in figure 12.

Table 24. Areal Extent of Selected NDVI-Value Ranges in Full Resolution and Spatially-Degraded AVHRR NDVI Imagery of Northeastern and Southern Spain

NDVI	Area in hectares x10^6				
	FR[a]	x16[b]	GVI[c]	x16-FR	GVI-x16
			April, 1985		
0.0-0.099	1.79 (6)[d]	1.53 (5)	0.47 (2)	-0.26 (1)	-1.06 (4)
0.1-0.199	15.66 (53)	17.45 (59)	8.56 (29)	1.79 (6)	-8.89 (30)
0.2-0.299	11.30 (38)	10.47 (36)	15.11 (51)	-0.83 (3)	4.64 (16)
0.3-0.399	0.70 (3)	0.08 (-)	5.15 (18)	-0.69 (2)	5.07 (17)
0.4-0.499			0.24 (1)		0.24 (1)
			July, 1985		
0.0-0.099	11.32 (38)	10.62 (36)	2.51 (9)	-0.70 (2)	-8.11 (28)
0.1-0.199	15.67 (53)	17.63 (60)	18.97 (64)	1.96 (7)	1.34 (5)
0.2-0.299	2.27 (8)	1.24 (4)	6.95 (24)	-1.03 (3)	5.71 (19)
0.3-0.399	0.25 (1)	0.03 (-)	0.95 (3)	-0.22 (1)	0.92 (3)
0.4-0.499	0.02 (-)		0.11 (-)	-0.02 (-)	0.11 (-)
			Integrated, 1985[e]		
0.0-0.099	6.70 (23)	5.44 (18)	0.85 (3)	-1.26 (4)	-4.59 (16)
0.1-0.199	22.12 (75)	23.77 (81)	14.63 (50)	1.65 (6)	-9.14 (31)
0.2-0.299	0.70 (2)	0.32 (1)	13.42 (45)	-0.38 (1)	13.10 (44)
0.3-0.399			0.64 (2)		0.64 (2)
			May, 1986		
0.0-0.099	2.08 (9)	1.25 (5)	0.31 (1)	-0.83 (4)	-0.94 (4)
0.1-0.199	13.34 (56)	14.99 (63)	5.89 (25)	1.65 (7)	-9.10 (39)
0.2-0.299	7.06 (30)	7.01 (30)	9.92 (42)	-0.05 (-)	2.91 (12)
0.3-0.399	1.15 (5)	0.39 (2)	6.19 (26)	-0.76 (3)	5.80 (25)
0.4-0.499	0.02 (-)		1.25 (5)		1.25 (5)
0.5-0.599			0.08 (-)		0.08 (-)
			August, 1986		
0.0-0.099	9.22 (39)	8.96 (38)	1.75 (7)	-0.26 (1)	-7.21 (31)
0.1-0.199	9.75 (41)	11.08 (47)	12.21 (52)	1.33 (6)	1.13 (5)
0.2-0.299	3.69 (16)	3.15 (13)	5.53 (23)	-0.54 (2)	2.38 (10)
0.3-0.399	0.98 (4)	0.45 (2)	3.24 (14)	-0.53 (2)	2.79 (12)
0.4-0.499			0.89 (4)		0.89 (4)
			Integrated, 1986[e]		
0.0-0.099	5.23 (22)	3.17 (13)	0.28 (1)	-2.06 (9)	-2.89 (12)
0.1-0.199	15.26 (65)	17.72 (75)	10.29 (44)	2.46 (10)	-7.43 (32)
0.2-0.299	3.14 (13)	2.75 (12)	9.21 (39)	-0.39 (2)	6.46 (27)
0.3-0.399			3.76 (16)		3.76 (16)

a. Full resolution AVHRR NDVI imagery
b. Spatially-degraded full resolution AVHRR NDVI imagery
c. Global Vegetation Index imagery
d. Percentage of total area (see table 22)
e. Presented as mean daily NDVI. The integration period for full resolution AVHRR imagery is 223 days. The integration period for Global Vegetation Index imagery is 182 days

Figure 12. AVHRR NDVI Imagery of Northeastern Spain, August 1986.
A) Full Resolution, B) Spatially Degraded Full Resolution,
C) Global Vegetation Index

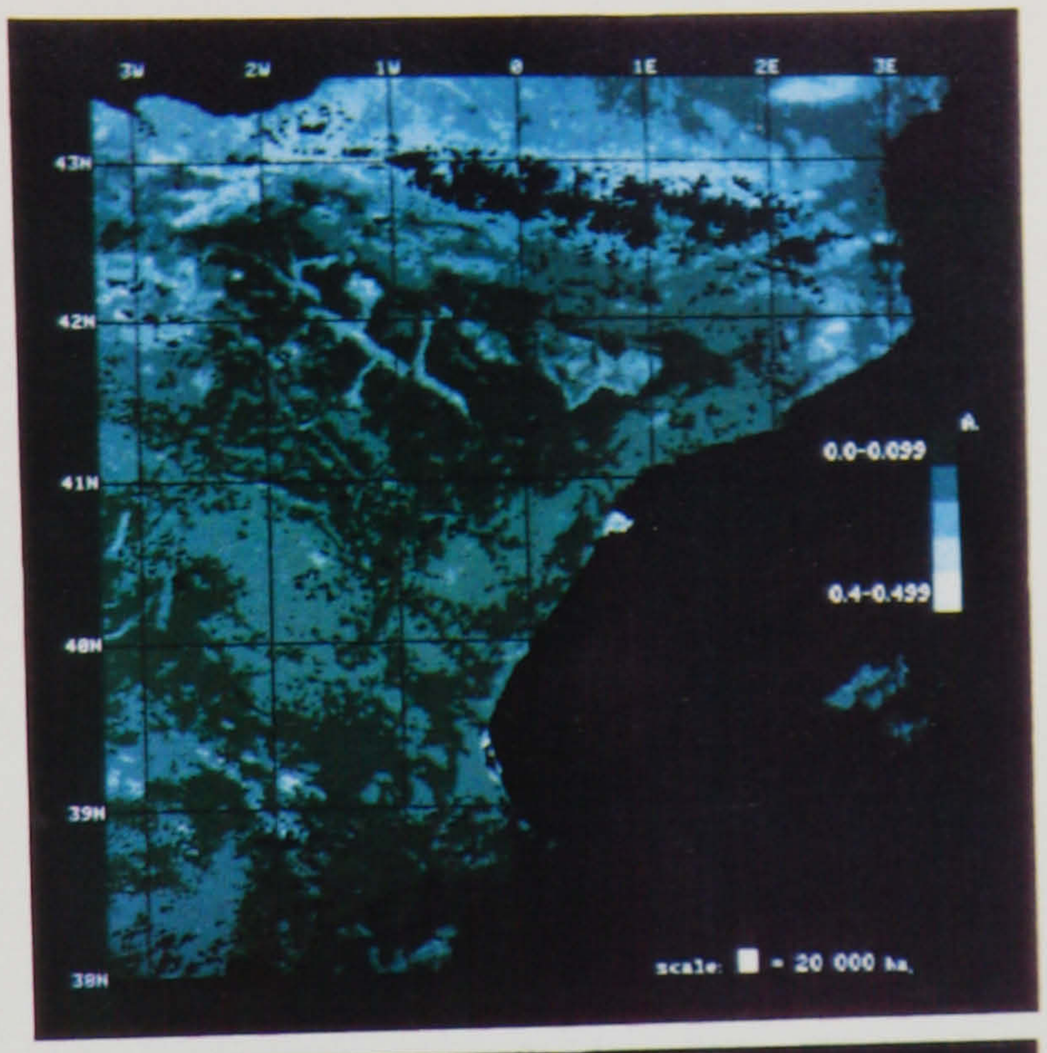

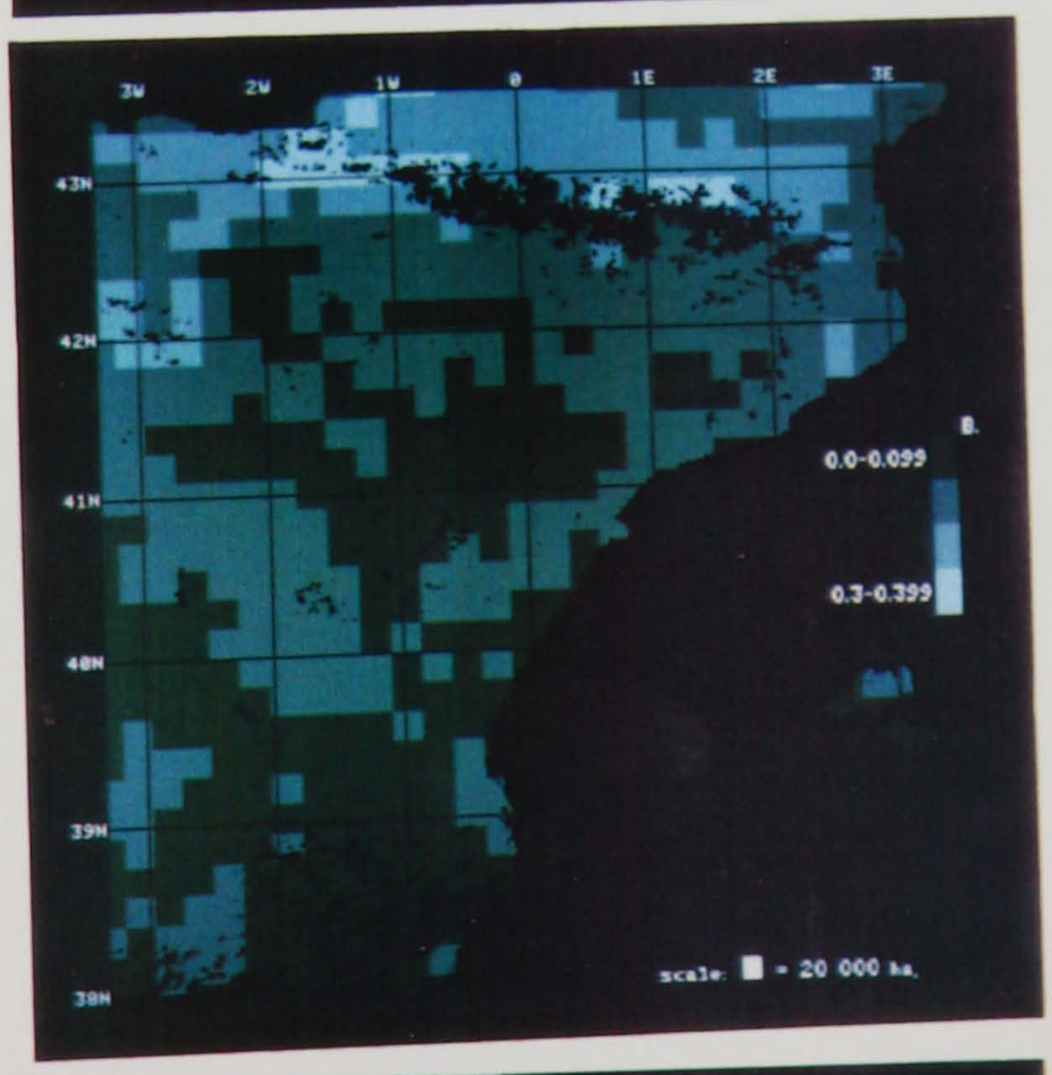

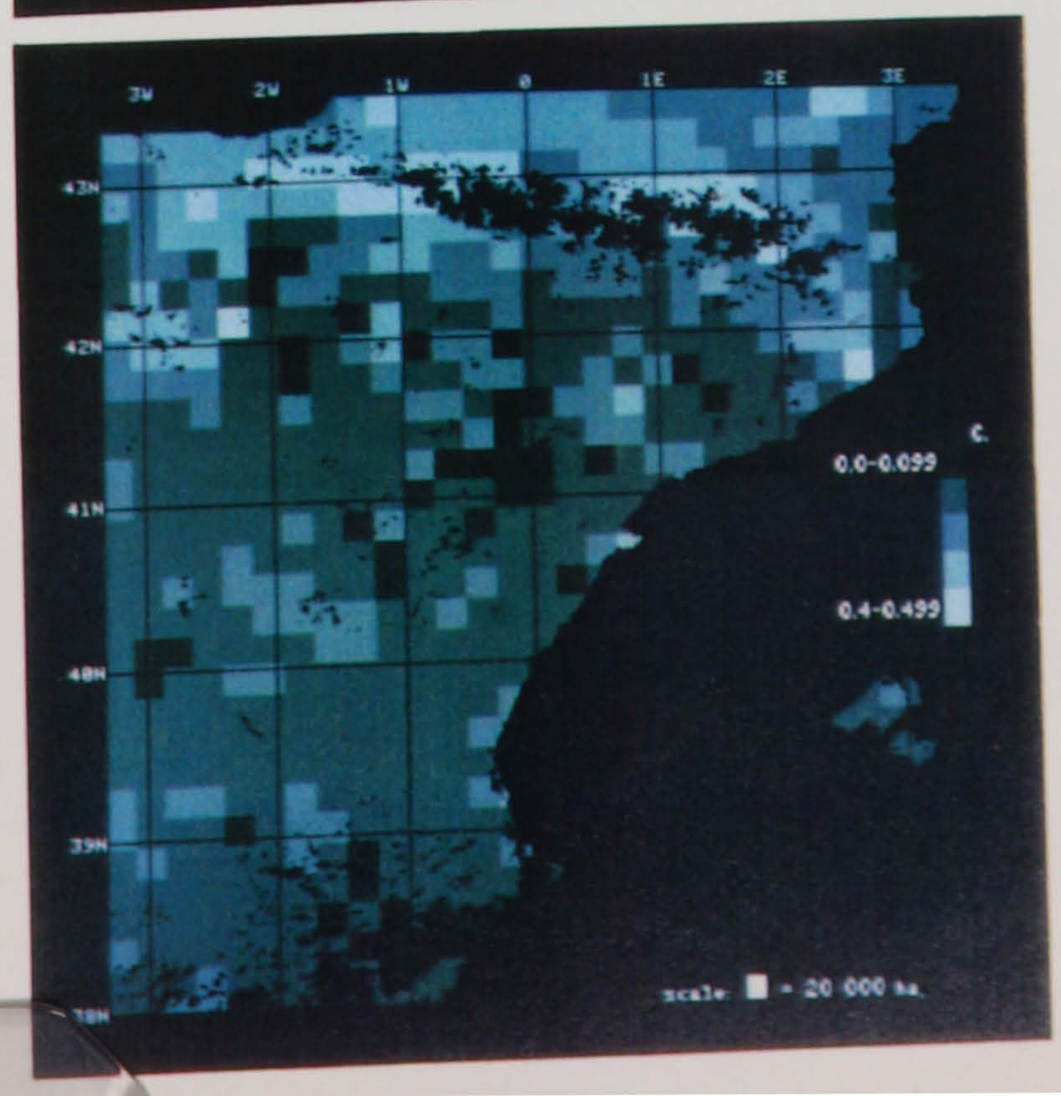

This comparison indicates that NDVI values that are the product of spatial and temporal subsampling, such as Global Vegetation Index NDVI values, are consistently higher than the area-integrated NDVI of the area on the ground that they represent (i.e. the corresponding x16 value). Presumably, the high values of Global Vegetation Index pixels are due to the combined effects of a temporal subsampling technique which consistently selects the highest NDVI value, and a spatial subsampling technique that makes it possible for relatively small areas of green, photosynthetically-active vegetation to represent much larger areas. Clearly, this tendency always to select the "greenest" NDVI value will occur whether it is vegetation type or vegetation productivity that is being mapped.

Three points arise from these findings. The first is that unrepresentative NDVI values will be less of a problem the closer together in areal extent are the actual measured area and nominal area of the pixel. For example, Global Area Coverage NDVI values represent the area-integrated NDVI response of the area represented by Global Area Coverage pixels more accurately than Global Vegetation Index NDVI values represent the area-integrated NDVI response of the area represented by Global Vegetation Index pixels. The second point is that the definition of meaningful threshold NDVI values for use with spatially and temporally subsampled NDVI imagery will be difficult. The problem is not simply that *all* NDVI values in temporally and spatially degraded NDVI imagery are higher than they should be, it is that they *may* be higher. There is no easy way of ascertaining whether an NDVI value in such imagery is representative or not.

The third point that arises from these findings is that NDVI values in spatially and temporally subsampled imagery are more likely to be representative when the target area is covered by a uniform vegetation cover. The analysis of full resolution imagery in Chapter Four has shown that sharp contrasts in vegetation activity are found over much of Spain. These contrasts make the interpretation of Global Vegetation Index imagery of the Iberian Peninsula in terms of vegetation cover type extremely difficult (Lloyd and Barrett 1986). For this reason primarily, Global Vegetation Index imagery is evaluated for purposes of vegetation mapping using imagery of Africa and not imagery of Spain. Of course, the importance of small areas of green, photosynthetically-active vegetation will be exaggerated in imagery of Africa as much as in imagery of Spain. However, the hope is that the exaggeration of NDVI values due to temporal and spatial subsampling will be relatively small compared with the variations in NDVI values due to regional variations in African phytophenology.

4. A phytophenological description of Africa

4.1 Introduction

The phenology of African vegetation has been studied by observers on the ground (e.g. Malaisse 1974) and, more recently, by image analysts using AVHRR NDVI imagery at several spatial scales. The small scale temporal dynamics of vegetation over the whole of Africa have been described by Justice *et al.* (1985)[3], Townshend *et al.* (1985)[4], Tucker *et al.* (1985a)[5], and Townshend and Justice (1986)[6]. These studies used twenty-one- or twenty-eight-day maximum NDVI value composite images to describe basic, seasonal patterns of vegetation photosynthetic activity. Larger scale analyses of AVHRR NDVI data have used either full resolution or Global Area Coverage AVHRR NDVI data or both (e.g. Tucker *et al.* (1983,1985b,1986b), Prince and Tucker (1986), Justice and Hiernaux (1986), Justice *et al* (1986)). Although these larger scale studies have investigated in more detail the phytophenological potential of AVHRR NDVI data (e.g. to map net primary production and length of the growing season), they have been limited spatially to regions of Africa. Apparently, full resolution AVHRR imagery of the entire continent presents the image analyst with unmanageable volumes of data (table 2).

The analysis of full resolution AVHRR NDVI imagery presented in Chapter Four suggested that maximum NDVI value imagery on its own provides relatively little phytophenological information compared with imagery of phytophenological variables. Yet the foregoing summary of investigations of AVHRR NDVI imagery of Africa indicates that an analysis of phytophenological variables for the whole of Africa has not been attempted. Consequently, the study presented here is a systematic evaluation of phytophenological variables derived from Global Vegetation Index imagery of Africa for the period January 1985 to December 1986. Clearly, meaningful interpretation of these data is greatly hindered by the temporal and spatial subsampling procedures that are used to produce them and also the extremely large area on the ground associated with an individual pixel. These factors should be borne in mind during the discussion of the images of these variables that follows.

The base map array of Africa used for all the imagery is shown in figure 14.

---

3 Using four, 8km spatial resolution, monthly maximum NDVI value composite images for the period May to November 1983

4 Using a principal components transform of eight twenty-one day maximum NDVI value Global Vegetation Index composites for the period April 1982 to February 1983

5 Using Global Vegetation Index imagery

6 Using 8km spatial resolution NDVI imagery for January, September and November 1984 and January 1985

Figure 13. Africa: Base Map Showing Political Divisions

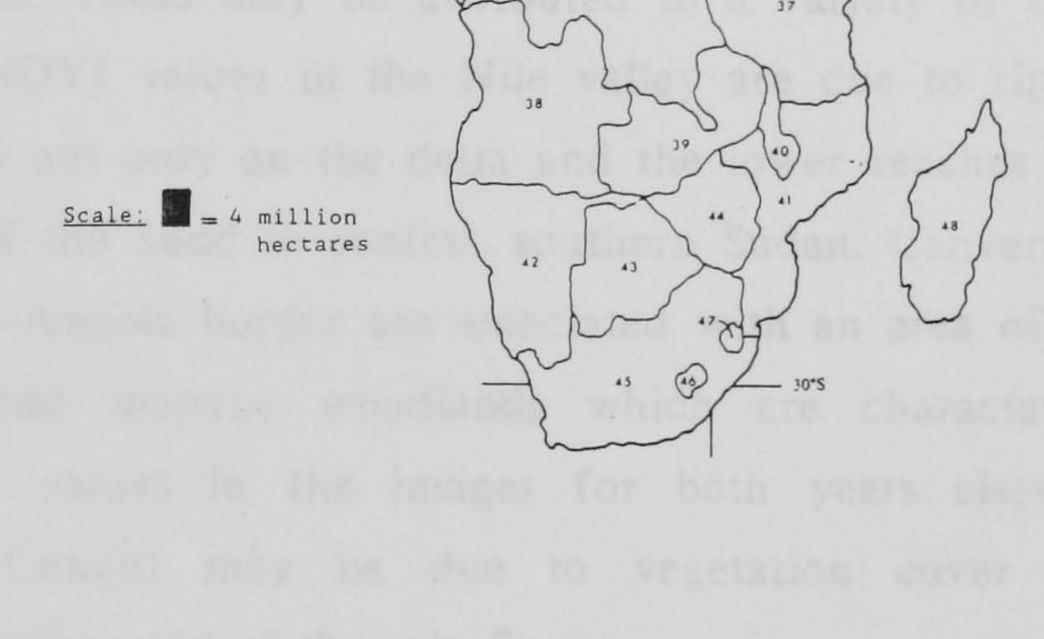

Key (numerical):

1. Morocco
2. Algeria
3. Tunisia
4. Libya
5. Egypt
6. Western Sahara
7. Mauritania
8. Mali
9. Niger
10. Chad
11. Sudan
12. Ethiopia
13. Djibouti
14. Somalia
15. Senegal
16. Gambia
17. Guinea Bissau
18. Guinea
19. Sierra Leone
20. Liberia
21. Ivory Coast
22. Burkina Faso
23. Ghana
24. Togo
25. Benin
26. Nigeria
27. Cameroun
28. Central African Republic
29. Equatorial Guinea
30. Gabon
31. Congo
32. Zaïre
33. Rwanda
34. Burundi
35. Uganda
36. Kenya
37. Tanzania
38. Angola
39. Zambia
40. Malawi
41. Mozambique
42. Namibia
43. Botswana
44. Zimbabwe
45. South Africa
46. Lesotho
47. Swaziland
48. Madagascar

Key (alphabetical):

Algeria (2)
Angola (38)
Benin (25)
Botswana (43)
Burkina Faso (22)
Burundi (34)
Cameroun (27)
Central African Republic (28)
Chad (10)
Congo (3)
Djibouti (13)
Egypt (5)
Ethiopia (12)
Equatorial Guinea (29)
Gabon (30)
Gambia (16)
Ghana (23)
Guinea (18)
Guinea Bissau (17)
Ivory Coast (21)
Kenya (36)
Lesotho (46)
Liberia (20)
Libya (4)
Madagascar (48)
Malawi (40)
Mali (8)
Mauritania (7)
Morocco (1)
Mozambique (41)
Namibia (42)
Niger (9)
Nigeria (26)
Rwanda (33)
Senegal (15)
Sierra Leone (19)
Somalia (14)
South Africa (45)
Sudan (11)
Swaziland (47)
Tanzania (37)
Togo (24)
Tunisia (3)
Uganda (35)
Western Sahara (6)
Zaïre (32)
Zambia (39)
Zimbabwe (44)

4.2 Annual mean daily NDVI

Images of annual mean daily NDVI for Africa for 1985 and 1986 are presented in figure 14. The method used to produce these images has been described already[7]. Figure 14 shows that, generally, high annual mean daily NDVI values are found in tropical areas, low values are found in subtropical areas and intermediate values are found in the areas between. The principal deviation from this latitudinal zonation is an east-west asymmetry, apparent in the images for both years, about the 25°E line of longitude. Western Africa north of the Equator has similar values to eastern Africa south of the Equator and *vice-versa.*

There are numerous local deviations from the simple, climatically-based pattern described above. These may be attributed to a variety of causes. For example, high annual mean NDVI values in the Nile valley are due to riparian irrigated vegetation which is found not only on the delta and the lower reaches of the river, but also the swampy area of the Sudd in central, southern Sudan. Conversely, relatively low values on the Zambia-Angola border are associated with an area of edaphic grassland within the miombo and mopane woodlands which are characteristic of these latitudes. Relatively low values in the images for both years elsewhere in tropical Africa (e.g. southern Congo) may be due to vegetation cover changes associated with agricultural development of the rain forest.

The lowest terrestrial annual mean daily NDVI values are associated with unvegetated areas. Thus, values less than 0.05 NDVI cover large parts of the great deserts of northern and southern Africa as well as local desert areas such as the Etosha and Makgadikgadi salt pans, in northern Namibia and northeastern Botswana respectively. The interpretation of values between 0.05 and 0.099 is less clear. Although these values are associated with desert fringes and therefore may be assumed to indicate usually a very sparse vegetation cover, they occur also over large parts of the Sahara. Furthermore, although the pattern produced by these values in the Sahara is very similar in 1985 and 1986, there is no obvious relation between these patterns and either the patterns of Saharan vegetation cover described by UNESCO (1983)[8] or Saharan physiography. Townshend and Justice (1986) suggest that NDVI values greater than 0.05 within desert areas are related to differences in the spectral response of surface materials. While this is probably true in most cases (Holben 1986), it is worth noting that there is no apparent correspondence between patterns of annual mean daily NDVI in the Sahara and soil type (UNESCO 1973b).

---

7 Section 3.1

8 See section 5.3

Figure 14. Africa: Annual Mean Daily NDVI. A) 1985, B) 1986

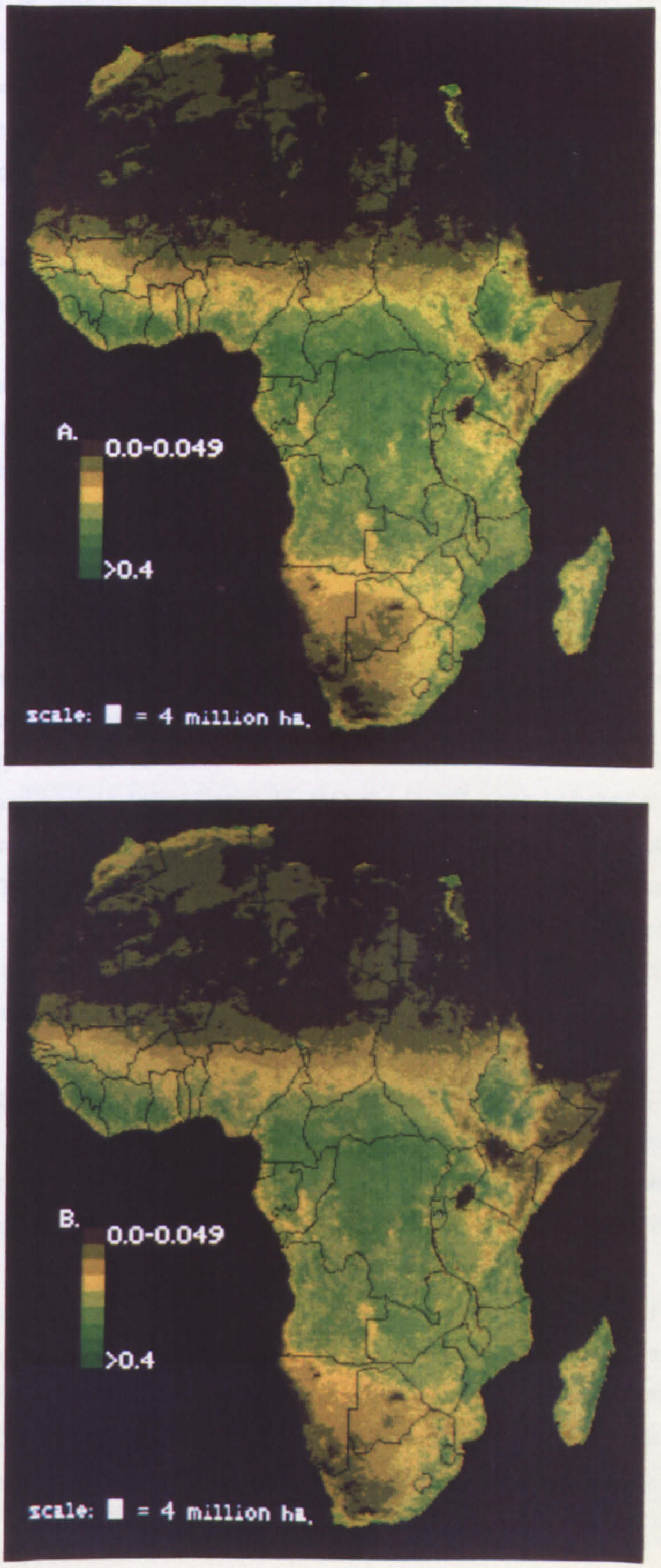

A careful comparison of the patterns associated with the various NDVI classes in the images of annual mean daily NDVI for 1985 and 19865 reveals interannual differences. For example, areas of southern Mozambique have higher values in 1985 than 1986, while the land around Lake Chad and the Kalahari, in Botswana particularly, have higher values in 1986 than 1985. Presumably, these interannual differences correspond to interannual variations in net primary productivity. This interpretation is supported by reports of interannual differences in crop condition, associated principally with meteorological conditions, in the aforesaid mentioned regions of Mozambique and Botswana (FAO 1985,1986).

4.3 Annual maximum NDVI

The annual maximum NDVI images for Africa for 1985 and 1986 are shown in figure 15. These images were made by retaining at each pixel the highest NDVI value of the twelve monthly values for each year. The lattice pattern that occurs at equatorial latitudes is an artefact of the remapping process.

The most obvious feature of the annual maximum NDVI images is their relative simplicity compared to the images of annual mean daily NDVI. Desert regions have values less than 0.1 while most areas outside the desert regions have values of at least 0.3. Relatively few areas have an annual maximum NDVI between 0.1 and 0.2. Although it may appear from figure 15 that the ">0.4" class imposes a ceiling value that is too low, only a very few pixels have annual maximum NDVI values greater than 0.45 NDVI. The relative simplicity of the patterns in these images compared with those in the images of annual mean daily NDVI, particularly the large number of pixels with high annual maximum NDVI values may be ascribed to the spatial and temporal subsampling techniques used to prepare the Global Vegetation Index.

Perhaps the most interesting feature of these images is the clarity with which they seem to define the limits of desert areas. A comparison between the apparent boundaries between desert and semi-desert areas in the images of annual mean daily NDVI and annual maximum NDVI suggests that the latter provide a more reliable indicator of the desertwards limit of ephemeral vegetation in semi-arid areas. Uncertainty over the meaning of the 0.05-0.099 annual mean daily NDVI class makes the delineation of a desert-grassland boundary for the Sahel using annual mean daily NDVI imagery difficult. However, the definition of this same boundary using annual maximum NDVI imagery would seem to be much less subjective. It would appear to correspond approximately with the 0.1 annual maximum NDVI isoline.

Figure 15. Africa: Annual Maximum NDVI. A) 1985, B) 1986

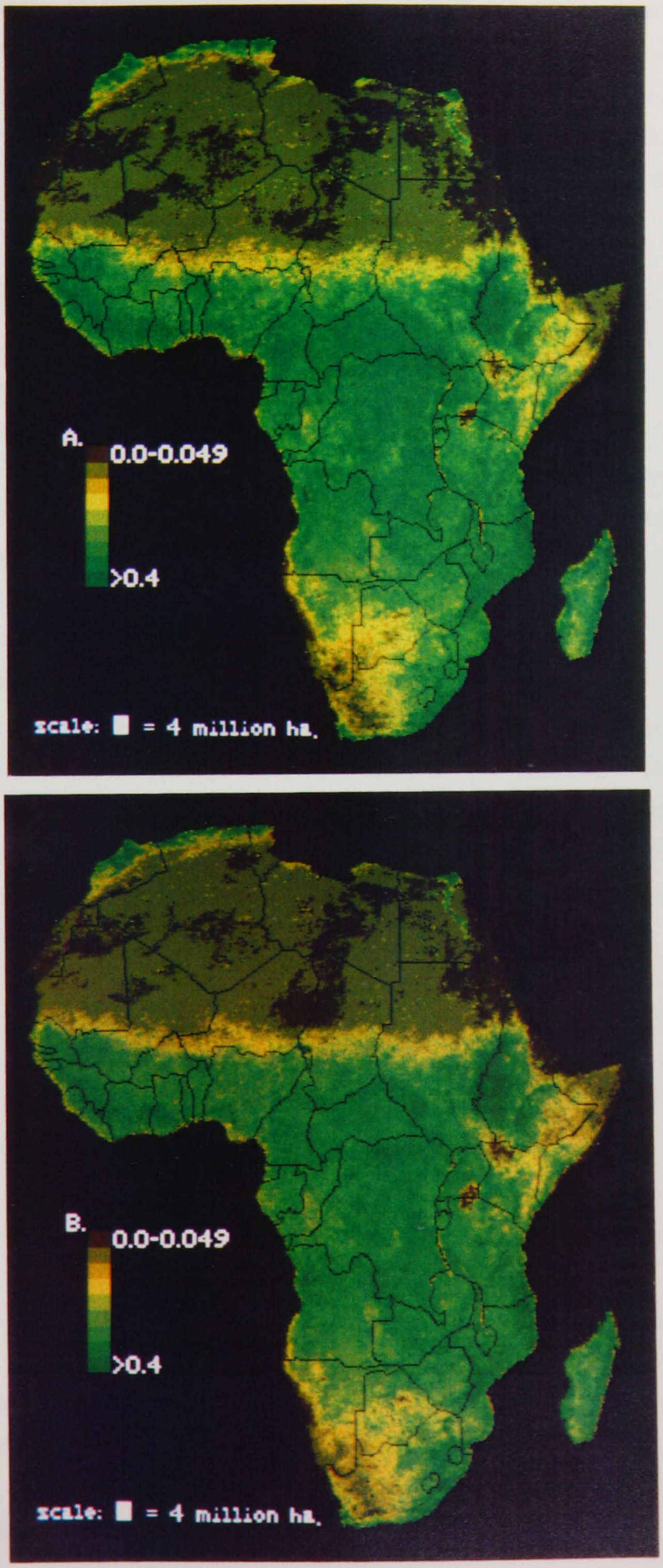

4.4 Timing of annual maximum NDVI

The months in which annual maximum NDVI values occurred for 1985 and 1986 are shown in figure 16. Generally, maximum NDVI values occur between May and October in most parts of northern Africa except the extreme northwest littoral and between November and April for most parts of southern Africa except the extreme southwest littoral. However, several distinct regional variations in the timing of annual maximum NDVI value are superimposed on this basic pattern.

The Sahel is clearly identified as an area with maximum NDVI values between July and September. Presumably, the northernmost limit of Sahelian grassland corresponds with the boundary between July-September maximum NDVIs and the arbitrary dates of maximum NDVI found in the Sahara. The clarity of this boundary is similar to that found in the annual maximum NDVI images. The delineation of the southern limits of the Sahel using these images is not so easy since Sahelian vegetation shares its timing of maximum NDVI with denser, more persistent vegetation cover classes located further south.

The pattern of the timing of maximum NDVI values along the Equator is complex and presumably reflects the distribution, timing and duration of the rains which are determined not only by the seasonal movement of the intertropical convergence zone but also by relief (Walter *et al.* 1975). The length, timing and reliability of the rains are particularly unpredictable in East Africa. Further west, in northern Zaïre, Congo and Gabon most maximum NDVI values occur during the period November to April.

Two major classes of vegetation may be discerned by the timing of their maximum NDVI values in Africa south of the equator. Southern Zaïre and much of Angola have annual maximum NDVI values in November and December while most of the countries along the east coast and Madagascar as well as much of Namibia have annual maximum NDVI values in February and March. Much of the southernmost part of the continent has annual maximum NDVI values in December and January.

There are many small differences between the images for 1985 and 1986. These variations are probably due to differences in the timing of seasonal rains. A particularly striking interannual variation in these images occurs in Kenya where the area with maximum NDVI values in December in 1985 is much smaller than it is in 1986. Since the 1985 October (long) rains were more favourable than the 1986 October rains (FAO 1986), the most likely explanation for the interannual difference is the

Figure 16. Africa: Timing of Annual Maximum NDVI. A) 1985, B) 1986

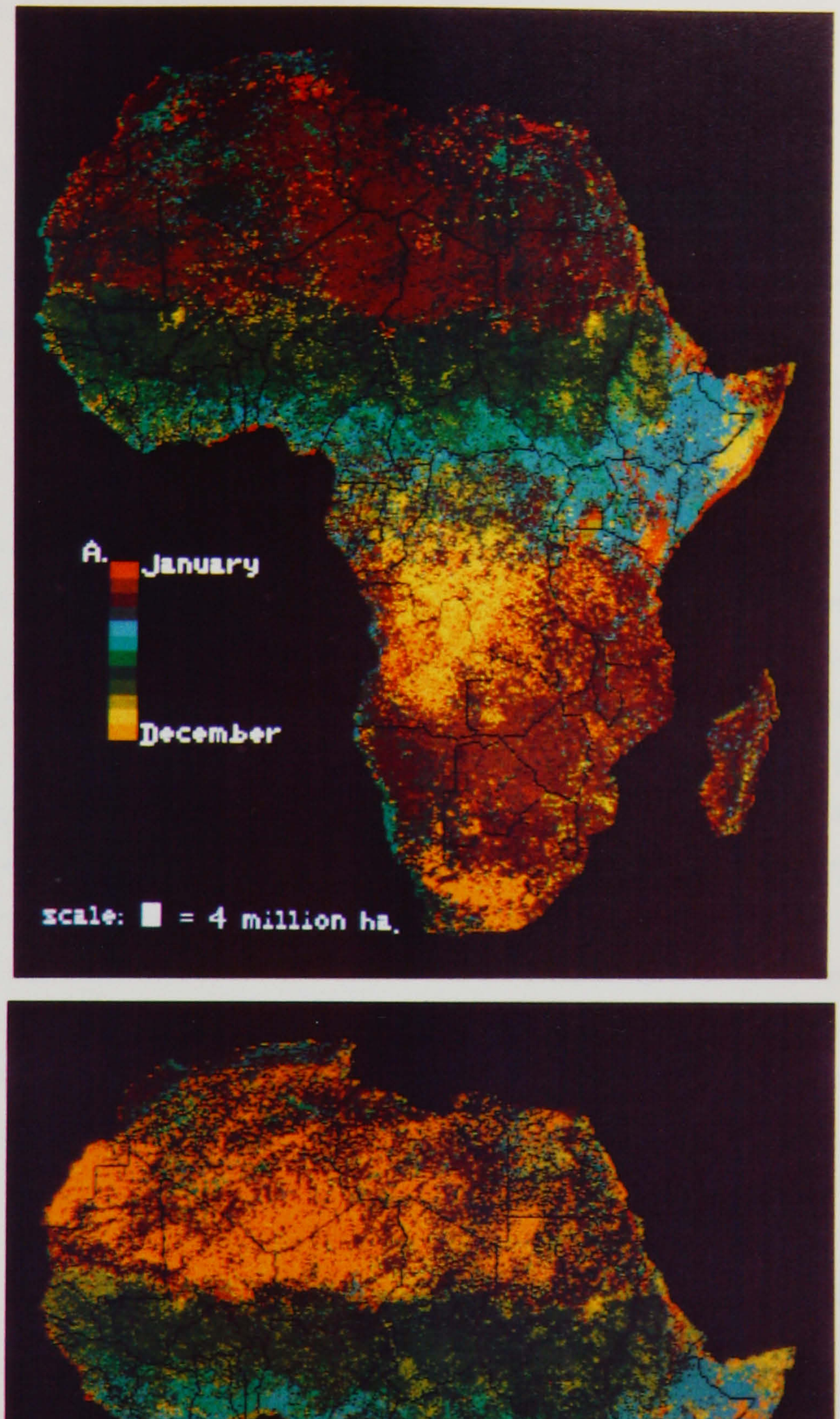

1986 March (short) rains were poor and that areas normally with an annual maximum NDVI in May had a December maximum in 1986.

Other notable examples of interannual differences occur in Botswana, Senegal and southwestern Mauretania. However, although these data suggest that the November (short) rains were more important than the March (long) rains in 1986 than 1985 in Botswana, and that the rains appear to have arrived almost a month later in 1986 than they did in 1985 in Senegal and southwestern Mauretania, suitable ancillary African rainfall data to support these interpretations are not available (Barrett and D'Souza 1986).

4.5 Period above 0.099 NDVI

Images showing the number of months of the year that NDVI values exceeded 0.099 NDVI are shown in figure 17. These images indicate that much of Africa is either above 0.099 NDVI throughout the year or else never above 0.099 NDVI. Thus, if NDVI values greater than 0.099 signify active vegetative growth[9], these images suggest that most African vegetation between 10°N and 20°S is never dormant. While it is true that tropical vegetation does not exhibit the marked seasonality of vegetation nearer the poles, nevertheless the complete absence of seasonality for the vegetation cover of such a large area is surprising. Presumably, the apparent perpetual photosynthetic activity of the vegetation in tropical Africa implied by these images is due, at least in part, to the spatial and temporal subsampling techniques used in the preparation of Global Vegetation Index imagery[10].

In spite of the detrimental effect of Global Vegetation Index preparation methods on the images in figure 17, several patterns suggested in the imagery of the other phytophenological variables appear clearly in these images of the period above 0.099 NDVI. In northern Africa, the Ethiopian highlands and Jos Plateau appear as islands of sustained photosynthetic activity surrounded by seasonal vegetation. Similarly, sustained photosynthetic activity along the East African coast is clearly distinguished from extremely seasonal vegetation inland. In southern Africa, the limits of sustained photosynthetic activity along the extreme south coast and the extent of extremely seasonal vegetation further north and west are clearly described. Over Africa as a whole, the asymmetrical distribution of photosynthetic activity about the Equator is very clear in these images. Vegetation with sustained photosynthetic activity appears

---

9 Chapter Two Section 4.4

10 A threshold NDVI value higher than 0.099 NDVI would produce a less uniform image. However, there would be no plant physical or physiological basis for interpreting the patterns in such imagery

Figure 17. Africa: Period Above 0.099 NDVI. A) 1985, B) 1986

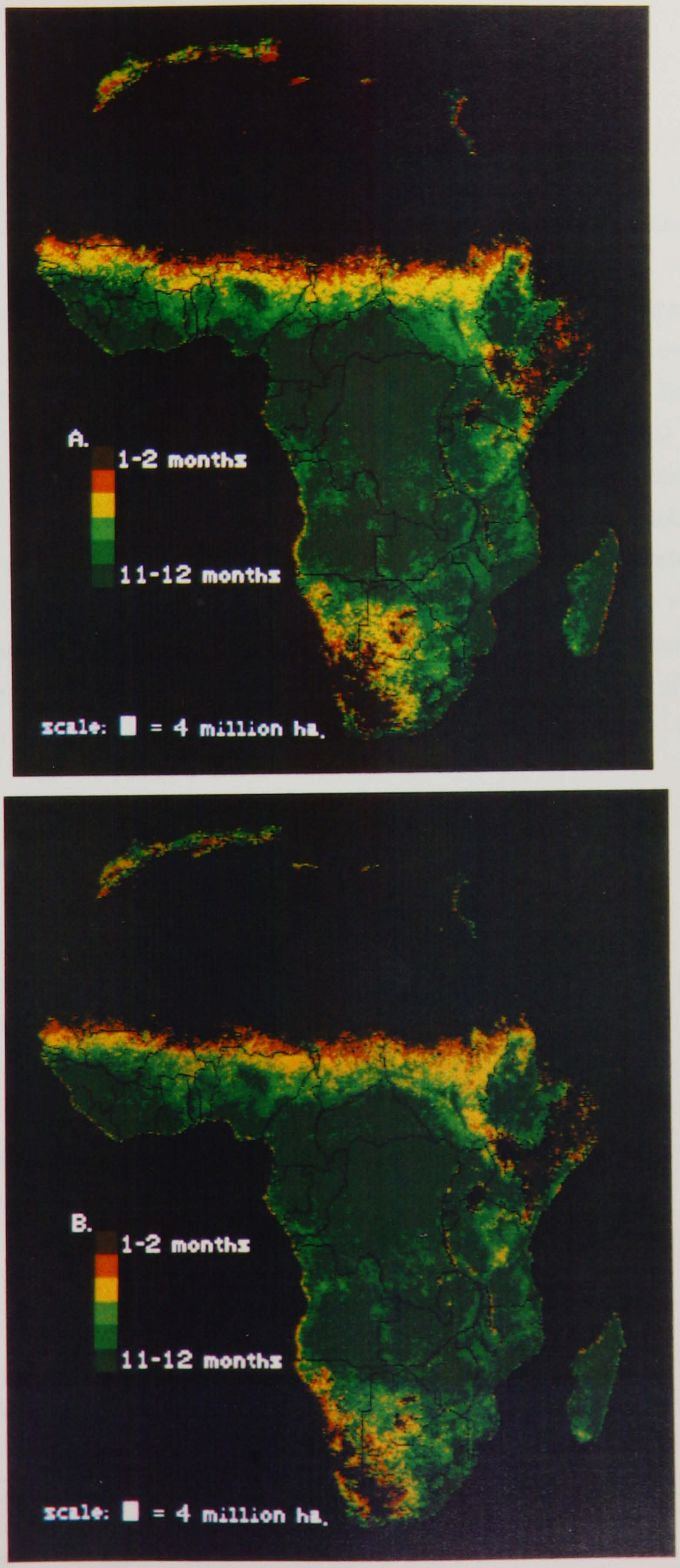

to extend further into the southern subtropical Africa than it does into the northern subtropical Africa.

4.6 Discussion

The images presented in figures 14 to 17 demonstrate, once again, the fundamental appeal of the phytophenological approach[11]. Vast amounts of digital data are reduced to a few, relatively simple images with a minimum of interference from or interpretation by the image analyst. Unfortunately, the evaluation of the Global Vegetation Index preparation procedure presented in Section 3 suggests that the distortion introduced by the temporal and spatial subsampling used to produce Global Vegetation Index imagery reduces considerably the reliability of these data. Thus, the striking similarity between the images of individual phytophenological variables for 1985 and 1986 may be due as much to the maximum NDVI value subsampling process as to genuine, interannual phytophenological similarities. Clearly, a Global Vegetation Index-type data set that did not suffer from drastic subsampling would be a major improvement. Nevertheless, in spite of these shortcomings, figures 14 to 17 demonstrate both the spatially-comprehensive phytophenological information that may be gleaned from multidate very small scale NDVI data and also the originality of the synoptic view that these data provide.

5. Mapping vegetation using the Global Vegetation Index

5.1 Introduction

The spatial scale of Global Vegetation Index data[12] and the uncertainty attached to individual Global Vegetation Index values due to temporal and spatial subsampling[13] make it imperative that attempts to map vegetation using Global Vegetation Index data should not stray too far from their primary phytophenological meaning. This is the reason why no attempt is made in this study to map physiognomic and agricultural vegetation classes using these data. Instead, two methods of mapping vegetation are presented based on the imagery of the phytophenological variables.

5.2 The "Peters Equality Atlas of the World"

In the course of my research I wrote to Professor Doctor Arno Peters asking for details of equal area radial projections. I enclosed a couple of maximum value Global

---

11 See Chapter Four Section 3

12 Discussed in Chapter Three Section 3

13 Discussed in Section 3

Vegetation Index composite images of Europe with my letter. In his reply Professor Peters expressed interest in the Global Vegetation Index. He was interested in the possibility of using the satellite data to assist with the depiction of vegetation in the *Peters Equality Atlas of the World*[14], a major new world atlas containing forty-three regional plates depicting the entire Earth's surface at a uniform spatial scale of 1 square centimetre:6000 square kilometres[15].

Ordinarily, physical cartographers use colour to describe elevation. Thus, low altitudes are frequently depicted shades of green while high altitudes are depicted shades of brown. However, in his new world atlas, Peters has chosen to describe elevation using a combination of shading and spot heights and to use colour to describe vegetation cover. Peters wanted to depict vegetation cover in a way that would be immediately comprehensible. In particular, he wanted not to use a complicated vegetation cover classification since usually these are region-specific, unavailable for all parts of the globe and intelligible only with constant reference to explanatory notes. Therefore, Peters chose to depict vegetation in the regional plates of his atlas according to a simple colour scheme that showed vegetated areas green and unvegetated areas brown. He requested a set of images derived from the Global Vegetation Index data that could be used to assist with the depiction of vegetation according to this scheme.

The imagery that was used to assist with the depiction of vegetation in Peters' atlas was mean daily NDVI imagery for the period January 1985 to December 1986. This imagery was chosen for four reasons. Firstly, it gives equal weighting to photosynthetic activity at all times of year. Secondly, it seems to be affected least of all the phytophenological variables by the temporal and spatial subsampling used to produce Global Vegetation Index imagery. Thirdly, it provides a very sensitive representation of spatial variations in photosynthetic activity[16]. Fourthly, imagery containing mean daily NDVI values for a two-year period is more likely to reflect average levels of primary productivity than imagery based on just twelve month's data.

The method used to make a mean daily NDVI image of the world from Global Vegetation Index imagery for the period between 1st January 1985 and 31st December 1986 is described in Appendix 2 Section 3. This polar-stereographic format world image was remapped[17] to equal area radial constructions corresponding with each of

---

14 Scheduled for publication (German edition) in July 1988

15 Equivalent to 77.5km^2

16 Nominally, there are two-hundred-and-fifty-six classes (i.e. grey levels) of mean daily NDVI

17 With assistance from Giles D'Souza

the regional plates in the atlas for which the satellite data had been requested[18]. A simple green-to-brown colour scheme was applied to each regional image. The colour scheme was devised so as to provide an acceptable representation of the Iberian Peninsula.

Photographs of the coloured regional images were sent to Oxford Cartographers (Oxford, England) who are producing the new atlas. In most cases the Global Vegetation Index images were used in conjunction with other information including maps of vegetation physiognomy, Landsat imagery, satellite photography and topographic maps. However, in some regions where information regarding vegetation cover is sparse (e.g. South America), the annual mean daily NDVI images were the primary information source. Occasionally the Global Vegetation Index imagery was used to update information from other sources. Thus the mean daily NDVI imagery for January 1985 to December 1986 was the basis for depicting a southwards expansion of the Sahara not described in the other, older information sources.

Two main problems were encountered with the images that were produced from the Global Vegetation Index. The first was that agricultural land frequently has quite low annual mean daily NDVI values. Presumably this is due to the fact that many agricultural areas have several months when the land is fallow. Since the decision had been made to depict agricultural land green, special care had to be taken to ensure that agricultural areas were not coloured wrongly[19].

The second problem encountered with the Global Vegetation Index imagery was its spatial scale. In particular, the small scale data proved unreliable for purposes of detecting small irrigated areas. This may seem surprising in view of the results of the comparative study presented in Section 3. However, the point is made there that the problem with Global Vegetation Index NDVI values is not simply that *all* NDVI values are higher than they should be, rather it is that the *may* be higher. Clearly, the fundamental solution to this problem is to use larger scale data.

In spite of these shortcomings, annual mean daily NDVI imagery provides an up-to-date, objective simplification of world vegetation based on vegetation

---

18 Mean daily NDVI imagery was requested for those areas where information relating to vegetation cover was sparse or unavailable (i.e. most of Africa, Asia, Australia, South America, the northern parts of North America and Mexico). Twenty-two of the forty-three regional plates in the atlas were produced using mean daily NDVI imagery

19 It would have been easier to identify many types of agricultural land using annual maximum NDVI imagery. However, this variable was not used for the atlas because of the reduction in its sensitivity due to the temporal and spatial subsampling procedures used to produce the Global Vegetation Index (see Section 4.3)

productivity that seems well-suited to the task for which it was commissioned. An example of an annual mean daily NDVI image and the corresponding plate from the *Peters Equality Atlas of the World* is shown in figure 18.

5.3 The supervised binary decision tree

Vegetation maps of Africa for 1985 and 1986 produced by a supervised binary tree classification of the phytophenological variables described in Section 4 are presented in figure 19[20]. The decision tree that produced these images is shown in figure 2. There are fewer classes in figure 19 than there are terminal nodes to the decision tree. The reason for this is the same as that given for the binary tree classifications of northeastern and southern Spain, namely, that several of the binary tree classes are either impossible or else represented by so few pixels that they were merged with closely related classes.

The definition of the various binary tree classes is as follows. Classes 1, 2 and 3 have maximum NDVI values between November and April and NDVI values greater than 0.099 for a period of nine months or more during the year. The difference between them is that Class 1 has annual mean daily NDVI values greater than 0.27, Class 2 has annual mean daily NDVI values between 0.2 and 0.269 and class 3 has annual mean daily NDVI values between 0.1 and 0.199. Class 4 has maximum NDVI values between November and April, NDVI values greater than 0.099 for a period of one to eight months during the year and an annual mean daily NDVI greater than 0.099. Class 5 has maximum NDVI values between November and April, NDVI values greater than 0.099 for a period of one to eight months during the year and an annual mean daily NDVI of less than 0.1. Classes 6 to 10 are identical to classes 1 to 5 respectively except that their annual maximum NDVI occurs between May and October. Class 11 has NDVI values that are never greater than 0.099 NDVI throughout the year and annual mean daily NDVI values less than 0.1.

The multidate NDVI values of the eleven binary tree classes are shown in table 25. Although the values for one standard deviation from the mean suggest that within-class variability is quite high, the values for 1985 and 1986 for each class are quite similar. This suggests that same-numbered classes in 1985 and 1986 are associated with vegetation cover that is similar phytophenologically. The NDVI temporal profiles in table 25 also show clearly that there is a consistent trend between classes 1 and 5, and classes 6 and 10. The lower-numbered classes in each case are associated with high

---

20 Slight geodetic misregistration, which occurs in all the imagery of Africa (Section 2), is particularly apparent in these images. It occurs most noticeably along the coasts of West Africa, Somalia and eastern Madagascar

Figure 18. Northwestern Africa. A) Annual Mean Daily Normalised Difference Vegetation Index (1st January 1985 - 31st December 1986), B) Plate from *Peters Equality Atlas of the World*

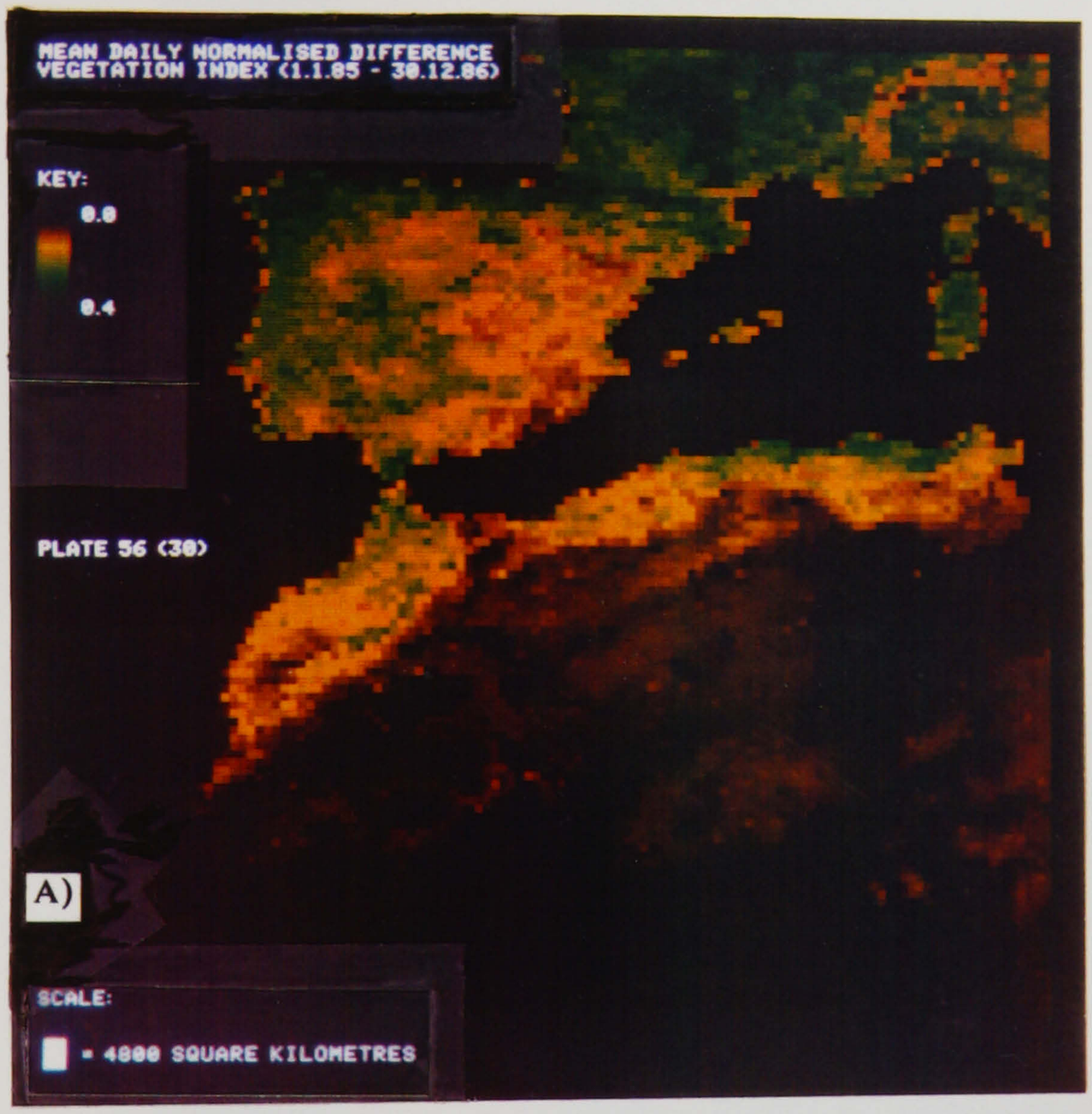

B)

Figure 19. Africa: Supervised Binary Decision Tree Classification of Multidate Global Vegetation Index Imagery. A) 1985, B) 1986

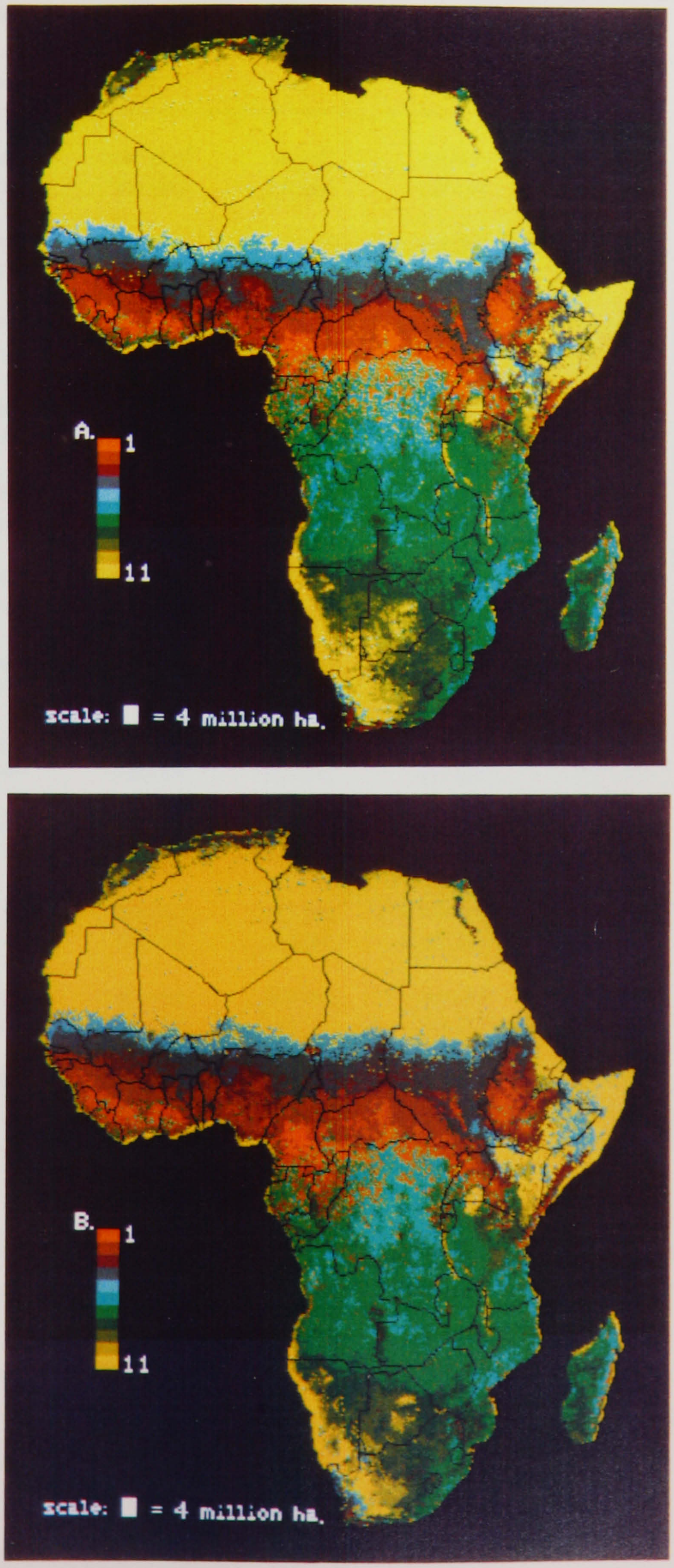

Table 25. Mean NDVI Values (in thousandths) of Classes Derived from a Supervised Binary Decision Tree Classification of Phytophenological Variables Derived from Multidate Global Vegetation Index imagery of Africa (continued on next page)

Month	Year	1	2	3	4	5
January	1985	147 (63)[a]	99 (69)	73 (57)	50 (30)	44 (24)
	1986	221 (66)	147 (66)	113 (48)	84 (30)	64 (27)
February	1985	250 (72)	176 (84)	133 (87)	110 (111)	84 (84)
	1986	239 (66)	159 (66)	107 (51)	76 (30)	61 (30)
March	1985	273 (72)	181 (75)	116 (57)	61 (30)	53 (27)
	1986	293 (57)	199 (69)	121 (51)	76 (30)	64 (24)
April	1985	316 (54)	239 (69)	150 (63)	87 (60)	64 (30)
	1986	301 (51)	221 (69)	139 (63)	73 (36)	61 (30)
May	1985	364 (48)	299 (66)	196 (72)	116 (90)	61 (51)
	1986	344 (45)	270 (72)	181 (84)	90 (63)	76 (54)
June	1985	336 (54)	293 (63)	199 (60)	127 (90)	39 (51)
	1986	324 (51)	276 (57)	190 (69)	110 (81)	53 (45)
July	1985	324 (66)	299 (81)	250 (87)	261 (93)	127 (69)
	1986	287 (69)	267 (75)	207 (24)	184 (84)	59 (48)
August	1985	327 (60)	299 (81)	250 (87)	261 (93)	127 (69)
	1986	321 (63)	296 (75)	241 (84)	267 (78)	110 (66)
September	1985	344 (57)	304 (78)	253 (93)	261 (93)	141 (87)
	1986	339 (54)	310 (72)	241 (93)	273 (81)	110 (66)
October	1985	339 (51)	279 (66)	219 (69)	297 (78)	87 (51)
	1986	333 (48)	287 (60)	227 (72)	230 (75)	101 (63)
November	1985	310 (45)	239 (54)	181 (42)	147 (54)	76 (33)
	1986	299 (45)	244 (45)	184 (48)	153 (54)	79 (27)
December	1985	241 (63)	167 (69)	124 (51)	93 (33)	64 (24)
	1986	230 (54)	170 (60)	136 (45)	104 (33)	76 (24)

a. One standard deviation from the mean (1σ)

NDVI values throughout the year and slight seasonality, and the higher-numbered classes are associated with lower NDVI values and marked seasonality.

It is apparent from figure 19 that the pattern produced by the various binary tree classes is very similar in 1985 and 1986. Table 26 shows precisely how many pixels changed classes between 1985 and 1986 and also the classes to which they changed. Unsurprisingly, most of the confusion is between neighbouring classes. For example,

Table 25. (conclusion)

Month	Year	6	7	8	9	10	11
January	1985	250 (75)[a]	523 (66)	184 (63)	141 (81)	81 (63)	33 (27)
	1986	293 (75)	287 (75)	199 (72)	170 (87)	87 (66)	39 (33)
February	1985	307 (72)	296 (66)	241 (72)	224 (99)	119 (105)	70 (99)
	1986	330 (66)	304 (69)	219 (72)	204 (84)	104 (75)	44 (36)
March	1985	344 (54)	316 (60)	247 (63)	224 (93)	110 (81)	44 (33)
	1986	359 (45)	313 (48)	233 (63)	213 (81)	113 (72)	47 (33)
April	1985	353 (48)	304 (48)	233 (51)	204 (78)	113 (57)	50 (42)
	1986	330 (48)	284 (48)	204 (57)	170 (81)	76 (60)	42 (39)
May	1985	330 (42)	273 (42)	193 (48)	147 (66)	64 (54)	42 (45)
	1986	319 (42)	259 (42)	181 (51)	136 (63)	67 (48)	44 (42)
June	1985	281 (48)	221 (45)	153 (39)	107 (45)	47 (51)	30 (36)
	1986	284 (51)	216 (45)	150 (42)	101 (36)	47 (45)	36 (33)
July	1985	250 (63)	176 (54)	133 (33)	87 (33)	42 (45)	24 (30)
	1986	233 (57)	173 (48)	127 (33)	84 (27)	44 (45)	30 (33)
August	1985	241 (69)	156 (57)	113 (30)	76 (36)	44 (45)	27 (33)
	1986	233 (72)	147 (24)	116 (30)	81 (30)	47 (45)	30 (33)
September	1985	264 (78)	156 (69)	104 (36)	76 (36)	44 (45)	27 (33)
	1986	253 (78)	150 (63)	104 (36)	76 (33)	44 (45)	30 (33)
October	1985	281 (75)	179 (78)	104 (39)	70 (33)	42 (36)	27 (30)
	1986	287 (66)	184 (75)	110 (42)	81 (36)	50 (42)	33 (33)
November	1985	333 (54)	264 (75)	161 (51)	107 (60)	53 (54)	36 (39)
	1986	321 (51)	270 (66)	173 (54)	136 (63)	73 (54)	44 (33)
December	1985	310 (69)	284 (66)	184 (57)	139 (78)	64 (63)	36 (33)
	1986	296 (72)	287 (66)	199 (60)	156 (81)	79 (66)	53 (36)

a. One standard deviation from the mean (1σ)

class 2 is confused particularly with classes 1 and 3. There is also some confusion with the corresponding classes from the opposite hemisphere (e.g. class 2 is confused with class 7 and, to a lesser extent, classes 6 and 8). Clearly, confusion between classes is a measure of the sensitivity of this classification approach to interannual variations in vegetation condition. Unsurprisingly, table 26 shows that, generally, least interannual variation is associated with the phytophenological classes at the two extremes of the photosynthetic activity scale (i.e. class 11, the desert class and classes 1, 2, 6 and 7). The number of pixels whose class label is different in 1985 and 1986 is higher for

Table 26. Confusion Matrix Showing the Correspondence Between Binary Tree Classifications of Multidate Global Vegetation Index Imagery of Africa for 1985 and 1986

	1986												
1985	1	2	3	4	5	6	7	8	9	10	11	Number of Pixels (1985)	Mean %[a]
1	2636	774	1	0	0	1111	182	3	0	0	0	4707 (56)[b]	59
2	721	6478	387	123	0	223	1053	163	9	1	8	9166 (71)	67
3	2	955	1653	479	12	1	139	304	33	8	52	3638 (45)	42
4	10	322	1445	5665	507	0	14	121	84	132	393	8693 (65)	68
5	0	4	26	1320	2973	0	1	30	100	325	1041	5820 (51)	52
6	791	252	1	0	0	2852	1164	11	1	0	1	5073 (56)	54
7	164	1138	150	14	1	1303	13 003	900	218	0	22	16 913 (77)	75
8	6	296	338	143	9	0	1884	3452	582	16	63	6789 (51)	52
9	4	17	85	121	147	8	254	1270	2083	267	366	4622 (45)	48
10	0	2	9	71	295	0	6	120	789	1337	1390	4019(33)	37
11	1	19	190	183	1751	0	9	112	196	1254	37 282	40 997 (91)	92
Number of Pixels (1986)	4335 (61)[b]	10 257 (63)	4285 (39)	8119 (70)	5695 (52)	5498 (52)	17 709 (73)	6486 (53)	4095 (51)	3340 (40)	40 618 (92)		

a. i.e. mean for 1985 and 1986 of the percentage of total number of pixels in each class classified as that class in both years

b. Percentage of total number of pixels in each class classified as that class in both years

those pixels associated with phytophenological classes associated with intermediate levels of photosynthetic activity.

It seems reasonable to suppose that the ability to identify, locate and quantify interannual variations in photosynthetic activity is one of the principal attractions of small scale NDVI data. Table 27 shows the area occupied by each of the binary decision tree classes in 1985 and 1986. The smallness of the interannual change in the area occupied by each phytophenological class is striking (e.g. 30×10^6 hectares is less than 1% of the total area of Africa). However, meaningful interpretation of interannual variations of this kind depends not only on having reliable data but also upon the definition of a reliable "mean" pattern. Since the imagery in figure 19 uses the Global Vegetation Index, which tends always to overestimate NDVI values, and just two years' worth of data, clearly, a detailed interpretation of the interannual variations in figure 19 is not possible. However, monthly reports by FAO (1985,1986) suggest that figure 19 depicts the distribution of phytophenological classes during years that, generally, were favourable for plant growth over most of Africa.

Table 27. Area Occupied by Classes Derived from a Supervised Binary Decision Tree Classification of Phytophenological Variables Derived from Multidate Global Vegetation Index Imagery of Africa

Binary Tree Class	Area in hectares x10^6[1] 1985	1986	1986-1985	% change
1	129	119	-10	8
2	252	282	+30	12
3	100	118	+18	18
4	250	230	-20	9
5	160	157	-3	2
6	140	151	+11	8
7	465	487	+22	5
8	176	172	-4	2
9	127	113	-14	12
10	111	92	-19	21
11	1127	1117	-10	1

[1] One (remapped) Global Vegetation Index pixel covers an area of 27 500 hectares (i.e. 1x10^6 hectares is equivalent to approximately thirty-six (remapped) Global Vegetation Index pixels)

No formal attempt is made to relate the phenological classes in figure 19 to physiognomic vegetation classes. However, a visual comparison with a simplified version of the *Vegetation Map of Africa* published at 1:500 000 by UNESCO (1983) (figure 20) suggests that the distribution of several of the phytophenological classes corresponds with the distribution of major African physiognomic classes[21]. Thus, generally-speaking, classes 1 and 6 represent Forest, classes 2 and 3 represent Forest Transition and Mosaic as well as Cape and Karoo Shrubland, class 4 represents Sudanian Woodland and Grassland, class 5 represents Sahelian Wooded Grassland and Bushland, class 7 represents Woodland, predominantly Miombo and Mopane, classes 8 and 9 represent Kalahari Wooded Grassland and Bushland and Karoo Grassy Shrubland and Highveld Grassland, class 10 represents Kalahari/Karoo-Namib Transition and class 11 represents Desert. Clearly, the correspondence between the phytophenological and the physiognomic vegetation cover classes is coincidental. It seems reasonable to suppose that the success with which the small scale NDVI data are able to reproduce the patterns in figure 20 might be improved if the phytophenological characteristics of the various physiognomic vegetation cover classes were taken into account.

21 The memoire accompanying the UNESCO vegetation map of Africa, by F. White, describes the classification that is used as "primarily physiognomic". Thus, although it is based on sixteen major physiognomic vegetation types, a total of one hundred cartographic units are shown on the map because the physiognomic types are grouped according to the floristic regions (phytochoria) in which they occur

Figure 20. Africa: Map Showing the Distribution of Major Vegetation Classes
(Redrawn from Tucker et al. (1985a), simplified from UNESCO (1983))

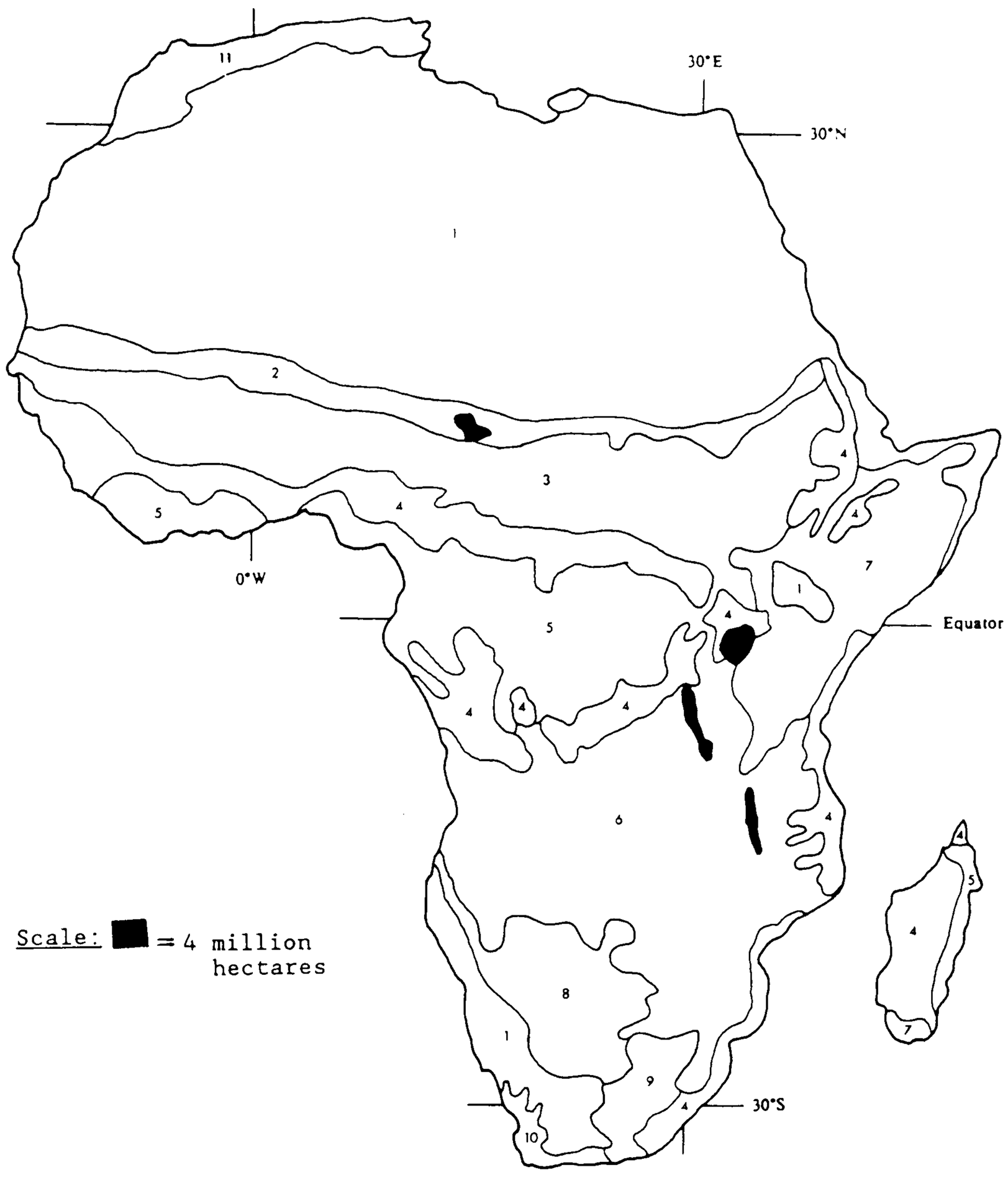

Scale: ■ = 4 million hectares

1. Desert and Semidesert Shrubland-Grassland
2. Wooded Grassland and Bushland (Sahel)
3. Sudanian Woodland and Grassland
4. Forest Transition and Mosaic
5. Forest
6. Woodland, predominately Miombo and Mopane
7. Woodland, predominately Somalia-Masai
8. Kalahari Wooded Grassland and Bushland
9. Karoo Grassy Shrubland and Highveld Grassland
10. Cape and Karoo Shrubland
11. Mediterranean Vegetation

5.4 Discussion

Perhaps the most intriguing feature of the phytophenological maps of Africa is the way in which they highlight contrasts between the phytophenology of northern and southern Africa. For example, the images in figure 19 show, and the figures in table 27 confirm, that class 7 covers a much larger area than its equivalent northern hemisphere class, class 2. Similarly, class 4 covers a larger area than its equivalent southern hemisphere class, class 9. Objective, phenologically-based comparisons of this type between vegetation canopies that are not only thousands of miles apart but also different, floristically and physiognomically, can be made easily using small scale NDVI imagery. They suggest that such data might provide the basis for a global vegetation classification. Unlike global vegetation classifications based on vegetation floristics or vegetation physiognomy which inevitably contain many classes, a classification scheme that used small scale multidate NDVI data could subdivide the world's vegetation into just few classes distinguished by the timing, the intensity and the duration of their photosynthetic activity. Ideally, a phytophenological classification of this type would use small scale NDVI imagery that were not a product of drastic temporal and spatial subsampling.

6. Summary

The characteristics of spatially-degraded AVHRR NDVI imagery are described and an evaluation of the effects of spatial and temporal subsampling on the NDVI values in Global Vegetation Index imagery is described. Twenty-four monthly maximum NDVI value composite images derived from one-hundred-and-four weekly Global Vegetation Index images produced between January 1985 and December 1986 are used to make images of phytophenological variables of Africa. The information these images reveal regarding the timing, intensity and duration of photosynthetic activity in Africa is discussed. The problems associated with the interpretation of classified images derived from Global Vegetation Index imagery are described and supervised binary decision tree classifications of the multidate Global Vegetation Index imagery of Africa are presented and their merits explained.

Chapter Six

Summary, Conclusions and Recommendations

The Advanced Very High Resolution Radiometer (AVHRR) onboard United States National Oceanic and Atmospheric Administration satellites is the only satellite-borne sensor producing small scale radiometric data suitable for studying vegetation. While it is true that these data are cheaper, more-frequently produced and more manageable than large scale radiometric data, perhaps the most significant feature of AVHRR imagery is the synoptic view of the Earth's surface that it provides since this is one of the unique scientific opportunities provided by satellite technology.

The phytogeographical potential of AVHRR imagery has been investigated using a variety of vegetation indices calculated from red and near-infrared reflectance measurements from AVHRR channels 1 and 2. The normalised difference vegetation index (NDVI) is one such physiologically-based vegetation index which is particularly suited to radiance data from satellite-borne sensors since, not only does normalisation compensate partially for variations in viewing and illumination angle, but also maximum NDVI value compositing can improve the quality of the imagery collected on consecutive days reducing especially the number of cloud-contaminated measurements.

AVHRR NDVI imagery at two spatial scales is the subject of this study. This imagery consists of twelve full resolution AVHRR NDVI images of northeastern and southern Spain for the period April to September 1985 and 1986 and twenty-four monthly AVHRR Global Vegetation Index images of Africa for the period January 1985 to December 1986. These two data sets, which represent the two extremes of AVHRR data in terms of spatial scale, were mapped to equal area radial projections. Although this map construction has not been used with radiometric imagery before, it is particularly well-suited to display small scale radiometric data since it provides a rectilinear graticule and a constant areal scale.

The analysis of the imagery of Spain and Africa is performed primarily using imagery of phytophenological variables. These variables, which are derived from multidate NDVI data, summarise qualitatively attributes of the phenology of vegetation photosynthetic activity in a concise, accessible from. Thus, the mean daily NDVI and

the seasonal maximum NDVI describe spatial variations in the intensity of vegetation photosynthetic activity, the timing of maximum NDVI describes spatial variations in the time of peak photosynthetic activity and the period above 0.099 NDVI describes spatial variations in the duration of photosynthetic activity. Although all these variables have been described elsewhere, this is the first study to evaluate them collectively.

The analysis of full resolution AVHRR NDVI imagery of Spain revealed the considerable sensitivity of these data to spatial and temporal variations in photosynthetic activity. Cluster analysis, a minimum distance classifier and an original supervised binary decision tree classifier were used to make classified images from the multidate full resolution AVHRR imagery. Although the results were promising, interpretation of the classes produced by these classifiers in terms of physiognomic and agricultural vegetation cover classes was ambiguous due to the phytophenological similarity of many physiognomic and agricultural vegetation classes. The most promising classificatory approach was the supervised binary decision tree classification of the phytophenological variables since the classes produced by this classifier have an unequivocal phytophenological meaning. Phytophenological maps of the type produced by the supervised binary decision tree classifier, which show spatial variations in the timing, intensity and duration of photosynthetic activity, have not been produced before.

Imagery of the phytophenological variables derived from the Global Vegetation Index imagery of Africa revealed a striking interannual similarity in the timing, intensity and duration of photosynthetic activity over much of the continent. The patterns contained in these images were associated with both patterns of vegetation cover and also interannual variations in environmental conditions. A supervised binary decision tree classification of these variables illustrated the potential of this classificatory approach to simplify natural diversity over very large areas using a parameter, photosynthetic activity, that is common to all vegetation.

This study has demonstrated the considerable potential of small scale shortwave vegetation index imagery for purposes of describing and classifying vegetation in terms of both physiognomy and phenology. It has also revealed the importance of data quality.

An attempt was made to acquire sufficient full resolution AVHRR imagery of the Iberian Peninsula to permit a thorough analysis of its vegetation. However, the results suggest that the analysis would have benefited had both more imagery for each

single-date maximum value composite, and also imagery from more dates been available. For example, it seems reasonable to suppose that discrimination among several of the physiognomic and agricultural vegetation cover classes that appear to be phenologically indistinct in this study would be possible if a *continuous* data set comprised of 15-day maximum NDVI value composite images were available. There are two reasons why this would be so. The first is that 15-day maximum NDVI value composites would have less cloud contamination than the images used in this study. The second is that a continuous data set would free the image analyst to pick the most appropriate (i.e. phytophenologically distinctive) data with which to classify individual vegetation cover classes.

The results of this study suggest that there are two ways in which the quality of Global Vegetation Index imagery would be improved. The most important change involves the adoption of a preparation process that does not involve drastic spatial subsampling. This study has shown clearly that the NDVI values in Global Vegetation Index pixels are consistently higher than the area-integrated NDVI values of the area on the ground those pixels represent. The result is a product that consistently overestimates the extent and vigour of photosynthetic activity. The second way in which Global vegetation Index imagery could be improved involves the adoption of an equal-area radial projection base map array. This study has shown that at both extremes of AVHRR spatial resolution, equal-area radial projections provide a representation of the Earth's surface that is better, both practically and ethically, to those currently used by the National Oceanic and Atmospheric Administration.

References

Aase, J.K. and F.H. Siddoway, 1981, Assessing winter wheat dry matter production via spectral reflectance measurements. *Remote Sensing of Environment*, **11**, 267-77.

Ahern, F.J., R.J. Brown, J. Cihlar, R. Gauthier, J. Murphy, R.A. Neville and P.M. Teillet, 1987, Radiometric correction of visible and infrared remote sensing data at the Canada Centre for Remote Sensing. *International Journal of Remote Sensing*, **8**, 1349-76.

Ajai, A.K., S. Gopalan and D.S. Kamat, 1985, Discrimination of winter crops using temporal spectral profiles. *International Journal of Remote Sensing*, 6, 1575-80.

Ali, A., D.A. Quadir and O.K. Huh, 1987, Agricultural, hydrologic and oceanographic studies in Bangladesh with NOAA AVHRR data. *International Journal of Remote Sensing*, **8**, 917-25.

Allen, T.D. (editor), 1983, *Satellite Microwave Remote Sensing*. Ellis Horwood, Chichester, England, 526pp.

Allen, W.A., H.W. Gausman and A.J. Richardson, 1973, Willstäter-Stoll theory of leaf reflectance evaluated by ray tracing. *Applied Optics*, **12**, 2448-53.

Allen, W.A. and A.J. Richardson, 1968, Interaction of light with a plant canopy. *Journal of the Optical Society of America*, **58**, 1023-8.

Allison, L.J. and A. Schnapf, 1983, Meteorological satellites. In *Manual of Remote Sensing* (second edition) edited by R.N. Colwell, American Society of Photogrammetry, Sheridan Press, Falls Church, Virginia, 651-662.

Ambroziak, R.A., 1984, Global crop monitoring: an integrated approach. *Society of Photo-Optical Instrumentation Engineers*, **481**, 238-44.

Amiran, D.H.K. and A.P. Schick, 1961, *Geographical Conversion Tables*. International Geographical Union, Aschmann and Scheller, Zürich, 315pp.

Asrar, G., M. Fuchs, E.T. Kanemasu and J.L. Hatfield, 1984, Estimating absorbed photosynthetic radiation and leaf area index from spectral reflectance in wheat. *Agronomy Journal*, **76**, 300-6.

Asrar, G., E.T. Kanemasu, R.D. Jackson and P.J. Pinter, 1985, Estimation of total above-ground phytomass production using remotely sensed data. *Remote Sensing of Environment*, **17**, 211-20.

Badhwar, G.D., 1980, Crop emergence date determination from spectral data. *Photogrammetric Engineering and Remote Sensing*, **46**, 369-77.

Badhwar, G.D., 1984a, Use of Landsat-derived profile features for spring small-grains classification. *International Journal of Remote Sensing*, 5, 783-97.

Badhwar, G.D., 1984b, Classification of corn and soybeans using multitemporal Thematic Mapper data. *Remote Sensing of Environment*, 16, 175-82.

Badhwar, G.D. and K.E. Henderson, 1981, Estimating development stages of corn from spectral data -an initial model. *Agronomy Journal*, 73, 748-55.

Badhwar, G.D., W. Verhoef and N.J.J. Bunnik, 1985, Comparative study of Suits and SAIL canopy reflectance models. *Remote Sensing of Environment*, 17, 179-95.

Bailey, D., 1987, NOAA 10. *Remote Imaging Group Newsletter*, 10, Remote Imaging Group, 14 Nevis Close, Leighton Buzzard, Bedfordshire, 6-9.

Baker, D., 1987, Remote future for Third World satellite data. *New Scientist*, 116, number 1583, 48-51.

Barnett, T.L. and D.R. Thompson, 1983, Large-area relation of Landsat MSS and NOAA-6 AVHRR spectral data to wheat yields. *Remote Sensing of Environment*, 13, 277-90.

Barrett, E.C. and R.W. Herschy, 1986, A European perspective on satellite remote sensing for hydrology and water management. In *Hydrologic Applications of Space Technology* edited by A.I. Johnson, IAHS Publication 160, International Association of Hydrological Sciences Press, Wallingford, 3-12.

Barrett, E.C. and G. D'Souza, 1986, An objective monitoring method for Africa rainfall based on Meteosat VIS and IR images. In *Proceedings of an International Satellite Land-Surface Climatology Project (ISLSCP) Conference held in Rome, Italy, 2-6th December 1985*, **ESA SP-248**, 305-13.

Bauer, M.E. (editor), 1984, Agriculture and Resources Inventory Surveys Through Aerospace Remote Sensing (AgRISTARS). *Remote Sensing of Environment* (special issue), **14**, 1-278.

Bauer, M.E., J.E. Cipra, P.E. Anuta, J.B. Etheridge, 1979, Identification and area estimation of agricultural crops by computer classification of Landsat MSS data. *Remote Sensing of Environment*, **8** , 77-92.

Baylis, P.E. and R.J.H. Brush, 1985, Satellite image data reception. In *Proceedings of the International Conference of the Remote Sensing Society and the Center for Earth Resources Management "Advanced Technology for Monitoring and Processing Global Environmental Data", University of London 9-12th September*, 13-20.

Beard, J.S., 1973, The physiognomic approach. In *Ordination and Classification of Communities (Handbook of Vegetation Science, Part V)*, edited by R.H. Whittaker, Dr. W. Junk, The Hague, The Netherlands, 355-86.

Becker, F. and B.J. Choudhury, 1988, Relative sensitivity of Normalized Difference Vegetation Index (NDVI) and Microwave Polarization Difference Index (MPDI) for vegetation and desertification monitoring. *Remote Sensing of Environment*, 24, 297-311.

Belward, A.S. and A. de Hoyos, 1987, A comparison of supervised maximum likelihood and decision tree classification for crop cover estimation from multitemporal LANDSAT MSS data. *International Journal of Remote Sensing*, 8, 229-35.

Billings, W.D. and R.J. Morris, 1951, Reflection of visible and infrared radiation from leaves of different ecological groups. *American Journal of Botany*, 38, 327-31.

Bizzari, B., 1986, Status of definition of the imaging radiometer for Meteosat second generation. In *Proceedings of the 6th Meteosat Scientific Users' Meeting, Amsterdam, The Netherlands, 25-27th November (Volume 1)* **EUM P 01**, Eumetsat, Darmstadt, 6pp.

Blümel, K. and W. Tonn, 1986, Satellite-derived vegetation index over Europe. In *Proceedings of an International Satellite Land-Surface Climatology Project (ISLSCP) Conference held in Rome, Italy, 2-6th December 1985*, ESA SP-248, 281-5.

Bowers, S.A. and R.J. Hanks, 1965, Reflection of radiant energy from soils. *Soil Science*, **100**, 130-8.

Brimacombe, C.A., 1981, *Atlas of Meteosat Imagery*. **ESA SP-1030**, European Space Agency Science and Technical Publication Branch, Noordwijk, The Netherlands, 495pp.

Brunel, P. and A. Marouin, 1987, An operational method using ARGOS orbital elements for navigation of AVHRR imagery. *International Journal of Remote Sensing*, **8**, 569-78.

Brush, R.J.H., 1985, A method for real-time navigation of AVHRR imagery. *Institute of Electrical and Electronic Engineers Transactions on Geoscience and Remote Sensing*, **GE-23**, 876-887.

Brush, R.J.H, 1988, The navigation of AVHRR imagery. *International Journal of Remote Sensing*, **9**, 1491-1502 .

Bunnik, N.J.J., 1977, *The Multispectral reflectance of shortwave radiation by agricultural crops in relation with their morphological and optical properties.* Mededelingen Landbouwhogeschool, Wageningen 78-1, The Netherlands, 172pp.

Caprio, J.M., R.J. Hopp and J.S. Williams, 1974, Computer mapping of phenological analysis. In *Phenology and Seasonality Modelling* edited by H. Leith, Springer-Verlag, 77-82.

Carlson, R.E., D.N. Yarger and R.H. Shaw, 1971, Factors affecting the spectral properties of leaves with special emphasis on leaf water status. *Agronomy Journal*, **63**, 486-9.

Carrillo Suárez, M.A., 1988, Drought in Spain. Paper presented at the *International Workshop on Natural Disasters in European-Mediterranean Countries, Perugia, Italy*, 22pp.

Celis-Ceusters, A.M., 1980, Ground truth radiometry (Exotech) on bare and overgrown Belgian soils. *Pedologie*, **30**, 43-66.

Chance, J.E., 1977, Application of Suits spectral model to wheat. *Remote Sensing of Environment*, **6**, 147-50.

Choudhury, B.J., 1987a, Relationships between vegetation indices, radiation absorption and net photosynthesis evaluated by a sensitivity analysis. *Remote Sensing of Environment*, **22**, 209-33.

Choudhury, B.J., 1987b, Estimation of primary productivity over the Thar Desert based upon Nimbus-7 37 GHz data: 1979 through 1985. *International Journal of Remote Sensing*, **8**, 1885-90.

Choudhury, B.J. and C.J. Tucker, 1987a, Monitoring global vegetation using Nimbus-7 37 GHz data: some empirical relations. *International Journal of Remote Sensing*, **8**, 1085-90.

Choudhury, B.J. and C.J. Tucker, 1987b, Satellite observed seasonal and inter-annual variation of vegetation over the Kalahari, The Great Victoria Desert and The Great Sandy Desert: 1979-1984. *Remote Sensing of Environment*, 23, 223-41.

Choudhury, B.J., C.J. Tucker, R.E. Golus and W.W. Newcomb, 1987, Monitoring vegetation using Nimbus-7 scanning multichannel microwave radiometer's data. *International Journal of Remote Sensing*, **8**, 533-8.

Claassen, M.M. and R.H. Shaw, 1970, Water deficit effects on corn. II. Grain components. *Agronomy Journal*, **62**, 652-5.

Coblentz, W.W., 1912, The diffuse reflecting power of various substances. *Bulletin of the Bureau of Standards*, **9**, 283-25.

Colucci, F., 1987, Selling SPOT. *Space*, **3**, 12-16.

Colwell, J.E., 1974, Vegetation canopy reflectance, *Remote Sensing of Environment*, 3, 175-83.

Colwell, R.N., 1956, Determining the prevalence of certain cereal crop diseases by means of aerial photography. *Hilgardia*, **26**, 223-86.

Colwell, R.N., 1963, Basic matter and Energy relationships involved in remote reconnaissance: Report of Subcommitte 1, Photo Interpretation Committee, American Society of Photogrammetry. *Photogrammetric Engineering*, **29**, 761-99.

Colwell, R.N. (editor), 1983, *Manual of Remote Sensing* (second edition). American Society of Photogrammetry, Sheridan Press, Falls Church, Virginia, 2440pp.

Comte, D.M. le, F.N. Kogan, C.A. Steinborn and L. Lambert, 1988, *Assessment of Crop Conditions in Africa.* NOAA Technical Memorandum **NESDIS AISC 13**, 66p.

Cracknell, A.P. and K. Paithoonwattanakij, 1987, Very accurate geocoding of AVHRR data. Poster presented at *the Third AVHRR Data Users Meeting held at Rutherford Appleton Laboratory, Didcot, 16-18th December.*

Crist, E.P. and R.C. Cicone, 1984, A physically-based transformation of Thematic Mapper data - the TM Tasseled Cap. *Institute of Electrical and Electronic Engineers Transactions on Geosience and Remote Sensing*, **GE-22**, 256-63.

Crist, E.P. and R.J. Kauth, 1986, The Tasseled Cap de-mystified. *Photogrammetric Engineering and Remote Sensing*, **52**, 81-6.

Curcio, J.A. and C.C. Petty, 1951, The near infrared absorption spectrum of liquid water. *Journal of the Optical Society of America*, **41**, 302-4.

Curran, P.J., 1981, Multispectral remote sensing of vegetation biomass and productivity. In *Plants and the Daylight Spectrum* edited by H. Smith, Academic Press, London, 65-99.

Curran, P.J., 1982, Multispectral photographic remote sensing of green vegetation biomass and productivity. *Photogrammetric Engineering and Remote Sensing*, 48, 243-50.

Curran, P.J., 1983, Multispectral remote sensing for the estimation of green leaf area index. *Philosophical Transactions of the Royal Society of London* A 309, 257-70.

Curran, P.J., 1985, Aerial photography for the assessment of crop condition: a review. *Applied Geography*, **5**, 347-60.

Curran, P.J. and E.J. Milton, 1983, The relationships between the chlorophyll concentration, LAI and reflectance of a simple vegetation canopy. *International Journal of Remote Sensing*, **4**, 247-255.

Curran, P.J. and S.E. Plummer, 1987, A polar platform for the remote sensing needs of ecology and agriculture: A view from the U.K. *International Journal of Remote Sensing*, **8**, 555-67.

Daughtry, C.S.T., K.P. Gallo and M.E. Bauer, 1983, Spectral estimates of solar radiation intercepted by corn canopies. *Agronomy Journal*, **75**, 527-31.

Dawe, B.R., C. Campbell, D. Finlayson and C. Clarke, 1986, The correlation of actual sea surface temperatures with NOAA AVHRR data and an assessment of the utility of this data to an inshore fisheries investigation. In *Proceedings of the Tenth Canadian Symposium on Remote Sensing, Edmonton, Alberta, 5-8th May*, 715 (abstract).

Dickinson, R.E., 1983, Land surface processes and climate-surface albedo and energy balance. *Advances in Geophysics*, **25**, 305-53.

Dijk, A. van, D. McCrary, S. LeDuc and M. Lyon, 1984, *AVHRR Training Set*. Prepared by National Oceanic and Atmospheric Administration/National Environmental Satellite, Data, and Information Service/Assessment and Information Services Center in co-operation with the Atmospheric Science Department and Geographic Resource Center of the University of Missouri-Columbia, 97pp.

Donoghue, D.N.M. and I. Shennan, 1987, A preliminary assessment of Landsat TM imagery for mapping vegetation and sediment distribution in the Wash estuary. *International Journal of Remote Sensing*, **8**, 1101-8.

Duchossois, G., 1985, ERS-1: Mission objectives and sytem description. *Progress in Astronautics and Aeronautics*, **97**, 536-53.

Duggin, M.J., 1985, Factors limiting the discrimination and quantification of terrestrial features using remotely sensed radiance. *International Journal of Remote Sensing*, **6**, 3-27.

Duggin, M.J. and D. Piwinski, 1984, Recorded radiance indices for vegetation monitoring using NOAA AVHRR data; atmosphere and other effects in multitemporal data sets. *Applied Optics*, **23**, 2620-3.

Duggin, M.J. and L.B. Schoch, 1984, The dependence of target discriminibility on systemmatic and random variations in recorded radiance. *International Journal of Remote Sensing*, **5**, 505-10.

Duggin, M.J., D. Piwinski, V. Whitehead, G. Ryland, 1982a, Evaluation of NOAA-AVHRR data for crop assessment. *Applied Optics*, **21**, 1873-5.

Duggin, M.J., L. Schoch and T.I. Gray, 1982b, Effect of sub-pixel sized cloud on vegetation assessment from satellite data. *Society of Photo-Optical Instrumentation Engineers*, **345**, 97-101.

Duggin, M.J., L. Schoch, T. Cunia and D. Piwinski, 1984, Effects of random and systemmatic variations in unresolved cloud on recorded radiance and target discriminibility. *Applied Optics*, 23, 387-95.

Dundee Satellite Receiving Station, 1985, *Advanced Very High Resolution Radiometer Ground Station*. Department of Electrical Engineering, University of Dundee, Scotland, 4pp.

Dundee Satellite Receiving Station, 1986, *Satellite Image Products available from Dundee University*. Department of Electrical Engineering, University of Dundee, Scotland, 9pp.

Egbert, D.D. and F.T. Ulaby, 1972, Effect of angles on reflectivity. *Photgrammetric Engineering*, **38**, 556-564.

Ellingsen, E., M.R. Boswell, O. Hogtun, J.P. Pedersen and C. McGeachy, 1986, *European utilisation of Tiros-N data -Proposal for a co-ordinated service (Final Report)*. ESA Contract Report **ESRIN 6296/86/HGE-1**.

Elvidge, C.D. and R.J.P. Lyon, 1985, Influence of rock-soil spectral radiation on the assessment of green biomass. *Remote Sensing of Environment*, 17, 265-79.

Eumetsat, 1987, *Meteosat Dissemination News (1)*, Eumetsat, 6100 Darmstadt-Eberstadt, Federal Republic of Germany.

Ezra, C.E., L.R. Tinney and R.D. Jackson, 1984, Effect of soil background on vegetation discrimination using Landsat data. *Remote Sensing of Environment*, 16, 233-242.

Falconer, A., 1985, Satellite remote sensing technology in East and Southern African development projects (unpublished manuscript). Regional Centre for Services in Surveying, Mapping and Remote Sensing, PO Box 18118, Nairobi, Kenya, 11pp.

FAO, 1984, Agroclimatological data for Africa. *Plant Production and Protection Series*, **22**, Food and Agriculture Organization of the United Nations, Rome.

FAO, 1985, *Food Crops and Shortages (Special Reports)*. Food information Group (ESC), Food and Agriculture Organization of the United Nations, Rome.

FAO, 1986, *Food Crops and Shortages (Special Reports)*. Food information Group (ESC), Food and Agriculture Organization of the United Nations, Rome.

Fischer, J.C., 1987, *Planning for future operational sensors and other priorities*. NOAA Technical Report **NESDIS 30**, 46pp.

Flint, H.L., 1974, Phenology and genecolgy of woody plants. In *Phenology and Seasonality Modelling* edited by H. Leith, Springer-Verlag, 83-95.

Fosberg, F.R., 1967, A classification of vegetation for general purposes. In *Guide to the Checksheet for IBP Areas* (compiled by G.F. Peterken), International Biological Program Handbook **4**, 73-120.

Fraser, R.S. and Y.F. Kaufman, 1985, The relative importance of aerosol scattering and absorption in remote sensing. *Institute of Electrical and Electronic Engineers Transactions on Geoscience and Remote Sensing*, **GE-23**, 625-33.

Fukshansky, L., 1981, Optical properties of plants. In *Plants and the Daylight Spectrum* edited by H. Smith, Academic Press, London, 21-40.

Fusco, L. and K. Muirhead, 1987, AVHRR data services in Europe - the Earthnet approach. *ESA Bulletin*, 49, 9-19.

Gallo. K.P. and C.S.T. Daughtry, 1987, Differences in vegetation indices for simulated Landsat-5 MSS and TM, NOAA-9 AVHRR, and SPOT-1 sensor sytems. *Remote Sensing of Environment*, **23**, 439-52.

Gallo, K.P. and T.K. Flesch, 1987, Crop development in the U.S. corn belt monitored with the NOAA AVHRR. Preprint volume of the *18th Conference on Agricultural and Forest Meteorology and the 8th Conference on Biometeorology and Aerobiology*, American Meteorological Society, Boston, 101-2.

Gallo, K.P., C.S.T. Daughtry and M.E. Bauer, 1985, Spectral estimation of absorbed photosynthetically active radiation in corn canopies. *Remote Sensing of Environment*, **17**, 221-232.

Garcia, O., 1985, *An Atlas of Highly Reflective Clouds for the Global Tropics 1971-1983*. National Oceanic and Atmospheric Administration Environmental Research Laboratories, Government Printing Office, Washington, D.C.

Gates, D.M. and W. Tantraporn, 1952, The reflectivity of deciduous trees and herbaceous plants in the infrared to 25 microns. *Science*, **115**, 613-6.

Gates, D.M., H.J. Keegan, J.C. Schleter and V.R. Weidner, 1965, Spectral properties of plants. *Applied Optics*, **4**, 11-20.

Gatlin, J.A., C.J. Tucker and S.R. Schneider, 1981, Use of NOAA-6 AVHRR channel one and two for monitoring vegetation. In *Proceedings of the 1981 International Geoscience and Remote Sensing Symposium, Institute of Electrical and Electronic Engineers, New York*, 454 (abstract).

Gatlin, J.A., R.J. Sullivan and C.J. Tucker, 1984, Considerations of and improvements to large-scale vegetation monitoring. *Institute of Electrical and Electronic Engineers Transactions on Geoscience and Remote Sensing*, **GE-22**, 496-502.

Gausman, H.W., W.A. Allen, R. Cardenas and A.J. Richardson, 1970, Relation of light reflectance to histological and physical evaluations of cotton leaf matirity (*Gossypium hirsutum L.*). *Applied Optics*, **9**, 545-52.

Gervin, J.C., A.G. Kerber, R.G. Witt, Y.C. Lu and R. Sekhon, 1985, Comparison of level 1 land cover classification accuracy for MSS and AVHRR data. *International Journal of Remote Sensing*, **6**, 47-57.

Gorman, R.W. and A. Sadowsky, 1986, Operational use of direct receive NOAA and Meteor satellite APT images for strategic route planning of an arctic class commercial vessel. In *Proceedings of the Tenth Canadian Symposium on Remote Sensing, Edmonton, Alberta, 5-8th May*, 775-84.

Goudriaan, J., 1977, *Crop Micrometeorology: a Simulation Study*. Centre for Agricultural Publishing and Documentation (PUDOC), Wageningen, 249pp.

Goward, S.A., C.J. Tucker and D. Dye, 1985, North American vegetation patterns observed with the NOAA-7 Advanced Very High Resolution Radiometer. *Vegetatio*, **64**, 3-14.

Goward, S.N., D.G. Dye, A. Kerber and V. Kalb, 1987, Comparison of North and South American biomes from AVHRR observations. *Geocarto*, 1, 27-39.

Gray, T.I. and D.G. McCrary, 1981, *Meteorological Satellite Data - a Tool to Describe the Health of the World's Agriculture*. AgRISTARS Report EW-N1-04042, Johnson Space Flight Center, Houston, Texas, 7pp.

Greaves, J.R. and W.E. Shenk, 1985, The development of the geosynchronous weather satellite system. *Progress in Astronautics and Aeronautics*, 97, 150-81.

GTT, 1987, Abstracts of papers presented at the *II Reunión Nacional del Grupo de Trabajo en Teledetección 17-18th December, Valencia*, 82pp.

Gutman, G., 1987, The derivation of vegetation indices from AVHRR data. *International Journal of Remote Sensing*, 8, 1235-43.

Hall, F.G. and G.D. Badhwar, 1987, Signature-extendable technology: Global space-based crop recognition. *Institute of Electrical and Electronic Engineers Transactions on Geoscience and Remote Sensing*, GE-25, 93-103.

Harrison, A.R. and R.M. Lucas, 1988, Multispectral classification of snow using NOAA AVHRR imagery. *International Journal of Remote Sensing* (in press).

Hatfield, J.L., 1983, Remote Sensing estimation of potential and actual crop yield. *Remote Sensing of Environment*, 13, 301-11.

Hatfield, J.L., G. Asrar and E.T. Kanemasu, 1984, Intercepted photosynthetically active radiation estimated by spectral reflectance. *Remote Sensing of Environment*, 14, 65-75.

Hayes, L., 1985, The current use of TIROS-N series of meteorological satellites for land-cover studies. *International Journal of Remote Sensing*, 6, 35-45.

Hayes, L. and A.P. Cracknell, 1984a, Vegetation depiction by AVHRR - a Scottish sampling. In *Proceedings of the 10th Annual Conference of the Remote Sensing Society, Reading*, 181-90.

Hayes, L. and A.P. Cracknell, 1984b, A comparison of Tiros-N series satellite data and Landsat data over Scotland. In *Proceedings of an EARSeL/ESA Symposium on Integrative Approaches in Remote Sensing (8-11th April 1984, Guildford, Surrey)*, ESA SP-214, 63-74.

Hayes, L. and A.P. Cracknell, 1985, An investigation of NOAA-7 LAC data for the provision of land cover information over large areas.In *Proceedings of the Poster Sessions at the International Conference of the Remote Sensing Society and The Center for Environmental Resources Management "Remote Sensing: Data Acquiation, Management and Applications" held in the University of London 9-12th September, 1985*, 81-90.

Henderson, K.E. and G.D. Badhwar, 1984, An initial model for estimating soybean develpoment stages from spectral data. *Remote Sensing of Environment*, 14, 55-63.

Henricksen, B.L. and J.W. Durkin, 1986, Growing period and drought early warning in Africa using satellite data. *International Journal of Remote Sensing*, 7, 1583-1608.

Hielkema, J.U., J. Roffey and C.J. Tucker, 1986, Assessment of ecological conditions associated with the 1980/81 desert locust plague upsurge in West Africa using environmental satellite data. *International Journal of Remote Sensing*, 7, 1609-22.

Hiernaux, P.H.Y. and C.O. Justice, 1986, Suivi du développement végétal au cours de l'été 1984 dans le Sahel Malien. *International Journal of Remote Sensing*, 7, 1515-31.

Hipps, L.E., G. Asrar and E.T. Kanemasu, 1983, Assessing the interception of photosynthetically active radiation in winter wheat. *Agricultural Meteorology*, 28, 253-9.

Ho, D. and A. Asem, 1986, NOAA AVHRR image referencing. *International Journal of Remote Sensing*, 7, 895-904.

Hoffer, R.M., 1984, Remote sensing to measure the distribution and structure of vegetation. In *The Role of Terrestrial Vegetation in the Global Carbon Cycle: Measurement by Remote Sensing* edited by G.M. Woodwell, John Wiley, 131-59.

Hogg, H.C. (editor), 1986, Agriculture and Resouces Inventory Surveys Through Aerospace Remote Sensing (AgRISTARS), *Institute of Electrical and Electronic Engineers Transactions on Geoscience and Remote Sensing* (special issue), GE-24, 3-184.

Holben, B.N., 1986, Characteristics of maximum-value composite images from temporal AVHRR data. *International Journal of Remote Sensing*, 7, 1417-34.

Holben, B. and R.S. Fraser, 1984, Red and near-infrared sensor response to off-nadir viewing. *International Journal of Remote Sensing*, 5, 145-60.

Holben, B.N., C.J. Tucker and F. Cheng-Jeng, 1980, Spectral assessment of soybean leaf area and leaf biomass. *Photogrammetric Engineering and Remote Sensing*, **46**, 651-6.

Holben, B., D. Kimes and R.S. Fraser, 1986, Directional reflectance response in AVHRR red and near-ir bands for three cover types and varying atmospheric conditions. *Remote Sensing of Environment*, **19**, 213-36.

Hopp, R.J., 1974, Plant phenology observation networks. In *Phenology and Seasonality Modelling* edited by H. Leith, Springer-Verlag, 25-43.

Horler, D.N.H. and J. Barber, 1981, Principles of remote sensing of plants. In *Plants and the Daylight Spectrum* edited by H. Smith, Academic Press, London, 43-63.

Howard, J.A. and C.W. Mitchell, 1980, Phyto-geomorphic classification of the landscape. *Geoforum*, 11, 85-106.

Huete, A.R., D.F. Post and R.D. Jackson, 1984, Soil spectral effects on 4-space vegetation discrimination. *Remote Sensing of Environment*, **15**, 155-65.

Huete, A.R., R.D. Jackson and D.F. Post, 1985, Spectral response of a plant canopy with different soil backgrounds. *Remote Sensing of Environment*, 17, 37-53.

Hussey, W.J., 1977, *The Tiros-N polar orbiting environmental satellite system*. National Oceanic and Atmospheric Administration, Department of Commerce, Washington, D.C., 33pp.

Hussey, W.J., 1985, The economic benefits of operational environmental satellites. *Progress in Astronautics and Aeronautics*, 97, 216-60.

IIS, 1984, *System 575 Software, Users' Manual*. International Imaging Systems, California.

Ives, R.L., 1939, Infrared photography as an aid in ecological surveys. *Ecology*, 20, 433-9.

Jackson, R.D., 1983, Spectral indices in n-space. *Remote Sensing of Environment*, 13, 409-21.

Jackson, R.D., P.N. Slater and P.J. Pinter, 1983, Discrimination of growth and water stress in wheat by various vegetation indices through clear and turbid atmospheres. *Remote Sensing of Environment*, **13**, 187-208.

Jordan, C.F., 1969, Derivation of leaf-area index from quality of light on the forest floor. *Ecology*, **50**, 663-6.

Justice, C.O. (editor), 1986, Monitoring the grasslands of semi-arid Africa using NOAA AVHRR data. *International Journal of Remote Sensing* (special issue), 7, 1383-1622.

Justice, C.O., and P.H.Y. Hiernaux, 1986, Monitoring the grasslands of the Sahel using NOAA AVHRR data: Niger 1983. *International Journal of Remote Sensing*, 7, 1475-97.

Justice, C.O., J.R.G. Townshend, B.N. Holben and C.J. Tucker, 1985, Analysis of the phenology of global vegetation using meteorological satellite data. *International Journal of Remote Sensing*, **6**, 1271-318.

Justice, C.O., B.N. Holben and M.D. Gwynne, 1986, Monitoring East African vegetation using AVHRR data. *International Journal of Remote Sensing*, 7, 1453-74.

Justice, C.O., J.R.G. Townshend and B.L. Markham, 1987, MODIS spatial resolution study. *International Journal of Remote Sensing*, **8**, 1119-21.

Justus, C.G., 1985, *Study of Cloud Screening and Analysis Methods for AgRISTARS Vegetation Index Products*. Georgia Institute of Technology, Atlanta, Georgia, 131pp.

Kamat, D.S., Ajai, M.N. Sashi Kumar, S.K. Sinha, G.S. Chaturvedi and A.K. Singh, 1983, Relationship of spectral parameters of wheat crop with yield. *Indian Journal of Agricultural Science*, **53**, 89-93.

Kauth, R.J. and G.S. Thomas, 1976, The Tasselled Cap- a graphic description of the spectral-temporal development of agricultural crops as seen by Landsat. In *Proceedings of the Symposium on Machine Processing of Remotely Sensed Data. Purdue University, West Lafayette, Indiana*, 4B41-4B51.

Kidwell, K.B., 1986, *NOAA Polar Orbiter Data Users Guide*. National Oceanic and Atmospheric Administration Satellite Data Services Division, Climatic Data Center, Washington D.C.

Kimes, D.S., 1984, Modeling the directional reflectance from complete homogeneous vegetation canopies with various leaf-orientation distributions. *Journal of the Optical Society of America*, **A1**, 725-37.

Kimes, D.S. and J.A. Kirchener, 1982, Radiative transfer model for heterogeneous 3-D scenes. *Applied Optics*, 21, 4119-29.

Kimes, D.S., B.L. Markham, C.J. Tucker and J.E. McMurtrey, 1981, Temporal relationships between spectral response and agricultural variables of a corn canopy. *Remote Sensing of Environment*, 11, 401-11.

Knipling, E.B., 1969, Leaf reflectance and image formation on color infrared film. In *Remote Sensing in Ecology* edited by P.L. Johnson, University of Georgia Press, Athens, Georgia, 17-29.

Knipling, E.B., 1970, Physical and physiological basis for the reflectance of visible and near-infrared radiation for vegetation. *Remote Sensing of Environment*, 1, 155-9.

Kollenkark, J.C., C.S.T. Daughtry, M.E. Bauer and T.L. Horsley, 1982a, Effects of cultural practices on agronomic and reflectance characteristics of soybean canopies. *Agronomy Journal*, 74, 751-8.

Kollenkark, J.C., V.C. Vanderbilt, C.S.T. Daughtry and M.E. Bauer, 1982b, Influence of solar illumination angle on soybean canopy reflectance. *Applied Optics*, 21, 1179-84.

Kubelka, P. and F. Munk, 1931, Ein beitrag zur optik der farbanstriche. *Zeitschrift für Technische Physik*, 12, 593-601.

Küchler, A.W., 1967, *Vegetation Mapping*. The Ronald Press Company, New York, 472pp.

Küchler, A.W., 1969, Natural and cultural vegetation. *Professional Geographer*, 21, 383-5.

Kumar, M. and J.L. Monteith, 1981, Remote sensing of crop growth. In *Plants and the Daylight Spectrum* edited by H. Smith, Academic Press, London, 133-144.

Kumar, R. and L. Silva, 1973, Light ray tracing through a leaf cross section. *Applied Optics*, 12, 2950-4.

Kumar, R. and L.F. Silva, 1977, Separability of agricultural cover types by remote sensing in the visible and infrared wavelength regions. *Institute of Electrical and Electronic Engineers Transactions on Geoscience and Remote Sensing*, GE-15, 42-9.

Lacaze, B. and R. Joffre, 1987, Caractérisation de formations végétales mediterranéenes à partir de donées 'Thematic Mapper'. Une étude de cas en Andalousie (Espagne). *International Journal of Remote Sensing*, 8, 1319-33.

Lagouarde, J.P. and Y. Kerr, 1986, On the effect of atmospheric conditions on NOAA-AVHRR normalised difference vegetation indices. In *Proceedings of an International Satellite Land-Surface Climatology Project (ISLSCP) Conference held in Rome, Italy, 2-6th December 1985*, ESA SP-248, 301.

Laubenfels, D.J. de, 1975, *Mapping the World's Vegetation: Regionalisation of Formations and Flora*. Syracuse University Press, New York, 246pp.

Lauritson, L., G.J. Nelson and F.W. Porto, 1979, *Data Extraction and Calibration of Tiros-N/NOAA Radiometers*. NOAA Technical Memorandum NESS 107, 58pp.

Leith, H., 1974a, *Phenology and Seasonality Modelling*. Springer-Verlag, 444pp.

Leith, H., 1974b, Purposes of a phenology book. In *Phenology and Seasonality Modelling* edited by H. Leith, Springer-Verlag, 3-19.

Lillesand, T.M. and R.W. Kiefer, 1987, *Remote Sensing and Image Interpretation* (second edition). John Wiley, 722pp.

Lloyd, D., 1988, A phenological description of Iberian vegetation using shortwave vegetation index imagery. *International Journal of Remote Sensing* (in press).

Lloyd, D. and E.C. Barrett, 1986, Mapping and monitoring the vegetation of the Iberian Peninsula using small-scale radiometric data from NOAA satellites. *Journal of the British Interplanetary Society*, 39, 535-41.

Lo, T.H.C., F.L. Scarpace and T.M. Lillesand, 1986, Use of multitemporal spectral profiles in agricultural land-cover classification. *Photogrammetric Engineering and Remote Sensing*, 52, 535-44.

MacDonald, R.B. and F.G. Hall, 1980, Global crop forecasting. *Science*, 208, 670-9.

Mack, A.R., E.J. Brach and C.R. Rao, 1984, Appraisal of multispectral scanner systems from analysis of high resolution plant spectra. *International Journal of Remote Sensing*, 5, 279-88.

Malaisse, F.P., 1974, Phenology of the Zambezian woodland area with emphasis on the miombo ecosystem. In *Phenology and Seasonality Modeling* edited by H. Leith, Springer-Verlag, 269-86.

Malingreau, J., 1986, Global vegetation dynamics: Satellite observation over Asia. *International Journal of Remote Sensing*, 7, 1121-46.

Malingreau, J.P., G. Stephens and L. Fellows, 1985, Remote sensing of forest fires: Kalimantan and North Borneo in 1982-83. *Ambio*, 14, 314-21.

MAPA, 1979, *Las Coniferas en el Primer Inventario Forestal Nacional*. Instituto Nacional para la Conservación de la Naturaleza, Ministerio de Agricultura, Pesca y Alimentación, Madrid, 174pp.

MAPA, 1980, *Las Frondosas en el Primer Inventario Forestal Nacional*. Instituto Nacional para la Conservación de la Naturaleza, Ministerio de Agricultura, Pesca y Alimentación, Madrid, 236pp.

MAPA, 1982, *Calendario de Siembra, Floración y Recolección* (third edition). Secretaria General Técnica, Ministerio de Agricultura, Pesca y Alimentación, Madrid, 553pp.

MAPA, 1986, *Avances de Superficies y Producciones Agricolas; Estimaciones en Noviembre*. Sevicio de Estadísticas Agrarias, Secretaría General Técnica, Ministerio de Agricultura, Pesca y Alimentación, Madrid, 62pp.

MAPA, 1988, *Mapas de Cultivos y Aprovechamientos de las Provincias de España a Escala 1:200 000* (series not yet completed). Dirección General de la Producción Agraria, Ministerio de Agricultura, Pesca y Alimentación, Madrid.

Matson, M. and B. Holben, 1987, Satellite detection of tropical burning in Brazil. *International Journal of Remote Sensing*, 8, 509-16.

Matson, M., G. Stephens and S. Robinson, 1987, Fire detection using data from the NOAA-N satellites. *International Journal of Remote Sensing*, 8, 961-70.

Maxwell, E.L., 1976, Multivariate system analysis of multispectral imagery. *Photogrammetric Engineering and Remote Sensing*, 42, 1173-86.

McGinnis, D.F. and J.D. Tarpley, 1985, Vegetation cover mapping from NOAA/AVHRR. *Advanced Space Research*, 5, 359-69.

Meador, W.E. and W.R. Weaver, 1980, Two-stream approximations to radiative transfer in planetary atmospheres: a unified description of existing methods and a new improvement. *Journal of Atmospheric Science*, 37, 630-43.

Mestre, H., 1935, The absorption of radiation by leaves and algae. In *Proceedings of the Cold Spring Harbor Symposia on Quantitative Biology*, 3, 191-209.

Milton, E.J. and N.W. Wardley, 1987, *Vegetation Canopy Reflectance Models: a review*. Discussion Paper 31, Department of Geography, University of Southampton, 45pp.

Moik, J.G., 1980, *Digital Processing of Remotely Sensed Images*. NASA SP-431, Government Printing Office, Washington, D.C., 330pp (out of print 1983).

Monteith, J.L., 1977, Climate and efficiency of crop production in Britain. *Philosophical Transactions of the Royal Society of London* B 271, 277-94.

Morain, S.A., 1974, Phenology and remote sensing. In *Phenology and Seasonality Modelling* edited by H. Leith, Springer-Verlag, 55-75.

Moss, R.A. and W.E. Loomis, 1952, Absorption spectra of leaves. I. The visible spectrum. *Plant Physiology*, 27, 370-91.

MTTC, 1982, *Guía Resumida del Clima en España*. Publication D-25, Servicio de Climatología, Instituto Nacional de Meteorología, Ministerio de Transportes, Turismo y Comunicaciones, Madrid, 52pp.

MTTC, 1983, *Atlas Climático de España*. Instituto Nacional de Meteorología, Ministerio de Transportes, Turismo and Comunicaciones, Madrid, 48pp.

Neblette, C.B., 1927, Aerial photography for study of plant diseases. *Photo Era Magazine*, 58, 346.

Neblette, C.B., 1928, Airplane photography for plant disease surveys. *Photo Era Magazine*, 59, 175.

Nelson, R. and B. Holben, 1986, Identifying deforestation in Brazil using multiresolution satellite data. *International Journal of Remote Sensing*, 7, 429-48.

Nelson, R., D. Case, N. Horning, V. Anderson and S. Pillai, 1987a, Continental land cover assessment using Landsat MSS data. *Remote Sensing of Environment*, 21, 61-81.

Nelson, R., N. Horning and T.A. Stone, 1987b, Determining the rate of forest conversion in Mato Grosso, Brazil, using Landsat MSS and AVHRR. *International Journal of Remote Sensing*, 8, 1767-84.

NOAA, 1986, *Global Vegetation Index Users Guide*. Satellite Data Services Division, National Climatic Data Center, National Oceanic and Atmospheric Administration, Washington D.C., 27pp.

Norwine, J. and D.H. Greegor, 1983, Vegetation classification based on Advanced Very High Resolution Radiometer (AVHRR) satellite imagery. *Remote Sensing of Environment*, 13, 69-87.

Norwood, V.T. and J.C. Lansing, 1983, Electro-optical imaging sensors. In *Manual of Remote Sensing* (second edition) edited by R.N. Colwell, American Society of Photogrammetry, Sheridan Press, 335-67.

NRSC, 1987, *SPOT Users Guide*. United Kingdom National Remote Sensing Centre, Farnborough.

Odenweller, J.B. and K.I. Johnson, 1984, Crop identification using Landsat temporal-spectral profiles. *Remote Sensing of Environment*, **14**, 39-54.

Ormsby, J.P., 1982, Classification of simulated and actual NOAA-6 AVHRR data for hydrologic land-surface feature definition. *Institute of Electrical and Electronic Engineers Transactions on Geoscience and Remote Sensing*, GE-20, 262-8.

Park, A.B., 1984, Coupling remotely sensed data to ground observation. In *The Role of Terrestrial Vegetation in the Global Carbon Cycle: Measurement by Remote Sensing* edited by G.M. Woodwell, John Wiley, 181-9.

Paris, J.F., 1986, The effect of leaf size on the microwave backscattering by corn. *Remote Sensing of Environment*, **19**, 81-95.

Perry, C.R. and L.F. Lautenschlager, 1984, Functional equivalence of spectral vegetation indices. *Remote Sensing of Environment*, **14**, 169-82.

Peters, A., 1967, *Die perspektivische Verzerrung von Raum und Zeit im historisch-geographischen Weltbilde der Gegenwart und ihre Überwindung durch neue Darstellungsweisen*. Vortrag an der Ungarischen Akademie der Wissenschaften in Budapest am 6.10.1967.

Peters, A., 1979, *The Europe-centred Character of our Geographical View of the World and its Correction*. Universum Verlag, Munich-Solln, 24pp.

Peters, A., 1982, *Space and Time: Their equal representation as an essential basis for a scientific view of the world* (lecture on 'Geo-Cultural Visions of the World', given at a symposium at the United Nations University, Cambridge, England, 29th March). Friendship Press, New York, 41pp.

Peters, A., 1983, *The New Cartography*. Friendship Press, New York. 163pp.

Pinter, P.J., R.D. Jackson, S.B. Idso and R.J. Reginato, 1981, Multidate spectral reflectance as predictors of yield in water stressed wheat and barley. *International Journal of Remote Sensing*, 2, 43-8.

Polunin, O. and B.E. Smythies, 1973, *Flowers of South-West Europe: a Field Guide*. Oxford University Press, London, 480pp.

Popham, R.W., 1987, HRPT station locations, applications, and communications. Papaer presented at the *Third AVHRR Data Users Meeting held at Rutherford Appleton Laboratory, Didcot, England, 16-18th December*.

Pratt, W.K., 1978, *Digital Image Processing*, John Wiley, New York, 750pp.

Price, J.C., 1987a, Calibration of satellite radiometers and the comparison of vegetation indices. *Remote Sensing of Environment*, 21, 15-27.

Price, J.C., 1987b, Radiometric calibration of satellite sensors in the visible and near-infrared: history and outlook. *Remote Sensing of Environment*, 22, 3-9.

Price, J.C., (editor), 1987c, Radiometric calibration of satellite data. *Remote Sensing of Environment* (special issue), 22, 1-158.

Prince, S.D. and W.L. Astle, 1986, Satellite remote sensing of rangelands in Botswana I. Landsat MSS and herbaceous vegetation. *International Journal of Remote Sensing*, 7, 1533-53.

Prince, S.D. and C.J. Tucker, 1986, Satellite remote sensing of rangelands in Botswana II. NOAA AVHRR and herbaceous vegetation. *International Journal of Remote Sensing*, 7, 1555-70.

Qing-Yun, S. and K.S. Fu, 1983, A method for the design of binary tree classifiers. *Pattern Recognition*, 16, 593-603.

Rabideau, G.S., C.S. French and A.S. Holt, 1946, The absorption and reflection spectra of leaves, chloroplast suspensions and chloroplast fragments as measured in an Ulbricht sphere. *American Journal of Botany*, 33, 769-77.

Rao, V.R., E.J. Brach and A.R. Mack, 1979, Bidirectional reflectance of crops and soil contribution. *Remote Sensing of Environment*, 8, 115-25.

Reader, R., J.S. Radford and H. Leith, 1974, Modelling important phytophenological events in eastern North America. In *Phenology and Seasonality Modelling* edited by H. Leith, Springer-Verlag, 329-42.

Richards, J.A., 1986, *Remote Sensing Digital Image Analysis*. Springer-Verlag, 281pp.

Richardson, A.J. and C.L. Wiegand, 1977, Distinguishing Vegetation from soil background information. *Photogrammetric Engineering and Remote Sensing*, 43, 1541-52.

Rouse, J.W., R.H. Haas, D.W. Deering and J.A. Schell, 1973, Monitoring vegetation systems in the Great Plains with ERTS. In *Third Earth Resources Technology Satellite-1 Symposium: Technical Presentations*, NASA-SP-351, 309-17.

Rouse, J.W., R.H. Haas, J.A. Schell, D.W. Deering and J.C. Harlan, 1974, *Monitoring the Vernal Advancement and Retrogradation (Green Wave Effect) of Natural Vegetation*. National Aeronautics and Space Administration/Goddard Space Flight Center Type III Final Report for the period September 1972 to November 1974, Greenbelt, Maryland, 371pp.

Sader, S.A. and A.T. Joyce, 1985, Global tropical forest monitoring. In *Proceedings of the International Conference of the Remote Sensing Society and the Center for Earth Resources Management "Advanced Technology for Monitoring and Processing Global Environmental Data" held at the University of London 9-12th September*, 41-50.

Saull, R., 1985, Land applications of the Advanced Very High Resolution Radiometer (AVHRR): a UK example. In *Proceedings of the Poster Sessions at the International Conference of the Remote Sensing Society and The Center for Environmental Resources Management "Remote Sensing: Data Acquisition, Management and Applications" held in the University of London 9-12th September, 1985*, 57-66.

Schnapf, A., 1982, *The Development of the Tiros Global Environmental Satellite System*. National Aeronautics and Space Administration Conference Publication 2227, 7-16.

Schnapf, A., 1985, The TIROS meteorological satellites- twenty-five years: 1960-1985. *Progress in Astronautics and Aeronautics*, 97, 51-70.

Schneider, S.R. and D.F. McGinnis, 1982, The NOAA/AVHRR: A new satellite sensor for monitoring crop growth. In *Machine Processing of Remotely Sensed Data Symposium*, Laboratory for Applications of Remote Sensing, West Lafayette, Indiana, 281-90.

Schowengerdt, R.A., 1983, *Techniques for Image Processing and Classification in Remote Sensing*. Academic Press, New York, 249pp.

Schwalb, A., 1978, *The Tiros-N/NOAA A-G satellite series*. NOAA Technical Memorandum NESS 95, United States Department of Commerce, 75pp.

Schwalb, A., 1982, *Modified version of the Tiros N/NOAA A-G satellite series (NOAA E-J) -Advanced Tiros N (ATN)*. NOAA Technical Memorandum NESS 116, United States Department of Commerce, 23pp.

Scott D., P.H. Menalda and R.W. Brougham, 1969, Spectral analysis of radiation transmitted and reflected by different vegetations. *New Zealand Journal of Botany*, 6, 427-49.

Seaford, P. (editor), 1987, *Remote Imaging Group Newsletter* 10. Remote Imaging Group, 14 Nevis Close, Leighton Buzzard, Bedfordshire, 36pp.

Sellers, P.J., 1985, Canopy reflectance, photosynthesis and transpiration. *International Journal of Remote Sensing*, 6, 1335-72.

Sellers, P.J. and F.G. Hall, 1987, *Experiment Plan: Konza Prairie 1987-1989*. First International Satellite Land Surface Climatology Project Field Experiment, 175pp (obtained from the first author).

Seybold, A. and A. Weissweiler, 1943, Clarification of some elementary problems in photophysiology. *Botanical Archives*, 44, 456-520.

Shimwell, D.W., 1971, *Description and Classification of Vegetation*. Sidgwick and Jackson, London, 322pp.

Shimwell, D.W.,1984, Vegetation Analysis. In *Themes in Biogeography* edited by J.A. Taylor, Croom Helm, Beckenham, Kent, 132-62.

Shull, C.A., 1929, A spectrophotometric study of reflection of light from leaf surfaces. *Botanical Gazette*, 87, 583-607.

Sieber, A.J., 1985, Forest signatures in imaging and non-imaging microwave scatterometer data. *ESA Journal*, 9, 431-48.

Simonett, D.S., 1983, The development and principles of remote sensing. In *Manual of Remote Sensing* (second edition) edited by R.N. Colwell, American Society of Photogrammetry, Sheridan Press, Falls Church, Virginia, 1-35.

Sinclair, T.R., M.M. Schreiber and R.M. Hoffer, 1973, Diffuse reflectance hypothesis for the pathway of solar radiation through leaves. *Agronomy Journal*, **65**, 276-83

Singh, A., 1984, Some clarifications about the pairwise divergence measure in remote sensing. *International Journal of Remote Sensing*, **5**, 623-7.

Singh, A., 1987a, Spectral separability of tropical forest cover classes. *International Journal of Remote Sensing*, **8**, 971-9.

Singh, S.M., 1987b, Lowest order correction to GVI data for solar zenith angle effect. Paper presented at the *Third AVHRR Data Users Meeting held at Rutherford Appleton Laboratory, Didcot, England, 16-18th December.*

Slater, P.N., 1980, *Remote Sensing: Optics and Optical Systems.* Addison-Wesley, Massachusetts, 575pp.

Smith, H. and D.C. Morgan, 1981, The spectral characteristics of the visible radiation incident upon the surface of the Earth. In *Plants and the Daylight Spectrum* edited by H. Smith, Academic Press, London, 3-20.

Smith, J.A. and R.E. Oliver, 1974, Effects of changing canopy directional reflectance on feature selection. *Applied Optics*, **13**, 1599-1604.

Smith, W.L., W.P. Bishop, V.F. Dvorak, C.M. Hayden, J.H. McElroy, F.R. Mosher, V.J. Oliver, J.F. Purdon and D.Q. Wark, 1986, The meteorological satellite: Overview of 25 years of operation. *Science*, **231**, 455-62.

Steiner, D., 1969, Time dimension for crop surveys from space. *Photogrammetric Engineering*, **35**, 187-94.

Steven, M.D., 1983, The physical and physiological interpretation of infrared/red spectral ratios over crops. In *Field Radiometry*, The Remote Sensing Society.

Steven, M.D., 1987, Ground truth: an underview. *International Journal of Remote Sensing*, **8**, 1033-8.

Steven, M.D. and T.H. Demetriades-Shah, 1987, Spectral indices of crop productivity under conditions of stress. In *Proceedings of the Thirteenth Annual Conference of the Remote Sensing Society held at Nottingham University, 7-11th September*, 593-601.

Steven, M.D., P.V. Biscoe and K.W. Jaggard, 1983, Estimation of sugar beet productivity from reflection in the red and infrared spectral bands. *International Journal of Remote Sensing*, **4**, 325-34.

Steven, M.D., P.V. Biscoe, K.W. Jaggard and J. Paruntu, 1986, Foliage cover and radiation interception. *Field Crops Research*, **13**, 75-87.

Suits, G.H., 1972a, The calculation of the directional reflectance of a vegetative canopy. *Remote Sensing of Environment*, **2**, 117-25.

Suits, G.H., 1972b, The cause of azimuthal variations in directional reflectance of vegetative canopies. *Remote Sensing of Environment*, **2**, 175-82.

Suits, G.H. and G. Safir, 1972, Verification of a reflectance model for mature corn with application to corn blight detections. *Remote Sensing of Environment*, 2, 183-92.

Swain, P.H. and S.M. Davis, 1978, *Remote Sensing: the Quantitative Approach*. McGraw-Hill, 396pp.

Swain, P.H. and H. Hauska, 1977, The decision tree classifier: Design and potential. *Institute of Electrical and Electronic Engineers Transactions on Geoscience and Remote Sensing*, **GE-15**, 142-7.

Talbot, S.S. and C.J. Markon, 1986, Vegetation mapping of Nowitna National Wildlife Refuge, Alaska using Landsat MSS digital data. *Photogrammetric Engineering and Remote Sensing*, **52**, 791-9.

Tarpley, J.D., 1984, Operational meteorological satellite products for agricultural monitoring. *Society of Photo-Optical Instrumentation Engineers*, **481**, 222-230.

Tarpley, J.D., S.R. Schneider and R.L. Money, 1984, Global vegetation indices from the NOAA-7 meteorological satellite. *Journal of Climate and Applied Meteorology*, **23**, 491-4.

Taylor, B.F., P.W. Dini and J.W. Kidson, 1985, Determination of seasonal and interannual variation in New Zealand pasture growth from NOAA-7 data. *Remote Sensing of Environment*, **18**, 177-92.

Taylor, J.C., A.S. Belward, D.G. Hewett and B.K. Wyatt, 1986, Mapping of vegetation and soils and estimation of biomass in the Sahel. Appendix III in *Monitoring of Pastureland Ecosystems in the Sahel and Mapping of Cloud Cover and Rainfall*, Final Report to the Commission of the European Communities Development Directorate (DG VIII), Natural Environment Research Council, 42pp.

Téran, M. de and L. Solé Sabarís (editors), 1978, *Geografía General de España*. Editorial Ariel, Barcelona, 549pp.

Thomas, J.R., V.I. Myers, M.D. Heilman and C.L. Weigand, 1966, Factors affecting light reflectance of cotton. In *Proceedings of the 4th Symposium on Remote Sensing of Environment*, Institute of Science and Technology, University of Michigan, Ann Arbor, 305-12.

Tissot, M.A., 1881, *Mémoire sur la Représentation des Surfaces et les Projections des Cartes Géographiques*. Gauthier-Villars, Paris, 397pp.

Townshend, J.R.G., 1981, The spatial resolving power of earth resources satellites. *Progress in Physical Geography*, **5**, 32-55.

Townshend, J.R.G. and C. Justice, 1981, Information extraction from remotely sensed data, a user view. *International Journal of Remote Sensing*, **2**, 313-29.

Townshend, J.R.G and C.O. Justice, 1986, Analysis of the dynamics of African vegetation using the normalised difference vegetation index. *International Journal of Remote Sensing*, 7, 1435-45.

Townshend, J.R.G. and C.O. Justice, 1988, Selecting the spatial resolution of satellite sensors required for global monitoring of land transformations. *International Journal of Remote Sensing*, **9**, 187-236.

Townshend, J.R.G. and C.J. Tucker, 1981, Utility of AVHRR of NOAA 6 and 7 for vegetation mapping. In *Proceedings of the Ninth Annual Conference of the Remote Sensing Society "Matching Remote Sensing Techniques and their Applications", held in the University of London, 16-18th December*, 97-109.

Townshend, J.R.G. and C.J. Tucker, 1983, Objective assessment of advanced very high resolution radiometer data for land cover mapping. *International Journal of Remote Sensing*, **5**, 497-504.

Townshend, J.R.G., T.E. Goff and C.J. Tucker, 1985, Multitemporal dimensionality of images of normalised difference vegetation index at continental scales. *Institute of Electrical and Electronic Engineers Transactions on Geoscience and Remote Sensing*, **GE-23**, 888-95.

Townshend, J.R.G, C.O. Justice and C.J. Tucker, 1986, Techniques for continental land cover classification using remotely sensed satellite data. In *Proceedings of an International Symposium organised by Commission IV of the International Society for Photogrammetry and Remote Sensing and the Remote Sensing Society "Mapping from Modern Imagery", Edinburgh, Scotland, 8-12th September*, 34-44.

Townshend, J.R.G, C.O. Justice and V. Kalb, 1987, Characterization and classification of South American land cover types using satellite data. *International Journal of Remote Sensing*, **8**, 1189-1207.

Tucker, C.J., 1978, A comparison of satellite sensor bands for vegetation monitoring. *Photogrammetric Engineering and Remote Sensing*, **44**,1369-80.

Tucker, C.J., 1979, Red and photographic infrared linear combinations for monitoring vegetation. *Remote Sensing of Environment*, **8** , 127-50.

Tucker, C.J., 1980, A critical review of remote sensing and other methods for non-destructive estimation of standing crop biomass. *Grass and Forage Science*, **35**, 177-82.

Tucker, C.J., 1986, Maximum normalised difference vegetation index images for Sub-Saharan Africa for 1983-1985. *International Journal of Remote Sensing*, 7, 1383-4.

Tucker, C.J. and B.J. Choudhury, 1987, Satellite remote sensing of drought conditions. *Remote Sensing of Environment*, **23**, 243-51.

Tucker, C.J. and M.W. Garratt, 1977, Leaf optical system modeled as a stochastic process. *Applied Optics*, **16**, 635-42

Tucker, C.J. and M. Matson, 1985, Determination of volcanic dust deposition from El Chichon using ground and satellite data. *International Journal of Remote Sensing*, **6**, 619-27.

Tucker, C.J. and E.L. Maxwell, 1976, Sensor design for monitoring vegetation canopies. *Photogrammetric Engineering and Remote Sensing*, **42**, 1399-1410.

Tucker, C.J. and L.D. Miller, 1977, Soil spectra contributions to grass canopy spectral reflectance. *Photogrammetric Engineering and Remote Sensing*, **43**, 721-6.

Tucker, C.J. and P.J. Sellers, 1986, Satellite remote sensing of primary production. *International Journal of Remote Sensing*, 7, 1395-416.

Tucker, C.J., B.N. Holben, J.H. Elgin, and S.E. McMurtrey, 1981, Remote sensing of total dry-matter accumulation in winter wheat. *Remote Sensing of Environment*, 11, 171-89.

Tucker, C.J., C. Vanpraet, E. Boerwinkel and A. Gaston, 1983, Satellite remote sensing of total dry matter production in the Senegalese Sahel. *Remote Sensing of Environment*, 13, 461-74.

Tucker, C.J., J.A. Gatlin, S.R. Schneider and M.A. Kuchinos, 1984a, Monitoring vegetation in the Nile delta with NOAA 6 and NOAA 7 imagery. *Photogrammetric Engineering and Remote Sensing*, 50, 53-61.

Tucker, C.J., B.N. Holben and T.E. Goff, 1984b, Intensive forest clearing in Rondonia, Brazil as detected by satellite remote sensing. *Remote Sensing of Environment*, 15, 255-61.

Tucker, C.J., J.R.G. Townshend and T.E. Goff, 1985a, African land-cover classification using satellite data. *Science*, 227, 369-75.

Tucker, C.J., C. Vanpraet, M.I. Sharman and G. van Ittersum, 1985b, Satellite remote sensing of total herbaceous biomass production in Senegalese Sahel: 1980-1984. *Remote Sensing of Environment*, **14**, 233-49.

Tucker, C.J., I.Y. Fung, C.D. Keeling, R.H. Gammon, 1986a, Relationship between atmospheric carbon dioxide variations and a satellite-derived vegetation index. *Nature*, **319**, 195-9.

Tucker, C.J., C.O. Justice and S.D. Prince, 1986b, Monitoring the grasslands of the Sahel 1984-1985. *International Journal of Remote Sensing*, 7, 1571-81.

UNESCO, 1973a, *International Classification and Mapping of Vegetation*. United Nations Educational, Scientific and Cultural Organisation, Paris, 14-37.

UNESCO, 1973b, *Soil Map of the World* (1:5 000 000).United Nations Educational, Scientific and Cultural Organisation, Paris.

UNESCO, 1983, *Vegetation Map of Africa* (1:5 000 000, including a descriptive memoir by F. White). United Nations Educational, Scientific and Cultural Organisation/Association pour l'Étude Taxonomique de la Flore de L'Afrique Tropicale/United Nations Sudano-Sahelian Office, Paris, 356pp.

USGS, 1984, *Landsat 4 Data Users Handbook*. United States Geological Survey, Alexandria, Virginia, 209pp.

Walter, H., 1985, *Vegetation of the Earth* (third edition). Springer-Verlag, 318pp.

Walter, H., E. Harnickell and D. Mueller-Dombois, 1975, *Climate-Diagram Maps of the Individual Continents and the Ecological Climatic Regions of the Earth*. Springer.

Wannamaker, B., 1984, An evaluation of digitized APT data from the TIROS-N/NOAA-A, -J series of meteorological satellites. *International Journal of Remote Sensing*, 5, 133-44.

Wardley, N.W., 1984, Vegetation index variability as a function of viewing geometry. *International Journal of Remote Sensing*, 5, 861-70.

Watson, R.M., 1981, Down market remote sensing. In *Proceedings of the Ninth Annual Conference of the Remote Sensing Society "Matching Remote Sensing Technologies and their Applications", held in the University of London, 16-18th December*, 5-36.

Whittaker, R.H., 1962, Classification of Natural Communities. *The Botanical Review*, **28**, 1-239.

Whittaker, R.H. (editor), 1973, *Ordination and Classification of Communities (Handbook of Vegetation Science, Part V)*. Dr. W. Junk, The Hague, The Netherlands, 737pp.

Whittaker, R.H., 1977, *Classification of Natural Communities*. Arno Press, New York, 239pp.

Wiegand, C.L. and A.J. Richardson, 1987, Spectral component analysis; Rationale and results for three crops. *International Journal of Remote Sensing*, **8**, 1011-32.

Wiegand, C.L., A.J. Richardson and E.T Kanemasu, 1979, Leaf area index estimates for wheat from Landsat and their implications fro evapotranspiration and crop modeling. *Agronomy Journal*, **71**, 338-42.

Wiegand, C.L., A.J. Richardson, R.D. Jackson, P.J. Pinter, J.K. Aase, D.E. Smika, L.F. Lautenschlager and J.E. McMurtrey, 1986, Development of agrometeorological crop model inputs from remotely sensed information. *Institute of Electrical and Electronic Engineers Transactions on Geoscience and Remote Sensing*, **GE-24**, 90-8.

Wiesnet, D.R. and J.D. Tarpley, 1987, The development of land remote sensing applications fro NOAA polar-orbiting and geostationary satellites. Paper presented at the *38th Congress of the International Astronautical Federation, October 10-17th, Brighton U.K.*, 8pp.

Willstätter, R. and A. Stoll, 1918, *Untersuchungen uber die Assimilation der Kohlensaure*. Springer, Berlin, 448pp.

Wong, C.L. and W.R. Blevin, 1967, Infrared reflectances of plant leaves. *Australian Journal of Biological Science*, **20**, 501-8.

Woodwell, G.M., J.E. Hobbie, R.A. Houghton, J.M. Melillo, B. Moore, A.B. Park, B.J. Peterson and G.R. Shaver, 1984, Measurement changes in the vegetation of the Earth by satellite imagery. In *The Role of Terrestrial Vegetation in the Global Carbon Cycle: Measurement by Remote Sensing* edited by G.M. Woodwell, John Wiley, 221-40.

Woolley, J.T., 1971, Reflectance and transmittance of light by leaves. *Plant Physiology*, **47**, 656-62.

Yates, H.W., J.D. Tarpley, S.R. Schneider, D.F. McGinnis and R.A. Schofield, 1984, The role of meteorological satellites in agricultural remote sensing. *Remote Sensing of Environment*, **14**, 219-33.

Yates, H., A. Strong, D. McGinnis and D. Tarpley, 1986, Terrestrial Observations from NOAA Operational Satellites. *Science*, **231**, 463-70.

Appendix One

Advanced Very High Resolution Radiometer Data

1. Introduction

The Advanced Very High Resolution Radiometer (AVHRR) measures electromagnetic radiance emanating from the Earth's surface and atmosphere. Four AVHRR sensors have been designed. In each case the sensor is able to respond simultaneously to various parts of the visible and infrared spectrum by means of multiple filters and a PN photodiode which converts the radiances into electric signals (table 28). These electric signals are converted to full resolution digital format by a 10-bit analog-to-digital converter (Lauritson *et al.* 1979; Schwalb 1978,1982; Brush 1985; Dundee Satellite Receiving Station 1986). The NOAA satellites on which the different AVHRRs have been or will be flown are listed in table 4.

The digital imagery produced for each AVHRR channel is processed by an on-board computer called the Manipulated Information Rate Processor to make full resolution AVHRR data, Global Area Coverage and Automatic Picture Transmission. In addition, Global Area Coverage is processed on the ground to make the Global Vegetation Index (Kidwell 1986).

2. Full resolution AVHRR data

There are two types of full resolution AVHRR data. These are High Resolution Picture Transmission and Local Area Coverage. The radiometric accuracy and precision of full resolution AVHRR data are described in table 29 and the geometric characteristics of full resolution AVHRR data are described in table 30.

High Resolution Picture Transmission is transmitted to ground stations by means of a split-phase/phase-shifted keyed signal at a bit rate of 614 400 bits per second. The carrier frequency is 1.7 GHz. This data stream may be received by any suitably equipped ground receiving station located under the satellite's flight path (Gatlin *et al.* 1984; Dundee Satellite Receiving Station 1985; Baylis and Brush 1985).

Table 28. Advanced Very High Resolution Radiometer Channel Bandwidths (μm)
(source: Fusco and Muirhead 1987)

Channel (Detector)	AVHRR	AVHRR/1	AVHRR/2	AVHRR/3[a]
Channel 1 (Si diodes)	0.55-0.90	0.58-0.68	0.58-0.68	0.58-0.68
Channel 2 (Si diodes)	0.72-1.10	0.72-1.06[b]	0.72-1.06[b]	0.82-0.8[illegible]
Channel 3A	-	-	-	1.57-1.78[c]
Channel 3 (indium antimonide)	3.55-3.93	3.55-3.93	3.55-3.93	3.55-3.93[d]
Channel 4 (HgCdTe)	10.5-11.5	10.5-11.5	10.3-11.3	10.3-11.3
Channel 5 (HgCdTe)	10.5-11.5	10.5-11.5	11.5-12.5	11.5-12.5

a. AVHRR/3 will fly on NOAAs K, L and M (table 4)
b. The oft-cited 1.10μm wavelength limit for channel 2 of AVHRR/1 and AVHRR/2 is misleading since these sensors have a filter response of less than 1% at wavelengths greater than 1.06μm (Gallo et al. 1987)
c. daytime
d. night-time

Table 29. Radiometric Accuracy and Precision of Full Resolution AVHRR Data
(sources: Norwood and Lansing 1983; Fusco and Muirhead 1987)

	Full-Scale Signal	Resolution	Accuracy (AVHRR/1,2)	Accuracy (AVHRR/3)
Channel 1	100% albedo[a]	10-bit[b]	3:1[c]	9:1
Channel 2	100% albedo	10-bit	3:1	9:1
Channel 3A	100% albedo	10-bit	-	20:1
Channel 3	≈320 K	10-bit	0.12 K[d]	-
Channel 4	≈320 K	10-bit	0.12 K	-
Channel 5	≈320 K	10-bit	0.12 K	-

a. i.e. brightest cloud
b. i.e. 1024 digital levels
c. signal-to noise-ratio at 0.5% albedo
d. noise equivalent differential temperature at 300 K

The coverage provided by a particular ground receiving station is limited to the area "seen" by the sensor for the period that its signal can be received by the ground station antenna. For example, when the satellite is at an altitude of 870km the period of contact between the sensor and the antenna on the ground is about fourteen

Table 30. Geometric Characteristics of AVHRR Data
(sources: Gatlin et al. 1984; Fusco and Muirhead 1987)

Instantaneous Field of View:	1.3-1.5 milliradians[a]
Scan Angle Range:	± 55.4°
Ground Coverage per Scan Line:	≈ 3000km ≈ 27° longitude at the Equator
Pixels per Channel per Scan Line:	2048
Dimension of One Pixel at Nadir:	1.1x1.1km[b]
Along-Track Dimension of One Pixel at ± 55.4° Scan Angle:	2.5km
Across-Track Dimension of one pixel at ± 55.4° Scan Angle:	7.0km

a. The instantaneous field of view is slightly different for the different AVHRR channels

b. There is overlap between adjacent instantaneous fields of view along the scan line. The dimension of one pixel at nadir excluding the area of across-track overlap is 0.8x1.1km

minutes, assuming that the spacecraft must be at least five degrees above the horizon for useful data to be acquired. Since a single scan line of AVHRR imagery covers an area on the ground approximately 3000x1.1km and the scan rate is six lines per second, the total coverage or swath that may be recorded by a single ground station during a single satellite pass is an area approximately 3000x5500km.

The orbital characteristics of NOAA Tiros-N series satellites are summarised in table 31. The repeat period for passes with precisely the same sub-satellite track is approximately nine days, based on westwards regression rate, and twenty-six days, based on eastwards precession rate. However, since the orbital period is one-hundred-and-two-minutes and equator crossings of consecutive orbits are separated by approximately twenty-five degrees of longitude, a single NOAA satellite returns to *approximately* the same longitude moving in the same north-south direction once every twenty-four hours. In that time it scans the entire Earth's surface twice- once during daylight hours and once at night. The operational configuration of the NOAA-series consists of two satellites in orbits with equatorial crossings approximately six hours apart. Thus, the operational AVHRR imaging system provides a minimum of four

Table 31. Orbital Characteristics of NOAA Tiros-N Series Satellites
(sources: Schwalb 1978; Holben and Fraser 1984; Gatlin et al. 1984; Kidwell 1986)

Type:	Retrograde sunsynchronous oblique polar
Inclination:	98.8° (Tiros-N: 102.3°)
Nominal Altitude:	853.7km
Period:	102 minutes
Mean Repeat Period:	≈ 9 days
Orbits per 24 Hours:	14.2
Westwards Regression Rate:	25.5° longitude per orbit
Eastwards Precession Rate:	0.986° longitude per day
Equatorial Crossing Time[a] (southbound):	0730 (NOAA 6, 8, 10) 1430 (NOAA 7, 9)
Equatorial Crossing Time[a] (northbound):	1930 (NOAA 6, 8, 10) 0230 (NOAA 7, 9)
Operational Configuration:	Two satellites in complementary orbits[b]

a. local solar time
b. i.e. two satellites with equatorial crossings in the same direction approximately six hours apart

images per twenty-four hours of anywhere on the Earth's surface (i.e. twice during the day and twice at night). In fact, areas at high latitudes may appear in as many as eight AVHRR passes per day due to the increasing overlap between consecutive passes polewards. Of course, the position of a particular location within these swaths relative to nadir varies and some of the extra coverage that can be obtained at midlatitudes may be of little practical value.

Some areas of Europe are covered by five or six ground receiving stations (Ellingsen *et al.* 1986; Fusco and Muirhead 1987). Other regions, such as East Africa, are not covered by one. Consequently, global coverage of High Resolution Picture Transmission is not possible at the moment. However, a maximum of ten minutes full resolution digital imagery corresponding to an area on the ground approximately 3000x4000km may be stored onboard the satellite per orbit. This imagery is called Local Area Coverage (Kidwell 1986).

Local Area Coverage is transmitted to either of the Command and Data Acquisition stations operated by NOAA at Wallops Island, Virginia and Gilmore Creek, Alaska. For areas not covered by a High Resolution Picture Transmission ground receiving station, Local Area Coverage is the only way to acquire full resolution AVHRR imagery.

Requests for Local Area Coverage are considered on a first-come-first-served basis. There is a long waiting list for these data (Kidwell 1986, personal communication). Since a priority system operates whereby United States national emergencies, situations where human life is in immediate danger, United States strategic requirements and commercial requirements all have higher priority than academic research, for many research purposes Local Area Coverage is too difficult to obtain. It is also unreliable. The top two priorities in the priority hierarchy cannot be predicted. Consequently, acquisitions planned months or even years in advance may be "bumped" at any time.

3. Global Area Coverage

Full resolution data from each AVHRR channel is spatially-degraded by the AVHRR Manipulated Information Rate Processor to produce Global Area Coverage. Global Area Coverage has 10-bit radiometric precision and is available from the Satellite Data Services Division of NOAA on a daily basis for the whole world in level 1b format[1]. Each Global Area Coverage array location contains the mean radiance of every four out of five samples along every third scan line of the full resolution AVHRR data. Thus, the mean areal integrated response of just four full resolution AVHRR pixels is assigned to each Global Area Coverage pixel. Clearly, the spatial subsampling is considerable. Four full resolution AVHRR pixels cover an area on the ground at nadir approximately 3.2x1.1km (i.e. taking across-track overlap into account (table 30)). This is equivalent to an area of approximately 350 hectares. A single Global Area Coverage pixel corresponds to an area on the ground at nadir nominally described as 4x4km (Kidwell 1986). This is equivalent to an area of approximately 1600 hectares.

---

1 Level 1b data have been quality controlled, assembled into discrete data sets and had Earth location and calibration information appended. A single day's Global Area Coverage level 1b imagery contains approximately 640 megabytes data produced from fourteen and occasionally fifteen orbits

4. Automatic Picture Transmission

The digital outputs of any two AVHRR channels selected by command from the National Environmental Satellite Service Spacecraft Operations Control Center are subsampled and selectively averaged by the Manipulated Information Rate Processor. The subsampling and averaging together remove the effects of the Earth's curvature in the imagery and create a data set in which individual pixels represent an area approximately 4x4km on the ground. After digital processing the data are time multiplexed along with calibration and telemetry data. These data are converted to an analog signal and amplitude modulated onto a 2.4kHz subcarrier which is in turn FM modulated on to 137 MHz for transmission (Lauritson *et al.* 1979; Wannamaker 1984; Brush 1985). This analog imagery has 8-bit radiometric precision and is called Automatic Picture Transmission. It is currently available for AVHRR channels 2 and 4 during the day and 3 and 4 during the night (Bailey 1987).

Although Automatic Picture Transmission has reduced spatial and spectral resolution compared with High Resolution Picture Transmission and is available only for two wavebands, it may be received easily by relatively low cost portable receiving stations comprising an omnidirectional antenna and unsophisticated imaging equipment. For this reason it is received on board ships to provide real time analyses of weather patterns and sea-surface temperature fronts (e.g. Gorman and Sadowsky 1986) and is also used by meteorologists and thousands of amateurs who use the cloud pictures for nephanalyses and weather forecasting (Wannamaker 1984; Fusco and Muirhead 1987; Seaford 1987).

5. The Global Vegetation Index

The Global Vegetation Index is mapped seven-day maximum NDVI value composite imagery that has been produced by NOAA since April 1982 (Tarpley 1984; Tarpley *et al.* 1984; NOAA 1986). Between April 1982 and January 1985 it was made using data from NOAA 7. Since January 1985 it has been made using data from NOAA 9.

First Generation Global Vegetation Index imagery was produced between April 1982 and March 1985. It was an experimental product funded as a research effort by the Agriculture and Resources Inventory Surveys Through Aerospace Remote Sensing project. Second Generation Global Vegetation Index imagery has been produced

operationally by the Satellite Data Services Division of NOAA since April 1985. Whereas the first generation product comprises AVHRR channels 1 and 2 and the NDVI, the second generation product comprises AVHRR channels 1, 2, 4, 5, the solar zenith angle, the scan angle and the NDVI. The first generation product is available on polar-stereographic (master) arrays between 90°N and 90°S only. The second generation product is produced between 75°N and 55°S[2]. These data are mapped first to a plate carrée master array and subsequently to both polar-stereographic and Mercator arrays. The representation of the Earth provided by these projections is discussed in Appendix 2.

Global Vegetation Index imagery is made in two stages. The first stage is data selection. Every day all Global Area Coverage level 1b data[1] from every second scan line are mapped to the Global Vegetation Index master array except those scan lines which contain night-time data, are missing Earth location or calibration information, or lie polewards of 75°N and 55°S[3]. Clearly, the spatial resolution of Global Area Coverage is much finer than the spatial resolution of the Global Vegetation Index and some method of degrading the Global Area Coverage data spatially is required. The method that is used by NOAA involves retaining in each Global Vegetation Index pixel the last value mapped to it from the Global Area Coverage data set. This selection process is regarded as random because the selection of the Global Area Coverage does not depend on its value. It should be noted, however, that there is no averaging of the Global Area Coverage values corresponding to a particular master array pixel and that only one Global Area Coverage value is used. Clearly, the Global Vegetation Index is based upon drastic spatial subsampling. The Global Area Coverage NDVI value for an area on the ground of approximately 350 hectares is assigned to a Global Vegetation Index pixel representing an area on the ground upwards of 12 800 hectares.

The second stage of Global Vegetation Index production involves production of maximum NDVI value composites. At each Global Vegetation Index master array pixel on each of the seven days the difference between the radiances of channels 1 and 2 is calculated (i.e. channel 2 minus channel 1). If the new value is greater than the value for the previous day, a new NDVI for that pixel is computed according to equation 2 based on the radiance values of the new day. At the end of every seven day period, each pixel in the Global Vegetation Index master array contains the highest NDVI value that occurred at that array location during the seven day period.

---

2 The latitudinal limits were selected to include significant land areas but also to minimise processing

3 i.e. second generation product

Appendix Two

Mapping NOAA AVHRR Imagery Using Equal Area Radial Projections

The main part of this Appendix is a letter published in the *International Journal of Remote Sensing* which I wrote with Giles D'Souza. A reprint of this letter is contained in the envelope inside the back cover. There are a two points, two minor corrections and one clarification that need to be added to the letter. I should like to thank M. H.M. Dufour, Ingénieur général géographe at the Institut Geographique National in Paris, for bringing these to my attention.

1. Practically all the projections described in the letter as equal area radial projections were described by Tissot (1881) as "*projections cylindriques authaliques*".

2. The geocentric latitude is known also as the authalic or the equivalent latitude.

3. Equations A1 and A3 are incorrect because they use the first eccentricity, e, rather than the second eccentricity, e', where

$$e^2 = (a^2 - b^2) / a^2,$$

$$e'^2 = (a^2 - b^2) / b^2$$

and a and b are the major and minor axes of the Earth. e and e' are related

i.e. $e / e' = b/a$

According to M. Dufour $e = 0.081819191$ and $e' = 0.082094439$.

Normally f is the flattening of the earth (i.e. $f = (a - b) / a$) and f and e are related by the equation

$$(1 - f)^2 = 1 - e^2$$

A1 may be corrected by replacing both occurrences of "$(1-f)^2$" by "$(1-e'^2)$". A3 may be corrected by replacing both occurrences *of* "e^2" by "$(1-e'^2)$". Elsewhere (i.e. A9, A10, A11 and A12) the use of the first eccentricity, e, is correct.

4. Equation A10 contains a misprint. "3.0" should read "e".

5. M. Dufour queries the method suggested for the derivation of the optimal standard parallels when the area of interest straddles the Equator. Considering the example of South America used in the letter, strictly, θ_p is 55° (i.e. $\theta_s \approx 40°$). The reason why we use a θ_p of 33° (i.e. $\theta_s \approx 24°$) is to take account of the fact that nominally there is twice as much of the area of interest between 0° and 11° (N and S) as is suggested by the equatorwards and polewards limits alone. This is a very simple form of areal weighting. In fact, it seems likely that the most effective areal weighting to produce the best equal area radial constructions for areas of interest distributed unequally either side of the Equator will be determined by local conditions and therefore be unique for every case.

Appendix Three

Geodetic Registration of Full Resolution AVHRR Imagery

Images made on different satellite overpasses contain different geometric distortion due not only to the Earth's curvature and rotation but also to variations in the satellite's speed, altitude, attitude, location and direction. Geometric distortions make intercomparison of images difficult and several algorithms have been developed which aim to effect geodetic registration of High Resolution Picture Transmission (e.g. Hayes and Cracknell 1984b; Ho and Asem 1986; Brunel and Marsouin 1987). The method of geodetic registration used in this study was developed by Dr. John Brush (1988) who generously made his software available to me for this research. Giles D'Souza and Dr. Andrew Harrison helped me to adapt the software to fit the computing system at Bristol and the needs of this study.

The first stage of the geodetic registration process involves *linearisation* of the raw data. An algorithm is produced, based on the mean satellite altitude and the Earth's radius at Madrid (i.e. 6369.5km), which creates new images with scan lines three times the length (i.e. 6144 pixels) of High Resolution Picture Transmission scan lines. Each linearised pixel has an across-track dimension of equal geocentric angle. Since this angle varies from pass to pass so too does the across-track distance on the ground corresponding to one linearised pixel although the approximate across-track dimension is 0.49km (i.e. 3000km/6144).

Linearisation removes gross geometric distortion from raw High Resolution Picture Transmission imagery. It also introduces considerable radiometric duplication, particularly towards the edges of the swath. Radiometric duplication is reduced by subsampling linearised imagery by a factor of two. Linearised imagery subsampled in this way has pixels representing areas on the ground approximately 1.1km (along-track) by 0.98km (across-track) (i.e. approximately the same dimensions as unprocessed High Resolution Picture Transmission at nadir). The subsampled, linearised data are assigned a precise latitude and longitude using ancillary information obtained from the Tiros Information Processor, whose output is included in the header of imagery obtained from Dundee, and the Satellite Orbits Group at the University of Aston. This ancillary

information comprises the equatorial crossing time and longitude (in degrees West), the time of the first line of the image, the mean anomaly at epoch, the ascending node equatorial crossing longitude, the orbital eccentricity, the orbital inclination and the rate of mean motion of the satellite.

INT. J. REMOTE SENSING, 1987, VOL. 8, NO. 12, 1869–1878

Remote Sensing Letters

Mapping NOAA-AVHRR imagery using equal-area radial projections

DANIEL LLOYD and GILES D'SOUZA

Remote Sensing Unit, Department of Geography, University of Bristol, University Road, Bristol BS8 1SS, England

(Received 3 July 1987; in final form 21 August 1987)

Abstract. The advantages of registering NOAA-AVHRR imagery to the world graticule of latitude and longitude using equal area radial projections are described and illustrated with normalized difference vegetation index imagery.

1. Introduction

Raw NOAA-AVHRR swaths are not registered to the world graticule of latitude and longitude. While there are some applications for which unmapped imagery may suffice, it is easiest objectively to compare and combine remotely-sensed imagery with related ancillary data (e.g. ground-based measurements, digitized map data and imagery recorded from other satellites) if all the data are registered to the same base map. Once imagery has been mapped it is the mapped imagery that usually forms the basis of all subsequent interpretation. The selection of appropriate map projections is therefore extremely important. Surprisingly, however, the subject has received little attention. The *Manual of Remote Sensing*, for example, gives just ten pages to the subject (Bernstein 1983).

Within the remote sensing community the plate carrée (or simple cylindrical), the Mercator and the polar-stereographic projections are widely used (e.g. NOAA 1986). Although both the Mercator and the polar-stereographic projections give true representation of shape locally (i.e. they are conformal), neither offers an optimal image of the globe; the Mercator cannot display all the Earth's surface, because the poles are located an infinite distance from the Equator, whilst the polar-stereographic splits the Earth's surface into two hemispheres. A more important failing common to all three projections is that they are not equal-area. In the plate carrée, which is neither equal-area nor conformal (but is relatively easy to construct), the linear scale in the longitudinal direction at 60°N and S is greater than it is at the Equator by a factor of two. In the Mercator projection the linear scales in both the longitudinal and the latitudinal directions at 60°N and S are greater than they are at the Equator by a factor of two. Whereas the plate carrée and the Mercator projections make areas near the poles appear larger than equally-sized areas near the Equator, the polar-stereographic projection exaggerates the size of equatorial areas compared to polar areas (Steers 1970). Thus, in the arrays of these three projections used by NOAA for its Global Vegetation Index the area on the ground represented by individual pixels varies from 162 square kilometres (Equator) to 567 square kilometres (at 60°N and S) for the polar stereographic, 256 square kilometres (Equator) to 128 square kilometres (at 60°N and S) for the plate carrée, and 380 square kilometres (Equator) to 95 square kilometres (at 60°N and S) for the Mercator.

Raw imagery of the Earth's surface produced by sensors such as the NOAA-AVHRR has nominally uniform spatial resolution (e.g. NOAA-AVHRR Global Area Coverage imagery (Kidwell 1984)). If such imagery is mapped to projections that are not equal-area, inevitably some parts of the Earth's surface will be shown in greater detail than others. This occurs not because the data are unavailable but because of either data duplication (i.e. a pixel value in the raw imagery is assigned to more than one array location in the mapped imagery) or data redundancy (i.e. the data available are not fully used) during the mapping process. Figure 15 in a recent paper by Malingreau (1986) illustrates the undesirable consequences of using a Mercator-type projection, probably Miller's (1942) second cylindrical projection (Hardy *et al.* 1988), for small-scale mapping. Assuming that Malingreau's images were made by remapping polar-stereographic format Global Vegetation Index data to the Miller projection, the lines of black dots that occur towards the poles in two of these images (figures 15 (*b*) and 15 (*c*)) are those pixels in the Miller array for which there was no corresponding pixel in the polar-stereographic array. The gaps in the data which the black dots illustrate can be filled (figure 15 (*a*)), but only by duplicating index values from the polar-stereographic array.

Data duplication and data redundancy assume particular importance when they occur in small-scale imagery due to the large areas on the ground associated with individual pixels. For this reason small-scale mapping and monitoring programmes in particular require a projection that effects registration of the imagery to the world grid with minimal duplication or redundancy of the raw data.

2. Equal-area radial projections

The characteristics of equal-area map projections have been examined by Peters (1979, 1982, 1983). Peters found that no single equal-area projection possessed all of the desirable properties that may coexist in a single map, and proceeded to develop a projection that did. Although this optimal equal-area projection was first published as a 'decimal map' (Peters 1967, Buccholz 1980), it may be closely approximated by a cylindrical equal-area projection with two standard parallels (Peters 1979). This latter construction, which Peters has termed a 'radial projection' (not to be confused with zenithal or azimuthal projections), is closely related to both Lambert's and Behrmann's cylindrical equal-area projections. The vital difference is that whereas Lambert's takes one standard parallel (the Equator) and Behrmann's two (at 30°N and S), Peters proposed that the two standard parallels should be chosen so as to locate shape distortion where it is least intrusive. The method for choosing the optimal standard parallels for a radial projection of a particular area and then converting points of latitude and longitude to co-ordinates in the corresponding equal-area radial projection array is described in the Appendix.

Peters identifies five mathematical qualities and five utilitarian and aesthetic qualities which together define radial maps (Peters 1979, 1983). For the present discussion the most important of these may be summarized as follows:

(1) Area fidelity. 1 cm^2 anywhere on the map represents the same unit area on the ground. There is no linear scale constant all over the map. However this applies to all projections which show large areas of the Earth's surface (Peters 1983).
(2) Fidelity of axis and position. Expressed as a rectilinear graticule, this property enables easy orientation in terms of the four points of the compass. The rectilinear graticule is also especially suitable for digital imagery since this is stored and processed in linear arrays.

Absolute conformality occurs only along the standard parallels (e.g. an area of 1 square kilometre is a square with sides of 1 km only at the standard parallels). Elsewhere the latitudinal distance in degrees per unit distance on the map varies so as to maintain the property of equal area. This variation may be described as the *ratio of shape distortion* which is defined as the longitudinal distance (i.e. east–west) on the globe in kilometres per unit distance on the map : latitudinal distance (i.e. north–south) on the globe in kilometres per unit distance on the map. The table shows the effect of this changing ratio on the dimensions of an area of 1 square kilometre for radial projections with standard parallels at 25°, 45° and 60°N and S.

Ratio of shape distortion and the dimensions of an area of 1 square kilometre at selected latitudes for radial projections with standard parallels at 25°, 45° (Peters Map) and 60°.

	Ratio of shape distortion (longitude : latitude)			Longitudinal (E–W) dimension (km)			Latitudinal (N–S) dimension (km)		
Latitude	25°	45°	60°	25°	45°	60°	25°	45°	60°
0°	1·2 : 1·0	2·0 : 1·0	4·0 : 1·0	1·10	1·42	2·01	0·91	0·71	0·50
25°	1·0 : 1·0	1·6 : 1·0	3·3 : 1·0	1·00	1·28	1·82	1·00	0·78	0·56
45°	0·6 : 1·0	1·0 : 1·0	2·0 : 1·0	0·78	1·00	1·42	1·28	1·00	0·71
60°	0·3 : 1·0	0·5 : 1·0	1·0 : 1·0	0·55	0·71	1·00	1·82	1·42	1·00
75°	0·1 : 1·0	0·1 : 1·0	0·3 : 1·0	0·29	0·37	0·52	3·51	2·74	1·93

3. Small-scale mapping using radial projections

Figure 1 shows mean daily normalized difference vegetation index imagery between 75°N and 55°S for the period 1 January 1985 to 31 December 1986 derived from NOAA Global Vegetation Index imagery (polar stereographic format) mapped to three different radial constructions. The data used in figure 1 (and in figures 2 and 3 also) were obtained as follows. Seven-day maximum value normalized difference vegetation index imagery obtained from NOAA was first processed to make either 28- or 35-day maximum value images corresponding approximately to calendar months. The index value at each array location for each 'monthly' image was then multiplied by the number of days in the 'monthly' period (i.e. 28 or 35) and the resulting twelve 'monthly' integrated images for each year were added together and then divided by the number of days in the year. Finally, the mean of the mean daily index images for 1985 and 1986 was calculated. High mean daily normalized difference vegetation index values are displayed as light grey tones and correspond to areas where healthy green-leaf vegetation has been present most persistently during the averaging period (Tucker and Sellers 1986).

Figure 1 shows how the shape of the landmasses varies considerably depending on the particular radial construction used, even though the areal scale for all three constructions illustrated is the same. For aesthetic, psychological, didactic and practical reasons Peters found that a radial projection with standard parallels at 45°N and S produces the 'best' global map (Peters 1982). This construction is widely known as the 'Peters Map' and provides an equal-area representation of the whole of the Earth's surface with distortion of shape between 0° and 60°N and S nowhere greater than 2 : 1 (see table). A practical advantage of using the Peters Map for global arrays of digital imagery is that the data may be stored and processed more efficiently than they are using other projections that are not equal area. A full global Peters Map array with individual pixels representing an area on the ground of 225 square kilometres, for

example, has dimensions 1886 × 1202. The arrays currently used for the Global Vegetation Index are a similar size yet they provide less information. The polar-stereographic array is 1024 × 2048, the Mercator array (between 75°N and 55°S only) is 2048 × 1038 and the plate carrée array (between 75°N and 55°S only) is 2500 × 904.

Although the Peters Map construction is arguably the optimal solution to the problem of representing the entire Earth's surface in two dimensions, figure 2 illustrates that the construction poorly represents areas away from the standard parallels. Equatorial areas appear elongated in the North–South direction whilst areas towards the poles are flattened. The ratio of shape distortion for Africa (i.e. 35°N–35°S) on the Peters Map ranges from 1·4 : 1·0 at 35°N and S to 2·0 : 1·0 at the Equator. Similarly the ratio of shape distortion for Northern Europe (i.e. 40°–65°N) ranges from 1·2 : 1·0 at 40°N to 0·4 : 1·0 at 65°N. Using the method described in the Appendix the optimal construction of both areas may be calculated. For the continent of Africa the optimal radial construction has standard parallels at 25°N and S and a

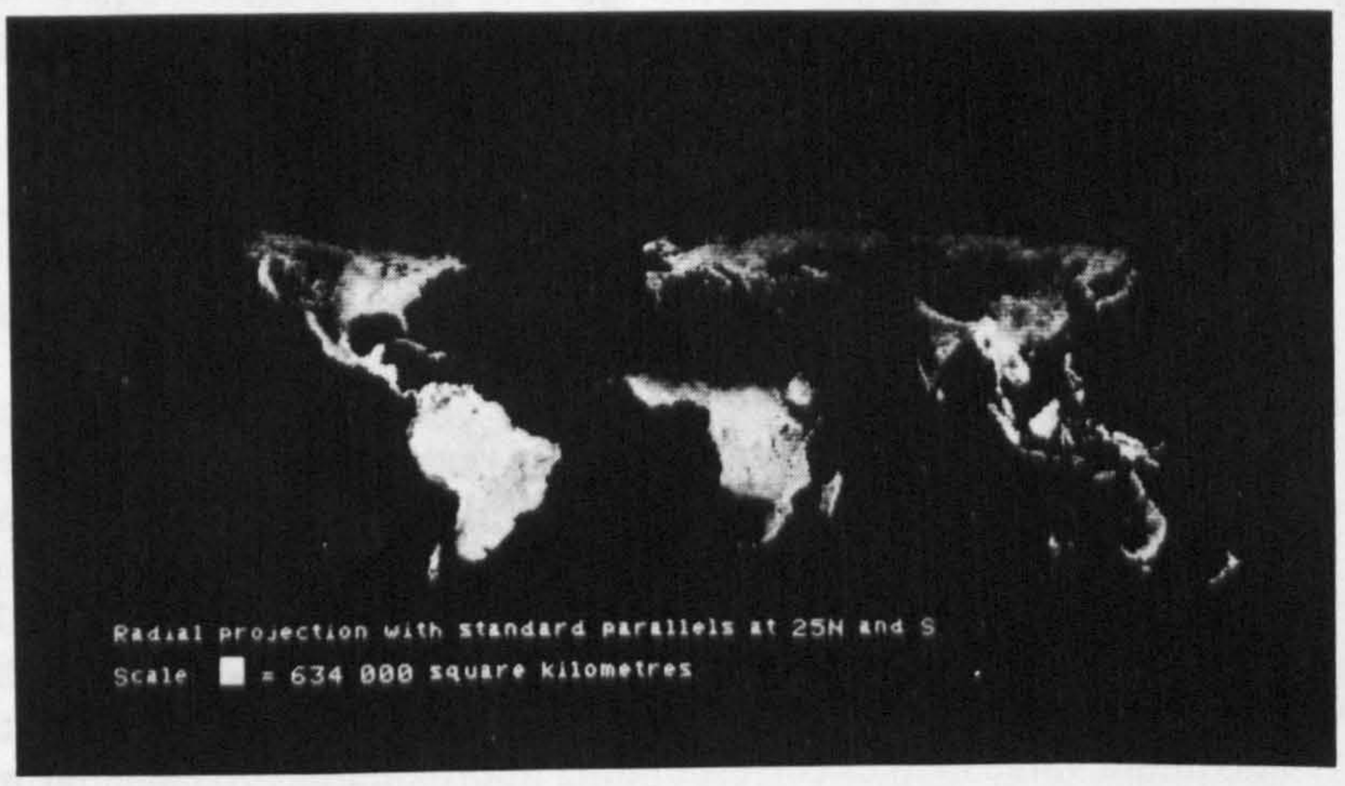

(*a*)

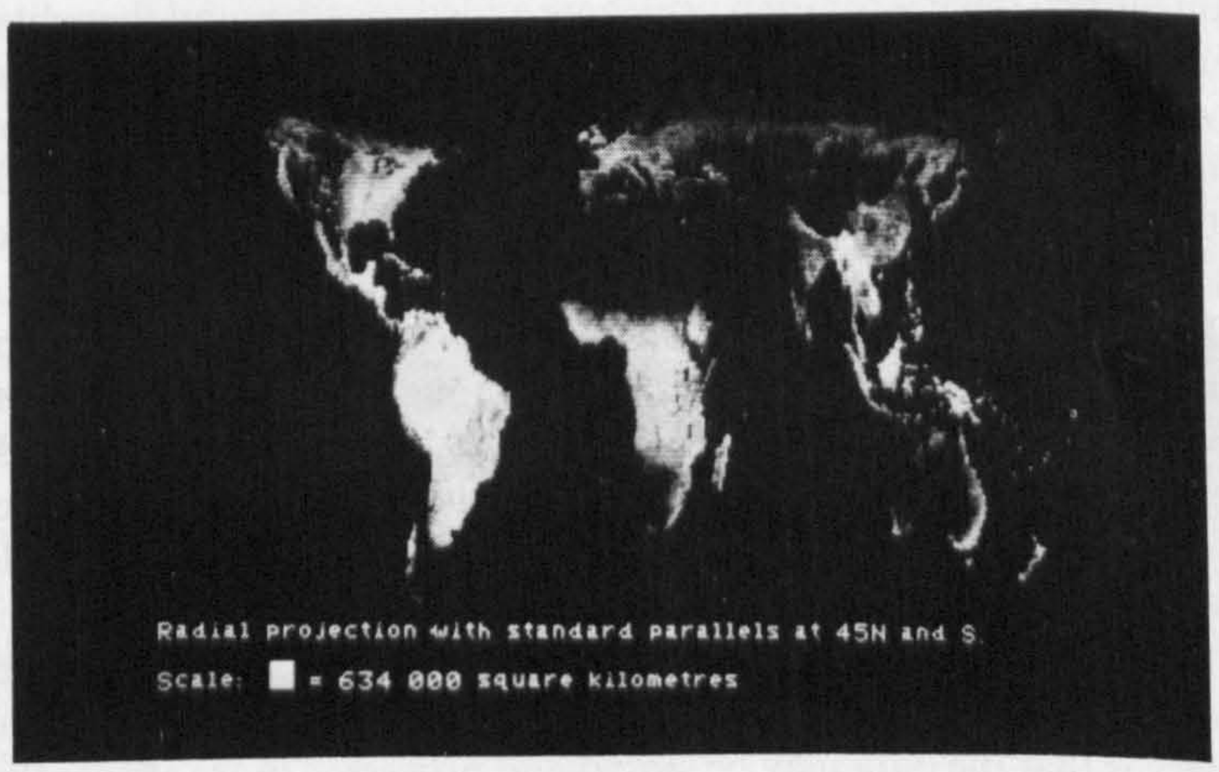

(*b*)

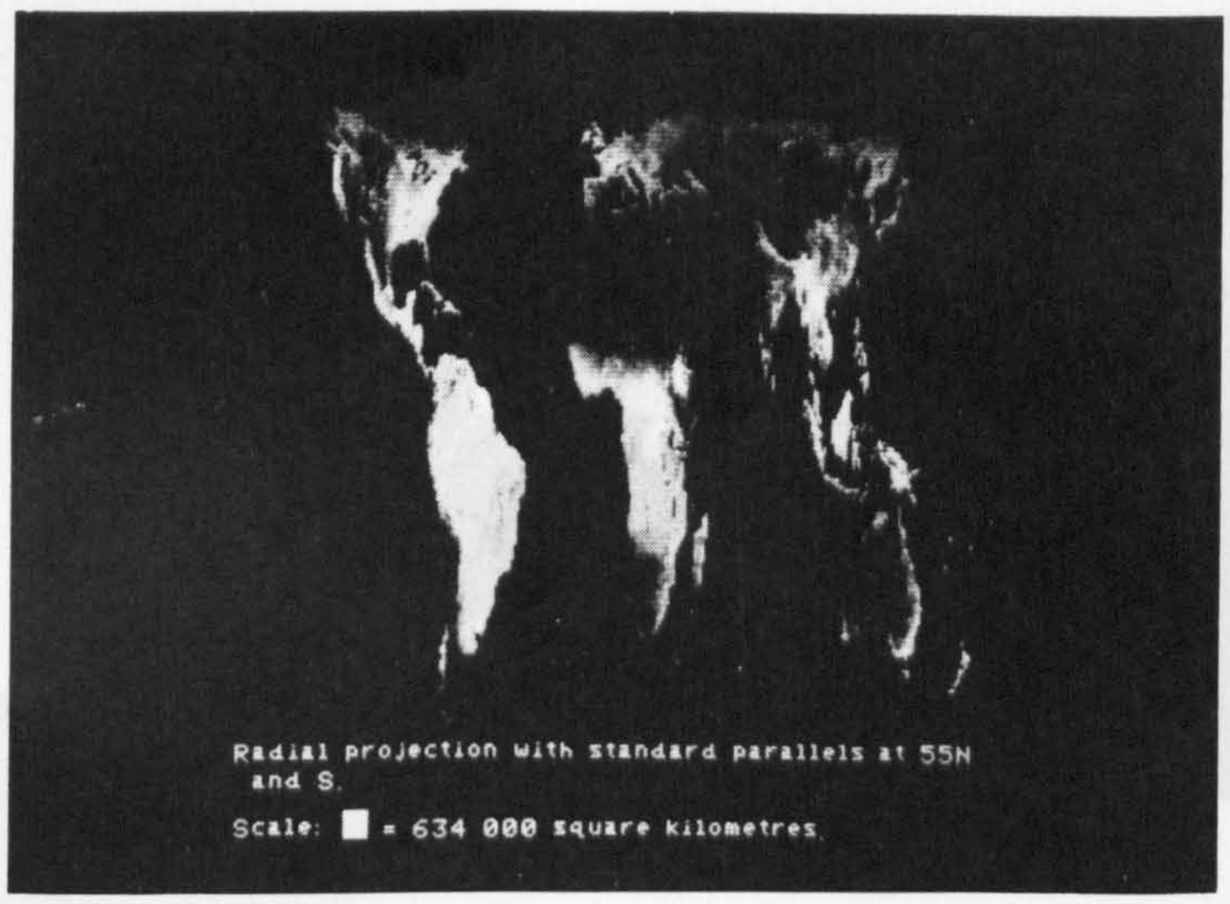

(*c*)

Figure 1. Mean daily normalized difference vegetation index imagery for the period 1 January 1985 to 21 December 1986 mapped to radial projections with standard parallels at (*a*) 25°N and S, (*b*) 45°N and S (the Peters Map) and (*c*) 55°N and S.

ratio of shape distortion of 0·8 : 1·0 at 35°N and S and 1·2 : 1·0 at the Equator. For Northern Europe the optimal construction has standard parallels at 55°N (and S) and a ratio of shape distortion of 1·8 : 1·0 at 40°N and 0·5 : 1·0 at 65°N. In both cases the ratio of shape distortion at the polewards latitudinal limit is approximately the reciprocal of the ratio value at the equatorwards latitudinal limit. Figure 3 shows how the depiction of both Africa and Northern Europe improves when optimal radial constructions are used. A world atlas containing 43 regional maps made using optimal radial constructions is being prepared (Peters 1988).

4. Remapping mapped imagery

Ideally, a definitive base map projection is chosen at the start of a project and raw satellite imagery is mapped directly on to this. A product like the Global Vegetation Index, however, is widely used for a variety of studies. Where these are regional rather than global it may be that representation of the area of interest in the global array is not satisfactory. Possibly as an attempt to sidestep this problem, NOAA market their Global Vegetation Index on three different map projections. It is first mapped to the plate carrée and then, from this, remapped again to either the Mercator or the polar-stereographic. While the intention may be to provide the user community with choice, this is limited since none of the projections used is equal area.

If the Global Vegetation Index were mapped first to the Peters Map instead of the plate carrée, remapping from this Peters Map array to any other radial construction could be done so as either to avoid data redundancy (at the cost of considerable data duplication), or else to avoid data duplication. The second of these two options is especially attractive since the avoidance of data duplication may be achieved with only a small amount of data redundancy. The new (larger) area on the ground represented

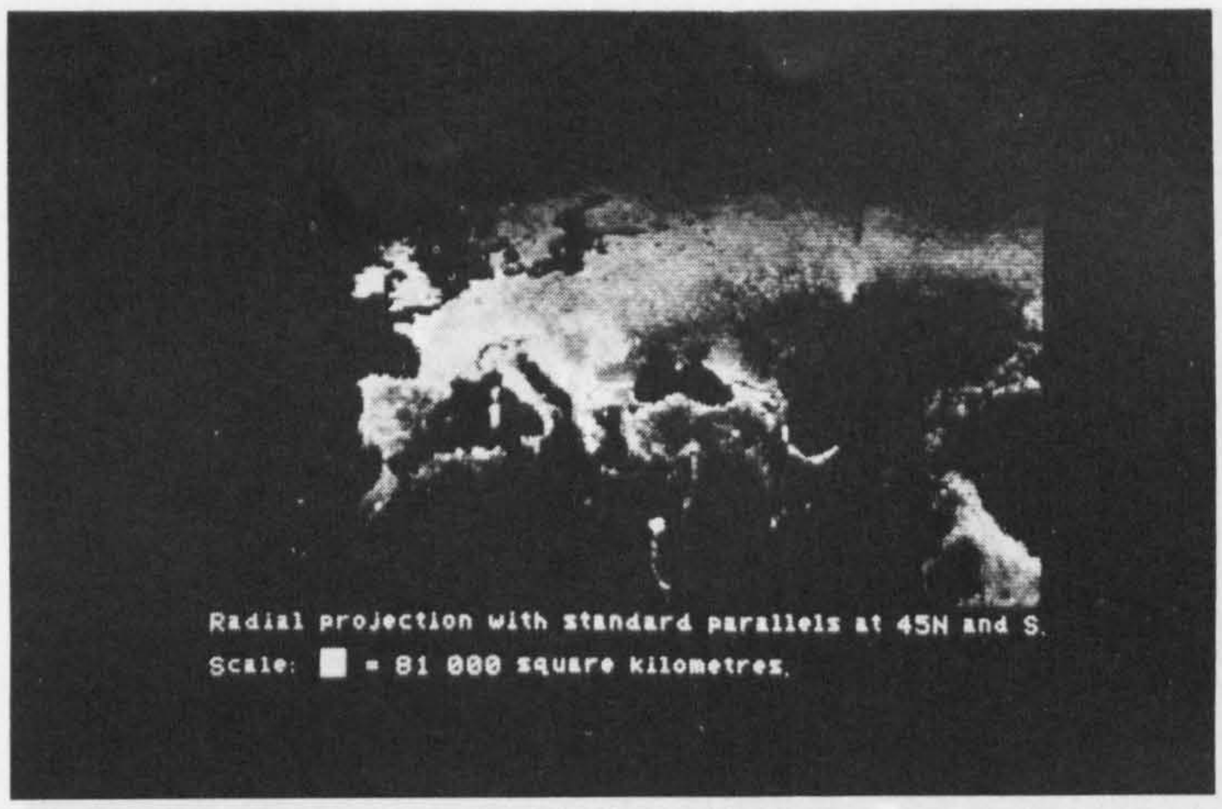

(*a*)

(*b*)

Figure 2. Regional enlargements of the Peters Map showing mean daily normalized difference vegetation index imagery for (*a*) Europe and North Africa (30°–75°N) and (*b*) Africa (35°N–35°S).

by a single pixel is determined by the location of the new standard parallels. For areas of interest lying equatorwards of the Peters Map standard parallels (i.e. 45°), the new pixel area, NPA_e, is calculated as

$$NPA_e = (\text{old pixel area}) \times (EW_{45} \text{ at } 0°/EW_0 \text{ at } 0°) \quad (1)$$

(*a*)

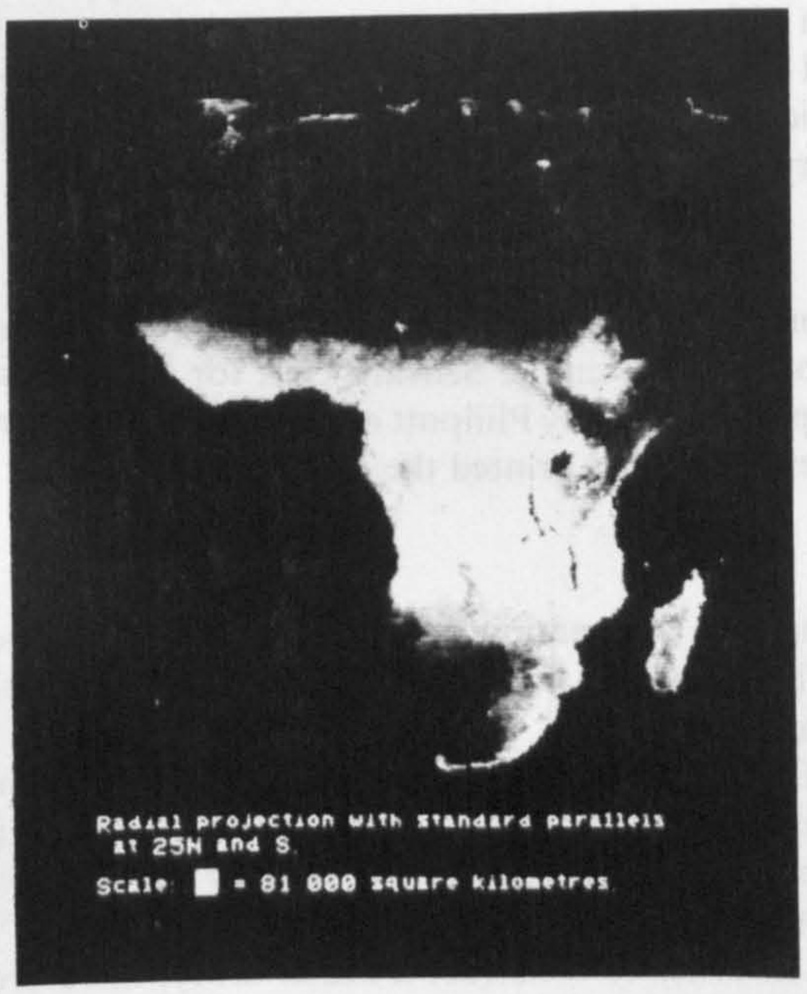

(*b*)

Figure 3. Mean daily normalized difference vegetation index imagery for (*a*) Europe and (*b*) Africa mapped to optimal radial constructions.

where EW_{45} and EW_0 are the longitudinal dimensions of an area 1 km^2 on the Peters Map and on the map with the new optimal standard parallels respectively. For areas of interest lying polewards of 45° the new pixel area, NPA_p, is calculated as

$$NPA_p = (\text{old pixel area}) \times (NS_{45} \text{ at } 0^\circ / NS_0 \text{ at } 0^\circ) \quad (2)$$

where NS_{45} and NS_0 are the latitudinal dimensions of an area 1 km^2 on the Peters Map and on the map with the new optimal standard parallels respectively. For example, if a

Peters Map with pixels representing 225 square kilometres on the ground were remapped to the optimal radial projection for Africa (i.e. standard parallels at 25°N and S) so as to avoid data duplication completely and minimize data redundancy, pixels in the new image would need to represent an area on the ground of 291 square kilometres (i.e. $225 \times (1{\cdot}42/1{\cdot}1)$). If, on the other hand, the same Peters map base map were to be remapped to a radial projection with standard parallels at 60°N and S then the pixels in the new image would need to represent an area on the ground of 320 square kilometres (i.e. $225 \times 0{\cdot}71/0{\cdot}5$)) in order to avoid data duplication completely and minimize data redundancy.

5. Conclusion

Radial projections provide a rectilinear graticule and a constant areal scale. The practical advantages of the rectilinear graticule not only for digital image processing but also for general map usage are complemented by the egalitarian representation of the Earth's surface that only an equal-area map projection can provide. The Peters Map radial construction is well-suited to provide the base map array for products such as the Global Vegetation Index since, in contrast to projections such as the Mercator, the polar-stereographic and the plate carrée, it may be remapped to any other preferred radial construction with no data duplication and minimal data redundancy. Although this paper has used normalized difference vegetation index imagery to illustrate radial projections, we believe that they will be of interest to users of other types of small-scale radiometric imagery.

Acknowledgments

The authors would like to thank Eric Barrett, Andrew Harrison and Tim Richards of the University of Bristol Remote Sensing Unit for their constructive criticism of early drafts of this paper and Tony Philpott of the University of Bristol Department of Geography who developed and printed the photographs.

Appendix

A full mathematical explanation of equal-area radial projections is given by Buccholz (1980). This Appendix describes the practical steps involved in constructing an equal-area radial array.

The graticule of a radial projection is constructed using two standard parallels and is symmetrical about the Equator. Although on the globe the length of 1° of longitude decreases from approximately 111 km at the Equator to 0 km at the poles, on radial projections this distance is constant and equal to the length of 1° of longitude at the standard parallels. In order to construct a radial array, therefore, two fundamental variables must be defined: the standard parallels of the construction, θ_s, and the area on the ground in square kilometres corresponding to one pixel in the radial array, A_p.

The optimal standard parallels for a radial projection of a particular area are calculated as follows. Firstly the polewards and equatorwards limits of the area within which minimum shape distortion is desired are identified (θ_p and θ_e respectively). If the desired area straddles the Equator $\theta_e = 0°$ and θ_p is found by multiplying by two the smaller of the two polewards limits and then subtracting this from the larger of the two polewards limits. For example, the continent of South America lies between 11°N and 55°S and so $\theta_e = 0°$ and $\theta_p = 33°$ (i.e. $55–(11 \times 2)$). Secondly, the radius of the Earth at θ_p and θ_e is calculated

$$r_\theta = \sqrt{\left(\frac{(1-f)^2 \, r_e^{\,2}}{(1-f)^2 + \tan^2 \theta}\right)} \qquad \text{(A 1)}$$

where r_θ = radius of Earth at latitude θ; r_e = radius of Earth at Equator; $(1-f)=(1-e^2)^{\frac{1}{2}}$, where e = numeric ellipsoidal eccentricity of the Earth = 0·081945.

Thirdly, the radius of the Earth at the optimal standard parallels, r_{θ_s}, is calculated from θ_p and θ_e

$$r_{\theta_s}=\sqrt{(r_{\theta_p}\times r_{\theta_e})} \tag{A 2}$$

Finally, the latitude corresponding to r_{θ_s} is calculated using

$$\theta_s=\tan^{-1}\sqrt{\left(\frac{e^2 r_e^2-r_{\theta_s}^2 e^2}{r_{\theta_s}^2}\right)} \tag{A 3}$$

Once θ_s and A_p have been defined the radial array for all the Earth's surface may be constructed. Firstly the radius of the Earth in kilometres at the standard parallels r_{θ_s} is calculated using equation (A 1). The number of pixels in the x direction (east–west), nx, may then be calculated

$$nx=(2\pi\, r_{\theta_s})/\sqrt{A_p} \tag{A 4}$$

The number of pixels per degree of longitude, $x$fac, is calculated as

$$x\text{fac}=(nx)/360 \tag{A 5}$$

The number of pixels in the y direction (north–south), ny, is calculated as

$$ny=A_e/(A_p\times nx) \tag{A 6}$$

where A_e = surface area of the Earth = 510 066 000 km^2.

Within the radial array nx,ny a point of latitude and longitude has coordinates (ix,iy) where

$$ix=(\text{longitude}+169{\cdot}0)\times x\text{fac} \tag{A 7}$$

$$iy=ny/2-((ny\times \text{area}_\theta)/(\text{area}_{90}\times 2)) \tag{A 8}$$

where (1,1) is the pixel located at the top left-hand corner of the array and area_θ and area_{90} are the elliptical surface areas between the equator and the geocentric latitude, l_g, of geographic latitudes θ and 90°, respectively. l_g is calculated as

$$l_g=arc\tan(1-e^2)\times\tan\theta \tag{A 9}$$

and area_θ is calculated as

$$\text{area}_\theta=(rr1+(\ln(rr2)/3{\cdot}0))\times(r_e\sqrt{(1-e^2)})^2\pi \tag{A 10}$$

where

$$rr1=\frac{\sin(l_g)\sqrt{(1-e^2\cos^2(l_g)(2-e^2))}}{(1-e^2)(1-e^2\cos^2(l_g))} \tag{A 11}$$

and

$$rr2=\frac{e\times\sin(l_g)+\sqrt{(1-e^2\cos^2(l_g)(2-e^2))}}{\sqrt{(1-e^2)}\times\sqrt{(1-e^2\cos^2(l_g))}} \tag{A 12}$$

The following should be noted:

(1) 169·0 is added to the longitude (equation (A 7)) in order to split the world map at 169°W (i.e. the central Pacific Ocean). This value may be changed as desired. Adding 30·0, for example, splits the world map at 30°W (i.e. the mid-Atlantic Ocean).

(2) In those instances where undistorted equal-area representation of the polar regions is desired an alternative method of equal area construction with circular parallels and straight meridians may be used (Peters 1983).

References

BERNSTEIN, R., 1983, Image geometry and rectification. In *Manual of Remote Sensing*, second edition, edited by R. N. Colwell (Falls Church, Virginia: American Society of Photogrammetry), pp. 873–958.

BUCCHOLZ, W., 1980, *Peters oder Winkel?* (Akademische Verlagsanstalt).

HARDY, J. R., SINGH, S. M., and NARRACOTT, A. S., 1988, Transformation of Global Vegetation Index (GVI) data from the polar stereographic projection to an equatorial cylindrical projection. *International Journal of Remote Sensing* (to be published).

KIDWELL, K. B., 1984, *NOAA Polar Orbiter Data Users Guide*. Satellite Data Services Division, (Washington, D.C.: National Climatic Data Center).

MALINGREAU, J. P., 1986, Global vegetation dynamics: satellite observation over Asia. *International Journal of Remote Sensing*, **7**, 1121–46.

MILLER, O. M., 1942, Notes on cylindrical map projections. *Geographical Review*, **32**, 424–430.

NOAA, 1986, *Global Vegetation Index Users' Guide*. Satellite Data Services Division (Washington, D.C.: National Climatic Data Center).

PETERS A., 1967, Die perspektivische Verzerrung von Raum und Zeit im historisch-geographischen weltbilde der gegenwart und ihre uberwindung durch neue darstellungsweisen. Votrag an der Ungarischen Akademie der Wissenshaften in Budapest am 6.10.1967.

PETERS, A., 1979, *The Europe-Centred Character of our Geographical View of the World and its Correction* (Munich-Solln: Universum Verlag).

PETERS, A., 1982, Space and time: their equal representation as an essential basis for a scientific view of the world. *Lecture on 'Geo-Cultural Visions of the World'*, given at a symposium at U.N. University, Cambridge, England, 29 March (New York: Friendship Press).

PETERS, A., 1983, *The New Cartography* (New York: Friendship Press).

PETERS, A., 1988, *Peters Equality Atlas of the World* (in preparation).

STEERS, J. A., 1970, *An Introduction to the Study of Map Projections* (London: University of London Press).

TUCKER, C. J., and SELLERS, P. J., 1986, Satellite remote sensing of primary production. *International Journal of Remote Sensing*, **7**, 1395–416.